Biogenic Polymers: From Barrier Coatings towards the Design of novel low-adhesive Release Liner

TECHNISCHE UNIVERSITÄT DARMSTADT

Vom Fachbereich Chemie
der Technischen Universität Darmstadt

zur Erlangung des akademischen Grades eines
Doctor rerum naturalium (Dr. rer. nat.)

Dissertation von
M.Sc. Sebastian von Gradowski
aus Ahlen

Referent:	Prof. Dr. Markus Biesalski
Korreferent:	Prof. Dr. Robert Stark

Darmstadt 2019

D17

Von Gradowski, Sebastian: Biogenic Polymers: From Barrier Coatings towards the Design of novel low-adhesive Release Liner
Darmstadt, Technische Universität Darmstadt,
Jahr der Veröffentlichung der Dissertation auf TUprints: 2019
URN: urn:nbn:de:tuda-tuprints-85795

Tag der Einreichung: 28.01.2019
Tag der mündlichen Prüfung: 15.03.2019

Darmstadt 2019

D17

Erklärung zur Dissertation

Hiermit versichere ich, die vorliegende Dissertation ohne Hilfe Dritter nur mit den angegebenen Quellen und Hilfsmitteln angefertigt zu haben. Alle Stellen, die aus Quellen entnommen wurden, sind als solche kenntlich gemacht. Diese Arbeit hat in gleicher oder ähnlicher Form noch keiner Prüfungsbehörde vorgelegen.

Darmstadt, den 20.01.2019

(Sebastian von Gradowski)

Sebastian von Gradowski
Mühlenkamp 21
40229 Düsseldorf

Düsseldorf, den 20.01.2019

Ich erkläre hiermit, dass die elektronische Version der Doktorarbeit mit der schriftlichen Version übereinstimmt. Die elektronische Version liegt dem Prüfungssekretariat vor.

_____

(Sebastian von Gradowski)

This present work is a result of the work from November 2014 until March 2019 accomplished at the Technical University of Darmstadt in the Department of Macromolecular Chemistry and Paper Chemistry at the Ernst-Berl-Institute for Technical and Macromolecular Chemistry, under the supervision of Prof. Dr. Markus Biesalski and in cooperation with Sappi Alfeld GmbH.

Part of this work has been presented at conferences:

I) **Oral presentation**: 'Biogenic coatings as building-blocks for release-liner applications', 5. Darmstädter Papierchemie-Kolloqium, Darmstadt, May 2018

II) **Poster presentation**: 'Development and investigation of a cellulose-based low adhesion coating for adhesive tapes', 253rd ACS National Meeting & Exposition, San Francisco, California, USA, April 2017

III) **Poster presentation**: 'Siliconization of clay-coated Paper by 3-Roller System', Doktorandentag, TU Darmstadt, January 2016

IV) **Manuscript**: Von Gradowski, S.; Torborg, C.; Biesalski, M. *Preparation and Characterization of Cellulose-based barrier coatings for producing a Release-liner out of a porous Base Paper*, Cellulose **2018**, 17(1), p. 6510. https://doi.org/10.1007/s10570-018-2152-1

Danksagung

An dieser Stelle möchte ich bei allen bedanken, die mich während meiner Promotion begleitet und unterstützt haben. Mein besonderer Dank gilt meinem Doktorvater Prof. Dr. Markus Biesalski, für die Betreuung dieser sehr anwendungsbezogenen Arbeit sowie für die vielen kontroversen Diskussionen. Die Gespräche haben mir besonders geholfen Beobachtungen besser zu verstehen und neue Lösungsstrategien zu entwickeln. Außerdem möchte ich mich für die Möglichkeit zur Teilnahme an zahlreichen internationalen und nationalen Konferenzen sowie die legendären Arbeitsgruppenausflüge nach Hirschegg bedanken.

Bei Dr. Christian Torborg bedanke ich mich recht herzlich für die Betreuung meiner Arbeit als Projektpartner seitens Sappi und für die Bereitstellung von verschiedenen Papiersubstraten. In zahlreichen Gesprächen und Besuchen konnte ich viel über die Papierherstellung und die Papierveredelung lernen. Es war mir außerdem eine sehr große Hilfe die Lösungsstrategien und Prozesse aus Sicht der Industrie zu betrachten und so die Herangehensweise zu optimieren. Ebenfalls möchte ich mich bei Dr. Peter Wenz für zahlreiche Gespräche und seinen Hilfestellungen durch seine langjährige Erfahrung in der Papierindustrie bedanken.

Ich danke Prof. Dr. Robert Stark für die freundliche Übernahme des Korreferats. Prof. Dr. Samuel Schabel sowie Herrn Dr. Schaffrath bedanke ich mich für die Möglichkeit am PMV messen zu dürfen und für die Einweisung in diverse Analysemethoden. Ein großer Dank an Maximilian Nau für die Bereitstellung von modifizierter Cellulose sowie für viele kontroverse Diskussionen und wissenschaftlichen Input. Ich bedanke mich außerdem bei ihm für die Unterstützung rund um das Thema Computer und Software (Unser „IT-Max"). Ich bedanke mich bei Prof. Robert Stark für die Möglichkeit in seinem Arbeitskreis messen zu dürfen sowie bei Dr. Christian Dietz und Julia Auernhammer für die Durchführung und Auswertungen der AFM-Messungen. Dr. Simon Trosien und Dr. Andreas Geißler danke ich herzlich für zahlreiche wissenschaftliche Gespräche und Unterstützung in vielerlei Hinsicht. Ich danke Dr. Tobias Meckel für die ausführliche Einführung in die Konfokalmikroskopie und Hilfestellungen bei den Untersuchungen der Proben.

Ich möchte mich beim gesamten Arbeitskreis Biesalski und beim Arbeitskreis Brunsen für eine tolle Zeit, eine sehr angenehme Arbeitsatmosphäre, einen super Zusammenhalt und für die vielen anregenden Diskussionen bedanken. Vor allem möchte ich mich bei Dr. Andreas Geißler, Dr. Simon Trosien, Dr. Cagla Söz, Maximilian Nau, Marcel Krauße sowie Mathias Diefenbach für die Durchsicht meiner Doktorarbeit bedanken. Herzlichen Dank auch an Martina Ewald für die Unterstützung in vielen verschiedenen Problemstellungen und für die sehr gute Organisation im Arbeitskreis (Die Frau, die für fast jedes Problem eine Lösung parat hat!). Ich danke Heike Herbert für diverse Hilfestellungen in der IR-Spektroskopie, dem Brookfield-Viskometer sowie vielen schönen Gespräche. Die fleißigen Frauen aus dem Sekretärsbüro Conny Golla, Vanessa Schmidt und natürlich Bärbel Webert danke ich sehr herzlich für die Hilfestellung in vielen organisatorischen Dingen. Meiner lieben Büronachbarin Mareike danke ich für die gegenseitige Unterstützung und eine tolle Zeit. Ich danke Fabian Nemitz und Frank Hartmann dich mich durch ihre Bachelorarbeiten in meiner Arbeit unterstützt haben.

Zu guter Letzt, danke ich meinen Eltern für eine ständige Unterstützung und Begleitung auf meinem Lebensweg, ohne dich ich nicht so weit gekommen wäre. Außerdem bedanke ich mich bei meiner Freundin Isabell, die mich während meiner Promotion mit viel Geduld und Kraft unterstützt hat.

Contents

Glossary

AFM	Atomic force microscopy
ATR	Attenuated total reflectance
CCD	Charge-coupled device
CCK	Clay-coated Kraft
CD	Cross direction
CMC	Carboxymethyl cellulose
CNC	Cellulose nanocrystals
$\overline{D}$	Polydispersity
DS	Degree of Substitution
eq.	Equivalent
EtOAc	Ethyl acetate
FINAT	Féderation Internationale des fabricants et transformateurs d'Adhésifs et Thermocollants sur papiers et autres supports
FITC	Fluorescein isothiocyanate
FT-IR	Fourier transform infrared spectroscopy
HEC	Hydroxyethyl cellulose
HPC	Hydroxypropyl cellulose
HRA	High release additive
IPA	Isopropyl alcohol
MC	Methyl cellulose
MD	Machine direction
MFC	Micro-fibrillated cellulose
NMR	Nuclear Magnetic Resonance
PDMS	Polydimethylsiloxane
PLA	Polylactic acid
Pr	Propyl
PSA	Pressure sensitive adhesive
PVA	Polyvinyl alcohol
r.H.	Relative humidity
RhB	Rhodamine B
rpm	Revolutions per minute
SEM	Scanning electron microscopy
THF	Tetrahydrofuran
TLC	Thin layer chromatography
WLI	White light interferometer
wt%	Weight percent

1 Introduction

1.1 Release liner

Since over 60 years release liner are used as a functional support for die cutting or as a delivery system for pressure sensitive adhesive (PSA), such as tapes or labels. The most used release material is based on polydimethylsiloxane (PDMS) due to its unique low-adhesion properties.[1,2] The release liner is produced from a substrate carrying a smooth and non-porous surface. In particular, a simple foil (polypropylene) or a clay-coated-Kraft (CCK) paper is used as release liner substrate (Figure 1). In case of CCK paper, hexagonal-shaped clay pigments from the group of the kaolinite, having the chemical composition of $Al_2Si_2O_5(OH)_4$, are usually used for this purpose.[3] The clay-coating is a complex mixture, consisting of various additives like binder, crosslinker and viscosity modifier. The porous paper surface is closed by the clay-pigments, which act as a barrier coating against the penetration of liquids.[4,5] The same principal is applied for silicone coatings in order to generate a homogeneous coating on the paper surface and to reduce silicone consumption. A thin silicone layer (1 g/m² or 1 μm) is applied on the substrate by a multiple roller coater and the coating is finally cured by UV light or heat.[2,6,7] Typically, a solvent-free silicone system is used as a release coating, which is cured and crosslinked by hydrosilylation reaction of vinyl groups of the silicone backbone with appropriate silane groups of the crosslinker.[8–11] Beside this, there exist also silicone systems on the base of aqueous emulsions or organic solvents. The silicone can undergo condensation reactions with hydroxyl groups, coming from the cellulose or from coating additives in the clay-coating, during storage. Hence, the anchorage of the silicone coating to the paper surface is improved by this post-curing process, which is accompanied with a good rub-off.[7,12–14] In a second step, the adhesive is coated on top of the silicone layer and additional substrate (Face-stock) is applied on the adhesive to get the adhesive tape. The release liner protects the adhesive against contamination and enables an easy release without impairing the adhesive performance. The release force have to be adjusted depending on the final application. Low release forces are required in label industry, whereas high release forces are needed in sealants for roofings or in graphic arts on foils for car wrapping.[1,15] The release forces can be tailored by the addition of silicone resins.[16] The release of an adhesive tape from a release liner is a complex process and depends on several parameters, such as on the type of adhesive, the release liner substrate, the silicone formulation, the coating process and on the peel-off process.[17] In a next part, a closer look will be placed on the adhesion in general and on adhesion of PSA on silicone release liner.

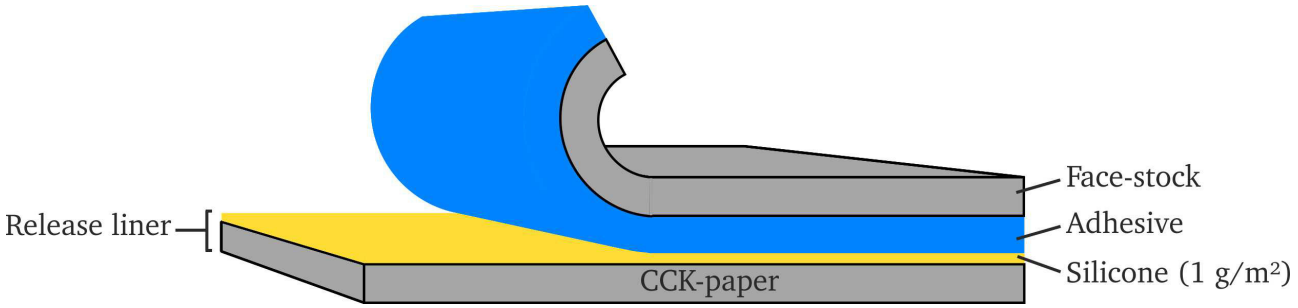

Figure 1: Layer structure of a release liner for the transportation of an adhesive tape.

1.1.1 Adhesion of a PSA

Adhesion between two substrates originates from interfacial forces, such as van der Waals, interdiffusion of polymer chains or chemical bonds. The adhesion force is mainly governed by the topography, surface energy and material properties.[18–20] The PSA is usually above its glass transition temperature (T_g) and it has got a viscoelastic behavior. Viscoelastic materials behave as a viscous liquid or as a elastic solid depending on the shear rate, time and temperature.[21,22] The adhesive is permanent tacky and it should possess a good cohesive strength in order to prevent adhesive failures. The thermodynamic work of adhesion is given by the Dupre equation and it focuses on fundamental adhesion between atoms in the interphase of two materials (Equation 1.1). This equation contains the surface energy of the solid and of the liquid with the vapour phase (γ_{SV} or γ_{LV}) and the interfacial energy (γ_{SL}) between the solid and liquid (Figure 2). As only γ_{LV} can be determined with sufficient accuracy by contact angle measurements, the Young equation (Equation 1.2) is used in order to calculate the thermodynamic work of adhesion.[23] Incorporation of the Dupre equation into the the Young equation gives the Young-Dupre equation (Equation 1.3), which directly correlates the contact angle (θ) and the liquid-vapour interfacial energy (γ_{LV}) to the thermodynamic work of adhesion.[19,23] If the contact angle is zero, the surface is fully wetted and the work of adhesion has its maximum value.

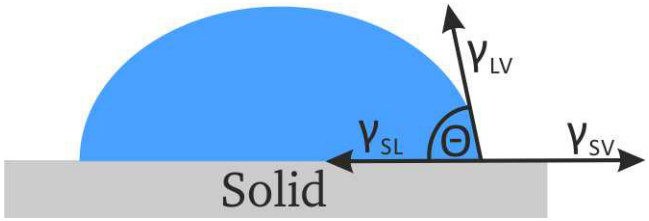

Figure 2: Contact angle measurement for the determination of the thermodynamic work of adhesion.

$$W_A = \gamma_{SV} + \gamma_{LV} - \gamma_{SL} \tag{1.1}$$

$$\gamma_{LV} cos\theta = \gamma_{SV} - \gamma_{SL} \tag{1.2}$$

$$W_A = \gamma_{LV}(1 + cos\theta) \tag{1.3}$$

Nevertheless, this equation is only valid with the assumptions that the adhesion process is reversible and does not dissipate energy, which is not true for a real case (Practical adhesion). During break of the bonding, energy is dissipated in several ways such as deformation, viscoelastic flow and heating of the adhesive. Thus, the practical adhesion is significant higher compared to the thermodynamic work of adhesion considering just surface energies.[18,19] For example, the surface adhesion of a liquid, which only interacts with the surface by van der Waals forces, is about 0.1 J/m^2, whereas fracture energies from

100 up to 1000 J/m^2 were measured for adhesives.[20] This shows that the debonding process and the creation of new interfaces are not the only parameters affecting the adhesion force.

In general, the interactions between two substrates are described not by one, but many different theories of adhesion (Figure 3). In the diffusion theory, the chain interdiffusion of the polymer chains in the interphase between two polymers is described, which contributes to the adhesion. Chain diffusion preferably arises in the interphase of two compatible materials having similar surface energy. The chains have to be mobile and not locked in a crosslinked network. Low molecular additives from the PSA, like tackifiers or surfactants, may migrate to the PSA/substrate-interphase and may also influence the adhesion.[1,21]

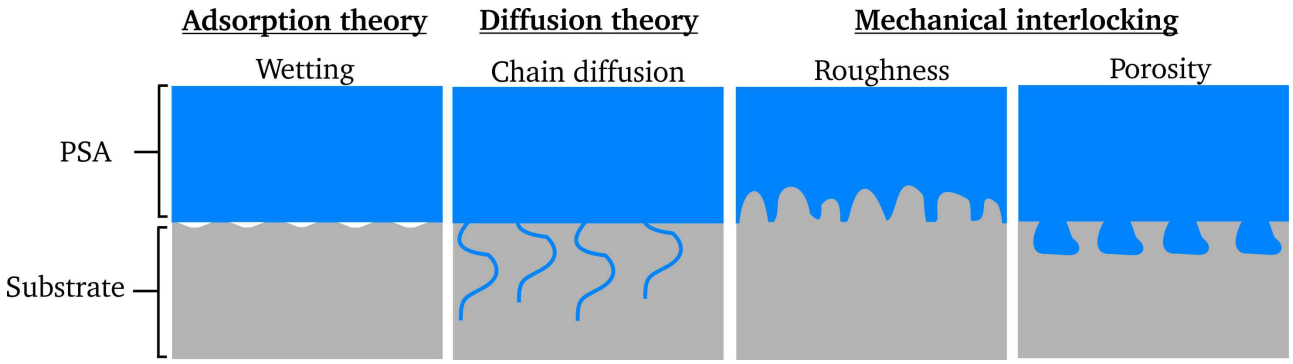

Figure 3: Schematic representation of adhesion mechanisms.

Beside this theory, the mechanical interlocking theory describes the influence of the surface roughness and surface porosity on the adhesion. Depending on the scale of roughness or the pore radius and the viscoelastic property of the adhesive, the adhesion can be decreased or increased compared to a smooth surface. For example, penetration of the adhesive into a microstructure increases the contact area and thus the surface interaction as well as the energy dissipation during peel-off. For this process, the viscosity of the adhesive has to be low enough in order to migrate into the cavities of the substrate. If the adhesive is not able to flow into the pores, the contact area is reduced and this results to lower adhesion.[1,21,24]

In adsorption theory (or wettability theory), the substrate has to be completely wetted by the viscoelastic adhesive in order to maximize the interfacial interactions and to guarantee good adhesion. The adhesive properties have to be tailored for an effective spreading of the adhesive. The wetting of a surface in general is influenced by the surface energy of the substrate and the surface tension of the liquid. Good adhesion and wetting are obtained, if the surface energy of the adhesive is smaller compared to the surface energy of the substrate.[1,22] Consequently, the substrate should have a low surface energy in comparison to the PSA (30-40 mN/m) in order to reduce the wetting of the surface. Additionally, strong physical interactions like hydrogen bonds have to be prevented to obtain low release forces.[21,25]. Silicone is the most prominent polymeric material for low adhesion applications, having a bulk surface energy of 22 mN/m. However, a low bulk surface energy is not the only prerequisite for low release properties. Fluorochemical release coatings should posses the lowest release forces due to a very low surface energy (< 20 mN/m), but this was not observed in experiments.[13,21,26]

1.1.2 Release mechanism of a PSA from different substrates

The release of an PSA from a substrate is a complex process and it depends on several parameters such as PSA rheology, chemical composition, surface energy, chemical and physical interactions as well as on the test method.[27] In general, it was found that the adhesion of a PSA is reduced with decreasing surface energy of the substrate, but this is not true for all cases.[21] The release of a PSA from different substrates and the understanding of the adhesion is subject to many publications.[27–30] For example, the mechanical behavior of an PSA, composed of an acrylic-styrene-copolymer, during peel test from a steel plate in an angle of 90° was investigated.[27] The formation of fibrils were observed during peel-off in the bending zone, which is explained by energy dissipation processes. The elongation of the fibrils depends on the chemical composition and the tack of the adhesive. Most fracture energy was dissipated in the region where the fibrils elongation was maximum (Figure 4). Additionally, the authors found out that the fracture energy raises linearly with increasing contact area.

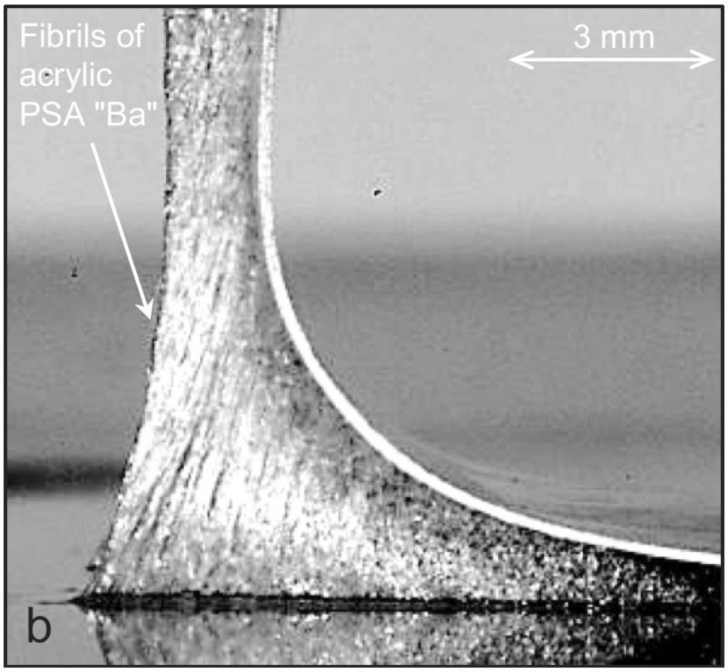

Figure 4: The image was recorded by a CCD-camera and it shows the development and elongation of fibrils of the adhesive in the fracture zone during 90°-peel-off from a steel plate. Figure reproduced with permission from reference.[27]

In another publication, the influence of the substrate surface energy and the roughness on the tack of an acrylic PSA was studied.[30] The surface energy mainly governed the tack properties of the PSA. The higher the difference in surface energy between the substrate and the PSA, the better is the tack. In addition, the viscoelastic property of the adhesive influences the peel-off force. A more viscous PSA dissipates more energy and this leads to higher peel force compared to a more elastic one. The adhesive is deformed at the fracture zone and the energy which is required for this process, is consumed and dissipated when the crack propagates.[20] The viscoelastic property of the adhesive is changed by addition of crosslinker and measured by the shear storage modulus (G') at low frequencies. This gives information about the cohesive strength of the adhesive. The storage modulus of the adhesive was increased by the

addition of crosslinker. Consequently, the tack decreases with increasing amount of crosslinker, because of less deformation of the adhesive. The adhesion force on smooth (R_a = 0.2 μm) and rough substrates (R_a = 3.3 μm) is also controlled by the viscoelastic behavior of the adhesive. In general, the adhesion force on the rough substrate was higher compared to the smooth surface. The adhesive is able to creep into the cavities of the surface at low concentrations of crosslinker. The contact area is larger compared to the smooth surface and adhesion is enhanced. In contrast to this, at higher crosslinker content, the adhesive does not penetrate into the cavities, the contact area is smaller compared to the rough surface which results in lower adhesion forces. Beside the viscoelstatic properties, adhesion is also affected by the PSA thickness.

The adhesion and the performance of a PSA is usually tested by peel-off experiments from a steel plate, but adhesion of PSA on a porous substrate like paper is different. Thus, the influence of paper properties on the peeling behavior of a PSA on a porous paper was investigated.[31–33] Three different fractures can occur during peel-off: The PSA can be removed from the paper surface by a paper failure, a cohesive failure of the adhesive or an interfacial failure. The interfacial failure is the ideal peel behavior in which the PSA is completely removed from the paper surface without destroying the paper or the adhesive. Interfacial failure is typically observed at low peel rate (100 $^{mm}/_{min}$), whereas paper rupture was observed at high peel rate (400 $^{mm}/_{min}$) (Figure 5).[33]

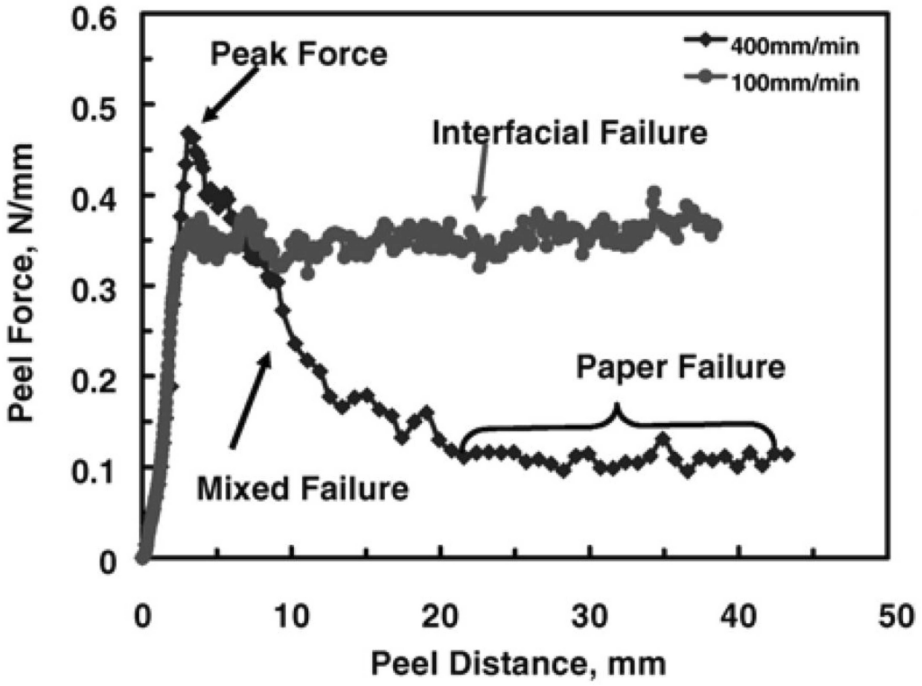

Figure 5: Peel curves of a PSA from a newsprint paper at peel rates of 100 $^{mm}/_{min}$ and 400 $^{mm}/_{min}$. Figure reproduced with permission from reference.[33]

Silicone release coatings are used in order to reduce the adhesion to the substrate and to maintain the adhesive performance. The unique low adhesion properties of the silicone cannot only deduced to a low surface energy. Comparing crosslinked PDMS with fluorinated release coatings the surface energy of the latter one is lower, but release forces are higher. Thus, release mechanism on silicone and fluorinated substrate was investigated in detail.[34,35] Fluorescent particles were introduced into the PSA bulk and

the adhesive/silicone interface and the displacement of the particles during peel-off was analyzed (Figure 6). It was found that the particles in the adhesive on the PDMS surface were moved up to 13 μm, whereas the particles on the fluorinated substrate were shifted by just 1-2 μm. This observation demonstrates a slip motion of the adhesive on the PDMS substrate during crack propagation, which supports the low release property. This interfacial slippage minimizes the shear deformation of the adhesive as well as the release force. Additionally, the force-dissipative character of the crosslinked PDMS also reduces the adhesion. Minor slippage on the fluorinated surface leads to higher shear deformation of the adhesive as well as more energy dissipation by friction, which leads to higher release forces. This shows that the unique low release property of the silicone is governed by interfacial slippage of the adhesive, which allows the shear stress to relax.[34,35] For a appropriate release, the adhesive of the PSA has to sufficiently stick to its facestock and the cohesive strength of the adhesive should sustain the peel forces. Additionally, the mechanical stability of the silicone coating and thus the rub-off has to be good so that the silicone is not removed by the adhesive during peel-off.[19,21]

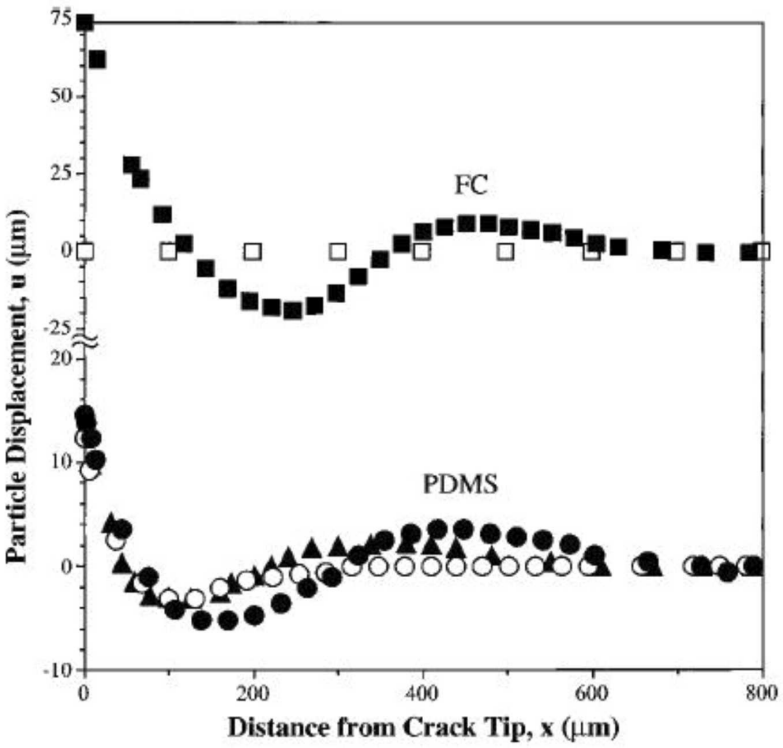

Figure 6: Motion of fluorescent particles in the bulk (black) of the adhesive and at the adhesive/silicone interface (white) on PDMS (∘) and fluorocarbon (□) substrate during peel-off. Figure reproduced with permission from reference.[34] Copyright (1997) American Chemical Society.

Depending on the application, the release forces have to be tailored by addition of high release additives (HRA). Most times silicate resins are incorporated into silicone release coatings in order to increase the release forces. In one study, an acrylic and a rubber-based adhesive were peeled-off from a siliconized paper substrate with different amounts of HRA.[36] It was found that the more HRA is added to the silicone formulation, the higher were the corresponding release forces. In order to understand this phenomena, the viscoelastic properties of the adhesive and of the cured silicone were determined in terms of the shear storage modulus (G'), loss modulus (G'') and loss tangent ($tan\,\delta = G''/G'$), which

describes the relationship between stored energy and dissipated energy during deformation. It was found that higher amounts of HRA increase the loss modulus G'' and thus $tan\,\delta$ of the release coating to more extent than the storage modulus G'. This means that the coating behaves more inelastic (viscous) and the silicone coating dissipates more energy during peel-off with raising amounts of HRA, leading to higher release forces. In addition to the silicone coating, the viscoelastic properties at different peel rates also affecting the release forces. The release forces of the acrylic tape were increased with higher peel rates, whereas the opposite was observed for the rubber adhesive. In both cases, the highest release forces were detected in the glass-rubber transition of the adhesive, where the loss modulus exceeds the storage modulus. It was found that the loss tangent correlates well with the release forces at different peel rates.[36] It was shown that low amounts of resin resulted in high slip and low shear deformation of the adhesive, leading to low release forces (Figure 7).

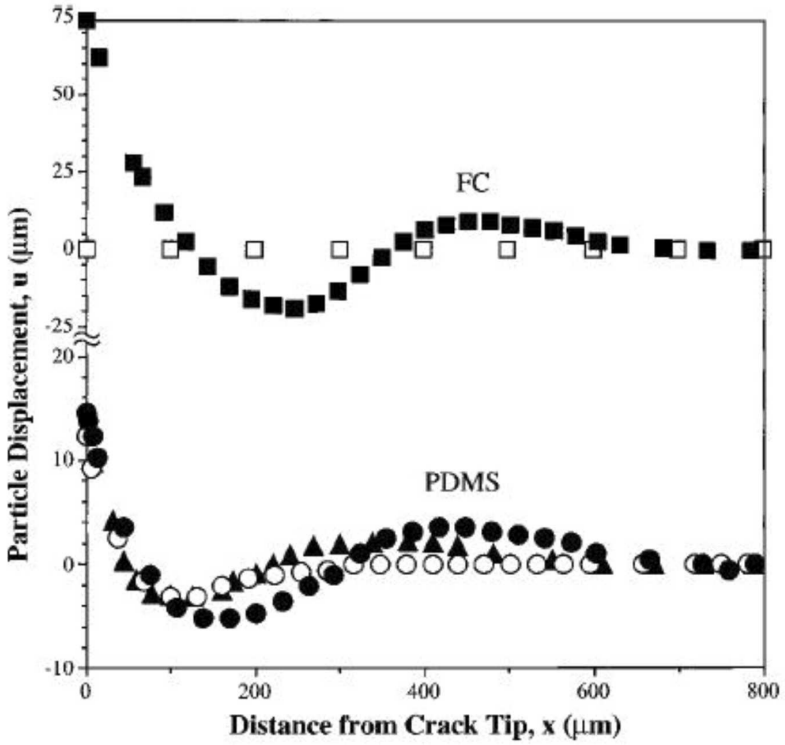

Figure 7: Displacement of fluorescent particles in the bulk (open symbols) and in the adhesive/silicone interface (solid symbols) during peel-off with different amounts of resin. The displacement of the particles (u) is plotted as a function of the distance (Vt) of the fluorescent particle from the peel front. Figure reproduced with permission from reference.[16] Copyright (2001) American Chemical Society.

The influence of HRA in silicone formulations on the interfacial slippage of an adhesive tape was studied in detail by determination of particle displacement in the adhesive/silicone interface.[16] In contrast to this, slip is reduced at higher amounts of resin and the adhesive deformed to more extent. Thus, more energy is dissipated during the peel process, which leads to higher release forces. Energy dissipation is possible in the fracture zone in the crack tip as well as in a region far away from the fracture tip. This dissipation process is either governed by shear deformation of the adhesive when resin was added to the silicone or by interfacial friction due to slip motion without any resin. The resins affect the viscoelastic

properties of the bulk, the interaction between the adhesive and silicone, and the amount of interfacial slip. Controlling the interfacial slip seems to be the key point in order to adjust peel forces of release systems. [16]

In summary, in high "adhesion systems", the surface energy of the substrate (e.g. glass or metal plate) is higher compared to the adhesive, the peel force as well as the deformation of the adhesive during peel-off are high and the adhesive bond brakes primary due to a cohesive failure (Table 1). In contrast to this, the surface energy of the substrate in a "release system" is lower compared to the adhesive. The peel force as well as the deformation of the adhesive during peel-off are low and the adhesive bond brakes primary due to an adhesive failure. [36]

Table 1: Comparison of peel system with a release system. [36]

Parameter	Adhesion system	Release system
Peel force	High	Low
Deformation	High	Low
Failure mode	Cohesive/Adhesive/Mixed failure	Adhesive
Surface energy	$\delta_{substrate} > \delta_{adhesive}$	$\delta_{adhesive} > \delta_{substrate}$

1.1.3 Silicone-free release liner

Silicone is the most widely used material for release coatings due to its unique properties and availability. Nevertheless, recyclability of silicone release papers is not trivial due to separation issues of the silicone contaminations from the pulp and strong acidic conditions. Additionally, silicone coatings contain unreacted silicone extractables, which are not desired for certain applications. The extractables can migrate to the backside of the release liner and this lead to printing issues. [37] Thus, in some research approaches the silicone was replaced by bio-based release coatings in order to produce sustainable release liner. [38–43] Additionally, an expensive platinum catalyst is required for curing reactions of the silicone and unreacted silicone chains can be transferred to the adhesive impairing its performance. Thus, there is a growing interest to replace the silicone by silicone-free alternatives (Figure 8). [44–49]

In one patent, a silicone-free release coating was synthesized from polyethylene. Different densities of the polyethylene were produced by using metallocene catalyst, whereas higher densities are related to higher crystallinity. It was found that the release forces were raised with increasing densities. The polymer was applied on the substrate at a film thickness of 0.1 to 0.15 mm, which is 100-fold higher compared to silicone release coatings (1 μm). Release forces of approximately 1 $^{N}/_{25\ mm}$ were measured. [44] This coating can be used as release coating for PSA, but a significant higher amount of coating is required, which is not sustainable.

Another invention describes the production of a synthetic release coating on the base of polyacrylate or a polyacrylate-copolymer. [46] The material was applied on the paper in a thickness of 3-10 μm by blade coating and the resulting release forces ranged from 2-4 $^{N}/_{50\ mm}$. The coating thickness and the release forces were significantly higher compared to silicone-based release coatings, but still practical for some high release applications. However, this coating does not improve the recyclabilityof the release liner, which is not sustainable.

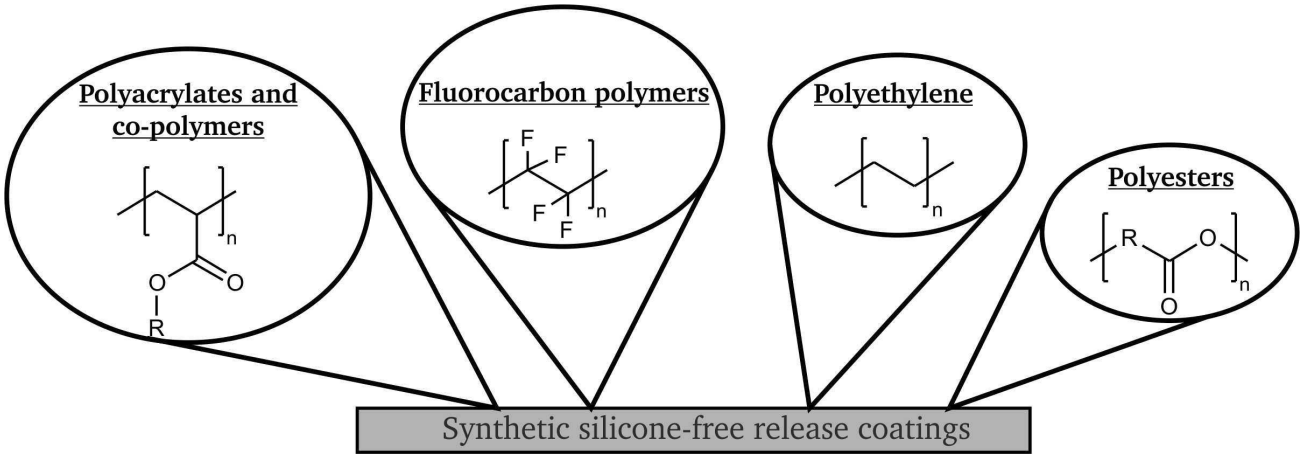

Figure 8: Chemical structure of synthetic silicone-free release coatings as reported in recent literature. [45–49]

Silicone-free release liners were also produced by direct modification of the substrate surface by using atmospheric pressure plasma. [49] The substrate was exposed to the plasma and an aerosol composed of a polymerizeable precursor, preferably acrylates. Active species, such as radicals or ions, evolved on the surface during plasma treatment and reacted with the added monomer. The release layer was finally cured by heat or UV light. Depending on the monomer, release forces of 2-3 $^{N}/_{25\ mm}$ were obtained.
In addition to the already mentioned release coatings, low adhesion coatings can be also composed of polyester or fluorocarbons, but the release forces of polyester were high and just limited applicable. In case of fluorocarbons, the costs were high and the environmental impact makes this system less appropriate for release liner. [49,50]
In addition to the silicone-free and synthetic release coatings, there is an increasing demand to introduce biogenic and biodegradable release coatings for a better sustainability. Phosphate esters were introduced as a new material for release applications. The phosphate ester were synthesized by the reaction of 1-octanol with phosphorus pentoxide (Scheme 1).

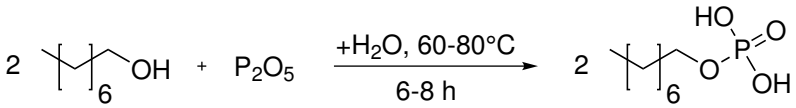

Scheme 1: Synthesis of phosphate esters. Figure reproduced from reference. [42]

The alkyl chains provide a hydrophobic character and a low surface energy, which is one requirement for a release coating. Additionally, the free hydroxy groups of the esters are supposed to undergo a thermal reaction with the hydroxy groups of the paper surface, which may lead to a stable anchorage to the paper surface. The phosphate ester were applied on a paper, which was previously coated by 10 $^{g}/_{m^2}$ of a PVA pre-coating. Release forces of approximately 0.5 $^{N}/_{25\ mm}$ were obtained, which is comparable to silicone release coatings. Nevertheless, a mass transfer of the release coating to the adhesive was observed likely due to a poor anchorage of the esters to the paper surface. This is not desired for release liner, because the esters on the adhesive tape may impair the adhesive performance. It is questionable whether the low release forces originate from the phosphate ester coating or from the undesired delamination process

of the coating from the paper surface, i.e. low adhesion between coating and PVA-pre-coating. The anchorage of the phosphate esters has to be studied in detail and improved by introducing covalent bonds in order to prevent mass transfer to the adhesive tape. [42]

In another approach, poly(vinyl N-alkyl carbamates) were used as release coatings. [39–41] Partially hydrolyzed poly(vinyl acetate) was reacted with decyl isocyanate and octadecyl isocyanate yielding polycarbamates with different alkyl side chains (Figure 9). The hydrophobic alkyl chains were exposed to the surface, shielding the inner-lying polar groups, and providing low surface energy. This is important to reduce the interaction of the PSA with the release material and enabling low adhesion.

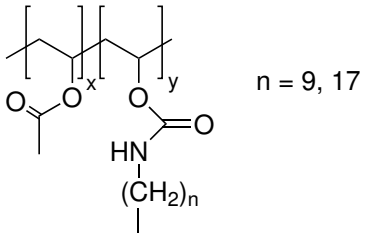

Figure 9: Chemical structure of polycarbamate release coating. Figure reproduced with permission from reference. [41]

Adhesion forces of a PSA containing acrylic acid moiety were determined by measuring the pull-off forces from the polycarbamate release coatings. It was found that the release forces of the acid-containing PSA was higher than compared to the reference PSA without any acid groups. The introduction of acrylic acid moieties to the PSA increases the interfacial energy with the release coating as well as the adhesion energy as a function of the contact time. Upon contact of the acidic PSA with the release coating, the polymer chains of the polycarbamates rearrange in the interface and the adhesion is enhanced. This rearrangement is driven by energetically favorable acid-base interaction between basic urethane groups from the polycarbamate with the acrylic acid groups from the PSA. The segmental mobility of the polymer chains has to be high enough to enable the restructuring process. The attractive force of the acidic PSA was higher at the polydecylcarbamate than the polyoctadecylcarbamate because the crystallinity of the latter one is higher, and chain mobility is reduced. Heating of the polyoctadecylcarbamate above the melting point increases chain mobility and attractive forces due to the restructuring process in the PSA/polycarbamate interface. Thus, for stable adhesion forces, the segmental mobility within the release coating has to kept low in order to preserve the surface structure. This can be obtained by introducing crosslinks as in silicone coatings or by using polymers with long alkyl side chains. It was found that the length of the alkyl side chains in the release coating has to be between 10 and 16 methylene groups in order to prevent polar interactions with the PSA. [39–41]

Long alkyl side chains were also introduced by reacting polyvinyl alcohol with stearic acid chloride. [38] The resulting polyester showed low adhesion towards PSA, but this property disappeared when heating the release coating above the melting temperature. This is most likely due to restructuring of the release coating as mentioned above.

In another invention, the paper surface was directly grafted by a steam of stearic acid chloride at elevated temperature (150-180 °C) (Scheme 2).[43,51–53] This modification process is known as "chromatogeny" and yielded a hydrophobic surface, which can be used as a water barrier as well as for a silicone-free release coating. For the application as a release coating, the porous paper surface is first closed by a PVA-precoating and then grafted with stearic acid chloride. Release forces of approximately 6 $^{N}/_{25\ mm}$ were obtained. Additionally, the recyclability of the grafted papers was still acceptable. Nevertheless, several side reaction occured during the modification step and only 15 to 28 % of the stearic acid chloride reacted with the paper surface depending on the paper substrate. Moreover, huge amounts of hydrochloric acid arise during the reactions and this can lead to corrosion of metal parts in the coating machine. The handling of the acid environment is still challenging and the papers have to be purified from unreacted by-products and hydrochloric acid.

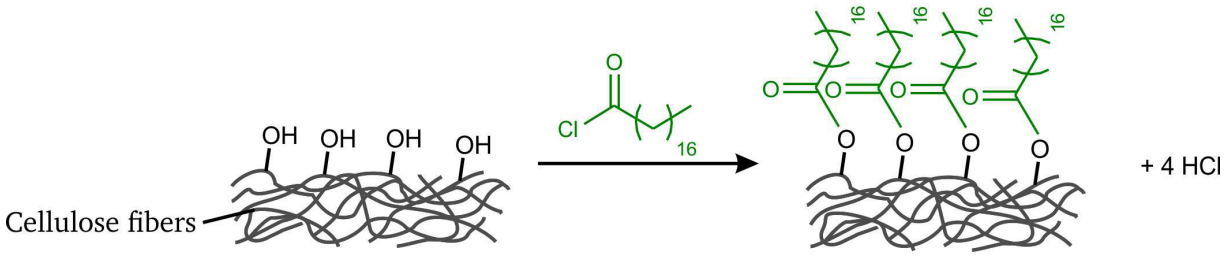

Scheme 2: Surface hydrophobization of hydroxy groups from the paper surface by the reaction with an aerosol of stearic acid chloride under release of hydrochloric acid.

The challenges of a poor grafting efficiency and high amounts of hydrochloric acid may be solved by modification of a bio-based polymer with stearic acid chloride and subsequent coating on the paper surface. It was already shown that hydroxy propyl cellulose (HPC) can be modified with different fatty acid chlorides and with precise tailoring the degree of substitution (DS).[54] Such materials were preferably used as a nanoparticle suspension in order to produce superhydrophobic surfaces, but they have yet not been used as a release coating.

1.2 Barrier coatings for paper substrates

Cellulose fibers are the main material used in packaging industry or for release liner applications due to its mechanical strength, flexibility and good recyclability. Nevertheless, paper exhibits a porous structure and suffers from poor barrier properties against water, water vapor, grease or oxygen (Figure 10). The paper must be treated by a surface coating or laminated with a plastic foil in order to provide barrier properties. This is important in order to protect the food product from contamination and to ensure high quality over time or prevent penetration of the surface coating (printing ink or release coating) into the paper. [55,56]

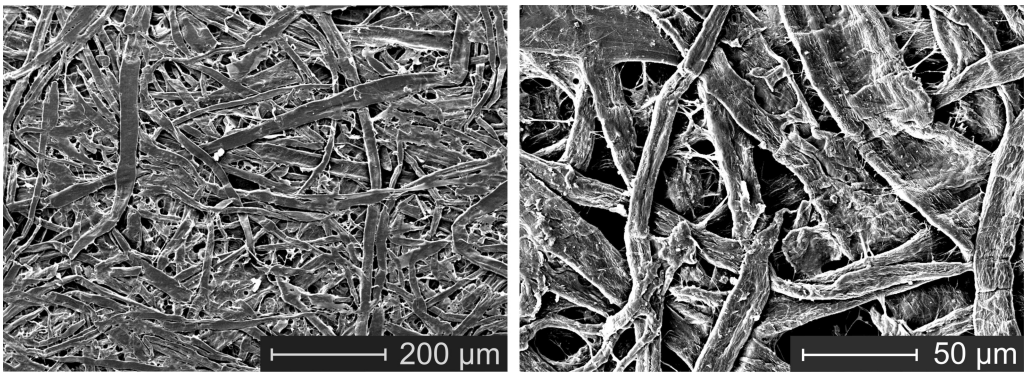

Figure 10: SEM images (topview) of the porous surface structure of paper at different magnifications.

1.2.1 Pigment-coated barrier coatings

Pigments like clay or calcium carbonate were used in combination with a binder as a mechanical barrier coating against penetration of liquids and in order to improve brightness, gloss and opacity. The paper pores were filled by the pigments, the surface is smoothed and penetration of liquids into the paper is reduced. [57] In one publication, the barrier properties of kaolin pigments, having different size and shape, against liquids, such as water and organic solvents, were tested in combination with different latex binders. [4,58] It was found that the barrier properties of highly aligned, thin platy kaolin were better compared to thick, fine kaolin. The platy kaolin particles posses a higher aspect ratio compared to particles of shapes such as spheres or cubes. The aspect ratio is defined as the particle diameter divided by the particle thickness. The barrier properties were improved by the platy shape of the particles because the pathway for the liquid to migrate is increased (Figure 11).

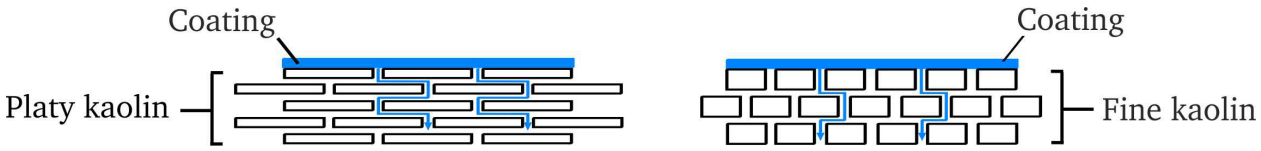

Figure 11: Schematic illustration of the influence of kaolin particle shape on barrier properties against liquids. The pathway for the liquid is longer for platy kaolin compared to fine kaolin resulting in better barrier properties. Figure redrawn from literature. [4]

It was found that the barrier properties were more governed by a high aspect ratio and by the orientation of the particles than by the particle size distribution. Large flakes with high aspect ratios were most

suitable for good barrier properties than small flakes with low aspect ratios. The barrier properties of platy kaolin were supported by addition of a latex binder, whereas best results were obtained for the ethylene acrylic latex. Other binders like styrene acrylate or styrene butadiene latex can also be used, but in case of coatings with organic solvents, the binder was dissolved and the barrier properties were reduced. [4,58]

The platy particle structure was also used as a barrier coating for silicone formulations. The hyperplaty talc particles, having an aspect ratio from about 60 to about 100, were mixed with a carboxylated styrene butadiene latex binder and coated on the paper substrate (Coat weight: 10 g/m²). The paper pores were closed and the surface porosity was decreased. This led to a reduced silicone penetration into the paper and more silicone remained on the surface. Thus, less silicone (0.5 – 1.5 g/m²) was overall required for desired release performance. In addition, this coating formulation showed a better cure and anchorage of the silicone coating compared to common clay-barrier coatings. [59]

The barrier properties can be further improved by addition of film-forming polymers to the pigments. In particular, waterglass, a substance composed of sodium and potassium silicates, was mixed with 30 wt% of film-forming polymers and coated on the paper substrate. The film-forming polymers were composed of polyvinyl alcohol and carboxymethyl cellulose. The pigment-coating was applied on the paper substrate (3.0 g/m²) followed by the silicone coating (0.5 – 0.9 g/m²) in order to produce the release liner. The film-forming polymers close small pores and this supports the barrier against silicone. Additionally, the silicone anchorage to the paper surface was improved. According to this method, small amount of a mixture consisting of water glass and film-forming polymers were used to reduce silicone consumption and at the same time maintaining the release performance. [60] The pigments acting as a filler and they support the sealing of the paper surface, but it has to be mentioned that the pigment coating is a complex mixture and those papers are cost-intensive.

1.2.2 Petrochemical polymers as barrier coatings

Beside mixtures of pigments and polymers, pure synthetic polymers were also used as barrier coatings. These barrier coatings can be composed of polypropylene, PVA or PVA which was co-polymerized with ethene providing a higher hydrophobicity. [55,61,62]

In one publication, the influence of corona treatment and hot calendering of the paper substrate on the barrier properties was studied. The surface energy of the paper substrate was increased by corona treatment of the cellulose fibers. This led to an improved wetting of the PVA-coating as well as to improved barrier properties. Additionally, barrier properties were further enhanced by hot calendering of the paper prior to coating. The paper was smoothed by the calendering process and this led to an improved spreading of the polymer solution and a better coating homogeneity. [62] Pure polymeric barrier coatings were most times applied on densified glassine papers. The fibers of these papers are highly refined and the paper is typically highly calendered, leading to a dense and smooth surface. The protruding microfibrils of the cellulose macrofibers increase the surface area and acting as a barrier against the migration of the polymer coating. [63,64] In order to enhance the anchorage of the silicone layer to the polymer-coated papers, PVA was modified by vinylic side chains, which can undergo covalent bonding with the solvent-free silicone system. The terminal vinylic functionality was initially introduced by the grafting-reaction of the hydroxy groups from PVA with acide chlorides of the vinylic organic molecule. This procedure was less

appropriate for industrial applications because organic solvents were used. Typical surface coatings in paper industry are applied as aqueous dispersion. Water is not compatible with acid chlorides because they undergo hydrolysis reactions, reducing the reactivity and high amounts of hydrochloric acid arise. Thus, in another approach, this modification step was performed by using a molecule with a vinyl functionality on the one side and an aldehyde functionality on the other side. The unsaturated aldheyde was covalently attached to the PVA by formation of an acetal. The vinylic functionality can then be used for catalyzed crosslinking reactions with silicones containing silane groups (Figure 12). This barrier coating prevented the penetration of the silicone into the paper and enabled fast curing and enhanced anchorage of the silicone to the paper surface, especially at low curing temperatures from 60 – 100 °C. [65]

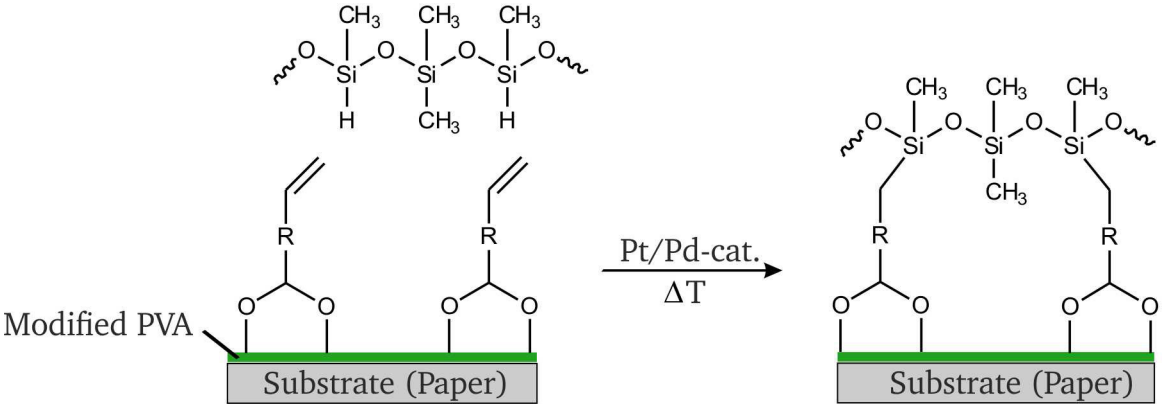

Figure 12: Covalent attachment of the silicone coating to the paper surface via the catalyzed addition reaction of silane groups with vinylic functionality of the modified PVA.

Nevertheless, the formation of acetals is a reversible reaction and the covalent bonding can be broken. Thus, in one invention vinylacetate was co-polymerized with a divinyl ether and the acetate groups were hydrolyzed by sodium hydroxide to receive the PVA. According to this procedure, the vinyl component was irreversibly attached to the PVA-backbone and silane-containing silicones can be covalently attached to the modified PVA-precoating. [66]

1.2.3 Biodegradable polymers as barrier coatings

Many petrochemical materials are being used in barrier coatings due to good availability and low price. However, these polymers suffer from a poor recyclability and they are not biodegradable. Hence, there is an increasing interest in replacing the petrochemical polymers by bio-based and recyclable materials from natural sources. [55,67]

Several biodegradable polymers such as starch, carboxymethyl cellulose (CMC) or polylactic acid (PLA) have been used as barrier coatings. [68,69] Most of them are hydrophilic and the barrier properties also depend on the humidity. Additionally, challenges occurred during industrial processing of these polymer coatings due to their crystallization behavior and brittleness. For example, starch is typically utilized as a surface sizing agent for paper substrates, but it has poor film-forming properties and it is brittle. The film-forming properties of starch have to be improved by addition of plasticizer, blending with other biopolymers or by chemical modification. Even after the modification step, the barrier properties of starch were still poor due to formation of cracks in the coating, i.e. non-homogeneous film formation.

Polylactic acid (PLA) is a synthetic, thermoplastic polymer, which is typically synthesized by catalytic ring-opening polymerization of lactic acid dimers (Scheme 3).[70] Nevertheless, this polymer is a compostable and renewable biopolymer, because the base materials is obtained from the fermentation process of corn or potato. Additionally, it possesses excellent mechanical and physical properties and can be processed by extrusion coating. The film-forming properties can be tailored by varying the ratio between D- and L-lactic acid in the polymer. The L-PLA increases the crystallinity, whereas the D-PLA improves the film-forming ability due to a higher amount of amorphous structures. PLA has a hydrophobic character and can be used as barrier coating against water. This polymer has a high potential for replacing commonly used petrochemical barrier coatings such as PE due to its low costs and good mechanical properties. However, PLA suffers from a low thermal stability and has to be stabilized by addition of pigments in order to preserve its functional properties, but maintaining its biodegradability.[68,71]

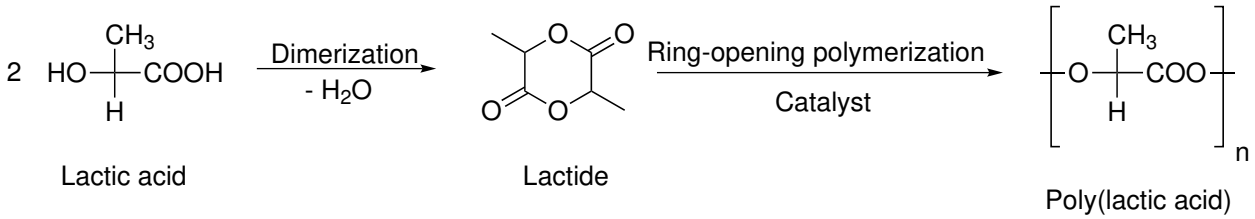

Scheme 3: Synthesis of poly(lactic acid) via a catalyzed ring-opening polymerization of lactic acid dimers. Figure redrawn from literature.[70]

Beside the usage of chemically modified cellulose derivatives, cellulose nanocrystals (CNC) were applied on the paper as barrier coatings.[72] The CNC were obtained by acid hydrolysis of wood and the rod-like shape structure carry a thickness of about 5 nm and a length of about 100 nm depending on the source. The amorphous part is removed and cellulose nanocrystals were isolated after sonification of the mixture. Multiple layers of CNC were coated on the paper by using the bar coater in order to improve the barrier properties (Figure 13). The paper pores were reduced with increasing coat weight and they were completely closed after the fourth coating cycle at a coat weight of 2.6 g/m². The brittle CNC-coating was reinforced by addition of 20 wt% polyethylene glycol, which further improved the barrier properties of the paper. Nevertheless, due to its low availability and complex production process, CNC is too expensive for large scale applications.[72]

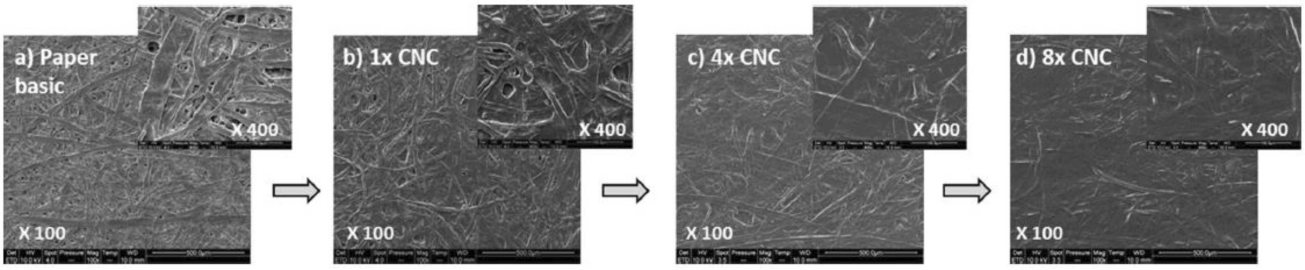

Figure 13: Surface SEM images of the base paper (a) and paper samples after x1 (b, 0.1 g/m²), x4 (c, 2.6 g/m²), x8 (d, 4.6 g/m²) coating with a 10 wt% suspension of CNC. Figure reproduced with permission from reference.[72]

As a similar biogenic coating, micro-fibrillated cellulose (MFC) was applied to the paper to improve the mechanical properties as well as the barrier properties.[73–75] MFC has got a broader size distribution compared to cellulose nanocrystals and a higher fibril diameter. Additionally, the MFC possesses a high aspect ratio with a diameter in the range of 10 – 50 nm and a length of several micrometers (Figure 14). The MFC was coated in several coating cycles on paper in order to obtain sufficient coat weight by using the size press and the bar coater. The coating homogeneity as well as the barrier properties of the paper were significantly higher when applying the MFC by the bar coater instead of size press. The water-based MFC suspension penetrated into the paper when using the size press, whereas the coating suspension stayed on the paper surface to more extent when using the bar coater. The mechanical properties of the paper were strengthened and the barrier properties were improved due to a reduced paper porosity by the MFC coating. However, multiple coating cycles are less appropriate for industrial scale and it is still challenging to obtain homogeneous coatings and sufficient high coat weights.[74]

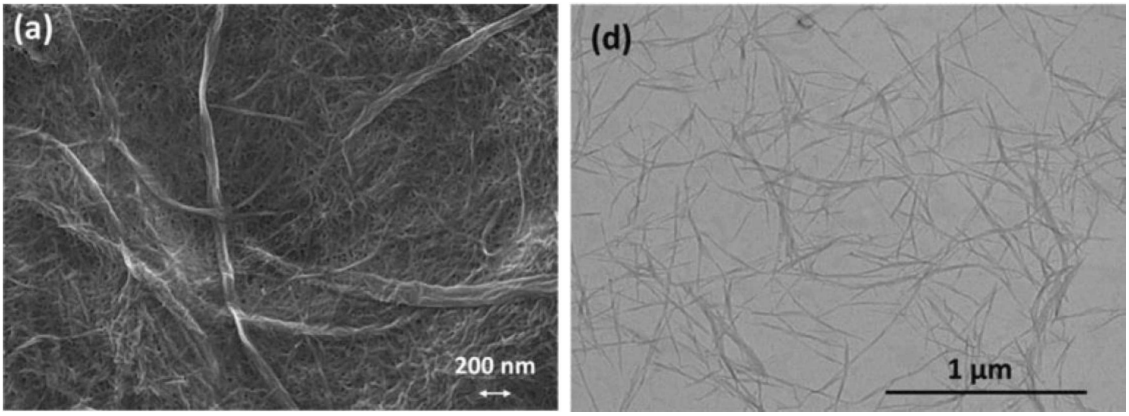

Figure 14: Surface SEM image of dried MFC (a) and TEM image of MFC suspension. Figure reproduced with permission from reference.[74]

1.3 Silicone polymers for release liner applications

Silicones on the base of PDMS are the main materials used in release liner. A low surface energy and high chain flexibility facilitate a poor wetting of the PSA and thus low release forces. Moreover, silicones can be easily synthesized with precise adjustment of the chain length and with different functional groups. Typically, the Si-O bonds are strongly polarized, which results in high intermolecular interactions. This is not the case in PDMS because the methyl groups are exposed to the surface, shielding the inner-lying polar segments of the silicone polymer and resulting in low surface energy (Figure 15). The high flexibility of the silicone chain is due to a low rotation energy of Si-O of about 3 $^{kJ}/_{mol}$, whereas the C-C rotation energy in polyethylene is about 13 $^{kJ}/_{mol}$ and higher than 19 $^{kJ}/_{mol}$ in polytetrafluoroethylene.[25] Thus, hydrocarbon polymers are more rigid compared to silicone polymers.[2,76]

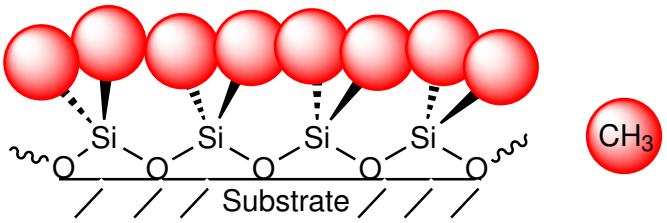

Figure 15: The methyl groups of the PDMS release coating are exposed to the surface. The inner-lying polar groups are shielded by the methyl groups. Figure redrawn from literature.[76]

1.3.1 Synthesis of silicone polymers

The commercial production of silicones, in specific polydimethylsiloxane (PDMS), started in the year 1940. The raw material, silicium, is produced by heating and reduction of silicium dioxide by using carbon (Scheme 4).[77,78]

$$SiO_2 + C \xrightarrow{1700\ °C} Si + CO_2$$

Scheme 4: Reduction of silicium dioxide to elemental silcium.[78]

In a next step, the silicium powder is reacted with methyl chloride according to the Müller-Rochow process in order to obtain dichlorodimethylsilane (Scheme 5).[77,78]

$$2\ H_3C{-}Cl + Si \xrightarrow[Cat.]{300\ °C} Cl{-}\overset{\displaystyle CH_3}{\underset{\displaystyle CH_3}{\overset{|}{\underset{|}{Si}}}}{-}Cl$$

Scheme 5: Synthesis of dichlorodimethylsilane according to the Müller-Rochow process.[78]

The dichlorodimethylsilane is hydrolyzed and a mixture of linear and cyclic PDMS oligomers is obtained (Scheme 6). The cyclic PDMS oligomers can be further polymerized to high molecular polymers by addition of acid or base and an end-blocker such as hexamethyldisiloxane. Herein, it is important to remove or neutralize the catalyst because it can also catalyze the depolymerization. Depolymerization is especially favored at high temperatures and in the presence of water. Labile catalysts have been developed, which are decomposed or volatilized by heating above the application temperature. Different functional groups such as vinyl, phenyl or trifluoropropyl can be introduced into the PDMS backbone by using the respective dichlorosilane.[2,79]

1.3.2 Curing mechanisms

As PDMS is an oil, it has to be cured for surface coating in order to guarantee sufficient stability on the substrate. First silicone systems were thermally cured by using the tin-catalyzed condensation reaction of hydroxy end-blocked PDMS groups with alkoxysilanes (Scheme 7). The alkoxysilane first reacts with water coming from the air and the resulting hydroxy group undergoes a condensation reaction with another alkoxysilane, thereby releasing propylalcohol. In another mechanism, silicones containing vinyl groups are crosslinked by a peroxide-initiated reaction via the formation of radicals.[2,12,79]

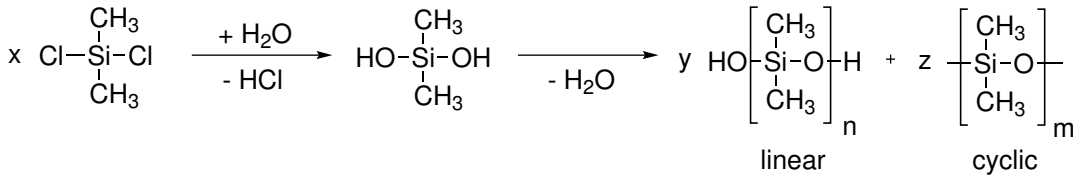

Scheme 6: Synthesis of linear and cyclic PDMS by hydrolysis of dichlorodimethylsilane. [2]

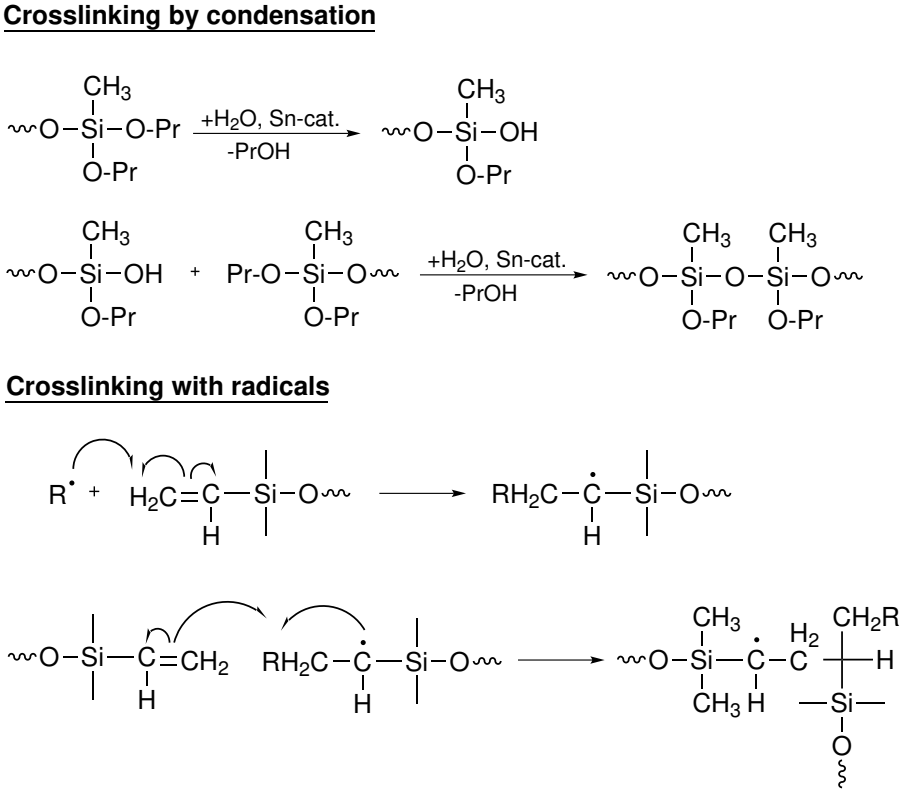

Scheme 7: Curing mechanisms by tin-catalyzed condensation reaction of alkoxysilanes and by an radical initiated crosslinking reaction of vinyl functionality. R· stands for a radical coming from an organic peroxide and Pr corresponds to a propyl group. Figure redrawn from literature. [79]

Thermal curing is the most widely used mechanism because of its easy processing. Silicone systems are mostly applied from an aqueous emulsion or organic solvents, but nowadays they are increasingly being replaced by the more commonly used solvent-free silicone systems. In this case, the vinyl-containing silicone is mixed with the polymeric crosslinker, carrying Si-H functionality, and with the catalyst, which is dispersed in the vinyl-containing silicone. Considering all three components, the platinum-containing silicone is the most expensive one and it has to be kept as low as possible. The silicone is crosslinked by a platinum-catalyzed addition reaction, also known as hydrosilylation (Scheme 8). The vinyl-containing silicone polymer reacts with appropriate silane groups of the crosslinker under the formation of a network. Inhibitors, such as maleic acid, are added in order to extend the bath life at room temperature. The inhibitors have significantly influence on the curing speed. Inhibition of the catalyst can also occur by poisoning agents coming from the substrate. Such poisoning substances are chemical compounds

having free electron pairs, which can coordinate to the Pt-catalyst. The catalyst is then blocked and the crosslinking reaction is inhibited. These are unwanted side reactions which have to be prevented. [7,12]

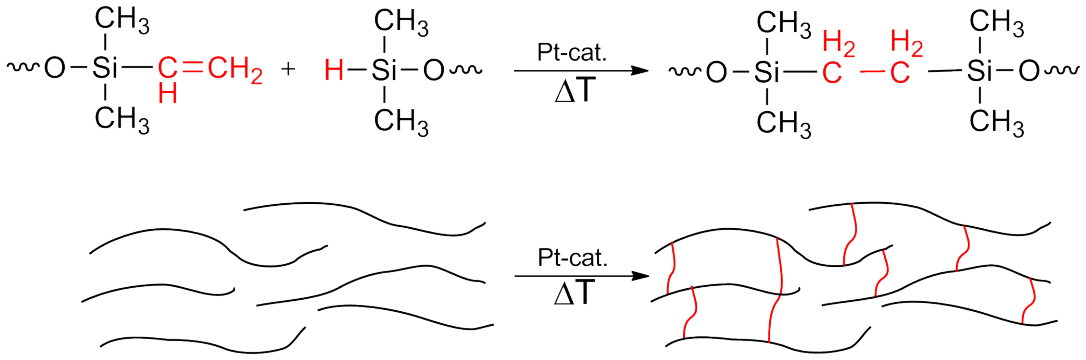

Scheme 8: Thermal-induced and Pt-catalyzed curing reaction of vinyl groups from the silicone polymer with silane groups coming from the crosslinker (Hydrosilylation). The initially freely-jointly silicone chains were connected by hydrosilylation reaction leading to a crosslinked network. The red joints represent the crosslinks by hydrosilylation reactions. Figure redrawn from literature. [7]

Residual Si-H functionality of thermally cured silicone release coatings can undergo post-curing reactions in which they are first hydrolyzed to silanols (Scheme 9). In a second reaction, the silanol groups can crosslink with other silanol groups from the silicone backbone or with hydroxy groups coming from the substrate surface in the presence of the Pt-catalyst (Scheme 10). The hydroxy groups from the substrate surface can originate from cellulose fibers, pigments or binders and the post-curing reaction significantly improves the silicone anchorage and leads to a good rub-off. Beside chemical reactions, anchorage can be improved by mechanical interlocking with the substrate surface. This process is preferred on porous substrates such as paper or pigment-coated papers having small pores. The silicone flows into the cavities of the porous material and cures between them. Stable anchorage of the silicone to the applied surface is important so that the silicone is not removed by the adhesive upon peel-off. Despite an improved anchorage by porous materials, the industry prefers a minimum penetration of silicone into the substrate in order to decrease silicone consumption and save costs. [7,12,13]

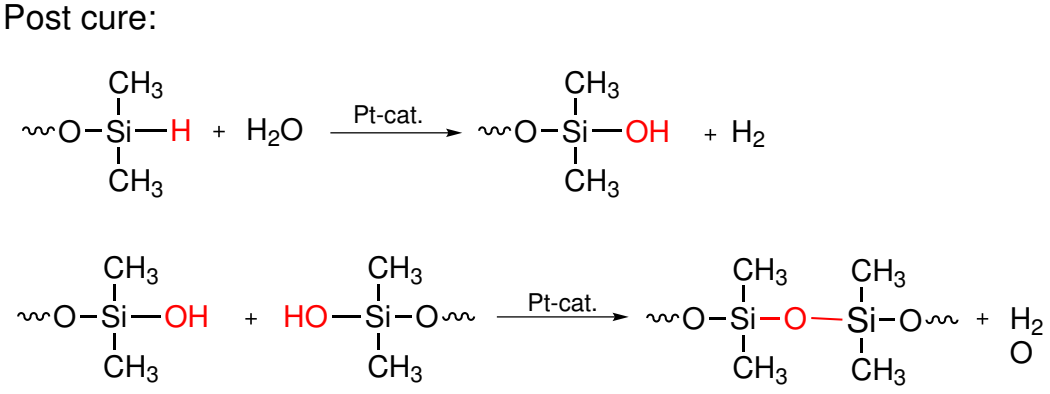

Scheme 9: Post-curing reactions of residual silane groups with water. The silane groups were condensated to silanol groups and they can be used for crosslinking reaction with other hydroxy-containing substances. Figure redrawn from literature. [7]

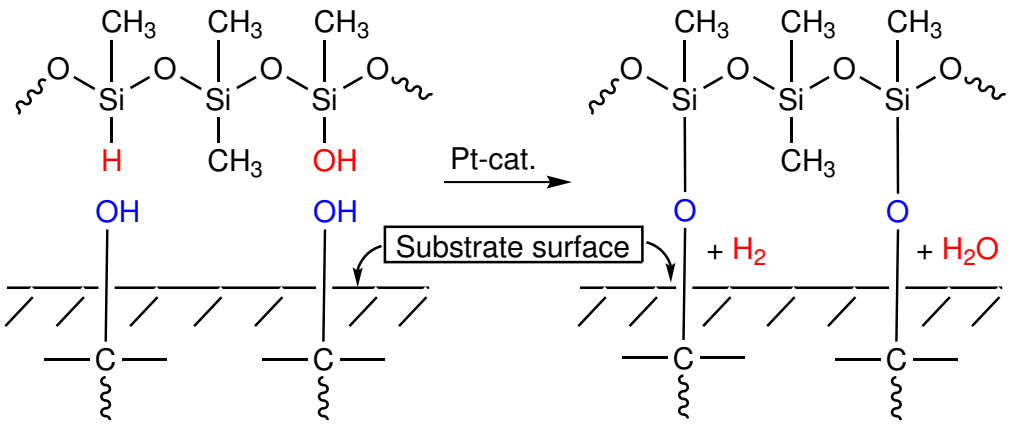

Scheme 10: Anchorage of the silicone layer to the substrate surface. Residual silane and silanol groups from the silicone coating react with hydroxy groups from the substrate surface in a post-curing reaction. Figure redrawn from literature.[7]

Beside the thermally cured silicone systems, silicones can also be crosslinked by irradiation with UV light or by an electron beam. These systems are important for curing reactions of silicones on thermal-sensitive substrates such as PE. Silicones are functionalized by epoxy groups and photochemically crosslinked by addition of a photocatalyst, which is decomposed into a strong acid upon irradiation with UV light. The acid catalyzes the ring-opening reaction of the epoxide under the formation of a three-dimensional network (Scheme 11). The silicone is completely cured, but silicone coatings on plastic substrates suffer from a poor anchorage to the substrate surface.[2,12]

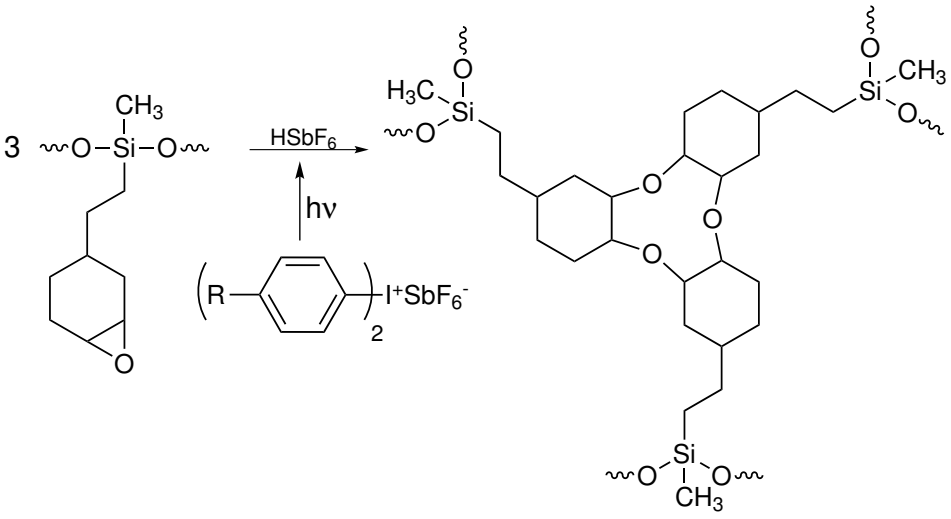

Scheme 11: Photochemical curing reaction of silicone polymer containing epoxy groups. UV irradiation of the diaryliodonium salt lead to the formation of a strong acidic acid, which induces the ring-opening reaction of the epoxy-containing silicone. This results in a three-dimensional network. Figure redrawn from literature.[12]

1.3.3 Silicone systems

The silicone can be applied from water-based emulsions, solvent-based or solvent-free silicone systems.[2] Solvent-based silicone systems are based on organic solvents and many different substrates can be siliconized by using this system. Low coat weights can be obtained and the anchorage to filmic substrates is excellent. Additionally, the silicone needs just moderate curing temperatures (100 °C). This also facilitates the siliconization of low-melting PVC-foils. Nevertheless, due to the organic solvents, the solvent-based silicones can be harmful and many safety precautions are necessary, such as an air exhausting system. Moreover, an installation for solvent recovery may be required or the solvent is incinerated.[80]

As a harmless alternative to the solvent-based silicone systems, water-based silicone dispersions are produced. This system allows an easy handling and no special safety precautions are needed. Water-based silicones require a higher curing temperature (120 °C) due to the higher boiling point of water and thus more energy is consumed. Another aspect is that water-based silicones have the tendency to penetrate into the substrate and affecting the release properties. Additionally, the water induces fiber swelling, which changes the paper structure and leads to paper curling.[49]

The most widely used silicone system is the solvent-free silicone, which is cured by a platinum-catalyzed addition reaction as shown above. It possesses several advantages over the other systems such as fast curing without formation of side products. As pure silicone is applied on the substrate, no shrinkage will occur.[79] Thus, the applied silicone thickness corresponds well with the finally cured layer allowing accurate adjustment of the silicone coat weight. However, one drawback is that the platinum-catalyzed curing reaction can be inhibited by sulphur- or phosphorus-containing poisoning agents coming from the paper.[81] Additionally, an expensive platinum catalyst is used, which cannot be recovered and high curing temperature (140 °C) or more catalyst is required for fast curing. Solvent-free silicones can also be cured by UV light, but these silicones are more expensive compared to thermal-curing silicones and a nitrogen atmosphere may be required for sufficient cure.[80]

The different kind of used silicone systems also influence the release forces (Figure 16). At low peel speeds, below 1 $^{m}/_{min}$, the release forces are similar, whereas the release profiles at higher speed differ significantly. The various release profiles are mainly governed by different crosslinking densities.[82] The correct silicone system has to be selected in consideration of the substrate, the costs and the final release application.

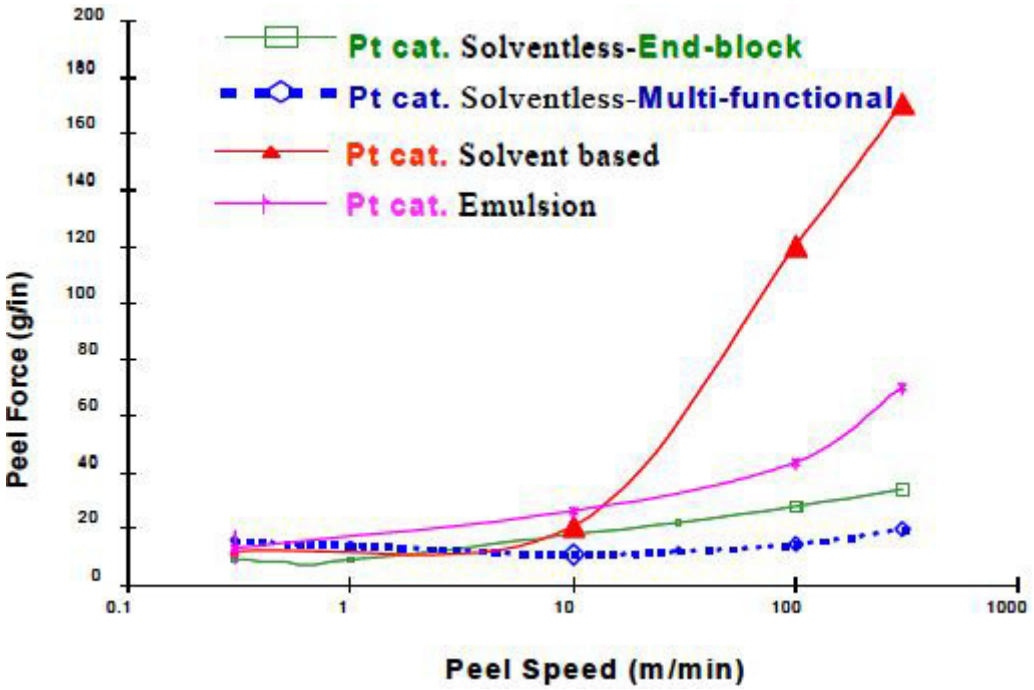

Figure 16: Influence of silicone system on release forces of a hot melt adhesive tape.[82]

2 Goals and Strategy

2.1 Goals

Since several years, release liners are produced following the same principal. The pores of the porous base paper are closed by a complex pigment coating and a thin silicone release layer is applied on the paper in a next step. As an alternative, non-clay-coated glassine papers were introduced for release liner applications. The paper surface is calendered to get a very dense and smooth surface and the fibers in glassine papers are highly refined. Additionally, a film-forming polymer is usually applied on the paper surface, which acts as barrier for silicone migration, similar to the clay coating in CCK papers. [64,65,83] Most polymers used in barrier coatings originates from synthetic sources and they are not biodegradable. Finally, the production of glassine papers is an energy-intensive process due to refining and several calendering steps. The production of siliconized release liner was continuously optimized in terms of efficiency and reduction of costs. The question is, if this is the end of optimization processes or is there still potential for new routes in order to save resources and energy?
The goal of this thesis is to address new strategies for the development of a release liner with the focus of implementing bio-based materials and simplifying the production process, as well as to address new ways to investigate the possibility of creating a "silicone-free" release liner. The following key-questions are to be addressed in this thesis (Scheme 12):

I) Is it possible to produce a release liner starting from a simple open-porous paper sheet without using a clay-coating?
   - Can silicone be mixed with particles and applied on porous papers to produce the release liner in one production step?
   - Can surface of the porous paper be closed by using film-forming polymers instead of pigment-coating, with special focus on bio-based polymers?

II) Can silicone be completely replaced by a silicone-free release coating on the base of a biogenic material with similar release properties?
   - Can we use modified cellulose polymers in such manner that it resembles similar properties of silicone?
   - Can such modified cellulose polymers be applied using non-toxic solvents and well-established coating methods?.

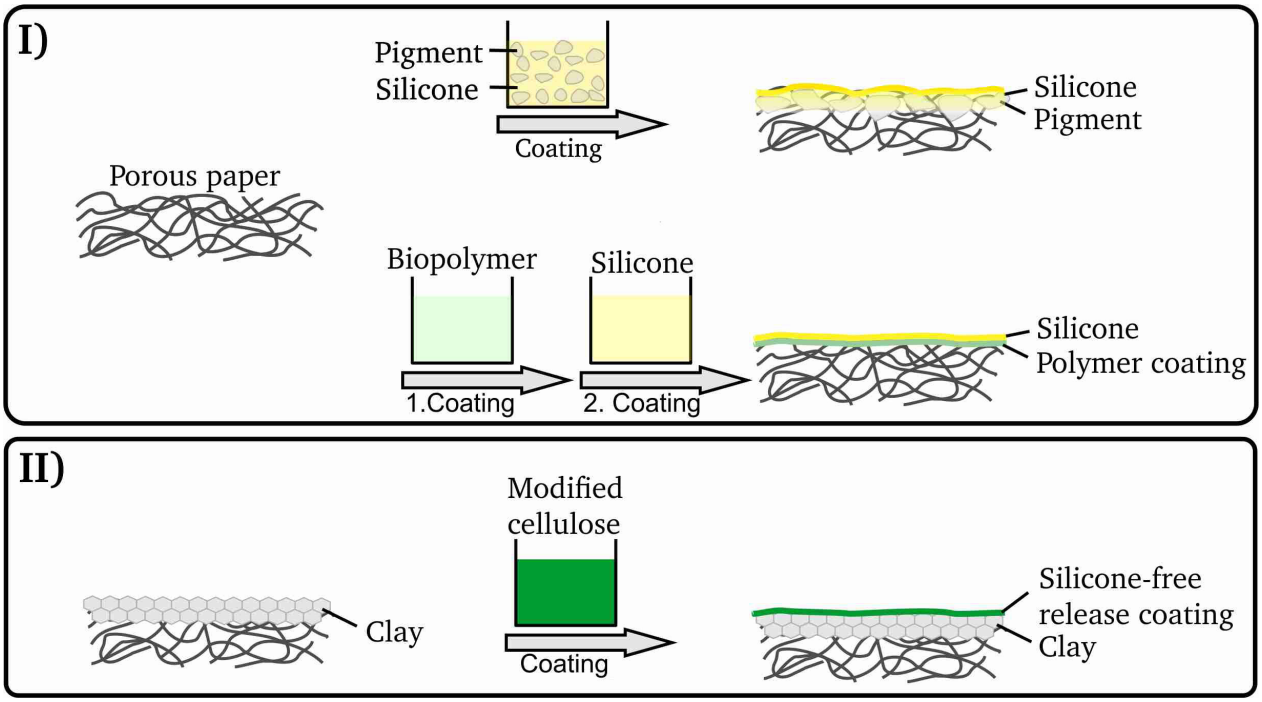

Scheme 12: Schematic overview of the main goals of this thesis.

2.2 Strategy

The following strategy was employed in order to address the questions mentioned before (Figure 17). First, specific porous base papers as well as clay-coated Kraft (CCK) papers will be selected from the product line of Sappi Alfeld GmbH. These papers will be characterized in terms of surface topography, porosity, contact angle and chemical composition. A thin silicone layer of about 1 g/m², which is a typical coat weight in industry, will be applied on the papers by using a multiple roller coater. Commonly used CCK papers will be utilized in order to adjust the silicone coat weight of a solvent-free silicone. This type of silicone is thermally cured by hydrosilylation reaction and commonly used in industry. In order to evaluate the siliconization process, the force will be measured which is required to release an acrylic tape from the siliconized paper surface. This measurement will be performed according to FINAT 10 method in an angle of 180°. The influence of paper roughness on the siliconization and on release forces will be investigated by using CCK papers with different degrees of roughness. Additionally, the stability of the release forces during storage and in dependency of the silicone coat weight will be analyzed.

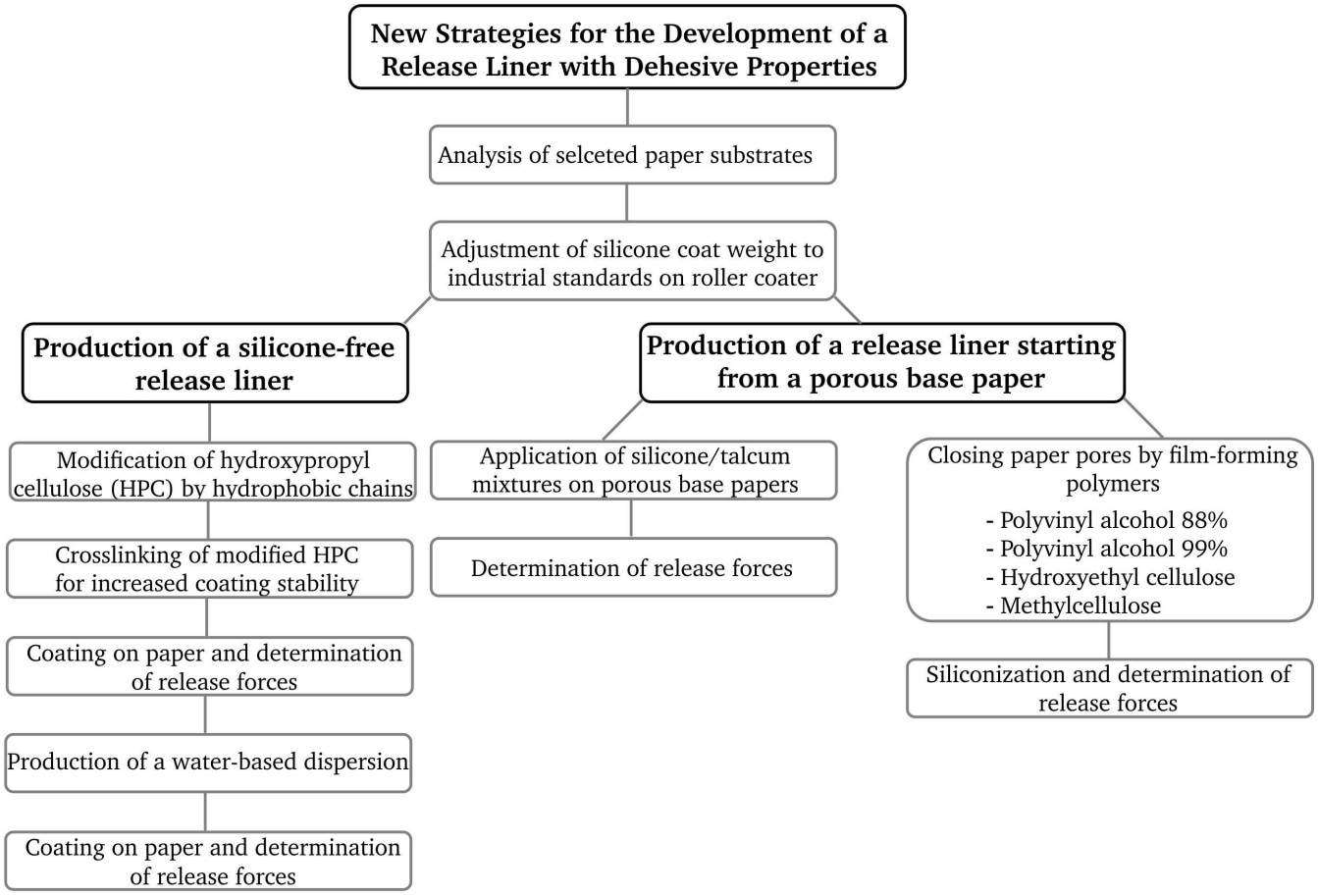

Figure 17: Developed strategy to answer the key questions addressed in this work.

In order to establish new strategies for the development of a release liner, in the first approach, the release liner will be directly produced from a non-clay coated, porous paper in one coating step. This process combines two individual coating steps, the clay-coating and the application of silicone, which saves energy and costs. In particular, a solvent-free and a water-based silicone will be mixed with different amounts of talcum and coated on a porous base paper. Talcum was selected as a pigment, because preliminary studies with this pigment by Sappi Alfeld GmbH showed promising results. The talcum should act as a mechanical barrier for silicone penetration into the paper as well as a viscosity modifier, which additionally reduces silicone migration. The resulting release forces should be in the range of siliconized CCK papers.

In another approach, the porous paper surface will be closed by using film-forming polymers, which should act as a barrier, similar to the clay-coating. Porous base papers with different sizing agents were selected in order to analyse the influence of the sizing agent on wetting behavior and on the siliconization process. In detail, synthetic barrier coatings, like polyvinyl alcohol (PVA) with 88% and 99% degree of hydrolysis, which are already used in industry, should be coated on porous base papers as a reference pre-coating. The barrier properties of these specific polymers should be compared to those of bio-based hydroxyethyl cellulose and methyl cellulose. These specific polymers were selected, because they possess good film forming capabilities and the hydroxyl groups can be used for crosslinking reaction with the silicone leading to a stable coating. The polymers will be applied by roller coater and blade coater

in order to compare the coating homogeneity of the respective methods as well as the resulting release forces. In order to study the distribution of the pre-coatings on the paper, PVA will be labeled by a fluorescent dye. After applying the polymer on the papers, the pre-coated papers will be characterized by fluorescence microscopy and scanning electron microscopy to examine the macroscopic homogeneity and surface morphology. The silicone layer will be applied in a second step and release forces will be determined. Additionally, the stability of the coating on the paper will be analyzed by a simple rub-off test. A stable anchorage of the coating to the paper surface is important in order to ensure stable performance of the adhesive tape.

Finally, the silicone should be replaced by a silicone-free alternative based on modified hydroxypropyl cellulose (HPC). This polymer was chosen, because it was shown in preliminary experiments that the hydroxy groups of the HPC can be easily modified with various degree of substitution (DS).[54] The HPC will be modified by long, hydrophobic alkyl chains in collaboration with a colleague in the Department of Macromolecular Chemistry and Paper Chemistry in order to generate hydrophobicity. A crosslinker will be introduced in order to investigate the influence on coating stability and anchorage to the paper surface. The modified polymer will be applied on CCK-paper from a solution in THF by using the blade coater. The release forces of the modified polymer will be measured and compared to silicone release liner. The hydrophobic HPC is usually dissolved in a organic solvent and applied on the paper. This is not applicable for industrial processes and thus a water-based dispersion of hydrophobic HPC will be developed to overcome this problem. The water-based dispersion will be applied on CCK-paper by blade coater and the release forces will be measured.

3 Methods

3.1 Coating techniques

3.1.1 3-Roller-coater

The roller-coating method is known to be a widely used technique to produce thin coatings on planar substrates in large scale. In Industry, this method is accomplished through consecutive connection of multiple rollers to obtain low coat weights. Roller coaters are especially used for laminating adhesives and solvent-free silicones in production of release coating. Beside the number of rollers, the roller pressure and coating speed significantly affect the coating thickness. The rollers can be arranged differently depending on the coating procedure and they can be moved in the same or reverse direction. In addition, composition of a roller is adapted in order meet the need for appropriate coatings. [84–86]
In this thesis, we use a lab-scale roller coater for coating of DIN A4-sized papers. The roller-coater contains a dosing roll, which is in intimate contact with the applicator roll upon applying pressure (Figure 18).

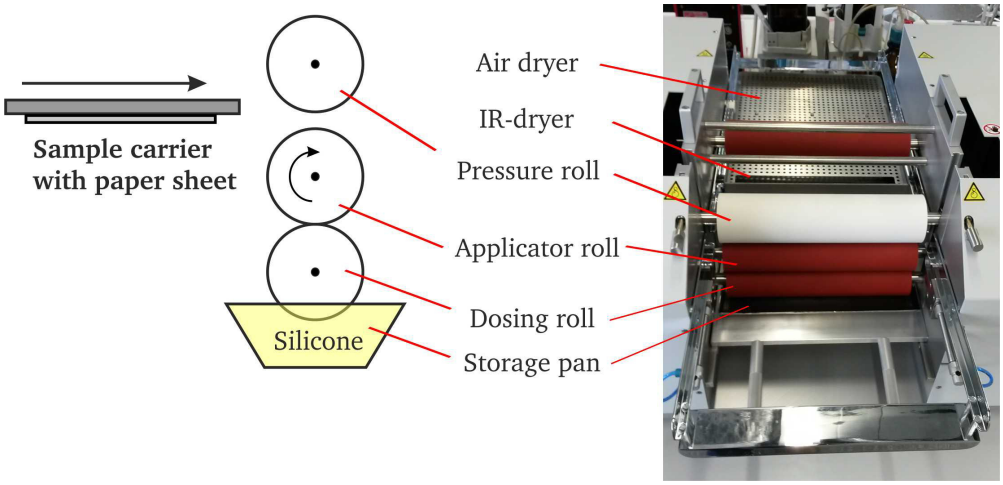

Figure 18: Coating setup of the 3-roller system.

During the coating process, the applicator roll starts to rotate, which makes also the dosing role to move so that both rollers have the same speed. The coating speed can be adjusted up to 8 $^{m}/_{min}$ and the pressure between dosing and applicator roll can be varied from 30-250 N depending on the intended application. The roller material is either composed of a rubber material or stainless steel. The coating material (e.g. silicone) is added to the storage pan so that it comes in contact with the dosing roll. The rotating dosing roll transports the coating material from the reservoir to the applicator roll and a nip is formed between these rolls. The liquid is forced to pass the nip between the rolls, the excess liquid is metered off by the applicator roll and the film is splitted into two films after the liquid exceeds the roller-roller contact point. The amount of coating material which is transferred from the dosing to the applicator roll depends mainly on the coating speed, the roller pressure, the roller material as well as on rheological properties of the liquid. [84] A paper, which is fixed on the sample carrier, is moved between the applicator roll and the pressure roll so that it is coated with a desired amount of material. The

pressure of the pressure roll can be adjusted up to 1200 N and it pushes the sample carrier together with the paper sheet onto the applicator roll so that the paper gets in intimate contact with the respective roller. An IR and hot-air dryer in the drying section can be utilized for drying and/or curing purposes. The IR dryer can be adjusted from 0 to 100% power and it is switched on when the paper passes the rollers. The temperature of the air dryer can be varied up to 150°C and the heating time can be adjusted.

3.1.2 Film-press setup

The roller-coater setup can be changed to the film-press setup if coatings with higher weights are desired or sizing agents like starch are applied. The film-press setup is build up of a storage pan, an applicator roll and a metering bar. The applicator roll is submerged in the coating material in the storage pan and transports the liquid to the substrate. During this process, the excess liquid is removed by the metering bar and a distinct coating thickness is transferred to the substrate. The coating thickness depends mainly on the pressure of the metering bar, the metering bar itself and the coating speed. The metering bar can have a smooth surface or it can be surrounded by a wire, whose diameter influences the coating thickness. A metering bar with a thick wire results in a thick coating, because less amount of coating material is metered off. The coating speed can be adjusted up to 35 $^{m}/_{min}$ and the pressure of the metering bar ranges from 10-110 N. As for the 3-roller system, the paper is fixed to the sample carrier and pushed between applicator and pressure roll. The coating can be cured by the IR-dryer or hot-air dryer.

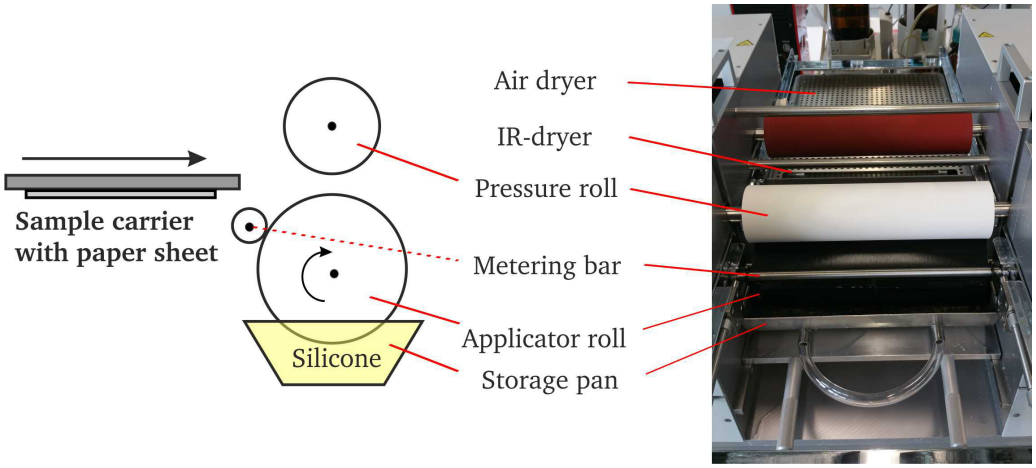

Figure 19: Coating setup of the film press system.

3.1.3 Blade-coating

The blade coating method was originally developed for the production of capacitors and piezoelectric materials.[87] In principle, the coating material is deposited on the substrate in front of the doctor blade and forms the reservoir. When the doctor blade moves over the fixed substrate with a constant speed, the coating material is metered off so that a homogeneous coating layer is formed on the substrate. The coating speed can be varied up to several meters per minute and the resulting coating thickness ranges from few up to hundred microns. The coating materials spreads over the substrate by using two different coating devices. In detail, a wire-wound rod and the doctor blade, a rectangular frame, are used for this purpose. The layer thickness is mainly governed by the width of the wire and the respective gap between the spirals, whereas the coating thickness at doctor blade is defined by the gap between the substrate and the metal frame.[88] Besides the gap width, the layer thickness is also affected by the viscosity, the coating speed, the surface tension and by the solid content. With this background, it is obvious that it is not trivial to predict the dry layer thickness and thus the coating parameters have to be separately adjusted for each coating material empirically. In general, considering a flat and non-porous substrate, a wet film thickness of half the coating gap is expected for the doctor blade.[88,89] However, this processing method is well established and some models were developed for specific coatings, like ceramic tape casting, in order to determine the dry coating thickness.[90–93] In addition, this method is used for the fabrication of different functional papers, such as barrier coatings, which are composed of microfibers or pigment coatings.[4,5,94,95]

A rectangular film applicator will be used for the prospective experiments in this thesis (Figure 20). The coating material is filled in front of the blade by a syringe and the blade is moved with a constant speed over the fixed substrate (paper). The liquid is homogeneously distributed over the paper and the resulting coating thickness is limited by the selected gap size of the doctor blade. The coated papers are either dried at room temperature or in oven at elevated temperature.

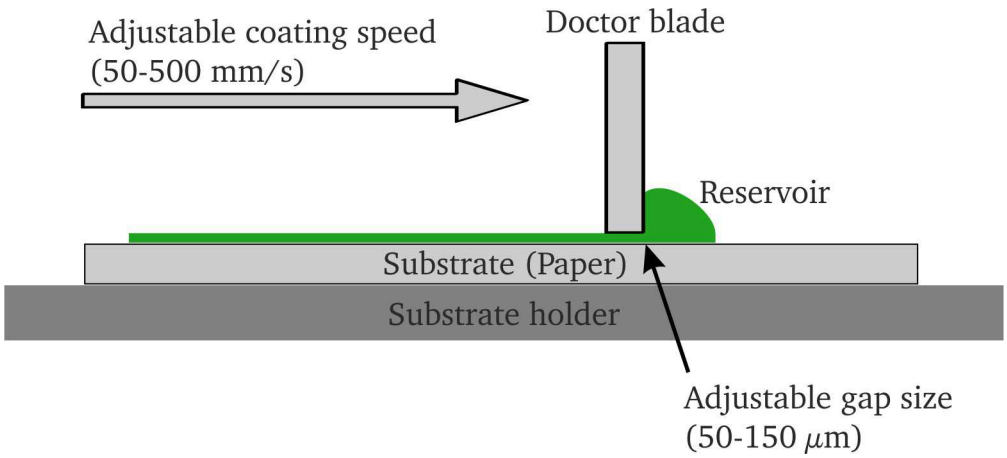

Figure 20: Coating setup of the film applicator.

3.2 Determination of release forces according to FINAT 10 method

A broad spectrum of different release properties are required for release liners depending on the final application. For example, release liners for automated peel-off applications of labels need low release forces, whereas the release forces for roof sealants have to be higher so that the product quality is maintained during transportation. The release forces of silicone release liner are usually tailored by addition of silicone resins to enable specific and stable release properties.[16,96] Thus, the measurement of release forces is essential in order to guarantee the desired release properties. The FINAT methods are usually implemented to determine the performance of adhesives as well as the release properties of release liner.[97] In this thesis, the peel-off forces (F_{peel}) are determined according to FINAT 10 method at an angle of 180° (Figure 21). The samples were prepared as follows: Siliconized papers are cutted so that a minimum number of five strips with a specific size (2.7 cm width, 17.5 cm length) were achieved. In a next step, an acrylic tape is applied onto the release liner under certain pressure by a standardized FINAT-pressure roll. The chemical composition of the adhesive tape should be identical to the adhesive of the final application. A double-sided adhesive tape was applied to the backside of the release liner. The test strips were stored between to flat glass plates under pressure and conditioned in climate room (23 °C, 50 % r. H.) prior to the measurement. The test strips were fixed to the steel plate by the double-sided adhesive tape and clamped into the 180°-peel-off setup at the Zwick Z 1.0 equipped with a 20 N load cell. Finally, the adhesive tape is removed from the silicone release liner with a constant speed and the respective force is recorded. The release force is related to the width of the adhesive tape and is stated as $^{N}/_{25\ mm}$ in our case.

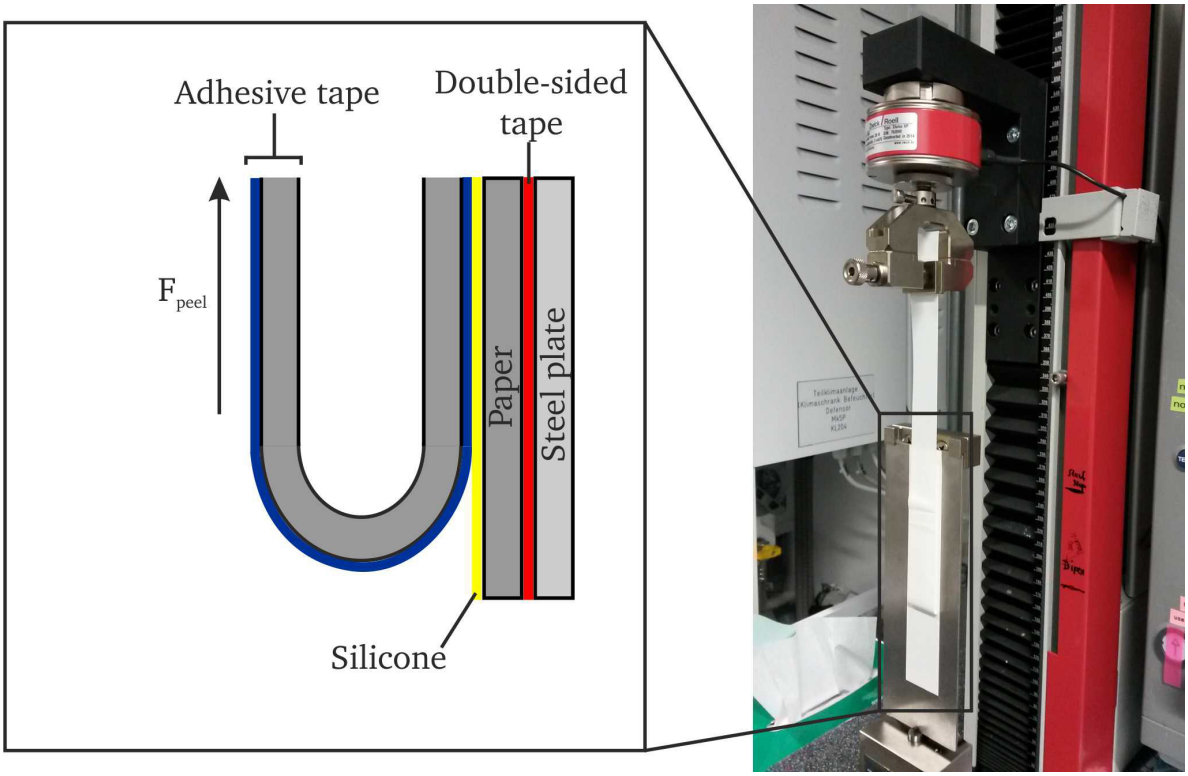

Figure 21: Setup for the determination of the release forces in accordance to FINAT 10 at an angle of 180°. Figure reproduced with permission from reference.[98]

The mean release force ($\overline{F}_{\text{peel,stripe x}}$) for every single test stripe (x) is calculated in the range of 100 to 200 mm according to the FINAT method (Figure 22). The selected area is located at the middle of the test stripe in order to prevent fringe effects and to obtain stable release forces. The mean peel-off force ($\overline{F}_{\text{peel,stripe x}}$) for each test stripe is calculated by considering the release force ($F_{\text{peel,n}}$) of 10 measuring points (n) in the respective range (Equation 3.1). The median release force of the five test strips are used in a second step to calculate the total median release force ($\overline{F}_{\text{peel,tot}}$) of one silicone release paper (Equation 3.2). The error of release force for each release paper is calculated by using the Gaussian error propagation and the standard deviation ($s_{\text{stripe x}}$) of the respective test stripe (Equation 3.3). Thus, the error indicates the variation of release force for each test stripe from the total median release force of the release paper.

$$\overline{F}_{\text{peel,stripe x}} = \frac{1}{n}\sum^{n=10} F_{\text{peel,n}} \tag{3.1}$$

$$\overline{F}_{\text{peel,tot}} = \frac{1}{x}\sum^{x=5} \overline{F}_{\text{peel,stripe x}} \tag{3.2}$$

$$\sigma(\overline{F}_{\text{peel,tot}}) = \sqrt{\left(\frac{\overline{F}_{\text{peel,tot}}}{\overline{F}_{\text{peel,stripe 1}}} \cdot s_{\text{stripe 1}}\right)^2 + \ldots \left(\frac{\overline{F}_{\text{peel,tot}}}{\overline{F}_{\text{peel,stripe 5}}} \cdot s_{\text{stripe 5}}\right)^2} \tag{3.3}$$

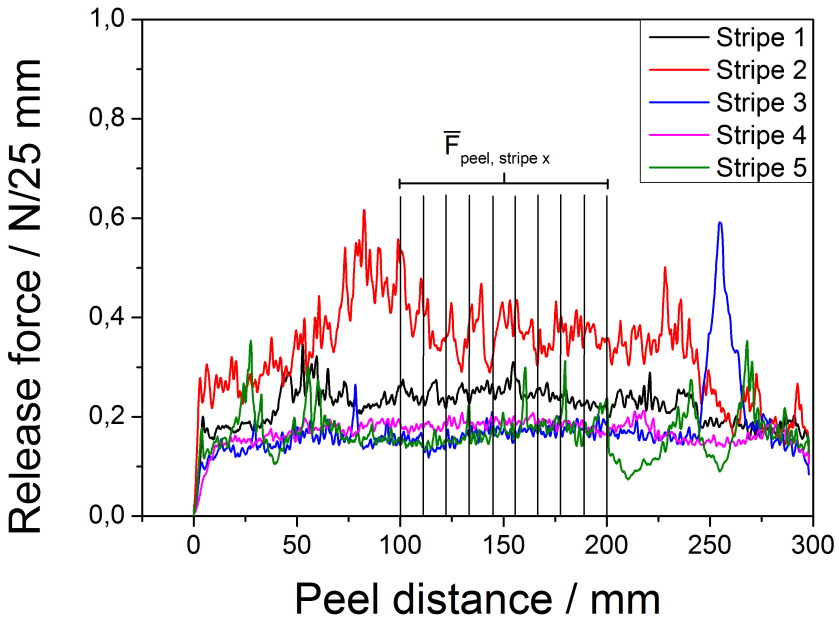

Figure 22: Release profiles of five release liner test strips. Release forces at every 10 mm in the range of 100 to 200 mm are considered for the calculation of the mean peel-off force ($\overline{F}_{\text{peel,stripe x}}$) for the respective test stripe.

3.3 White light interferometer

Interferometric techniques are used for long time as a non-destructive method in order to obtain topographical images with sizes of millimeter to nanometer scale. The interference pattern of two light beams is utilized to obtain a surface topography image. The sample must be light reflective and if a non-reflective substrate is investigated, light reflection has to be generated by sputtering of a thin gold film. The interference pattern of two light beams is determined as follows: If two light waves with same frequency are superposed, the amplitudes are reinforced when the waves are in phase or completely canceled when the beams are out of phase (optical coherence). The phase difference of the light waves results in light and dark bands, which are known as fringes. The interference pattern is utilized in order to visualize the topography of the sample. In detail, the location of the fringes during scanning in z-direction corresponds to the height of the sample. [99]

Lasers were initially used as a light source, but the interference fringe can be better detected by using white light due to its low coherence length. [99] In this case, LED or halogen lamp is used as a light source which possesses a Gaussian spectral intensity distribution. In the case of white light, interference is possible just in limited coherent areas, because of the short coherence length of the light. This simplifies the detection of interference fringes. [99–101] The first and most commonly known technique is based on two-beam interferometry, also known as Michelson Interferometer (Figure 23).

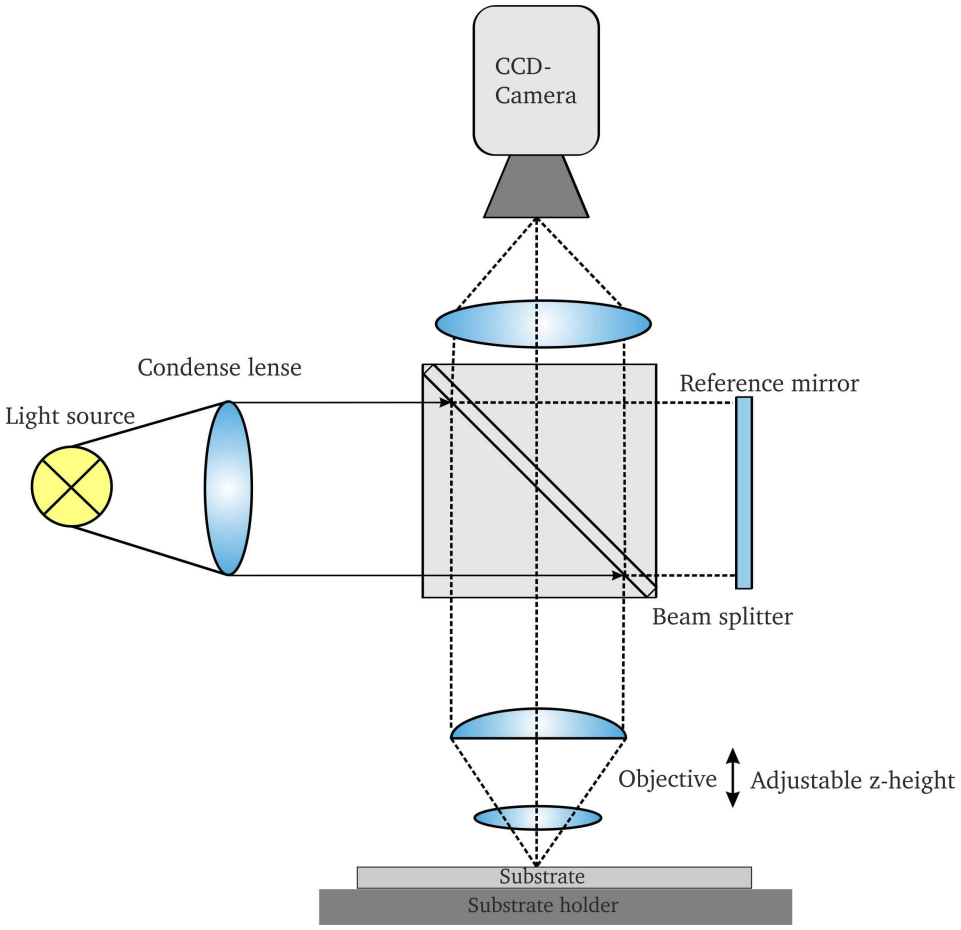

Figure 23: Schematic setup of Michelson Interferometer (Figure redrawn [102]).

The beam of the light source is splitted into two parts by a semi-reflecting coating on the beam splitter. One part is directed to the reflective sample surface and the other part is reflected back by the mirror and acts as a reference. A phase change between both beams occurs, because of different optical path (time delay). The beams are recombined at the beam splitter to form an interference pattern (interference fringe). The light intensity, which depends on the sample height and the resulting phase shift, is recorded by the CCD-camera (Charge-coupled device) as the objective moves by a piezo driven system in z-direction. Finally, the interference pattern is converted by Fourier transformation into a topographical image.[102–104] The resulting image show the different heights, which are indicated by red colour (high) or blue colour (low) (Figure 24, A). The roughness of the sample can be visualized by a line depth profile (Figure 24, B). The arithmetic roughness (R_a) is calculated by averaging the absolute deviation values from the imaginary mean line in z-direction. R_a describes the arithmetic deviation from the mean line over the sampling length, whereas the mean line is defined by a fitting parameter (Figure 25).[105] The arithmetic average roughness (R_a) is calculated by the absolute values (z_n) divided by the number of elements n (Equation 3.4). Multiple line depth scans were performed in order to obtain the arithmetic average roughness (R_a) for the whole surface image. This allows an estimation of the surface roughness for the investigated surface.

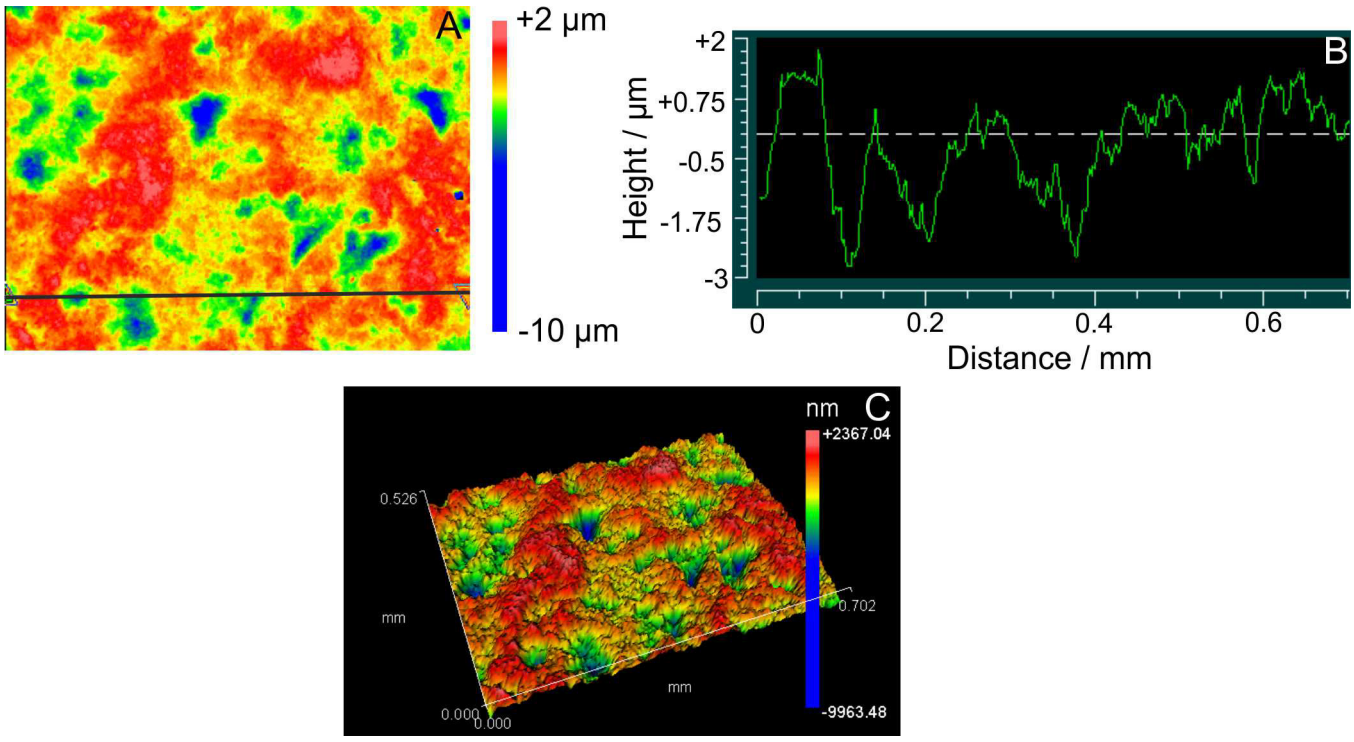

Figure 24: Image of white light interferometer (A) with the corresponding depth profile in x-direction (B) and a topographical map (C).

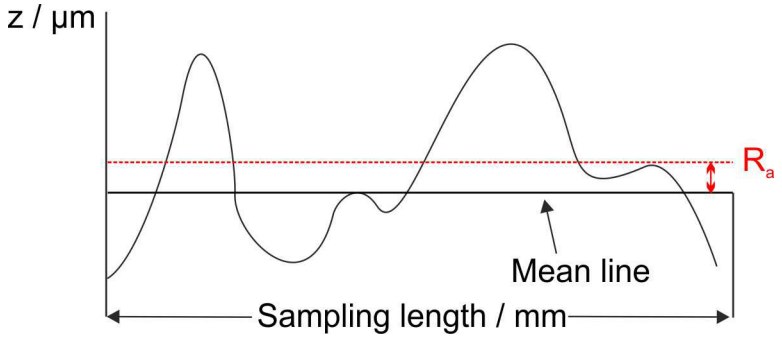

Figure 25: Surface profile and the determination of the arithmetic average roughness (R_a).

$$R_a = \frac{1}{n}\sum^{n}|z_n| \tag{3.4}$$

4 Characterization of model paper substrates

Specific non-clay-coated base papers and clay-coated papers were selected in agreement with Sappi Alfeld GmbH in order to produce a release liner (Table 2). In detail, cheap and non-clay-coated base papers (L40, L90) as well as various CCK papers were used. The base papers were sized with alkyl ketene dimer (L40) or with resin (L90), the fibers were refined to 30 °SR and one-side machine glazed. The papers were selected in order to investigate the influence of the sizing agent on the siliconization process. In addition to the porous papers, commonly used CCK papers, which were calendered (S98, DNC135) or not calendered (DN135), were chosen as reference papers and for the production of silicone-free release liners in this thesis. In detail, the influence of calendering process (DN135 ⟷ DNC135) as well as the influence of different clay coating recipes (S98 ⟷ DNC135) on release forces should be analyzed. Main differences between DNC135 and S98 were that double the amount of clay-coating was applied on the DNC135 paper. The papers were first characterized with special focus on surface topography, surface chemistry and wetting behavior, respectively. This is essential in order to interpret the different coating results.

Table 2: Overview of selected papers.

Abbreviation	Grammage / g/m²	Info
L40	40	AKD-sized, one-side machine-glazed, not calendered
L90	90	Resin-sized, one-side machine-glazed, not calendered
S98	98	CCK topside coating, calendered
DN135	135	Double amount of clay compared to S98, not calendered
DNC135	135	Double amount of clay compared to S98, calendered

4.1 Chemical analysis

All selected papers were characterized by FT-IR in order to compare the composition of the paper surface before and after the coating process. FT-IR analysis of sized base papers (L40, L90) do not show significant differences (Figure 26, A). The broad vibration band of OH-groups (3310 cm^{-1}) as well as signals from CH- (2896 cm^{-1}) and CH_2- (1310 cm^{-1}) groups arise, which can be assigned to signals from the cellulose backbone. The absorption band at 1640 cm^{-1} is caused by the stretching vibration of adsorbed water on cellulose.[106] Variations of L40 and L90 spectrum due to different sizing agents were not detected, probably because of less amount of sizing agent. The signals from the cellulose disappear, when the paper surface is coated by clay (Figure 26, B). Signals at around 3668 cm^{-1} arise from the clay-coating representing inner lying hydroxyl groups and weakly formed hydrogen bonds with the oxygen from Si-O-Si bonds. The small vibration bands for CH- (2913 cm^{-1}) and CH_2- (1445 cm^{-1}) groups may probably arise from polymeric aliphatic additives in the clay-coating. Strongest signals from Si-O vibration appears at 993 $cm^{-1}$and at 905 cm^{-1} for Al_2-OH vibrations of the clay pigments.[107,108] FT-IR absorption bands are summarized and characterized in detail in table 3. The spectrum of DNC135 paper was not depicted, because it is identically to the spectrum of DN135 paper.

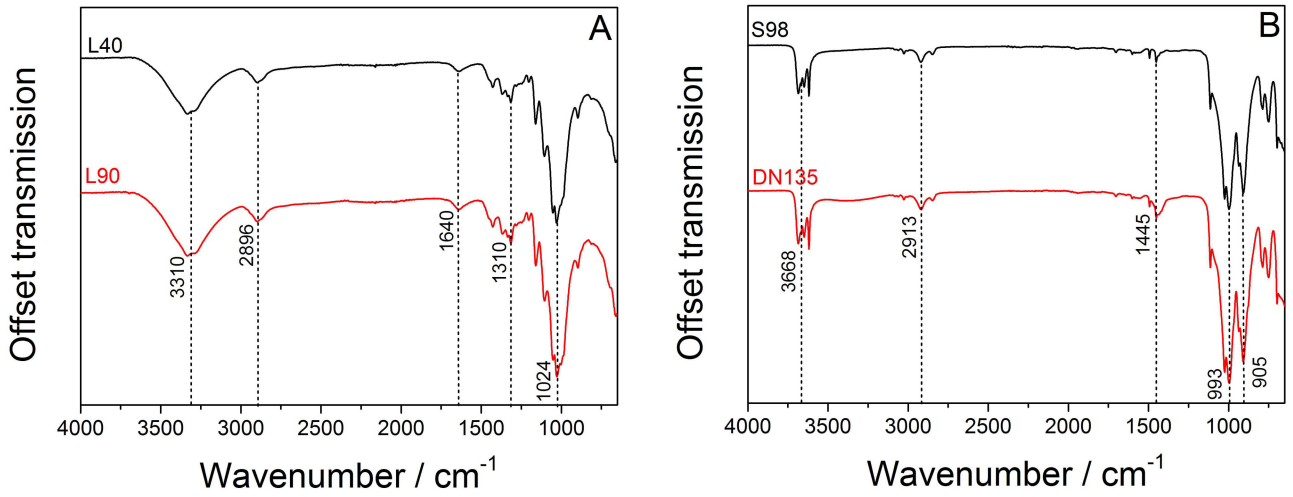

Figure 26: FT-IR analysis of sized base papers (A) and CCK papers (B).

Table 3: Detailed overview of the observed FT-IR absorption bands of various paper samples.

Paper	Wavenumber/ cm^{-1}	Assignment
L40 + L90	3310	O-H stretching vibration
	2896	C-H stretching vibration
	1640	stretching vibration of adsorbed water on cellulose
	1310	CH_2 deformation vibration
	1024	C-OH stretching vibration
S98 + DN	3668	O-H stretching vibration
	2913	C-H stretching vibration
	1445	CH_2 deformation vibration
	993	Si-O stretching vibration
	905	Al_2-OH stretching vibration

4.2 Morphological analysis

The papers were investigated by SEM in order to visualise the topographies of the paper surfaces. The images show the porous and open structure of the surface sized base paper (L40) (Figure 27). This can be also seen for L90 (see Appendix, Figure 108). The fibers are mostly randomly oriented and the fiber width ranges from 10 to 40 μm. The fiber structure is preserved and only a few microfibrils are sticking out of the cellulose fiber, due to the moderate refining process on the fibers. Some pores were closed by the sizing agent but most of them remain open. The sizing agent is located at the fiber-fiber crossing points and on the fiber surface. Sometimes holes in the sizing layer on the fibers can be observed which arise from defects during drying process. The surface structure of both sized base papers (L40 + L90) look similar and does not show significant differences. This is reasonable, because the production process for both papers is the same and the only difference is the grammage and the sizing agent. In contrast to that, the paper pores on CCK paper (S98) were closed by clay pigments (Figure 28). These pigments posses a hexagonal structure and most of them were smaller than 2 μm. Large paper pores ($>$ 10 μm) were closed and just small pores ($<$ 1 μm) remained on the paper surface. The fiber structure, as from

the non-clay coated papers, was overlaid by the clay in most parts and is just partially visible. The surface of the other CCK papers (DN135, DNC135) seems to be smoother compared to S98, which is likewise caused by a double amount of clay-coating (Figure 29). Additionally, the fiber structure disappeared completely at DNC135 paper compared to S98 paper.

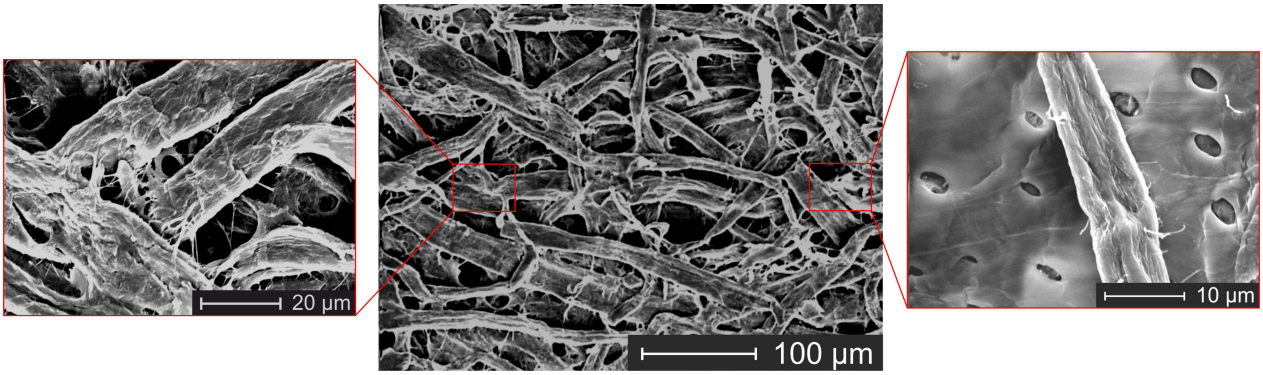

Figure 27: SEM images (topview) of sized base paper (L40) at different magnifications.

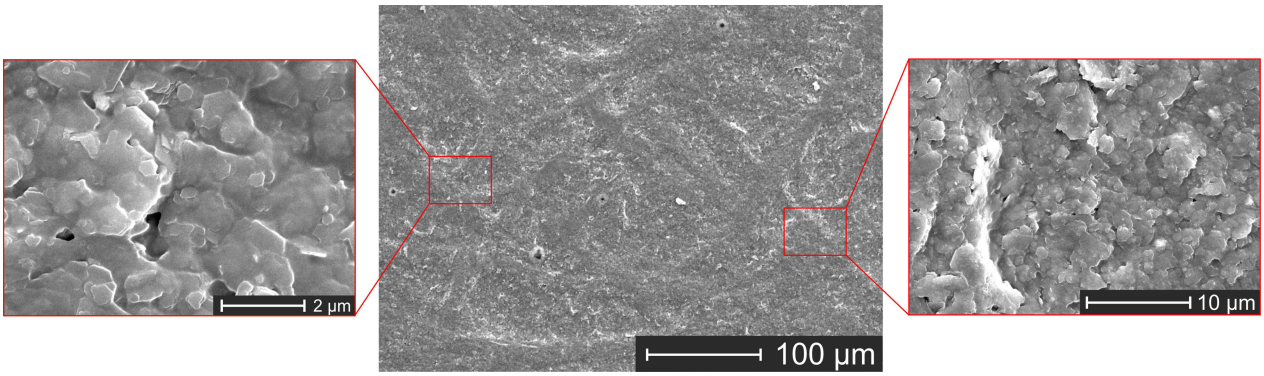

Figure 28: SEM images (topview) of CCK paper (S98) at different magnifications.

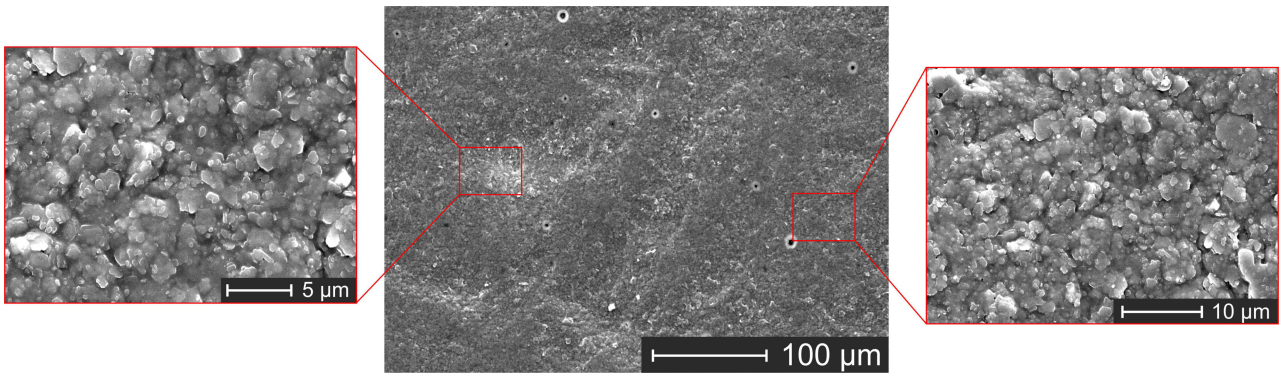

Figure 29: SEM images (topview) of CCK paper (DNC135) at different magnifications.

The paper porosity and pore diameter are important parameters in order to interpret the coating results. The ability to homogeneously close the paper surface is higher, when the paper porosity and the pore size were small. The coating will be retained by the cellulose fibers and penetration into the paper is diminished. The paper parameters may affect the coat weight as well as the coating homogeneity. Thus,

the porous base paper L40 and L90 as well as the CCK paper S98 were investigated by mercury intrusion experiments (Table 4).

Table 4: Results of the mercury porosimetry measurements: pore diameter d and porosity P for selected papers.

Paper	d / μm	σ(d) / μm	P / %	σ(P) / %
L40	12.5	0.5	59	12
L90	11.2	0.3	54	10
S98	6.8	0.1	39	4

The median pore diameter of the porous base papers was between 11-12 μm (Figure 30), whereas the pore diameter of the CCK paper was reduced to 7 μm. This is induced by the clay-coating, because part of the huge pores on the paper surface were closed by the clay coating and just small pores remain. The small pores in the clay-coating were still accessible for the mercury and were therefore detected during the measurement. Thus, the clay-coating affects the overall pore diameter of the paper. The differences between porous and clay-coated papers can be also seen in the porosity. The porosity of the clay-coated paper was smaller compared to the porous base papers, because the pore volume was reduced by the clay-coating. However, the results of this method have to be considered carefully. In addition to the errors of the standard deviation, errors during the measurement may occur, which influence the results. Artificial pores may be generated between paper sample and glass wall of the penetrometer and the flexible paper structure may be changed at higher pressures of the mercury.

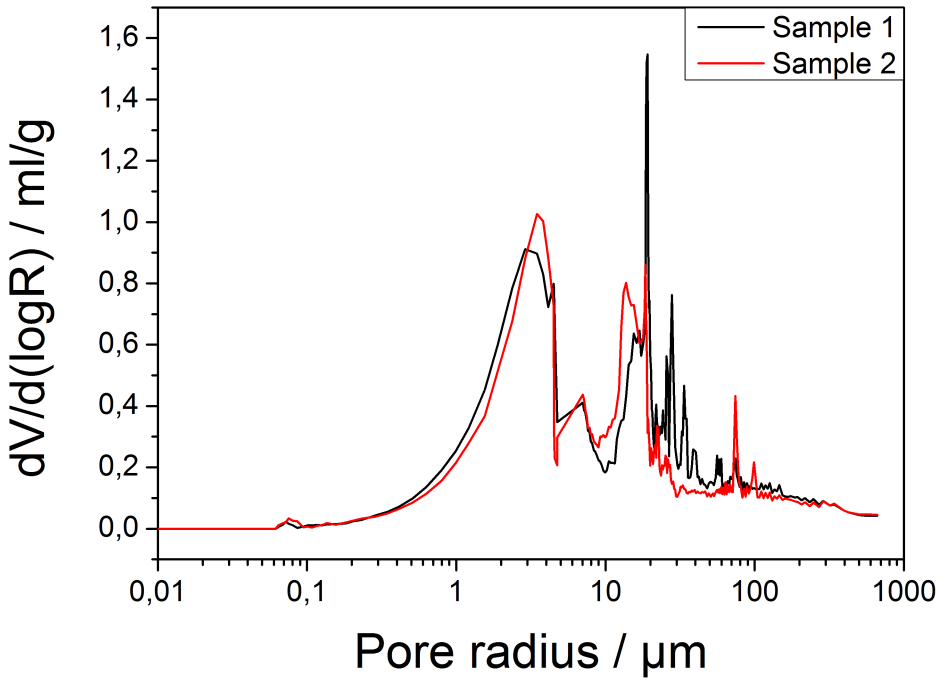

Figure 30: Pore size distribution of L90 paper obtained by mercury intrusion experiments.

Additionally, some mercury remained in the paper after complete depressurization, which leads to higher amounts of intruded mercury. Many assumptions were done in order to calculate the pore diameter. For example, the pore shape is expected as cylindrical, which in case of paper is not true. This shows, that the results depend on various assumptions and experimental factors.[109] The results, which were determined by mercury intrusion experiments, relate to the complete paper, but especially the surface properties of the paper were crucial for the coating experiments. Therefore, the paper surface was investigated by white light interferometry in a next step.

In order to investigate the influence of the paper roughness on the release forces, the arithmetic average roughness (R_a) was measured with a white light interferometer. A high paper roughness may lead to higher release forces compared to a smooth release paper, because of a higher contact area between the adhesive and the siliconized paper, respectively. Additionally, the coating homogeneity may also be affected by the roughness of the base paper. The porous base paper (L90) possesses a rough surface, because it is not calendered and the pores on the paper surface are not closed, i.e. by a pigment coating (Figure 31, A). The fiber structure is visible and the depth profile varies over several microns. An arithmetic average roughness (R_a) of about 2.2 μm was calculated for the non-clay coated base papers L40 and L90 (Table 5). In contrast to this, the paper roughness is significantly reduced, if the paper surface is covered by clay pigments. Hence, a median paper roughness of 1.3 μm was obtained for the S98 paper. Part of the fiber structure can be still seen, but the paper surface is smoother compared to the non-clay coated papers (Figure 31, B). The fiber structure disappears when double amount of clay is applied on the paper in contrast to S98 paper (Figure 31, C).

The paper surface looks more homogeneous and the paper roughness is even more reduced when the paper surface is smoothed by calendering steps. The median paper roughness for DNC135 is decreased to 0.8 μm. Nevertheless, even with highly surface-smoothed paper, some unevenness (blue) persists, which may lead to defects in the silicone top-coating. These results show that the selected papers possess different surface roughnesses, which may affect the coating results and release forces.

Table 5: Determination of the arithmetic average roughness (R_a) by white light interferometer.

Paper	R_a / μm	$\sigma(R_a)$ / μm
L40	2,3	0,2
L90	2,2	0,2
S98	1,3	0,3
DN135	0,9	0,0
DNC135	0,8	0,1

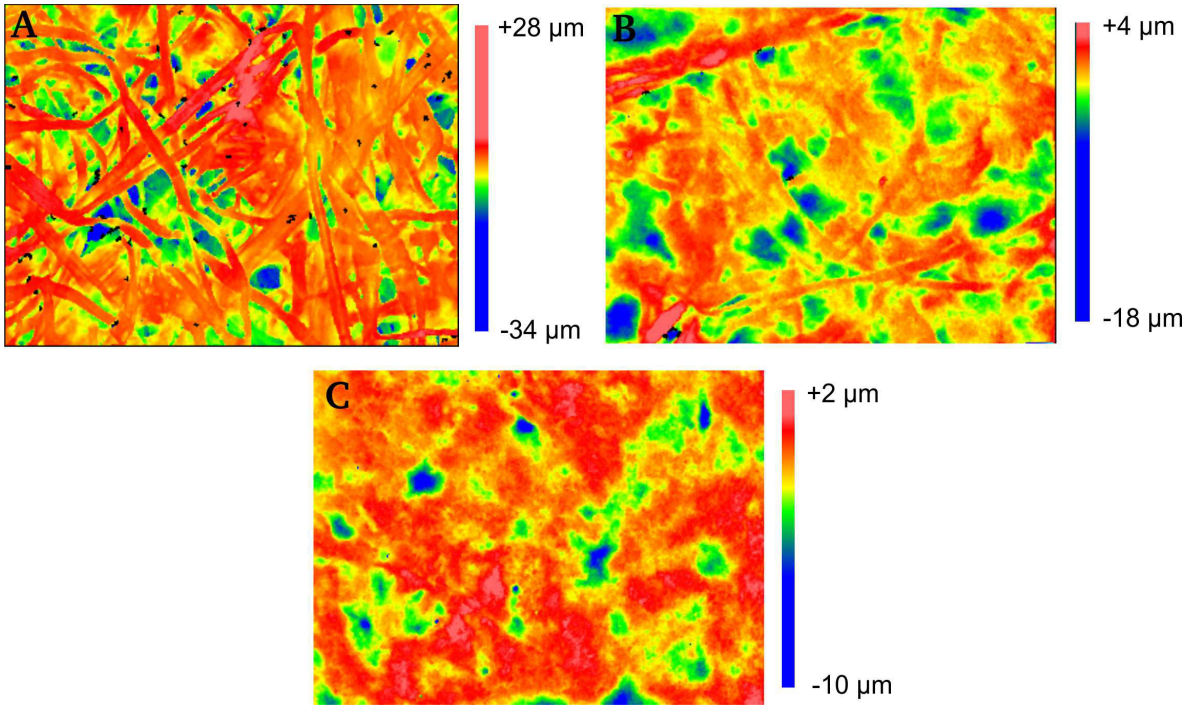

Figure 31: Analysis of paper surface by white light interferometer. A: L90; B: S98; C: DNC135.

4.3 Wetting behavior

In order to characterize the behavior of the chosen paper samples in contact with fluids, the wetting behavior was studied by means of contact angle measurements. This is important, because the surface properties may influence the coating results. Both base papers (L40, L90) show hydrophobic contact angles ($\theta > 90°$) and a dewetting behavior for water (Figure 32). The hydrophobic character was provided by the sizing agent. The contact angle of L40 was approximately 10° higher compared to L90. This result may be due to the different sizing agents, which were used for the hydrophobization of the papers. Nevertheless, despite the hydrophobic character of the papers, it was observed, that the fibers start to swell after 15 s. This is due to the fact that the fibers were not fully covered by the sizing agent and micropores exist on the fiber surface, which was previously shown by SEM analysis. The water penetrates through the micropores into the fibers, inducing swelling of the fibers. Because this swelling may be accompanied with a more polar surface, water uptake by capillary forces is dynamically enhanced. In contrast to this, the contact angles of the CCK papers (S98, DN135, DNC135) were more hydrophilic (∼65°) from the beginning. The CCK papers do not contain hydrophobic additives in the coating. Usually, the contact angle of kaolinite is at around 50°[110], which in our case is slightly increased, because of more hydrophobic polymer binders in the clay-coating formulation.

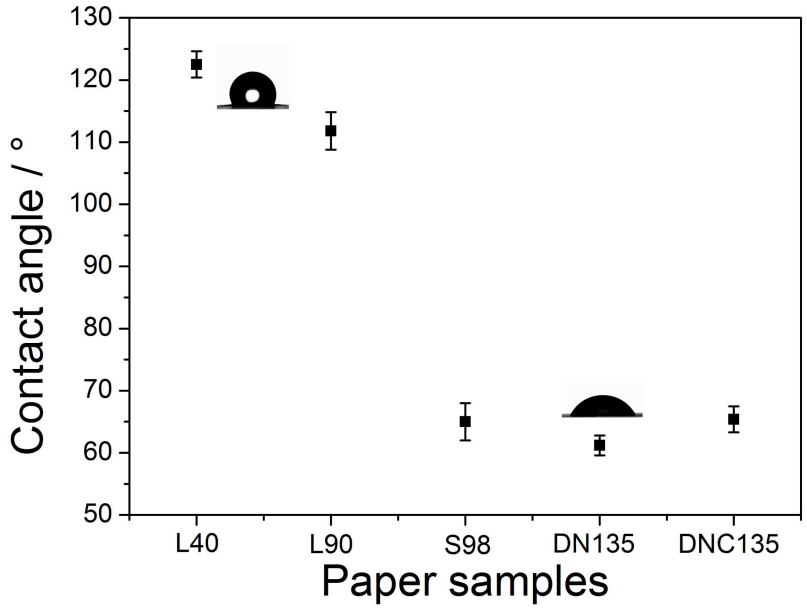

Figure 32: Water contact angles (drop size = 4 μL) of sized base papers and CCK papers. The sized base papers (L40 and L90) show a hydrophobic contact angle, whereas the CCK papers (S98, DN 135 and DNC 135 have a hydrophilic contact angle

4.4 Conclusion

Characterisation of selected papers by various methods demonstrated the differences between base papers and the CCK papers. The base papers carries a highly porous structure with pore sizes bigger than 10 μm. The fiber structure can be clearly visualized, whereas the surface of CCK papers was closed by clay pigments and just small pores ($<$ 10 μm) exist. The clay-coating acts as a barrier and prevents penetration of the coatings into the paper substrate. The different pore sizes were also determined by mercury intrusion experiments. The sized base papers carry similar mean pore diameter of about 11 μm, whereas the pore diameter of CCK paper was reduced by the clay to around 7 μm. The clay-coating also reduces the paper porosity. Analysis of the paper surface by WLI revealed that the non-clay-coated papers carry an average roughness of about 2.2 μm. The surface roughness was significantly reduced below 1 μm, when the paper was coated with clay and smoothed by calendering steps. The different roughness may influence any subsequent coating process as well as the release forces. The chemical composition of the paper surface was analyzed by FT-IR. The spectra of L40 and L90 show typical IR-absorption bands of cellulose, whereas the cellulose signals disappeared, if the paper surface is covered by clay-coating. New signals arise, which can be assigned to the clay pigments, respectively. The wetting behavior of the selected papers were investigated by static contact angle measurements. The sized base papers show a high water contact angle, which is due to the hydrophobic sizing agents. In addition, L40 (122°) was coated with another sizing agent compared to L90 which leads to a slightly lower contact angle (112°). This may also result in different wetting during coating with aqueous solutions in subsequent experiments. In contrast, CCK papers possess a more hydrophilic character due to the clay coating, with water contact angles below 90°.

5 Investigation and control of coating parameters for the production of a silicone release liner

The silicone coat weight of solvent-free silicone should ideally be adjusted to ∼1 g/m² in order to reach industrial standards and to compare the results to commercial available release liner. The film press setup as well as 3-roller system were used here. Different adjustments in coating parameters were performed to investigate the influence on silicone coat weight. CCK papers (S98) were used for these measurements. Papers are hygroscopic and thus stored in climate room over night (23 °C, 50 % r. H.) for constant conditions prior to weighing after each coating step. The silicone coat weight was determined by gravimetrical means. The silicone coat weight was calculated by dividing the silicone mass by the surface area of a DIN A4 paper (DIN A4: 0.06237 m²; Equation 5.1).

$$\text{Silicone coat weight} = \frac{m_{silicone}}{A_{paper}} \tag{5.1}$$

5.1 Comparison of different methods for the determination of silicone coat weight

The silicone coat weight was determined by weighing and measuring the coating thickness using a micrometer screw. As paper has a rough surface, the paper thickness differs by some μm and it is thus important to mark the measuring points for quantitative analysis of the silicone thickness by SEM-crosssections. Paper thickness was measured prior and after siliconization on the selected points. The silicone thickness can be directly compared with the silicone coat weight, because the silicone has a density of roughly one (0.97 g/cm³ [111]). Thus, silicone coat weight of 1 g/m² corresponds to an apparent silicone thickness of ∼1 μm, if an ideal flat surface is considered. The results from the micrometer screw and the determination of silicone coat weight by weighing were compared with silicone thicknesses which were received from cross sections of siliconized papers by SEM (Figure 33). SEM cross sections were recorded on the previously marked points. Minimum six measuring points from micrometer screw and SEM images were used to calculate the silicone coat weight. Silicone thicknesses from SEM investigations containing errors because the interface between silicone and clay coat cannot be determined accurately for each sample. The results of all three methods are similar for high coat weights, but the error is highest for the micrometer screw. Determination of coat weight by micrometer screw for lower coat weights fails completely whereas the results from the balance and SEM investigations are similar. It has to be mentioned that the error of the micrometer screw given by the product is ± 2 μm. Additionally, some part of the silicone may penetrate in to the clay coat which cannot be detected by the micrometer screw. Thus, this method is improper for measuring low coat weights. Best results in agreement with SEM measurements were obtained by weighing, which is as a simple and fast method. Silicone coat weight can also be determined by using X-ray fluorescence spectrometer (XRF). The sample is irradiated by x-rays and the released fluorescence of secondary electrons, which is specific for each element, is detected. This device is expensive and calibration standards with precise silicone coat weights were necessary for every paper substrate and for each specific type of silicone. Thus, silicone coat weight is determined by gravimetrical means using the balance for all further experiments.

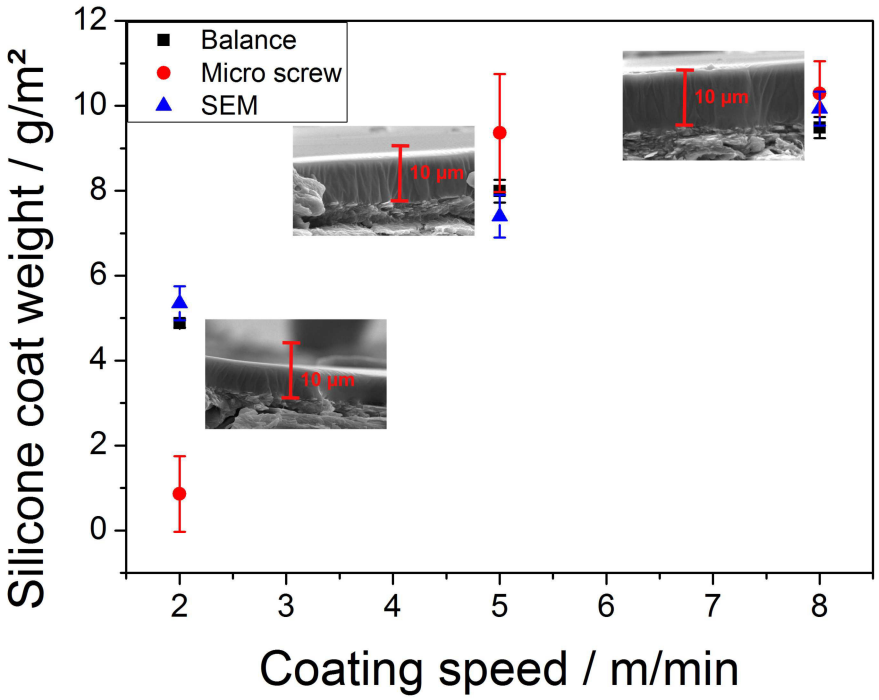

Figure 33: Comparison of different methods for the determination of the silicone coat weight on CCK-paper. The silicone coat weight is increased with increasing roller pressure. The micrographs feature SEM-crosssections of siliconized papers with a scale bar of 10 μm.

5.2 Siliconization via a film press setup

In order to adjust the silicone coat weight to a target of approximately 1 g/m^2, the coating speed (10, 20, 35 m/min) and the pressure of the blade to rubber roller (40 N, 80 N, 110 N) were altered. Additionally, the influence of various metering bars (0 μm, 10 μm, 20 μm, 30 μm) on the coat weight were investigated. Results are shown for a blade pressure of 110 N (Figure 34, A). Prior to the measurements, it was assumed that the silicone coat weight is increased at low coating speed because the paper/roller contact time is longer compared to high coating speeds. This was not observed in our experiments. The silicone coat weight is increased with increasing coating speed. This is most likely due to the fact that the roller material is deformed by some μm due to the high viscosity of the silicone (500 mPa·s [111]). The influence of different metering bars on coat weight is less significant. More silicone should be transferred going from bar 0 μm to bar 30 μm because the rills are getting deeper and wider. Most silicone should be removed from the roller by using bar 0 μm without any rills leading to lowest silicone transfer. However, this was not the case. Similar amounts of silicone were obtained by using blades 0 μm, 10 μm or 20 μm. Furthermore, lowest silicone coat weight was obtained by using bar 30 μm carrying most distinct rills. This observation is in contrast to the expectation. One explanation may be that the counter-pressure of the highly viscous silicone is higher than the adjusted pressure (110 N) and the blades (0 μm, 10 μm, 20 μm) are not completely in contact with the roller. The counter-pressure of the silicone may be reduced by using bar 30 μm with the largest rills. The metering bar is now in contact with the roller and more silicone can be displaced. Coating experiments with bars 20 μm and 30 μm at 35 m/min, respectively, were not done because the paper was detached from the sample carrier at high speeds and it has been

creased. Similar amounts of silicone were transferred using 80 N pressure (Figure 34, B). More silicone is transferred to the paper when using 40 N pressure, because less silicone is removed by the metering bar (Figure 34, C). Minimum silicone coat weight of 5 g/m^2 was obtained with bar 30 μm, a coating speed of 10 m/min and a pressure of 110 N. Since this coating method could not met our requirements, the setup was changed to the 3-roller system.

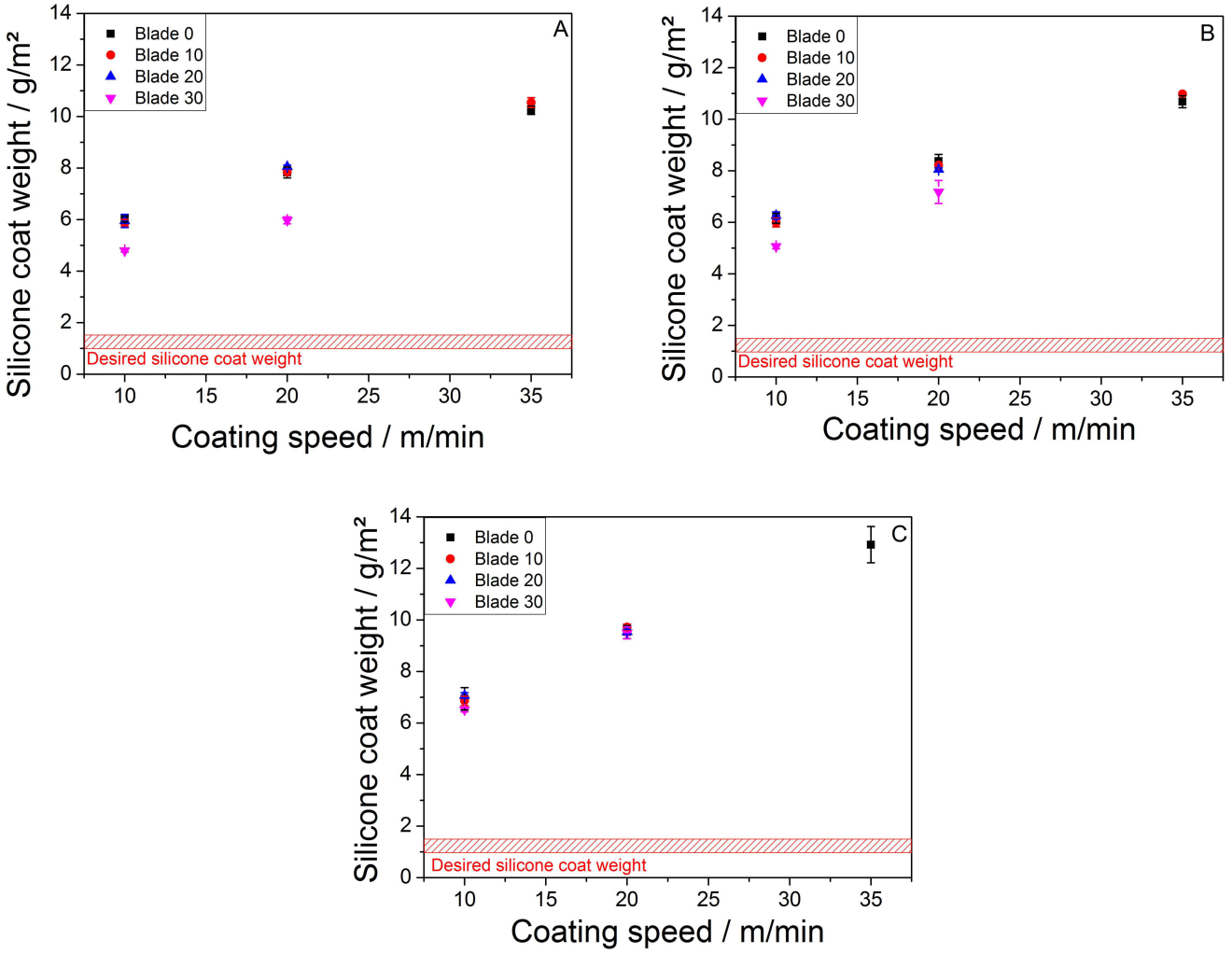

Figure 34: Siliconization with film press setup at 110 N (A), 80 N (B) and 40 N (C) blade pressure and at different coating speeds. The silicone coat weight is increased with increasing coating speed and with decreasing roller pressure.

5.3 Siliconization by means of 3-roller coating system

Similar to film press siliconization, the pressure between the two roller (50 N, 100 N, 150 N, 200 N) as well as the coating speed (2, 4, 8 m/min) were changed to investigate the influence on the silicone coat weight. The silicone coat weight is raised going from slow to fast coating speeds (Figure 35).
This is presumably due to a deformation of the rubber roller by some μm. More silicone is coated on the paper when the roller pressure is decreased. Additionally, a macro structure was observed on the roller and on the paper sheet which was more distinct for low coat weights. Less silicone is displaced by the roller when the roller pressure is reduced, which leads to an increased coat weight. Changing

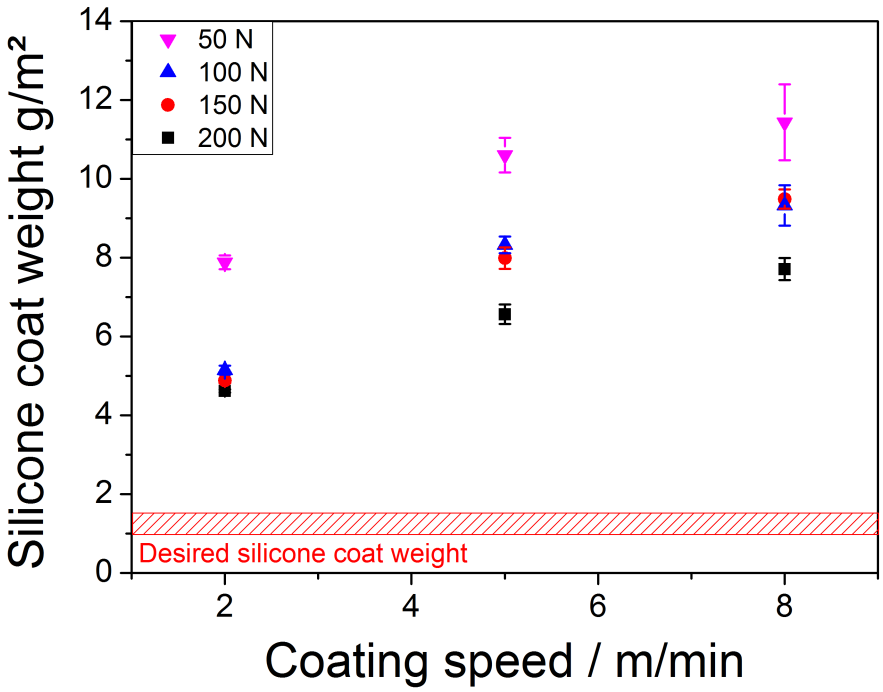

Figure 35: Siliconization of paper by 3-roller coater at different coating speeds and various roller pressures. The silicone coat weight is increased with increasing coating speed and with decreasing roller pressure.

roller pressure from 150 N to 100 N lead to only minor influence on silicone coat weight. Additionally, the silicone coat weight at slow coating speed of 2 $^{m}/_{min}$ is only significantly increased, if the pressure is 50 N. Nevertheless, silicone coat weight of ~1 $^{g}/_{m^2}$ was not achieved. SEM investigations of siliconized papers show that the silicone formed a ribbing structure build up of hills and valleys (Figure 36).

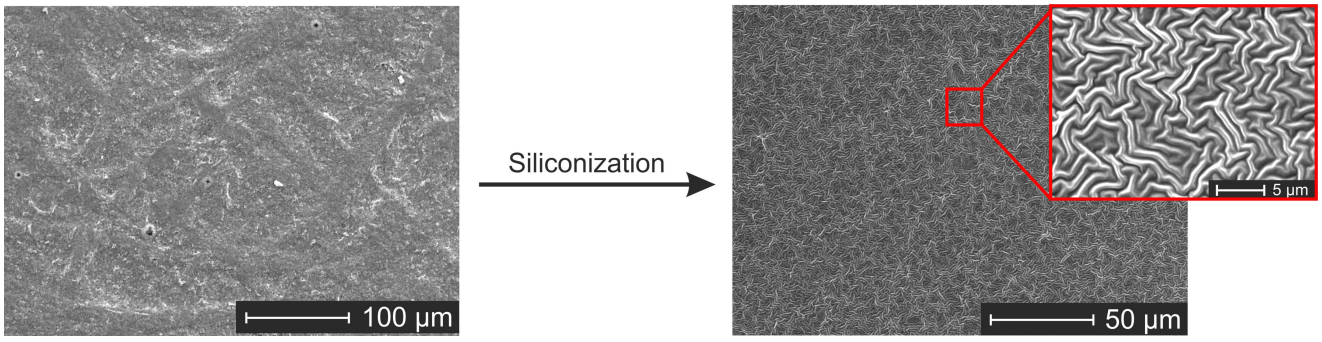

Figure 36: SEM images (topview) of CCK paper (S98) prior (left) and after siliconization (right) by the 3-roller-system.

Brighter parts display a maximum, because more electrons can be detected by the SE detector. It is known from literature that such structures arise during sputtering a gold layer (50 nm) on a thick PDMS-substrate. The gold layer is deposited on the PDMS-substrate by electron beam evaporation and the sample is heated during this process. The sample is cooled and the different thermal expansion of

the metal and the elastomer results in compressive stress in the metal film that is relieved by buckling of the surface.[112,113] In a next step, it has to be checked, whether the structuring of the silicone layer arises from the sputtering process or from other processes.

5.3.1 Investigation of ribbing structure on siliconized papers

The surface of siliconized paper samples were investigated by light microscope prior to sputtering process in order to learn more about the origin of the ribbing structure. As the structuring of the silicone layer was observed on the paper samples after silicone coating, the pattern does presumably not emerge from the sputtering process. The structuring can be disordered (Figure 37, A), ordered (Figure 37, B) or completely vanished (Figure 37, C).

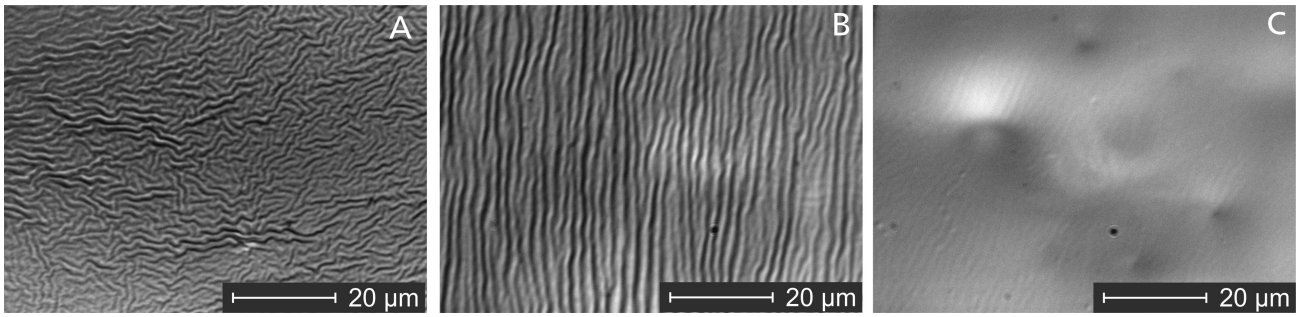

Figure 37: Investigations of siliconized papers by light microscopy carrying disordered (A), ordered (B) and no structuring (C) of the silicone.

The geometric dimensions of structures were investigated by atomic force microscopy (AFM). The maxima of the stripes had a height of 20 – 50 nm and the distance between two maxima was about 1 – 2 μm (Figure 38). Additionally, the elastic modulus of the maxima are higher compared to a minimum. The E-modulus is influenced by the crosslink density because more crosslinks lead to a stiffer silicone. Thus, crosslink density seems to be higher at the maxima compared to the softer valleys.
The structuring occurs most likely due to the curing process of the silicone. The extent of structuring may depend on silicone thickness, coating procedure as well as on curing temperature and curing time. Silicone was coated by blade coater (30 μm, 200 mm/s) and cured for several hours at room temperature until the silicone was crosslinked. For comparison reason, silicone was cured for 1 min at 150 °C. Investigation of silicone surface by light microscopy showed that ribbing structure occured in both cases (Figure 39). The structuring seems to be independent of curing temperature and curing time. Additionally, the coating procedure does not influence the microstructure, but the macrostructure. Papers siliconized by blade coater look smoother and do not possess macrostructuring as on papers coated by roller coater.

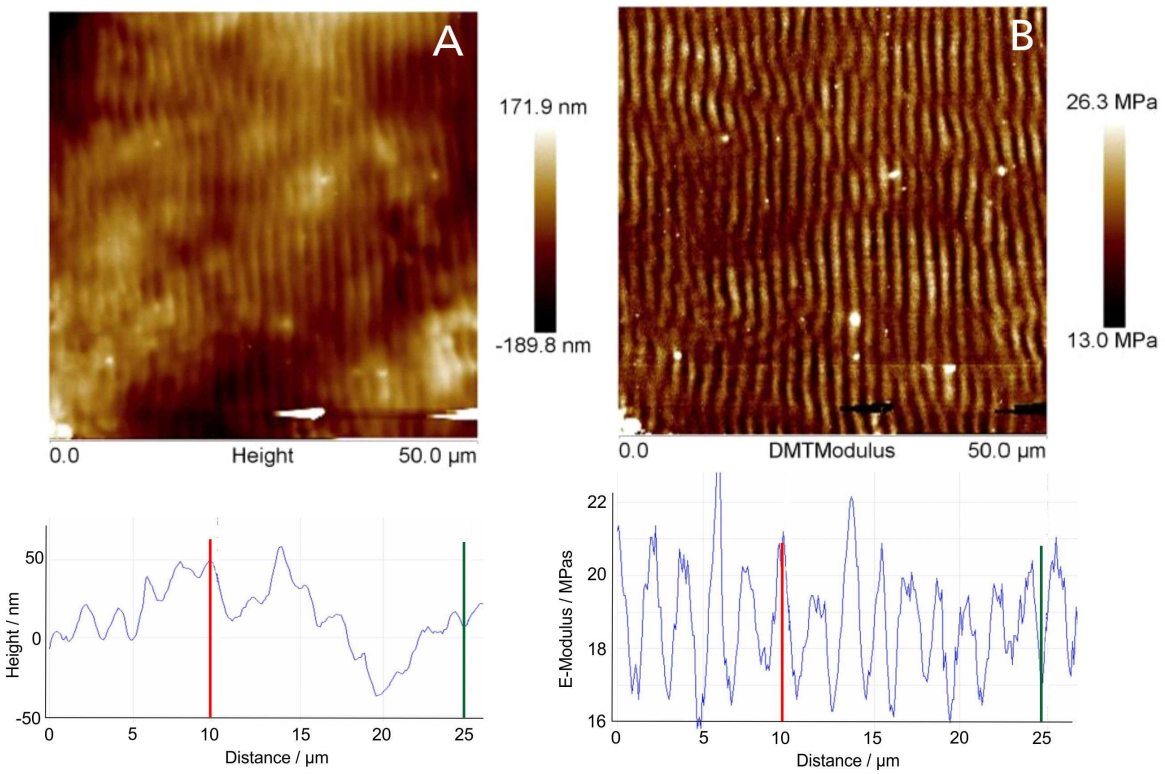

Figure 38: AFM images of siliconized papers recorded by the height sensor (A) and in DMT-mode (B). The height profile and the E-Modulus was determined by a cross section analysis over the width of the micrograph. The red line determines a maximum and the green line indicates a minimum.

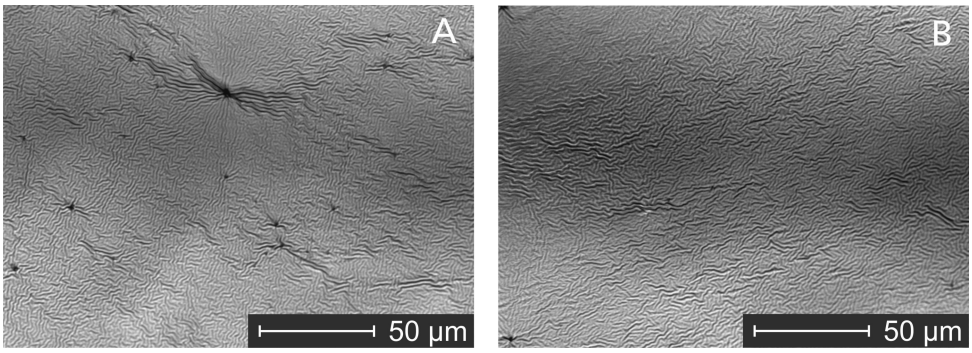

Figure 39: Light microscope images of siliconized papers by blade (30 μm, 200 mm/s) cured at room temperature (A) and for 1 min at 150 °C (B). Both papers posses a structured surface.

5.3.2 Reducing silicone coat weight by dilution

Next the influence of the dilution of the silicone coating material with different solvents, and its effect on the silicone coat weight was studied. The solvent-free silicone was diluted by ethyl acetate (EtOAc) and methyl isobutyl ketone (MIBK). Dilution of silicone by EtOAc with 30 and 50 wt% did not have a significant effect on coat weight (Figure 40, A).

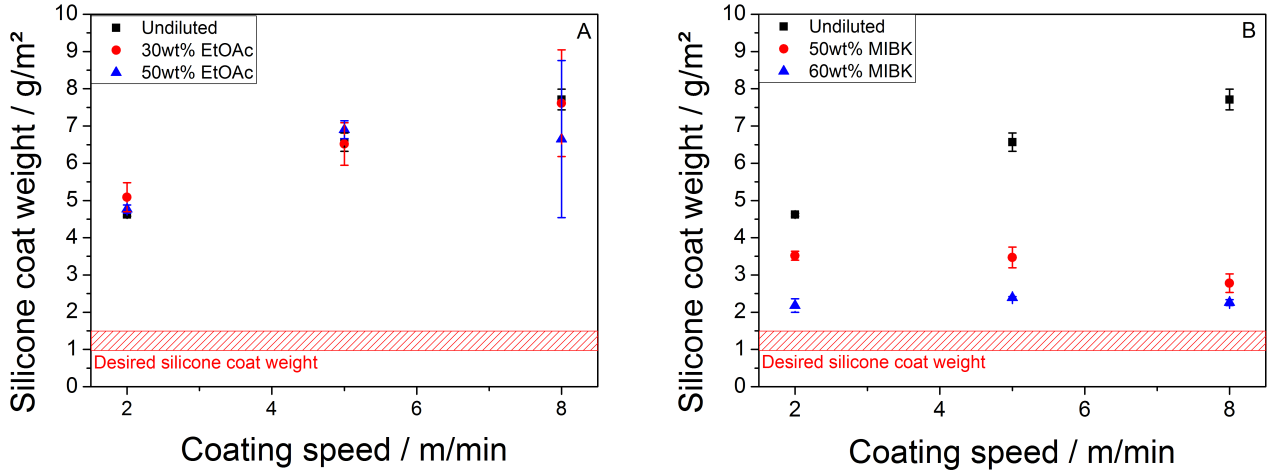

Figure 40: Solvent-free silicone was diluted by EtOAc (A) and by MIBK (B) in order to reduce the silicone coat weight. The diluted mixtures were coated on CCK-paper at different coating speeds.

The standard deviation is significantly raised at 8 $^{m}/_{min}$ and the coat weights stayed almost constant. Large errors are presumably due to an improper miscibility of EtOAc with the silicone and an inhomogeneous coating, respectively. Thus, MIBK was used as another solvent for dilution experiments (Figure 40, B). It can be seen that the silicone coat weight is remarkably reduced to about 2 $^{g}/_{m^2}$ using 60 wt% MIBK, which may be attributed to a more homogeneous miscibility of the solvent and the silicone, respectively. Additionally, the influence of coating speed on the coat weight is diminished. The coat weight is similar for various coating speeds. This is probably due to a decreased viscosity, which lowers the deformation of the roller. One challenge of this method is that the solvent is evaporated over time and this leads to a thickening of the solution, which influences the coat weight. Furthermore, the papers are not homogeneously coated by the silicone and defects in the coating appear, which was detectable by SEM analysis (Figure 41). The wetting behavior of the coating solution on the rubber roller may be different and it affects the coating homogeneity, as well. This method can thus be used in order to reduce the silicone coat weight, but the target coat weight was not obtained and this process suffers from a lack of coating homogeneity. The roller materials has to be changed to stainless steel to further reduce the silicone coat weight without dilution. The stainless steel roller cannot be deformed by the roller pressure and this should lead to lower silicone coat weights.

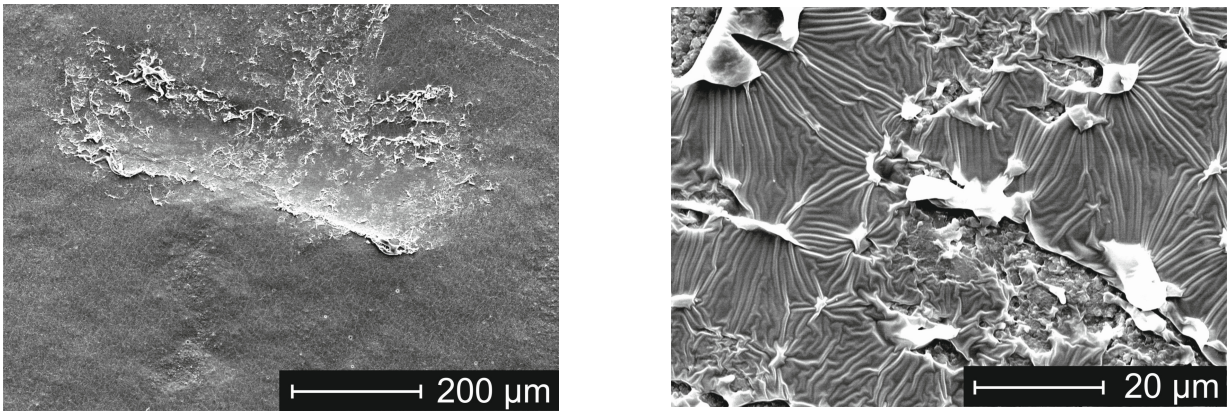

Figure 41: SEM images (topview) of CCK-papers which were coated by the diluted silicone mixtures. The images showing huge defect in the silicone coating.

5.3.3 Influence of roller material on silicone coat weight

Silicone coat weight was investigated by using different combinations of roller material at 200 N. Changing the bottom roller to a steel roller does not have any effect on silicone amount when compared with both roller composed of rubber (Figure 42). This changed, if the steel roller is placed to the top. Silicone coat weight is reduced by 1 g/m^2, but it is still not sufficiently low, which shows that less silicone is transferred from the bottom to the top roll when using a steel roller at the top position. During experiments with both rollers made of steel it was observed that the bottom roller rotates slower compared to the top roller especially at high coating speeds (5 and 8 m/min). This is presumably due to a reduced grip between the smooth and rigid rollers.

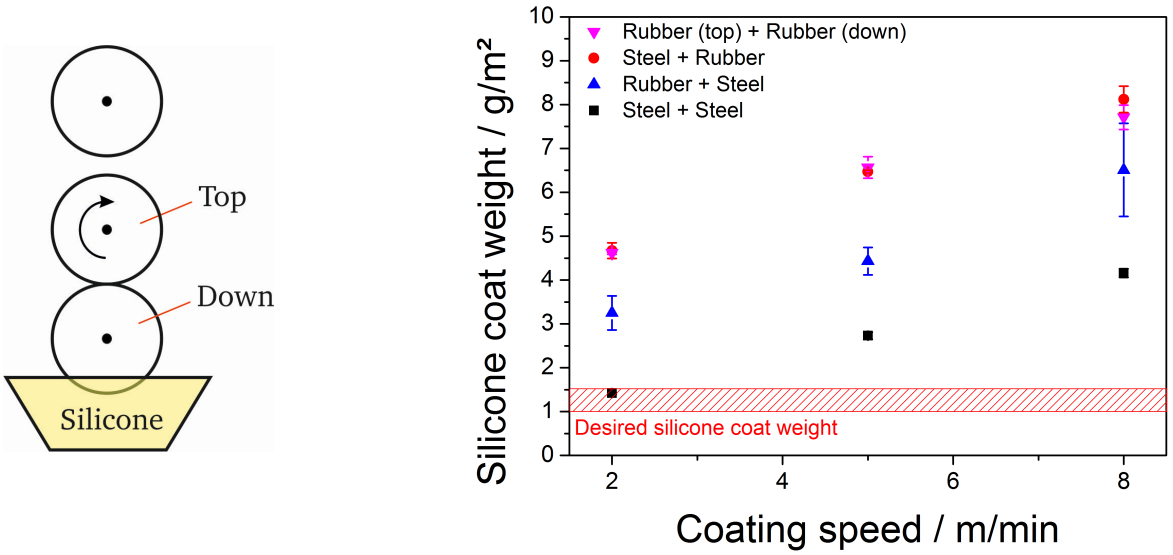

Figure 42: Influence of various roller material on silicone coat weight at 200 N pressure and 110 N for steel + steel combination.

Thus, a connection bridge consisting of two rubber rollers between bottom and top roll was installed outside the coating system. It has to be mentioned that 90 N are necessary to bring both rollers in contact. Thus, when the pressure is adjusted to 200 N, the actual pressure is 110 N. This is just valid for steel + steel roller combination. In order to enable higher coating pressures, a second pressure cylinder was installed (Figure 43). This ensures same rotation speeds of both rollers. The silicone coat weight was successfully reduced to the desired coat weight of ∼1 g/m^2, if both rollers are composed of stainless steel. This is because stainless steel rollers are not flexible and the silicone can be removed properly. However, silicone coat weight still increases with increasing coating speed which was observed for all combinations of roller material. This is due to the fact that the rollers of the connection bridge are made of rubber and they may be deformed by some μm due to the highly viscous silicone. The improved system with stainless steel rollers was used for further coating experiments.

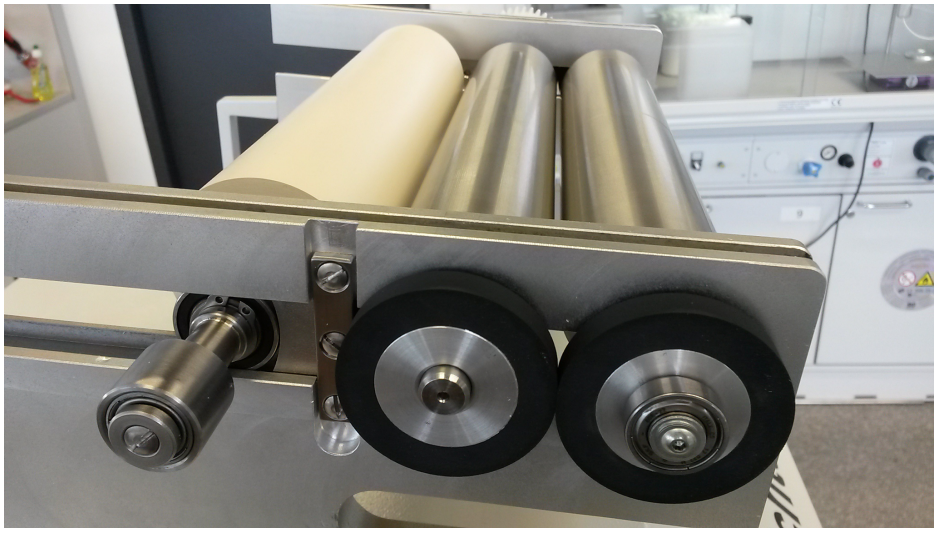

Figure 43: Connection bridge between the top and bottom roller for same rotation speeds of the steel rollers.

5.4 Determination of release forces

Release forces of papers which were coated with silicone by two different methods were investigated according to FINAT 10. The coating direction of silicone can have an influence on release forces. Thus, release forces on siliconized paper determined in machine direction (MD) may have different release forces as in cross direction (CD). Furthermore release forces may vary during storage due to condensation reactions. Depending on the application, specific release forces are needed. In literature there are no standard definitions how the release forces are categorized into various fields of applications. In one publication, release forces are stated as premium (0.03 – 0.25 $^{N}/_{25\ mm}$), modified (0.25 – 1.25 $^{N}/_{25\ mm}$) and tight (1.25 – 12.5 $^{N}/_{25\ mm}$) [21]. One company defines the release forces as easy ($\leq$0.15 $^{N}/_{25\ mm}$), moderate (0.15 – 0.5 $^{N}/_{25\ mm}$) and tight release ($\geq$ 0.5 $^{N}/_{25\ mm}$) [15]. Another company classifies release forces in premium, easy, medium, tight and extra tight [114]. This shows that there exist a variety of different names and ranges for various release applications. Hence, an own definition for release applications with specific release forces was developed for this thesis (Table 6). Release forces are categorized as easy and medium release for applications like labels in which the sticker is removed by machine or tight release for medical applications or tapes where the adhesive is removed by hand. The focus of this project is on release liner which can be are in the range of easy and medium release, however, there also exist a number of applications where tight-release ranges are in focus, such as for die cutting of or roof sealants. [115,116]

Table 6: Definiton of release forces.

Definition	Release forces / $^{N}/_{25\ mm}$	Application
Easy	< 0.25	Automated peel-off
Medium	0.25 – 1	Automated peel-off / Hand peel-off
Tight	> 1	Hand peel-off

5.4.1 Analysis of the adhesive tape (Tesa 7475)

The release forces are determined by using the adhesive tape Tesa 7475 as reference PSA. This pressure sensitive adhesive was selected, because it is recommended in the FINAT 10 method and the adhesive is widely used in label industry.[117] The adhesive is composed of an acrylic base polymer which is characterized by FT-IR analysis (Figure 44). The signals at 2957 cm^{-1}, 2873 cm^{-1} and 1457 cm^{-1} arise from the aliphatic backbone of the acrylic polymer. The ester functionality is detected at 1475 cm^{-1} for the C=O group and at 1024 cm^{-1} for C-O stretching vibrations. The IR-spectrum does not show any characteristic signals for hydroxy or carboxylic groups. All signals are depicted in detail in table 7. The adhesive may be a homopolymer or co-polymer and the glass transition temperature of the adhesive is below the room temperature. The wetting behavior of the adhesive was investigated by static contact angles measurement of a water droplet. A water contact angle of about 92° was determined, which displays a hydrophobic character and confirms the absence of hydrophilic groups. The adhesive is homogeneously applied on a PET-substrate tape and the adhesive thickness was determined to 100 μm by SEM-cross section of the adhesive tape (Figure 45).

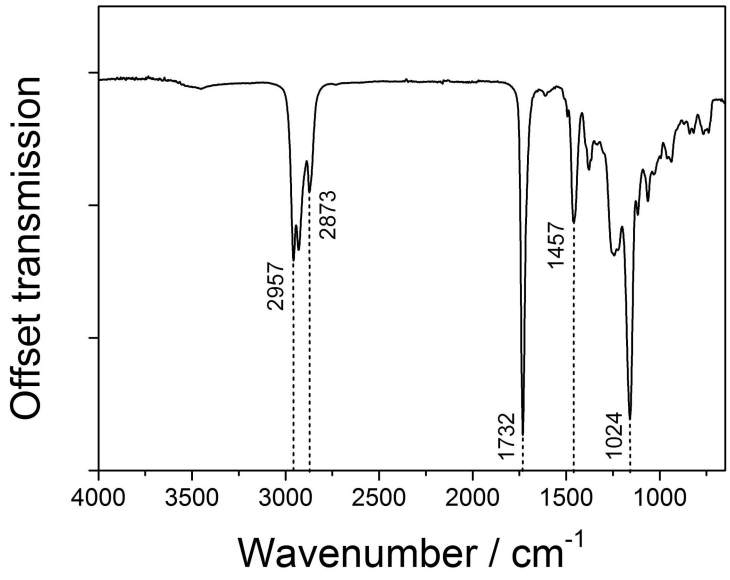

Figure 44: FT-IR analysis of acrylic adhesive tape Tesa 7475.

Table 7: Detailed overview of the observed FT-IR absorption bands of Tesa 7475.

Sample	Wavenumber/ cm^{-1}	Functional group
Tesa 7475	2957	C-H stretching vibration
	2873	C-H stretching vibration
	1732	C=O stretching vibration
	1457	CH_2 deformation vibration
	1024	C-O stretching vibration

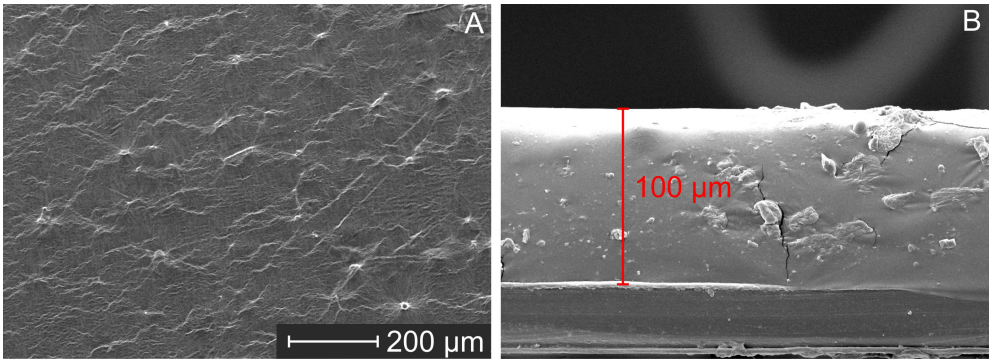

Figure 45: SEM images of the adhesive surface (A) and the cross section (B) of Tesa 7475.

5.4.2 Papers siliconized by film press

As previously shown, higher silicone coat weights were achieved by using film press setup. Nevertheless, it is interesting to see, how the release forces are influenced by the silicone coat weight in general. Peel-off measurements were performed and the release forces observed is plotted as a function of silicone coat weight (Figure 46). The resulting release forces of siliconized papers at 110 N are in the range of easy release (0.04 – 0.1 N/25 mm) and do not show significant differences.

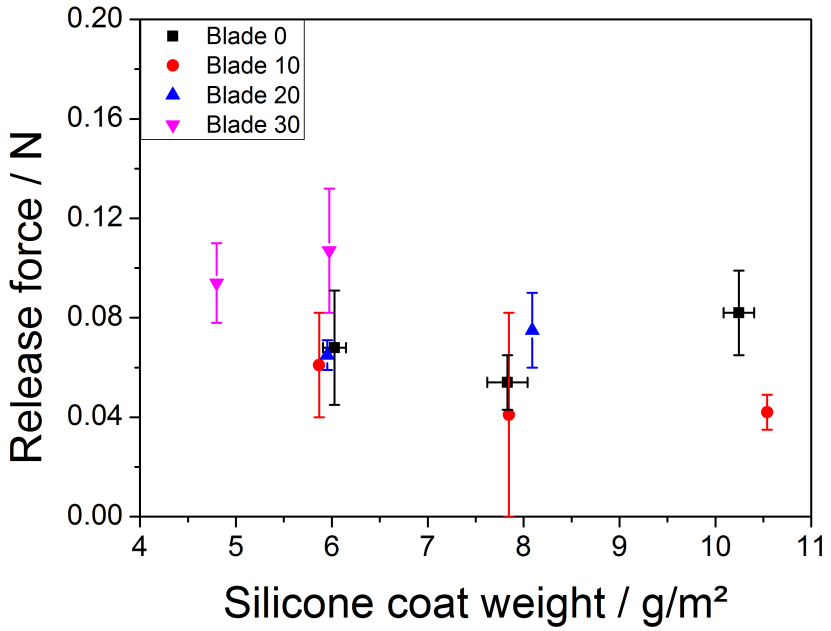

Figure 46: Release forces of papers with different silicone coat weights. The papers were siliconized by film press setup at 110 N.

As inferred from the figure, the release forces are independent from the silicone coat weight for high amounts of silicone (> 4 g/m²). Release forces of coated papers by metering blade 30 are slightly higher compared to the other blades. This was also observed for papers which were coated at 40 N and 80 N pressure of the metering bar. A more distinct structuring of the silicone layer may increase the contact area and thus the release forces when using blade 30. This assumption was not deeper investigated

because the differences are negligible and received coat weights are not in the desired range. Release forces were measured after 2 days and 6 weeks storing in climate room (23 °C, 50 % r. H.). It is known that hydroxy groups can be formed during storage originating from condensation reaction of residual silanes with water.[76] This may lead to an increase of release forces. However, the release forces measured here are not affected by prolonged storage times (Figure 47, A).

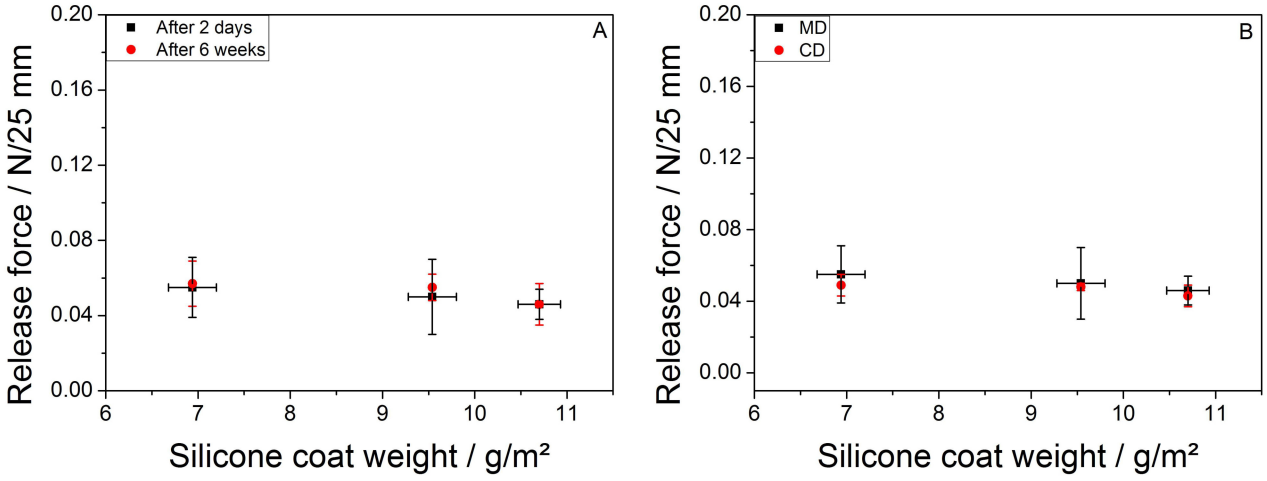

Figure 47: Influence of aging (A) and coating direction (B) on release forces. The release forces were measured in machine direction (MD) and cross direction (CD). The silicone was applied on the paper at 40 N in combination with blade 30.

This suggests that all silane groups reacted after 2 days by condensation or hydrosilylation reaction. Release forces were also measured in direction of the coating (MD) and perpendicular to it (CD). The macro-structure which arises during coating in MD may have an influence on release forces. The release forces of the adhesive tape which is removed in MD may vary from the release forces measured in CD. The results show that release forces are not influenced by the coating direction. The differences in release forces are all in the range of the experimental error (Figure 47, B).
Release forces are mainly governed by the low surface energy of the silicone. Structuring has minor effect because the highly viscous adhesive penetrates into the structures of the silicone and thus the effect is diminished. More distinct structures where the adhesive is not able to penetrate may lead to reduced release forces cause of decreased contact area. Nevertheless, further peel-off experiments will be performed in MD according to FINAT 10.

5.4.3 Papers siliconized by 3-roller-system

The release forces of siliconized papers by 3-roller system were also investigated. The resulting forces are in the same range of easy release like release forces from the film press (Figure 48). Similar release forces were obtained up to a silicone coat weight of 1.4 g/m^2. At this point, the release forces are increased to ~0.2 $N/25\ mm$. Reason for this may be an inhomogeneous silicone film on the applicator roll or impurities on the paper. The adhesive comes in contact with the clay and this results in higher release forces. The paper roughness may also influence the coating process and the silicone coverage. Analysis of the siliconized papers (S98) by SEM revealed that small parts of the paper were inhomogenously coated by

silicone (Figure 49). More data points in addition with release forces should be acquired for low silicone coat weights (< 1.4 g/m²) in order to visualize the influence of coat weight on release forces. Additionally, the paper surface should be investigated by microscopy to check homogeneity and defects in the silicone layer. This will be discussed in detail later in this thesis, below.

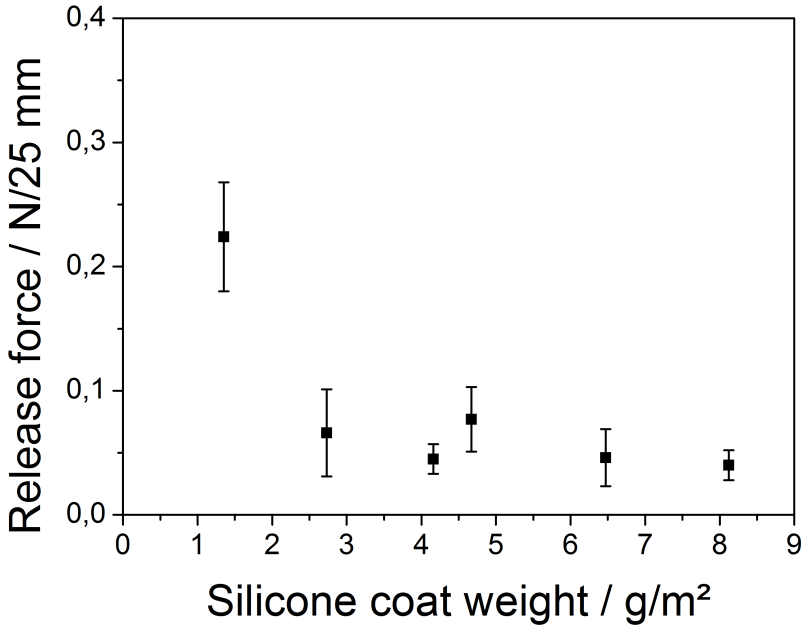

Figure 48: Release forces of papers (DN135) with different silicone coat weights. The silicone was applied by using the 3-roller system at 200 N.

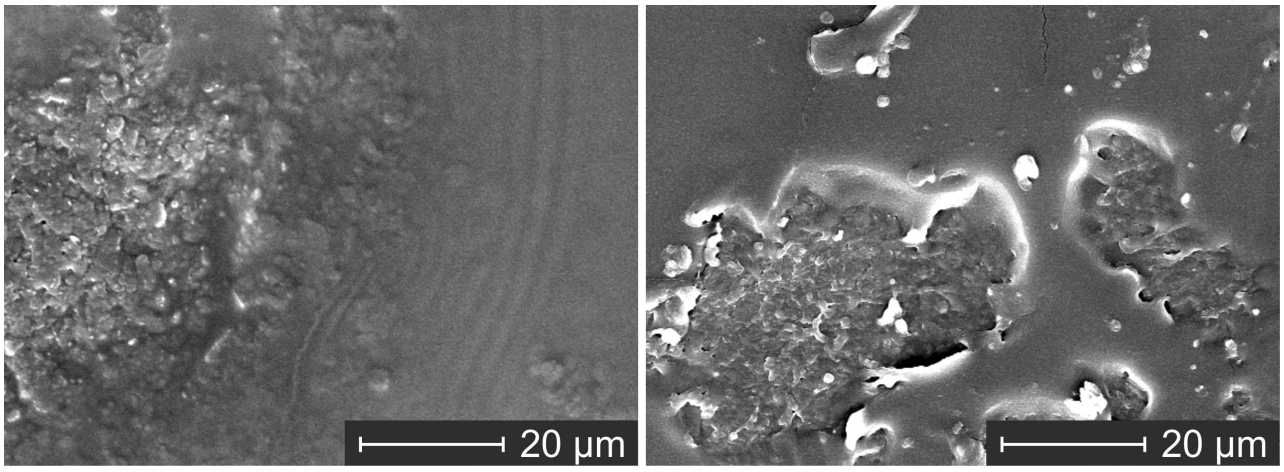

Figure 49: SEM images (topview) of siliconized CCK paper (S98) with 1.4 g/m² silicone coat weight. The images show defects in the silicone coating.

5.4.4 Influence of pressure roll on release forces

The pressure of the pressure roll was changed during siliconization of CCK papers (S98) in order to investigate the impact on release forces and on silicone anchorage to the paper. More silicone may be pressed into small pores of the clay-coated paper at high pressures leading to defects in silicone coating along with higher release forces. The pressure between the dosing and applicator roll was held constant to 110 N and the coating speed was adjusted to 2 m/min for coat weights of ~1.3 g/m² or 5 m/min for coat weights of ~2.6 g/m². The pressure of the pressure roll was changed to 200 N, 800 N and 1200 N (Figure 50).

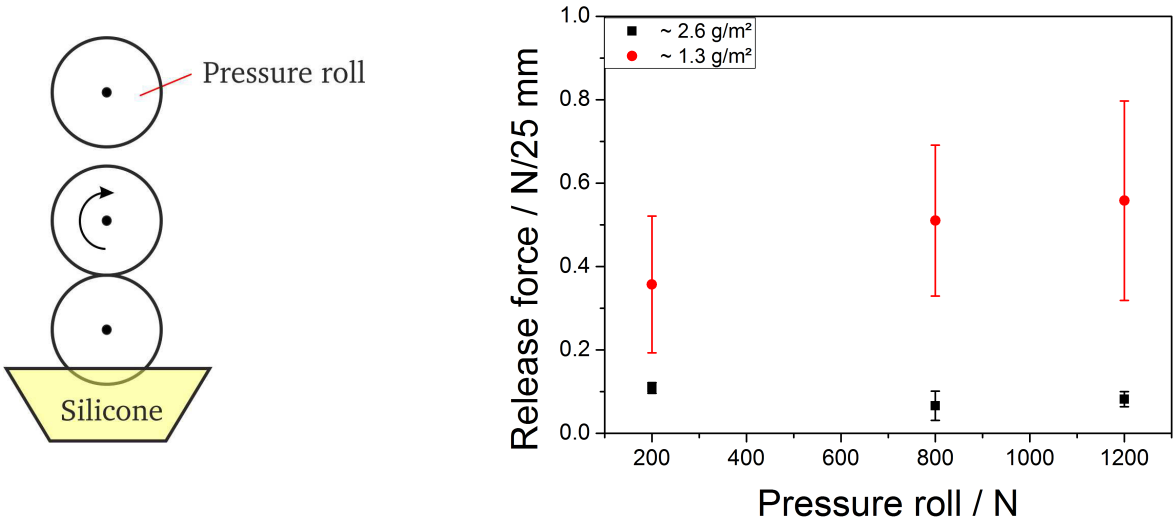

Figure 50: Influence of pressure roll on release forces at different silicone coat weights. CCK papers (S98) were siliconized by 3-roller system at 110 N and 2 m/min (red) or 5 m/min (black) with various pressures of the pressure roll.

The pressure was also reduced to 50 N but this pressure was too low so that the paper was not completely in contact with the applicator roll. Large uncoated areas occurred and as a consequence, release forces of these papers could not be measured. It can be seen that the papers with low amounts of silicone (~1.3 g/m²) possess higher release forces and errors compared to papers having higher silicone coat weights of about 2.6 g/m². This was also observed in previous sections and is most likely due to defects in the silicone layer. In contrast, release forces are not affected by the pressure roll, but influenced the rub-off. Anchorage of the silicone to the paper was poor at 200 N pressure, presented in a high rub-off. No rub-off was detected at 800 N and 1200 N. This is because the silicone is pushed even into small pores of the clay coat at high pressures which improves the mechanical anchorage of the silicone to the paper and thus decrease the rub-off. One drawback of high pressure (1200 N) is that the handling is of the coating process is inconvenient for the applicator. The sample carrier with the paper sheet must be pushed between the applicator and pressure roll and this is difficult at pressure of 1200 N. Influence of pressure roll was also investigated for non-clay-coated paper (L90). This base paper has got an open surface with large pores. Thus, the silicone is able to penetrate into the paper to more extent. This may be enhanced by high pressures of the pressure roll and leading to higher release forces. Indeed, the

release forces are significantly increased to ~7 $^{N}/_{25\ mm}$ compared to the CCK paper, but release forces are similar for various pressures (Figure 51). The silicone is absorbed by the paper and less silicone stays on the surface. Thus, the adhesive tape is not just in contact with silicone but also with fibers which lead to significant higher release forces. Additionally, the adhesive is also able to penetrate into the paper pores which increases the contact area and allows mechanical interlocking.[118] The silicone anchorage is also improved by this process. The rub-off is good for all pressures. The pressure roll was adjusted to 800 N for further experiments, because 1200 N is difficult to process and 200 N showed bad rub-off for siliconized CCK papers.

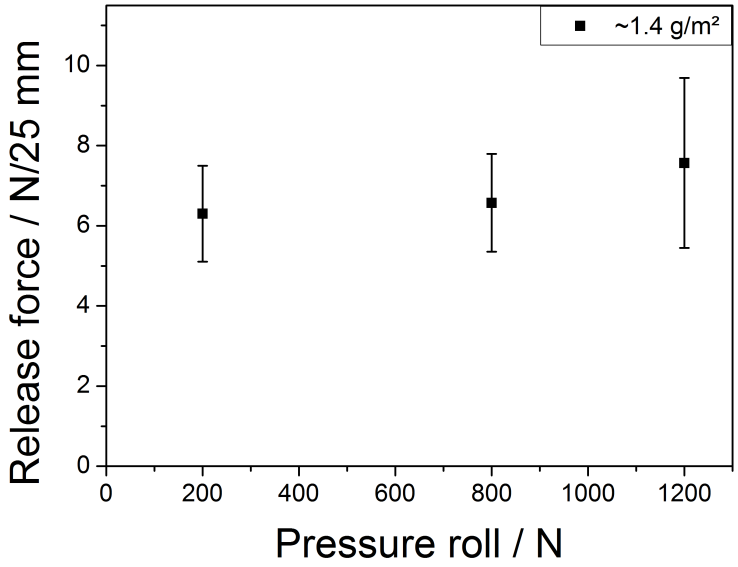

Figure 51: Influence of pressure roll on release forces of siliconized base papers (L90). Porous base papers were siliconized by 3-roller system at 110 N and 2 $^{m}/_{min}$ with various pressures of the pressure roll.

5.4.5 Influence of paper roughness and silicone coat weight on release forces

The CCK papers (S98, DN135, DNC135) with various roughness were coated with different amounts of silicone in order to investigate the influence of paper roughness and silicone coat weight on the release forces. The release forces of siliconized papers are all below 0.25 $^{N}/_{25\ mm}$ and thus in the range of an easy release. Nevertheless, papers which were coated with 2.3 $^{g}/_{m^2}$ possess lower release forces and smaller errors compared to papers with 1.5 $^{g}/_{m^2}$ silicone coat weight (Figure 52). The influence of silicone coat weight on release forces was most prominent for S98 papers.

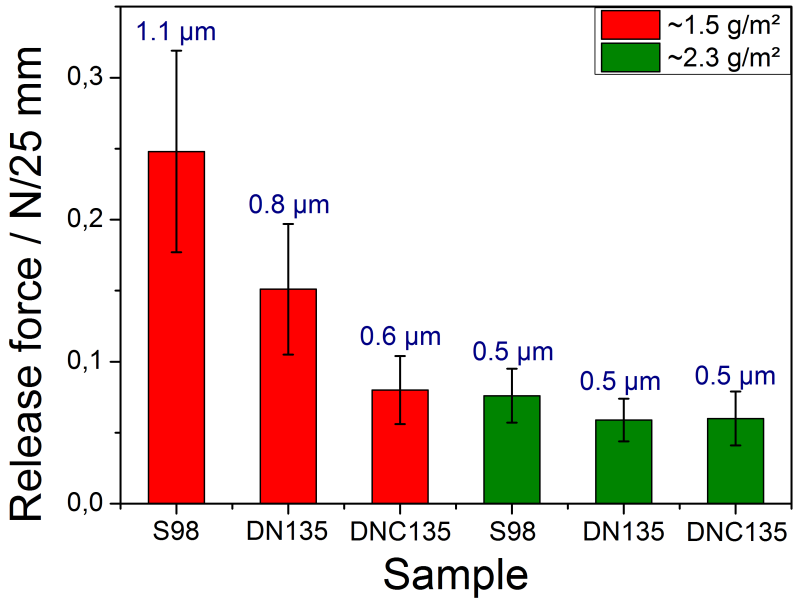

Figure 52: Influence of paper roughness and silicone coat weight on release forces. Papers were siliconized by using stainless steel rollers at a pressure of 110 N with a coating speed of either 2 $^{m}/_{min}$ or 5 $^{m}/_{min}$. The median roughness (R_a) of the siliconized papers was determined by WLI measurements and is featured in blue colour.

Investigation of siliconized S98 papers by SEM reveals that the paper surface is very homogeneously covered by the silicone at 2.3 $^{g}/_{m^2}$ (Figure 53, B). In contrast to this, defects in the silicone coating were observed when less silicone is applied on the paper (Figure 53, A). No or significantly less silicone is present in these defects and the underlying clay-coating is visible. The adhesive comes in contact with the clay-coating and this results in high release forces. In a next step, the influence of the paper roughness on release forces was studied. The paper roughness differs, depending on the amount of clay coating (S98 ⟷ DNC135) as well as on paper calendering process (DN135 ⟷ DNC135). Analysis of the base paper roughness by white light interferometer showed that S98 paper (R_a = 1.3) carries the highest paper roughness, followed by DN135 (R_a = 0.9) and lowest roughness was observed for DNC135 (R_a = 0.8). The roughness after siliconization of 1.5 $^{g}/_{m^2}$ is reduced to 1.1 μm (S98), 0.8 μm (DN135) and 0.6 μm (DNC135), but the differences are still visible. The release forces of DNC135 are 0.25 $^{N}/_{25\ mm}$ lower compared to S98.

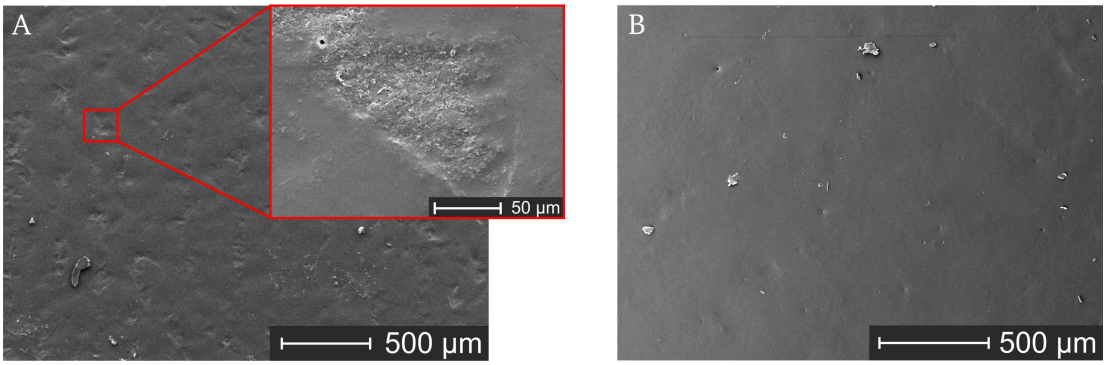

Figure 53: SEM images (topview) of siliconized S98 paper with 1.5 g/m² (A) and with 2.3 g/m² (B) silicone. Coating defects in the silicone layer are visible at low silicone coat weights (A).

Nevertheless, other additives in the clay-coating of DN135 and DNC135, which cannot be disclosed in detail, may also have a reducing effect on release forces. Considering papers with silicone coat weight of 1.5 g/m², it seems that the release forces correlate well with the median paper roughness. Nevertheless, as the adhesion is mainly governed by the silicone, the main reason for this observation originates most likely from defects in the silicone coating, which occur during the coating process. These defects arise, because the thin silicone layer on the roller comes not in contact with the paper surface in some parts due to its rough morphology and thus it was not transferred to the paper (Figure 54).

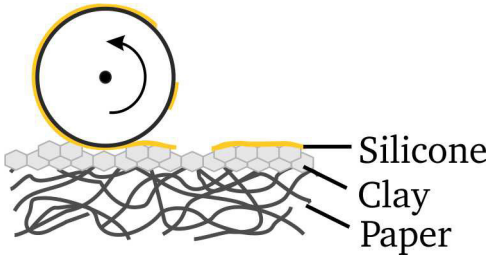

Figure 54: Schematic illustration of the formation of coating defects in silicone during roller coating. The silicone on the roller is just partially in contact with the paper due to its roughness, which leads to coating defects.

Less defects in the silicone coating were observed when the base paper roughness is decreased (Figure 55). The effect of calendering on release forces at ~1.5 g/m² coat weight can be clearly seen. Peel-off forces are reduced by 0.05 N/25 mm when the paper is calendered (DN135 ⟷ DNC135). The clay-coating is densified during calendering process leading to less open pores and a smooth surface. Thus, the silicone will stay mainly on the paper surface and less defects in the silicone coating occur, which leads to low release forces. However, even if the paper surface is completely covered by silicone without defects the surface roughness may also influence the release forces due to a different silicone/adhesive contact area. It is known from literature that depending on the roughness scale of the surface and the glass transition temperature of the adhesive, release forces can be reduced or increased.[1,21,24] As the roughness of our siliconized paper determined by AFM measurement was in the range of 20-50 nm, it is not expected that release forces will be significantly influenced by the latter.

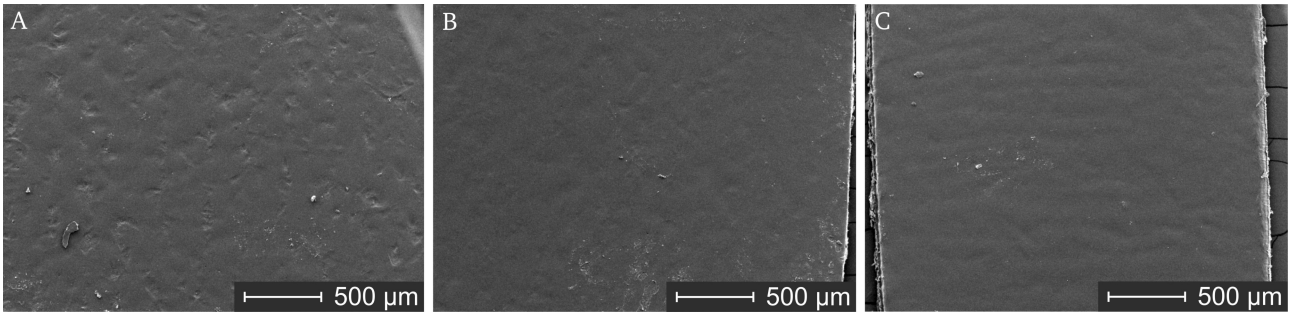

Figure 55: SEM images (topview) of S98 paper (A), DN135 (B) and DNC135 (C) coated with 1.5 g/m² silicone.

The paper roughness is reduced to 0.5 µm, if 2.3 g/m² silicone is applied to the paper surface. The initial paper roughness is thereby smoothened by the silicone and the release forces of all three papers are similar. The influence of paper roughness on release forces at higher silicone coat weights (2.3 g/m²) is less pronounced, because less defects occur in the silicone coating. Low release forces of about 0.08 N/25 mm can be obtained by either using a calendered base paper with high amounts of clay coating (DNC135) or by applying higher amounts of silicone on CCK paper with lower amounts of clay-coating (S98).

5.5 Siliconization of CCK papers and porous base papers

Siliconization of CCK papers (S98) and porous base papers (L40 and L90) was performed at various roller pressures with stainless steel rollers in order to investigate the influence on silicone coat weight. As in the preceding experiments, the silicone coat weight is reduced with increasing roller pressure because less silicone is transferred from the dosing to the applicator roll (Figure 56).

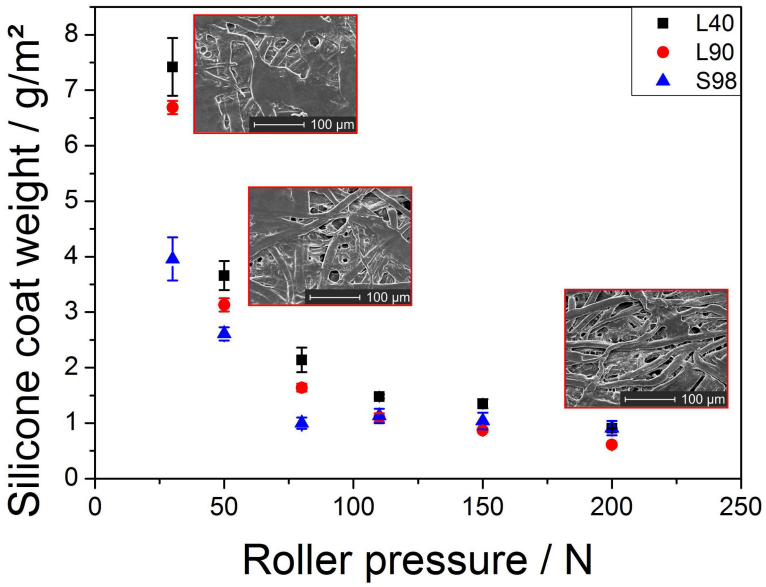

Figure 56: Influence of pressure between dosing and applicator roll on the silicone coat weight of various paper substrates at 2 m/min using stainless steel rollers. SEM images of siliconized L90 with different silicone coat weights at 30 N, 50 N and 200 N. The silicone coat weight is reduced with increasing roller pressure.

SEM images of siliconized L90 show that the paper surface is closed to more extent with increasing amounts of silicone, but paper structure and pores can be still seen even at high silicone coat weights. Analysis of the silicone distribution on the paper surface by Si-EDX-mapping indicates that most silicone is located on the fibers and the fiber-fiber crossings (Figure 57).

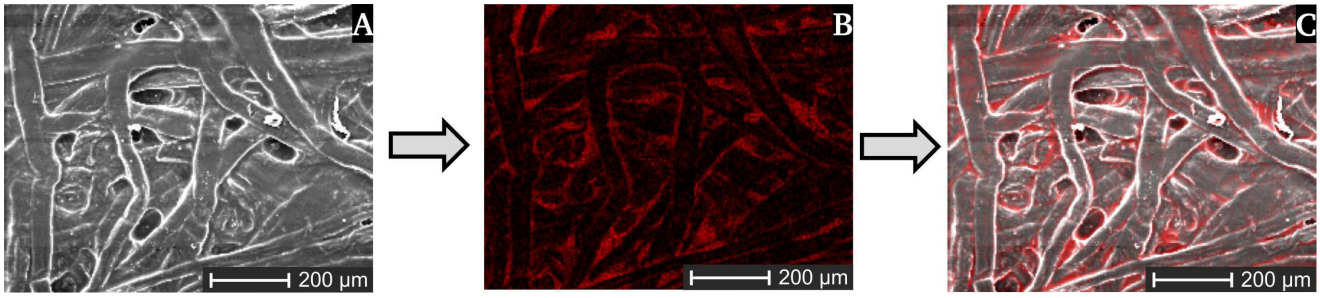

Figure 57: Surface analysis of siliconized L90 with silicone coat weight of about 6.7 g/m² by SEM (A), Si-EDX-mapping (B) and an overlaid image of SEM and Si-EDX-mapping (C).

The graph features an exponential increase of the silicone coat weight with decreasing roller pressure. The silicone coat weight is just minor affected by roller pressures in the range of 110 N to 200 N, but increases drastically at roller pressure smaller than 110 N. It can be seen that the amount of transferred silicone is influenced by the paper substrate. Different amounts of silicone at same roller pressure were applied to the various papers, which is due to a different surface coating. This behavior is most significant at low roller pressure of 30 N. Highest silicone coat weight was achieved for L40 (7.5 g/m²) and approximately 0.8 g/m² less silicone was transferred to L90 which is probably due to the different surface sizing of these papers. The porous papers exhibit different wetting behavior, which was previously shown by contact angle measurements. Considering the non-clay-coated papers, the paper porosity may also affect the silicone transfer, but just to a small part because the paper porosity of the respective paper samples is similar as previously shown. Lowest silicone coat weight at 30 N roller pressure was obtained for the CCK paper (S98). The reason for the different transfer rates of silicone to either CCK papers or non-clay coated papers originates from the surface porosity. The surface of base papers is not closed and carries huge pores in the range of 10 – 50 μm in which the silicone can be absorbed. Thus, almost complete silicone is transferred and pushed from the applicator roll into the paper in this case. In contrast, CCK papers just have small pores (<1 μm) and the paper surface is closed rather by pigments. Hence, less silicone is absorbed by the paper and huge part of the silicone stayed on the applicator roll. These results are very useful in order to precisely adjust the silicone coat weight for various paper substrates by simply changing the roller pressure. In a next step, release forces of siliconized papers were measured. Evaluation of peel off experiments from siliconized CCK papers revealed that release forces reached a minimum of ~0.05 N/25 mm with increasing silicone amount (Figure 58).

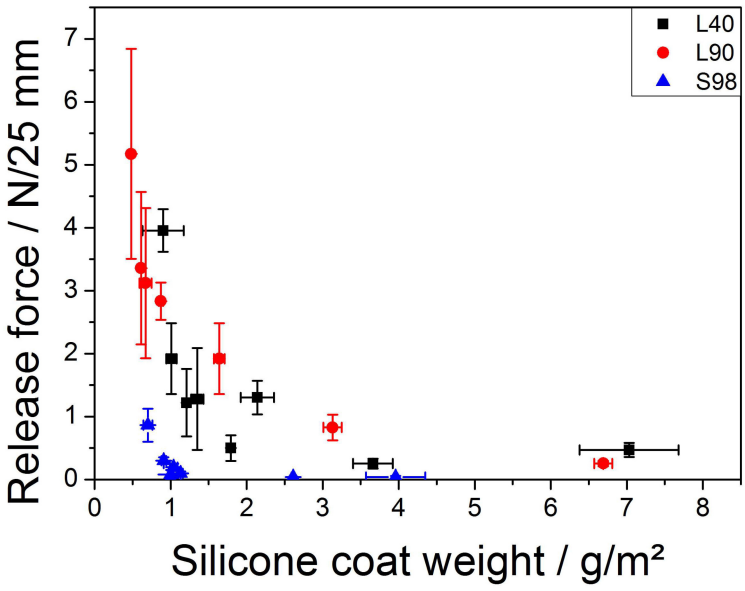

Figure 58: Influence of silicone coat weight on the release forces of various papers. Papers were coated at 2 m/min using stainless steel rollers. The release forces are reduced with increasing silicone coat weight.

Silicone coat weights above 1.2 g/m² does not lead to remarkably lower release forces for CCK paper, because the paper is almost completely covered by silicone (Figure 59).

Silicone coat weights smaller as 0.7 g/m² leads to an increase of release forces to ~0.9 N/25 mm. This is because the paper surface is not fully covered by silicone and the adhesive tape comes in contact with the clay in some parts leading to higher release forces. Hence, a minimum coat weight of 1 g/m² is necessary for easy release applications. Release forces of L90 with similar coat weights are significant higher compared to S98. Release forces up to 5 N/25 mm were obtained for L90 and can be considered as high. In addition, paper is partially destroyed during peel-off which makes this paper improper for release liner applications. This is because major part of the silicone is pushed into the paper pores and does not stay on the paper surface. Some pores are closed by the silicone, but several pores remain open (Figure 59). The adhesive is pushed into them and comes in contact with the fibers leading to higher release forces. More pores are closed at higher silicone amounts and the penetration of the adhesive into the paper is diminished which results in lower release forces. Nevertheless, even at high silicone coat weights (>4 g/m²) the release forces are higher compared to CCK paper which is likely due to a mechanical interlocking of the adhesive into paper pores and a rougher surface, respectively.

Release forces of L90 behave similar to L40 depending on the silicone amount, but it seems that the peel-off forces at same coat weights are higher compared to L40. The range in which the release forces of the base papers are influenced by the silicone amount is larger as compared to CCK paper. The silicone coat weight on CCK papers shows an influence on release forces beneath a threshold of <1.2 g/m², whereas release forces of siliconized base papers (L40, L90) are affected starting from coat weights of <4 g/m². For this reason, a smooth and closed surface is required to get good release properties with a minimum amount of silicone. It should be noted that release forces correspond to the silicone coat weight and they are exponentially reduced with increasing silicone amount. Strongest increase of release forces for base

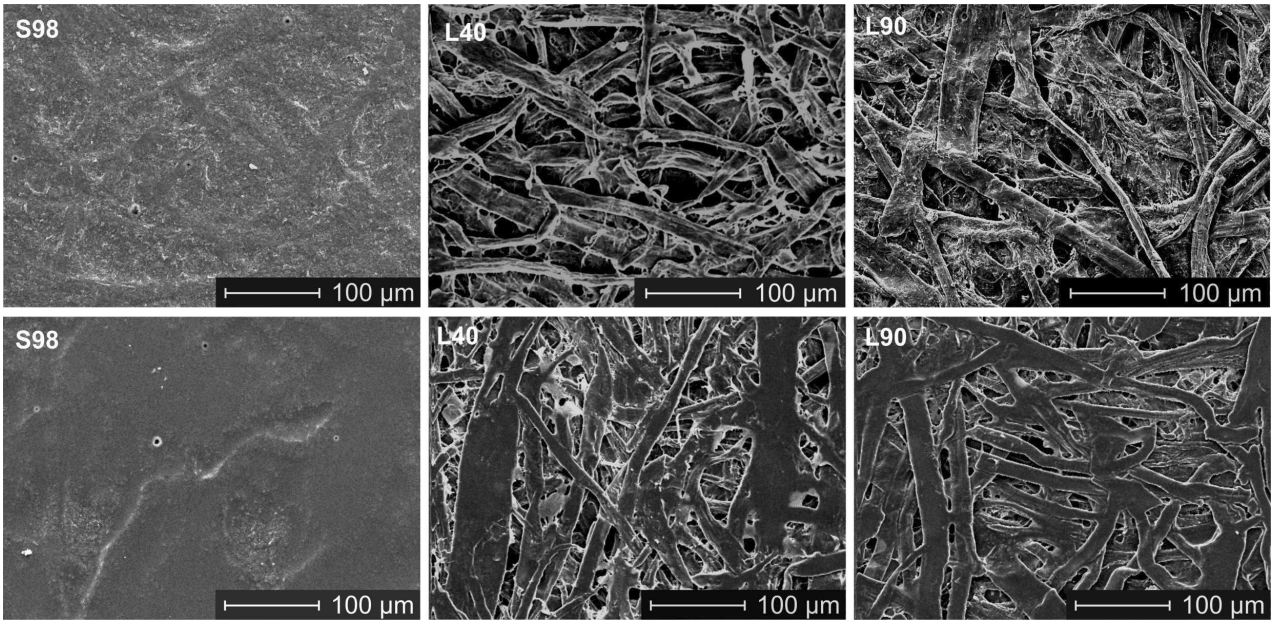

Figure 59: SEM images (topview) of various papers before (top) and after siliconization of ∼1.2 g/m² (bottom).

paper was observed at a silicone coat weight of <1.2 g/m² as for the CCK paper. This value seems to be a threshold, the silicone coat weight should not fall below this value. The silicone coat weight as well as release forces can be precisely tailored for various papers with this results.

5.6 Analysis of siliconized papers by FT-IR and contact angle

Next, the chemical identity of siliconized papers was investigated by FT-IR. As an example, spectra of L40 base paper before and after siliconization are compared (Figure 60, A). Most signals of the non-siliconized base paper are still visible because the paper surface is not completely covered by silicone which was also shown by SEM images. New signals arise from the silicone coating at 1260 cm^{-1} coming from CH_3 deformation and at 796 cm^{-1} assigned to Si-C stretching of Si-CH_3 group. One more new small signal at 2965 cm^{-1} can be ascribed to CH_3 asymmetric stretching vibration of Si-CH_3 group. Additionally, the absorption band of Si-O-Si appearing at around 1020-1074 cm^{-1} may be overlaid by the signal at 1024 cm^{-1}.[119] As a candidate for CCK papers, S98 was investigated by FT-IR. Signals from the uncoated CCK paper at 3668 cm^{-1} and 993 cm^{-1} are still visible after silicone coating (Figure 60, B). Same signals representing the silicone coating were detected for siliconized CCK paper as for the siliconized L40 paper. New signals show up at 2965 cm^{-1}, 1260 cm^{-1} and 796 cm^{-1} which are assigned to the silicone coating. Characterized FT-IR absorption bands of silicone are summarized and featured in detail (Table 8). The contact angle is increased for CCK papers (S98, DN135, DNC135) but decreased for sized base papers (L40, L90) after silicone coating.

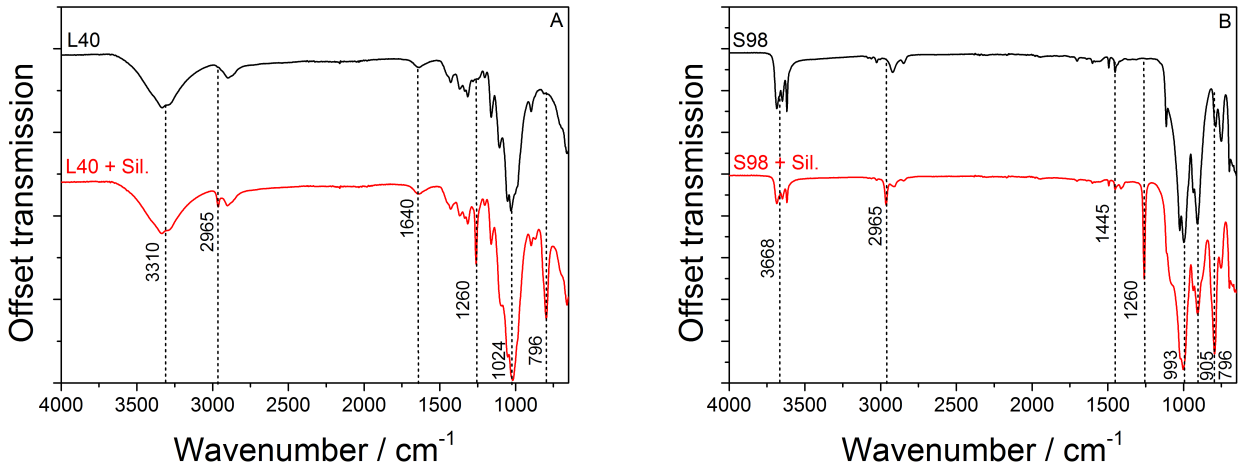

Figure 60: Comparison FT-IR spectra of L40 (A, black) and S98 paper (B, black) and after silicone coating of 1.4 g/m² (red).

Table 8: Detailed overview of the FT-IR absorption bands from silicone coating.

Paper	Wavenumber/ cm^{-1}	Assignments
L40 + S98	2965	CH_3 asymmetric stretching vibration of Si-CH_3
	1260	Si-O-Si stretching vibration
	1020	CH_3 deformation of Si-CH_3
	796	Si-C stretching of Si-CH_3

5.7 Conclusion

At the first part of the thesis, a method was developed to accurately determine the silicone coat weight on different reference paper sheets. Best results for determination of coat weights were obtained by weighing the papers prior and after coating, which was confirmed by SEM cross sections of siliconized papers. The influence of various coating parameters on the silicone coat weight was investigated. In detail, the coating system, roller pressure as well as coating speed were changed and silicone amount on CCK paper was determined. The silicone coat weight is reduced with increasing roller pressure and decreasing coating speed. Following this finding, the 3-roller system was selected as the most appropriate method to obtain low, and controlled silicone coat weight. Further investigations were focused on coatings with combinations of different roller materials in order to reduce the silicone coat weight. The desired coat weight in the range of 1 – 1.4 g/m^2 was reached by using stainless steel rollers at a pressure of 110 N and a coating speed of 2 m/min. This coat weight fits to industrial produced release liner. Coating experiments at different coating pressures were also conducted on non-clay coated and porous base papers. The silicone coat weight is reduced with increasing roller pressure, but the papers show different silicone coat weights at same coating conditions. Significant more silicone was absorbed by the base papers (L40, L90) in contrast to the CCK paper (S98). This is because more silicone can be pushed into the paper pores which is not possible at CCK paper, because the pores are closed by the clay. Important point for a release liner is how much force is needed in order to remove an adhesive tape from the siliconized paper. Thus, peel off experiments were performed which showed that release forces are decreased with increasing silicone coat weight. High release forces arise when the adhesive tape comes in contact with parts of fibers or the clay-coating, which was not siliconized. Such defects of the silicone coating were shown by SEM images. Release forces are significantly increased for silicone coat weights smaller than 1.2 g/m^2. In addition, release forces of base paper are significantly higher compared to CCK paper. An explanation for this is that most part of the silicone is absorbed by the paper and paper pores are still open. The adhesive tape penetrates into these pores leading to mechanical interlocking and comes in contact with non-siliconized parts of the paper resulting in high peel off forces. Thus, a closed and smooth surface is required to produce a release liner with easy release properties from a minimum amount of silicone coated on top of the paper.

6 Towards a silicone-based release liner starting from a porous base paper

Base papers (L40, L90) were directly coated by solvent-free silicone in order to investigate release forces. As previously shown, peel-off forces of about 3 $^{N}/_{25\ mm}$ with silicone coat weight of approximately 1.0 $^{g}/_{m^2}$ were achieved for porous base papers. This is high compared to siliconized CCK papers. Additionally, the errors are large and the paper was partially destroyed during peel-off. The reason for this may be that the silicone is absorbed by the paper and does not stay on the paper surface. A silicone coat weight of 4 $^{g}/_{m^2}$ is required in order to obtain low release forces comparable to CCK papers. This specific coat weight is too high and not economic, from a resource-saving point of view. Release liner coated in this way are therefore not appropriate for release liner applications. Thus, new ways for the production of a release liner starting from a porous base paper needed to be explored.

6.1 Siliconization of base paper by mixtures of silicone and talcum

As a first step, the porous base papers should be coated by a mixture of silicone and talcum with different particle sizes according to an experiment performed by Sappi in the year 2002. In this trial, a water-based silicone was mixed with about 40wt% talcum and applied on the porous base paper by blade coater. Release forces obtained by this coating mixture were as low as common release liner on CCK paper. The talcum presumably act as a barrier in order to reduce silicone absorption into the paper. Additionally, a release liner is commonly produced in two individual production steps, namely closing paper pores by a pigment coating followed by calendering steps and applying the silicone coating to get the final release liner. These two steps may be combined within one production process by using the method mentioned above, which decreases costs. The idea behind this approach is, that the pigments are mechanically retained on the paper surface by the cellulose fibers and silicone penetration into the paper is reduced (Scheme 13). This should lead to lower release forces compared base papers siliconized without any pigments.

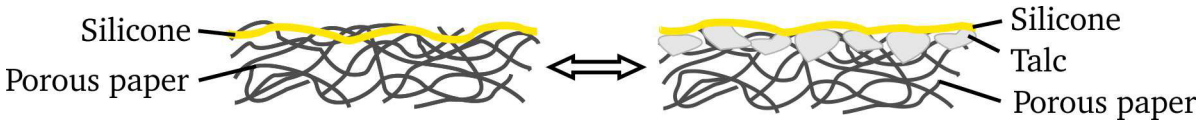

Scheme 13: Schematic representation of silicone penetration into paper without any pigments (left) and with talc particles (right).

6.1.1 Roller coating of solvent-free silicone/talcum mixtures on porous papers

In previous experiments performed by Sappi, water-based silicone was mixed with talcum and used as release coating. Nevertheless, solvent-free silicone may also be mixed with talcum and applied on base paper to reduce release forces compared to pure silicone coating. SEM images of talcum (Talcum T1 CA) features particle sizes ranging from 4-12 μm (see Appendix, Figure 109). This talcum is named as talcum (8 μm) in further experiments. Solvent-free silicone was mixed with 20wt% or 40wt% talcum (8 μm), respectively and coated on porous base paper by roller coater using stainless steel roller at constant coating conditions (110 N, 2 $^{m}/_{min}$). This coating method was used instead of blade coating in order to obtain low coat weights. It can be seen that the coat weight is raised with increasing talcum

content, because more talcum is transferred to the paper (Figure 61, A). In addition, talcum has a higher density (2.8 g/cm³ [120]) compared to silicone (1.0 g/cm³ [111]) which also increases the coat weight. About 0.3 g/m² more coating were transferred to L40 compared to L90 which was previously observed and is most likely due to a different sizing of the base papers. It has to be mentioned that the talcum was poorly transported from the storage pan to the roller in the solvent-free silicone and finally to the paper. Huge part of the talcum settled down in the storage pan during coating. Thus, just a minor part of the talcum was transferred to the paper. This may explain that release forces of papers coated with 20wt% and 40wt% are similar compared to the reference without any talcum (Figure 61, B). Release forces of about 3.5 N/25 mm were obtained for siliconized L40 as well as for silicone mixtures with talcum (8 µm). Higher release forces were measured for coated L90 papers (6.0 N/25 mm), because less silicone was transferred compared to L40. These specific release forces are too high for release liner applications. Moreover, the standard deviations were increased when talcum is mixed to the silicone. This may originate from a rougher surface due to the talcum pigments. SEM analysis of siliconized base papers show that the paper surface is just partially closed by silicone and many open pores remained (Figure 62). Some pigments can be seen on the cellulose fibers when the silicone is mixed with talcum, but most talcum particles stayed in the storage pan and just minor part was transferred to the paper. Thus, the paper surface was not closed to more extent when talcum is added to the silicone and huge part of the silicone penetrates into the paper. The adhesive tape is able to creep into the paper pores which leads to high release forces as discussed above. Thus, mixtures of solvent-free silicone with talcum can not be used in order to produce a release liner with appropriate release forces.

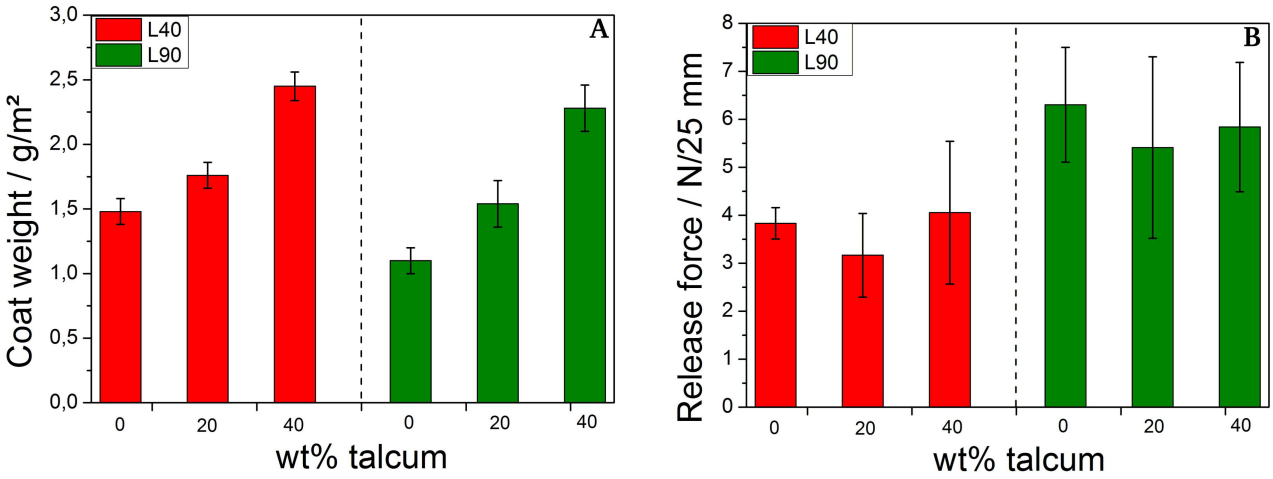

Figure 61: Influence of talcum content on the coat weight (A) and on release forces (B) of L40 and L90 base papers. The silicone coat weights of L40 papers are about 0.3 g/m² higher compared to L90.

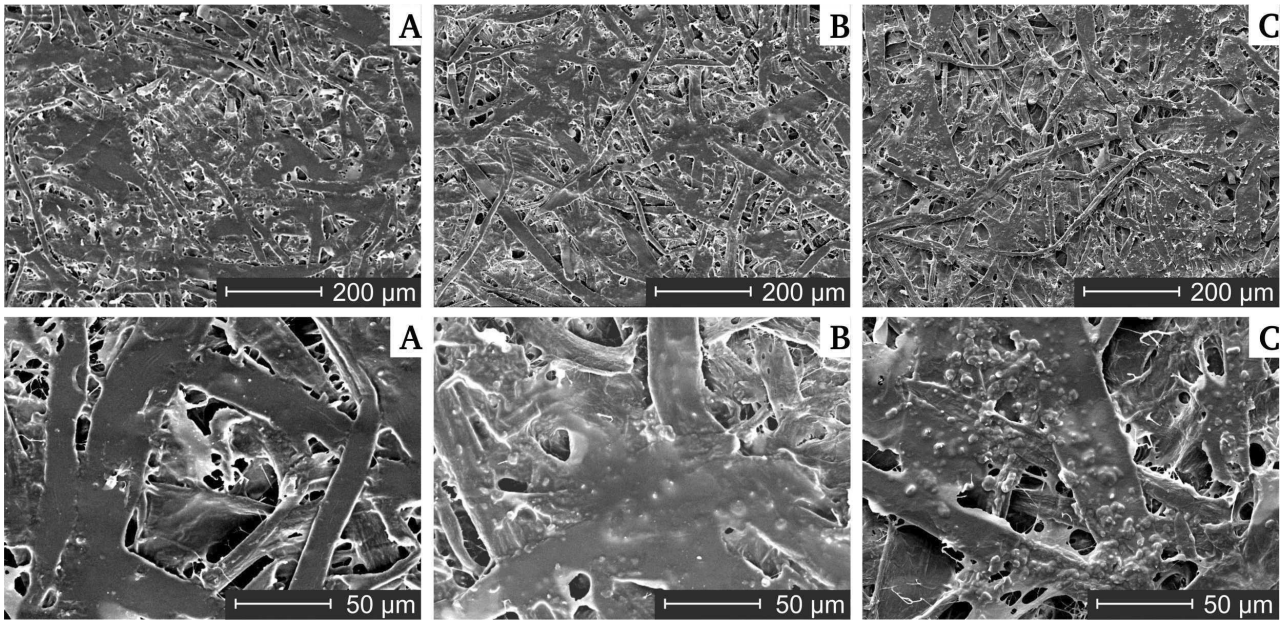

Figure 62: SEM images (topview) of L40 coated with pure silicone (A), silicone + 20wt% talcum (8 μm) (B) and silicone + 40wt% talcum (8 μm) (C). Most silicone is pushed into the paper pores and the paper surface is just partially closed by the silicone mixtures.

6.1.2 Roller coating of water-based silicone on various papers

In another experiment, water-based silicone was mixed with talcum (8 μm) and applied on the porous base papers by roller coater. The solid content of this specific silicone was determined to about 50wt% by a drying balance. The water-based silicone showed an instability in film formation on the rollers, which is known in literature as ribbing (Figure 63).[121,122] This formation of stripes originates from hydrodynamic effects of the coating. The tendency to form ribs can be estimated by the capillary number. In general, a higher capillary number, which is correlated to a higher coating speed, as well as a high viscosity and low surface tension support the formation of a ribbing structure.[123–125] This phenomenon may result in an inhomogenous coating film on the paper, which has to be investigated.

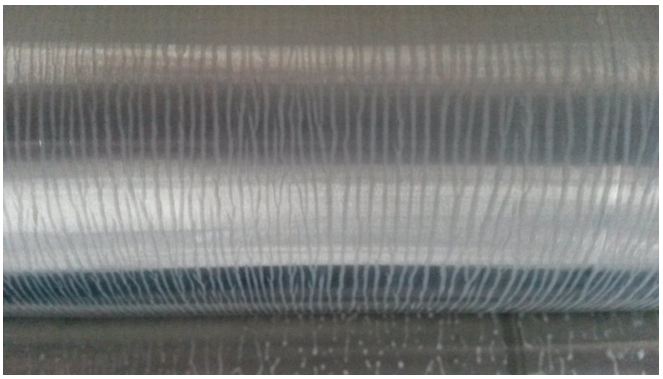

Figure 63: Incomplete wetting of the stainless-steel rollers by water-based silicone due to ribbing effects.

First, the influence of the roller pressure between dosing roll and applicator roll on the silicone coat weight was studied in order to adjust the silicone coat weight. As one can infer from figure 64, the silicone coat weight is increased with decreasing roller pressure for all paper samples.

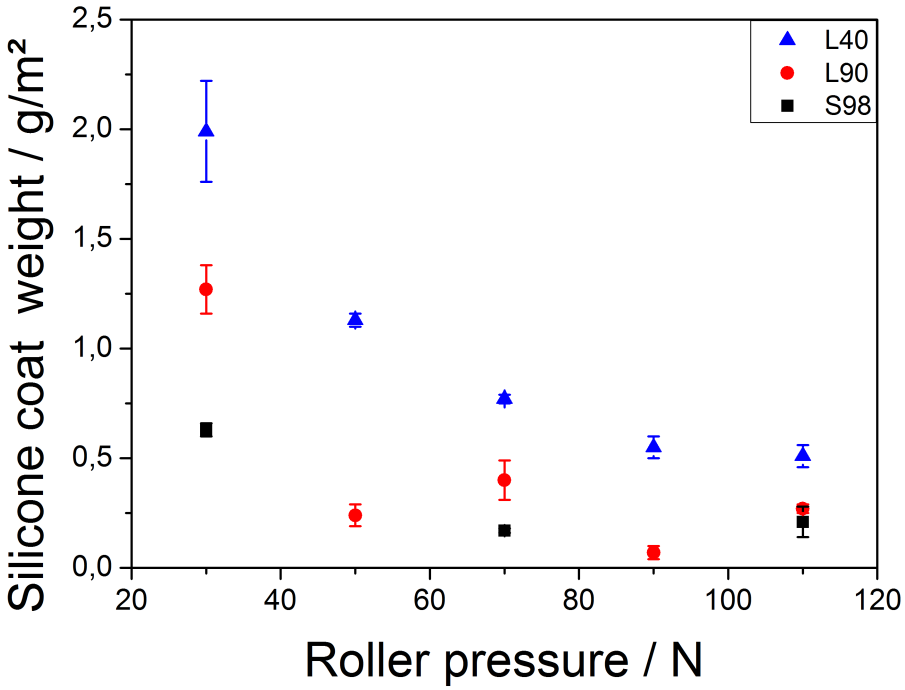

Figure 64: Influence of roller pressure between the dosing and applicator roll on the silicone coat weight of water-based silicone on various paper substrates.

More silicone is transferred from the dosing roll to the applicator roll, if the pressure between them is reduced. This was also observed when applying solvent-free silicone. Thus, water-based silicone coat weight can be adjusted by changing the roller pressure. The amount of how much silicone is transferred from the applicator roll to the paper surface depends on the paper substrate. Considering a similar roller pressure, most silicone was coated on L40 paper, followed by L90. As for the solvent-free silicone, the different silicone transfer rates of L40 and L90 is presumably due to a different surface sizing. Lowest amount of silicone was transferred to the CKK paper S98, because the paper surface is closed by pigments and just small pores remain. Thus, small amount of silicone is absorbed by the paper. The silicone coat weights at 50 N and 90 N for L90 should be closer to coat weights of L40. This probably occurred due to inhomogeneous silicone distribution on the roller during coating process. Significant less silicone is applied to the paper compared to the solvent-free silicone. One reason is a lower solid content of the water-based silicone and another reason may be the instability in film formation on the roller. In order to investigate the silicone coverage on the surface, papers were analyzed by SEM (Figure 65). It can be seen that a huge part of the paper is covered by silicone. Nevertheless, all paper samples show an inhomogeneous coating which is displayed by uncoated stripes on the paper surface. These stripes were previously observed on the roller during coating process and transferred to the paper.

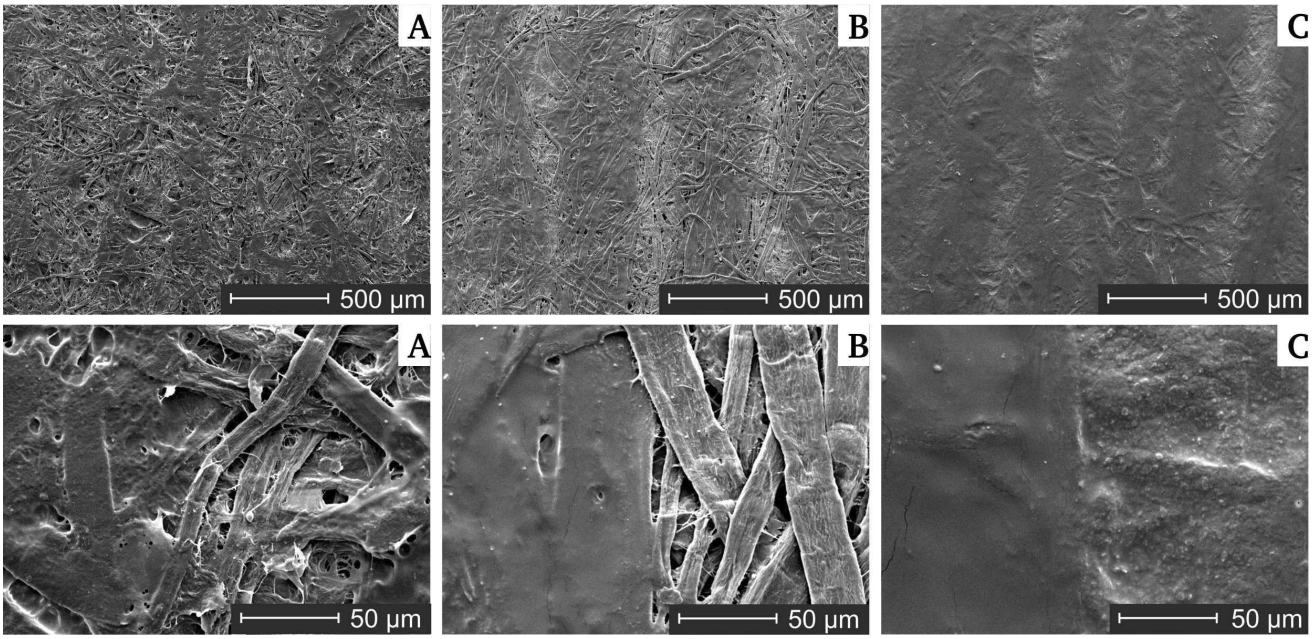

Figure 65: SEM images (topview) of L40 (A), L90 (B) and S98 (C) coated with water-based silicone at 30 N roller pressure and 2 $^{m}/_{min}$ coating speed at different magnifications. Papers are inhomogeneously coated by the silicone due to ribbing on the rollers.

Still, release forces of papers which were coated by water-based silicone were measured (Figure 66). Release forces were reduced, if the silicone coat weight is increased. This behavior was also observed for solvent-free silicone. The adhesive tape is in contact to silicone to more extent when the silicone coat weight is increased. This leads to lower release forces. Additionally, paper pores are closed by the silicone and penetration of the adhesive tape into paper pores is diminished. Nevertheless, peel-off forces of papers which were coated by water-based silicone are high and errors are large compared to similar coat weights of solvent-free silicone systems. For example, about 2 g/m^2 solvent-free silicone is necessary to obtain release forces of 2 $N/25\ mm$. For those release forces, silicone coat weights between 3 and 4 g/m^2 of the water-based silicone are required. Even the CCK paper S98 which does not have large big paper pores shows high release forces in the range of 4 to 9 $N/25\ mm$. In this case, it has to be mentioned that the maximum silicone coat weight was smaller than 0.8 g/m^2. Nevertheless, release forces of solvent-free silicone with similar coat weights are significant lower with respect to the water-based system, with one exception. The S98 paper which is coated with 0.7 g/m^2 showed release forces of 0.4 $N/25\ mm$ which is comparably low. The silicone coating on this paper was presumably more homogeneous leading to lower release forces and smaller standard deviation. It was not possible to measure the release forces of L40, because these papers suffer from a weak stability due to its low thickness and they were partially destroyed during peel-off. The biggest drawback of the water-based silicone system is an inhomogenous wetting of the rollers, which leads to an incomplete coating of the paper. The adhesive tape is coming into contact with parts of the paper which were not siliconized leading to a significant increase in release forces. In order to circumvent these limitations, 0.75wt% of hydroxyethyl cellulose (HEC) related to the amount of silicone was added as a surfactant in order to help improving roller wetting.

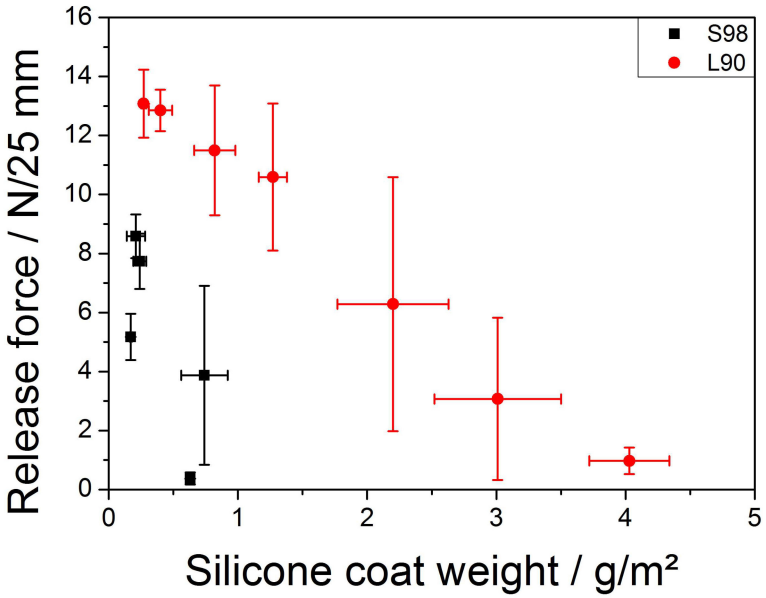

Figure 66: Influence of silicone coat weight on release forces. The release forces are reduced with increasing silicone coat weight.

Silicone coat weights were increased by about 0.2 g/m² by addition of HEC, but the rollers were still not completely covered by the water-based silicone (Figure 67). The higher silicone transfer is attributed to thickening effects of the silicone by the HEC. It can be seen from SEM images that the inhomogenous wetting on the rollers still leads to coating defects on siliconized S98 papers. Hence, it was not possible to ensure a homogeneous silicone coating by addition of HEC.

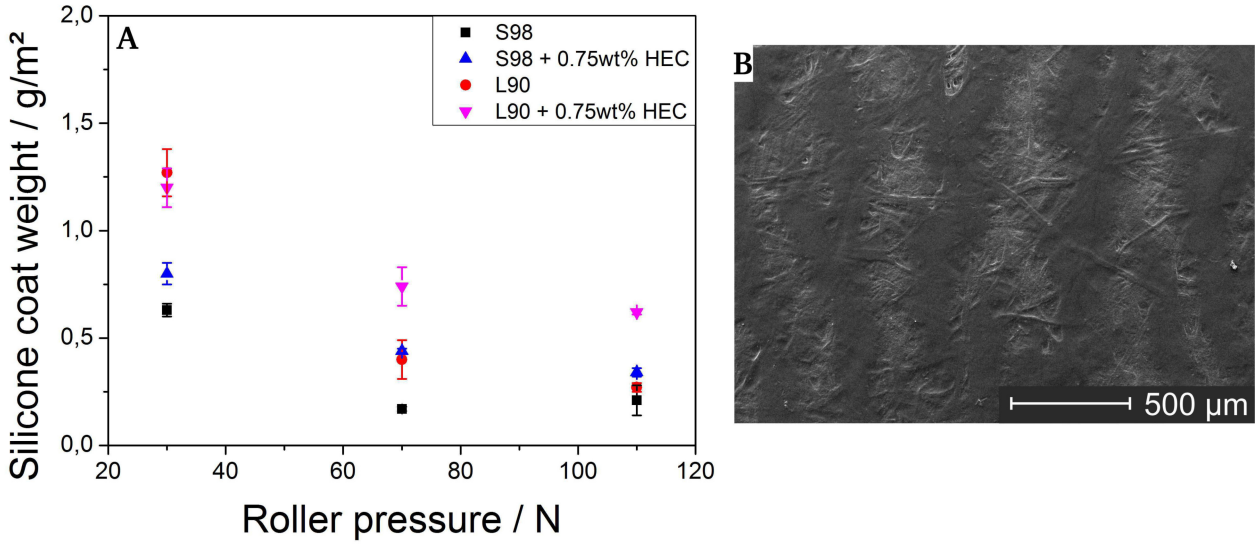

Figure 67: Influence of dispersion additive (HEC) on silicone coat weight (A). SEM image of siliconized S98 paper (B) with 0.75wt% HEC showing an inhomogenous coating.

Another approach in order to improve the coating homogeneity was performed by multiple coating cycles of S98 papers (Figure 68). The silicone coat weight was increased with every coating step and the release forces were significant decreased even after second coating cycle. This is attributed to more

homogeneous coverage of the paper by silicone, which was also shown by SEM analysis. Thus, the adhesive is in intimate contact with the silicone coating which results in low release forces. This method represents a way to obtain homogeneous silicone coatings by multiple coating cycles. Nevertheless, this method is in contradiction to the preceding aim in which two individual coating steps should be combined into one. Despite the fact, that the papers were insufficiently covered by pure silicone, talcum was added to the silicone and applied on paper in the next step. The coating homogeneity may be improved by the addition of talcum, because it will also positively influence the rheological properties of the silicone coating formulation.

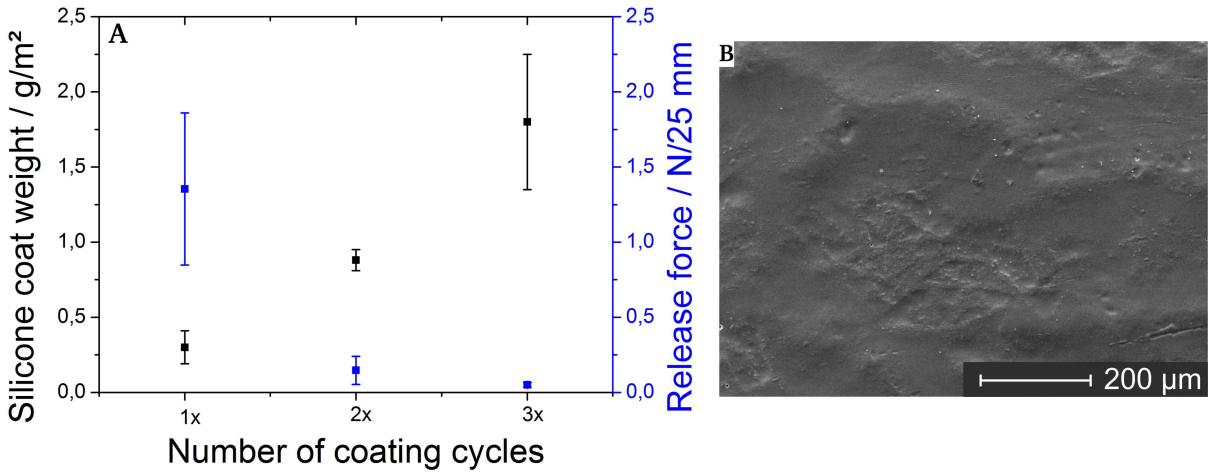

Figure 68: Influence of multiple coating cycles of S98 on silicone coat weight and release forces (A). Papers were coated at 30 N and 2 m/min by using stainless-steel rollers. SEM micrographs (topview) of S98 paper after third coating cycle (B). Voids in the silicone coating are still visible

6.1.3 Roller coating of water-based silicone/talcum mixtures on different paper substrates

After detailed investigations of the coating procedure of water-based silicone and the influence on coat weights and release forces, the silicone was mixed with different amounts of talcum (8 μm) in the next step. Porous L90 paper was coated by silicone/talcum mixtures containing 20wt% and 40wt% talcum related to the amount of silicone. The mixtures were also applied on clay-coated S98 paper as a reference in order to investigate the influence of talcum content on release forces on a closed paper surface. As one can infer from figure 69, A, the coat weight is raised with increasing talcum content for both papers. More coating is transferred to L90 as compared to S98, because the silicone mixture is pressed into the open pores of the paper. Maximum coat weights of about 2 g/m² were achieved for S98 and about 5 g/m² for L90 with a talcum content of 40wt%. It has to be considered that 60% of the coat weights are attributed to the silicone amount. Thus, papers coated with 40wt% talcum contain about 1.2 g/m² silicone for S98 or about 3 g/m² silicone for L90, respectively. This calculation is valid with the assumption that the silicone/talcum mixture is transferred in the same ratio to the paper as in the storage pan. Indeed, sedimentation of the talcum in the storage pan was not observed in contrast to the solvent-free silicone. This is because talcum has a high affinity to water and the water is adsorbed from the talcum particles

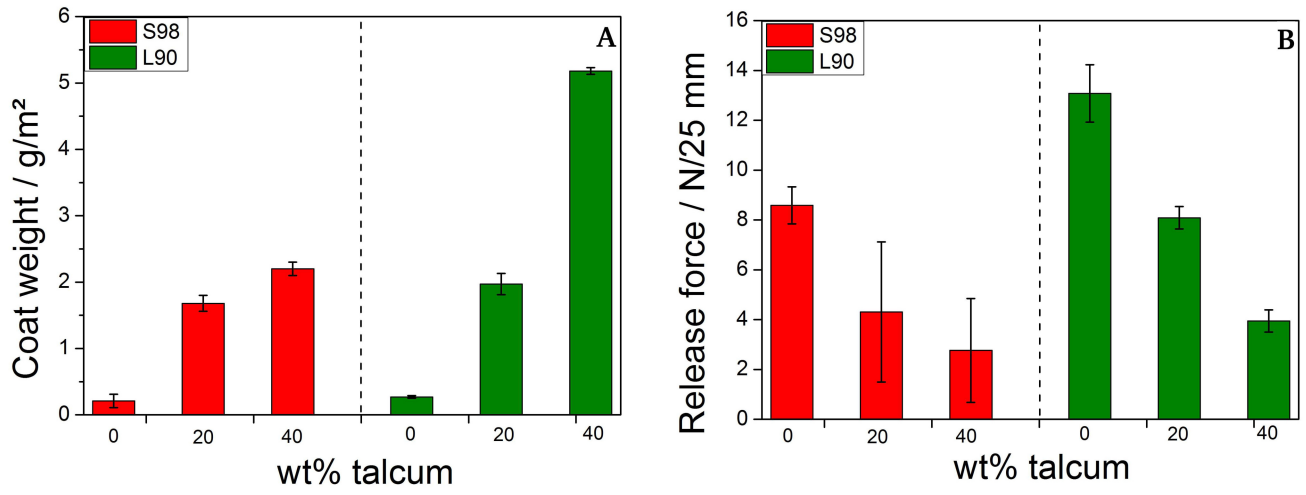

Figure 69: Influence of talcum content on the coat weight (A) and on release forces (B) of S98 and L90 paper. Coatings were applied by roller coater at 2 m/min coating speed and 110 N roller pressure. The release forces are reduced with increasing coat weight.

leading to a stable suspension.[126] The viscosity of the silicone is also increased when talcum is added. This leads to higher coat weights, because more coating is transported by the rollers to the paper.

In the next step, the release forces of the coated papers were studied (Figure 69, B). The release forces were reduced with increasing talcum content for both papers, because more silicone is transferred to the paper and the silicone stays on the surface in most parts. SEM analysis of the coated papers shows that the porous surface of L90 is increasingly closed with higher talcum content, but paper surface still exhibits some open pores (Figure 70).

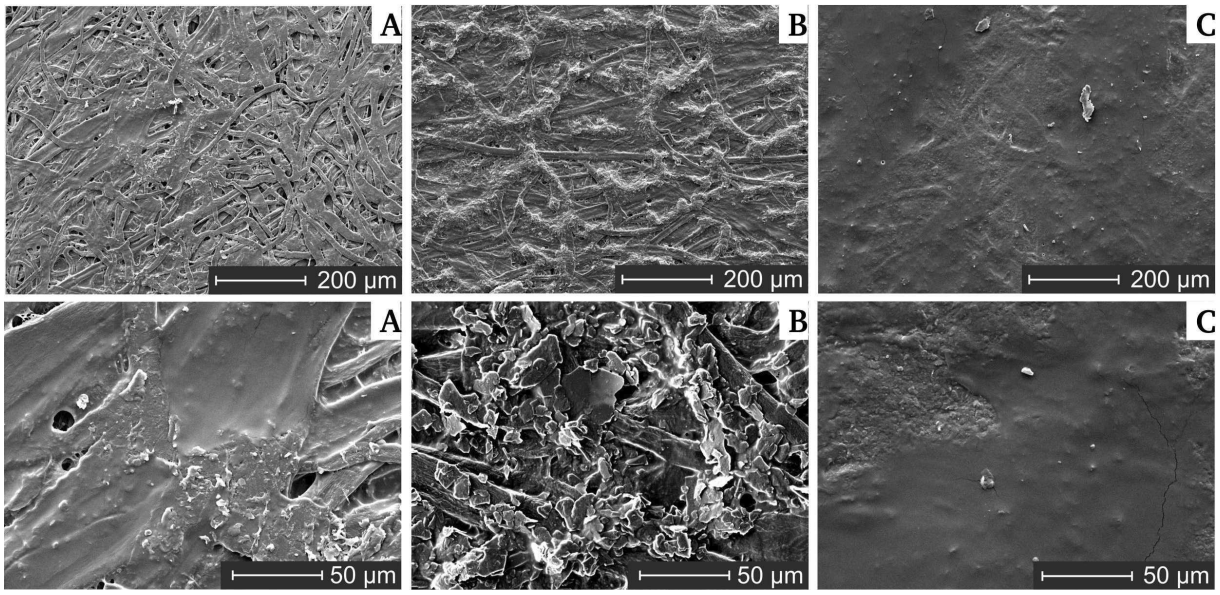

Figure 70: SEM images (topview) of L90 coated with mixtures of water-based silicone and 20wt% talcum (8 μm) (A), 40wt% talcum (8 μm) (B) and S98 coated with water-based silicone and 40wt% talcum (8 μm) (C) at 110 N roller pressure and 2 m/min coating speed at different magnifications.

The coating is mechanically retained on the paper surface to more extent due to the talcum particles. Furthermore, flow of the coating mixture into the paper is diminished by the increased viscosity. Despite the fact that the paper pores are closed in most part, release forces of L90 with 40wt% talcum of about 4 N/25 mm are still high compared to common silicone release liner. This may be explained, because paper roughness is increased by the talcum particles which was observed in SEM images. It seems that the talcum particles accumulate leading to a rough surface. Thus, the contact area of the adhesive tape to the paper surface is increased compared to a smooth siliconized CCK paper which may lead to higher release forces. Additionally, the adhesive penetrates into some small open pores, which results in high release forces. Nevertheless, the error of release forces is significantly reduced compared to coated paper with pure water-based silicone (Figure 66) comparing same coat weight of 3 g/m². This is because the silicone is retained on the paper surface to more extent and paper pores are blocked.
As a reference experiment, release forces of talcum/silicone mixtures on a smooth clay-coated paper (S98) were studied (Figure 69). It can be seen, that release forces were reduced with higher coat weights but the errors were increased. Lower release forces were obtained, because the paper surface is covered by silicone to more extent. Nevertheless, some uncoated areas on the paper occur which lead to huge errors.
Additionally, the rollers were still not complete covered by the coating mixture (Figure 71) and the mixture leaked out of the storage pan, especially at 40wt% talcum content due to the high viscosity. Nevertheless, other talcum particles with an averages particle size of 2 μm and 4 μm were mixed with silicone and coated on paper by roller coater in order to investigate the release forces. Smaller particles may lead to a stable suspension and improved wetting of the rollers. Maximum talcum content of 10wt% for talcum (2 μm) and 20 wt% for talcum (4 μm), respectively were used for paper surface coatings. Mixtures of higher talcum content were not applicable, because of high viscosity and leaking issues.

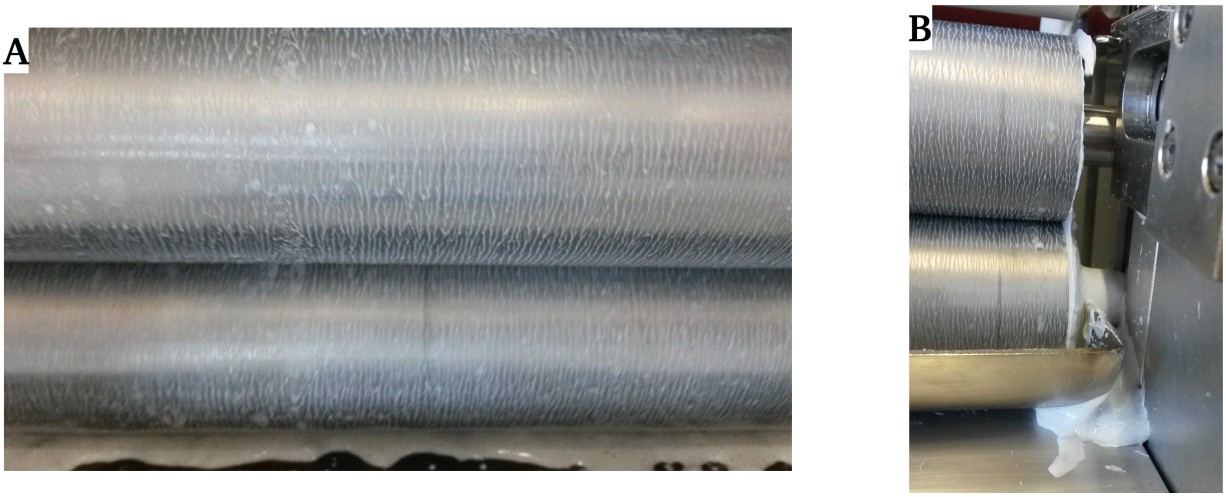

Figure 71: Incomplete wetting of the stainless-steel rollers by water-based silicone due to ribbing effects (A). Mixture of water-based silicone and 40wt% talcum (8 μm) is leaking out of the storage pan during coating (B).

In order to study the influence of different talcum particles on release forces, coat weights of about 2 g/m² were compared (Figure 72). The rollers were still not homogeneously wetted by the coating. Nevertheless, all release forces were reduced, once talcum is added to the silicone with respect to the reference (0wt% talcum). Especially, talcum (2 μm) and talcum (8 μm) reduce the release forces from 12 N/25 mm to 8 N/25 mm, respectively. Silicone coverage is improved by addition of talcum and the adhesive/silicone contact area is increased leading to lower release forces. Additionally, many paper pores are closed by the coating and penetration of the adhesive tape into paper pores is reduced.

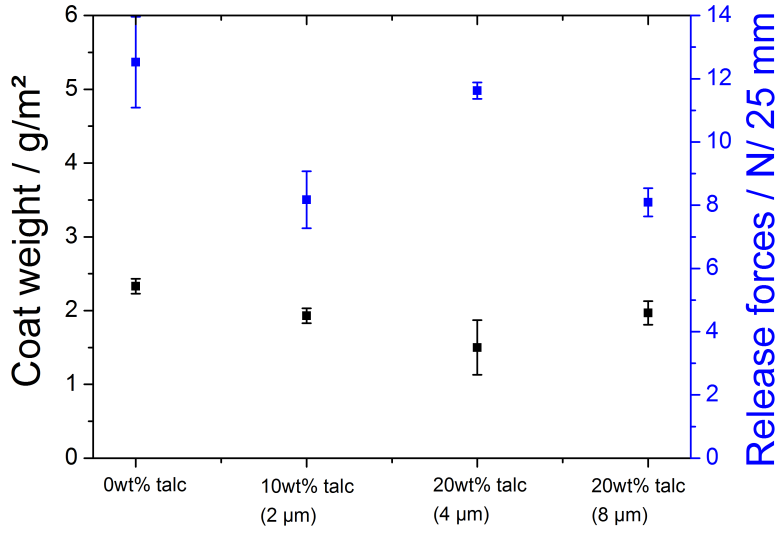

Figure 72: Coating of water-based silicone mixed with different talcum particles on L90 papers and determination of the release forces.

Analysis of the coated paper surface by SEM presents the paper surface which is covered by pure silicone (Figure 73, B) or silicone/talcum mixture (Figure 73, A). The paper surface with the talcum mixture seems to be rougher which is induced by the particles. The resulting release forces of 8 N/25 mm are too high for release liner applications. High release forces were induced by the arising micro-roughness and open pores on the paper surface. Additionally, the inhomogeneous wetting of the roller lead to defects in the coating. Thus, this coating procedure is less appropriate for coating of silicone/talcum mixtures. The mixtures have to be applied on paper by blade coating method in order to overcome these issues.

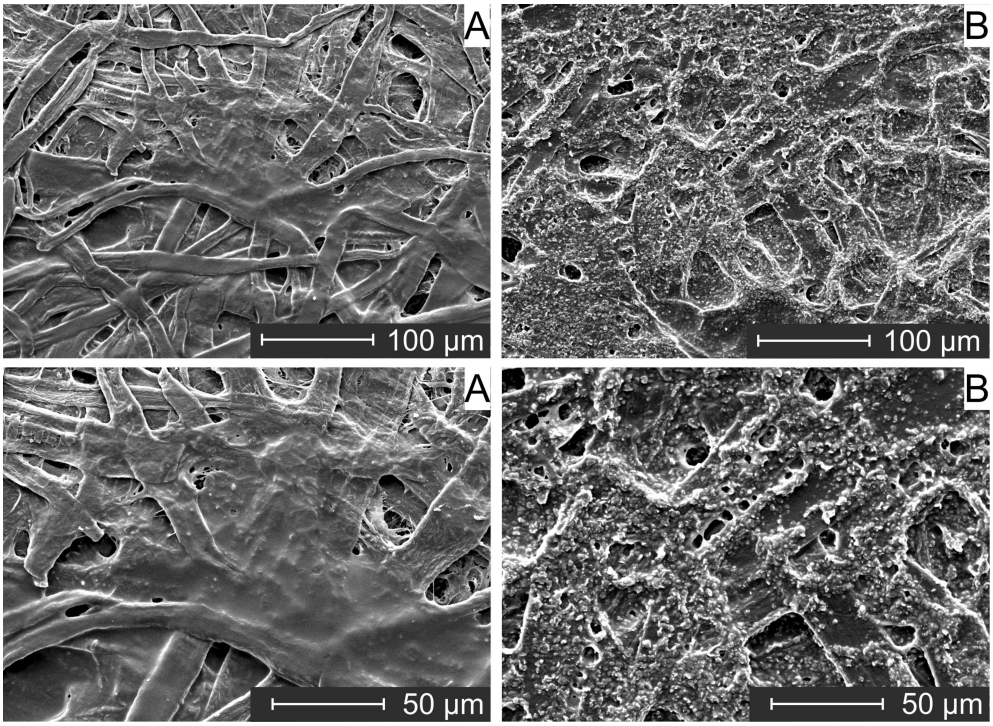

Figure 73: SEM images (topview) of L90 paper coated by roller coater (30 N, 2 $^{m}/_{min}$) with water-based silicone (A) and silicone mixed with 10wt% talcum (2 μm) (B) at different magnifications.

6.1.4 Blade coating of water-based silicone/talcum mixtures on different paper substrates

The mixtures of water-based silicone and talcum were not homogeneously applied on the paper surface by roller coater, because of an inhomogeneous coverage of the rollers. Thus, in order to receive better coating results, water-based silicone mixed with various talcum particles was applied by blade coater first on L90 papers. For this, the blade with the smallest gap size of 50 μm was selected in order to obtain low coat weights. Water-based silicone coating without any talcum gave a coat weight of about 9 $^{g}/_{m^2}$, which is high compared to common coat weights in release liner applications (1 $^{g}/_{m^2}$) (Figure 74). As a result of the high coat weights, the release forces were very low and comparable to siliconized CCK papers. Analysis of the coated paper surface by SEM showed that almost all pores were closed by the silicone (Figure 75, A). Thus, the adhesive tape is in complete contact with silicone and penetration of the adhesive into open paper pores is prevented. If talcum was added to the silicone, the coat weight was increased in all cases due to a higher viscosity. It has to be mentioned that maximum talcum content of 10wt% was applicable for talcum with a particles size of 4 μm and 2 μm, respectively. Higher concentrations were not suitable for blade coating, because the coating mixture got stuck on the blade and the coating was not transferred to the paper surface. The talcum should reduce silicone penetration into the paper and should lead to a closed paper surface. This behavior could not be confirmed by this measurement, because paper pores were blocked even if the paper was coated by silicone without any talcum. Even more, the release forces were slightly increased to about 0.5 $^{N}/_{25\ mm}$, if talcum is added to the silicone. This is probably due to a rough surface which is depicted in the SEM images (Figure 75, B). The coat weight has to be further reduced by using blades with smaller gap sizes in order to investigate the ability of the talcum to prevent silicone penetration into the paper. The lab blade coater in our

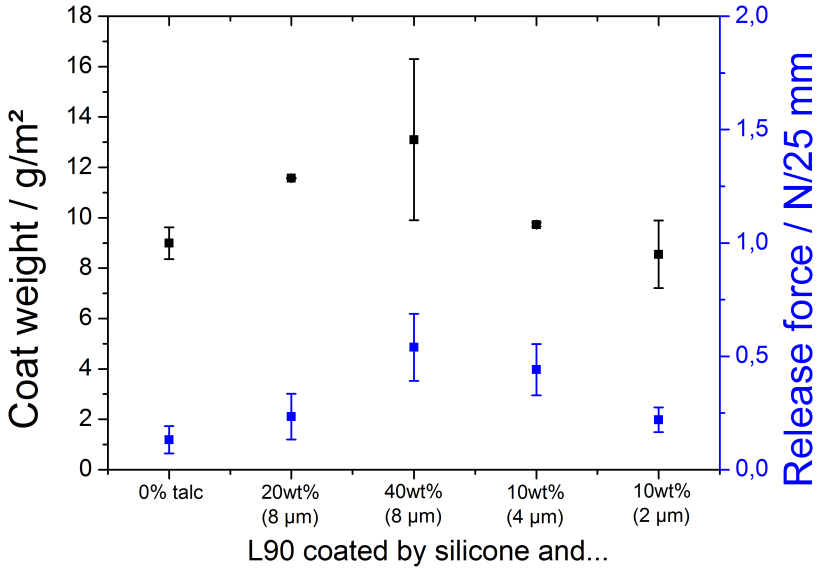

Figure 74: Application of mixtures of water-based silicone and different sorts of talcum by blade coater (50 μm, 50 mm/s) and determination of the release forces.

institute is not appropriate in order to reach low coat weights in the range of 1-2 g/m². The preceding experiments showed that talcum can be used as a viscosity modifier in order to reduce penetration of the silicone into the paper. Thus, as a last step the influence of the different talcum sizes on the viscosity will be analyzed.

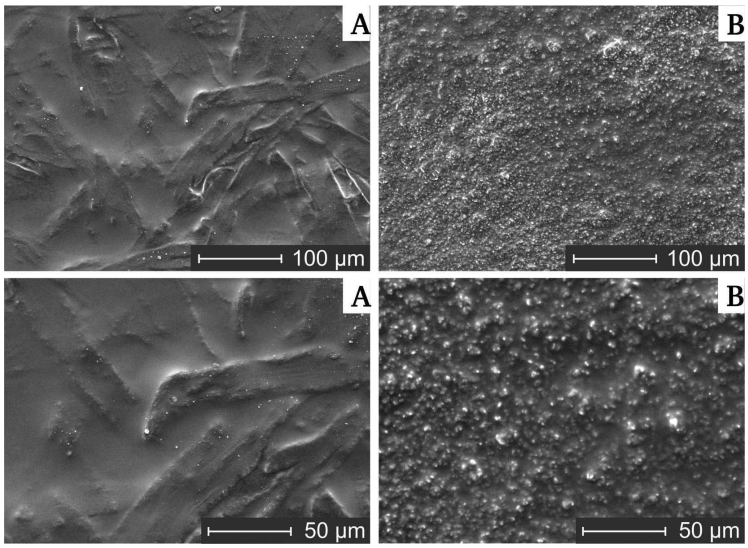

Figure 75: SEM images (topview) of L90 paper coated by blade coater (50 μm, 50 mm/s) with water-based silicone (A) and silicone mixed with 10wt% talcum (2 μm) (B) at different magnifications.

6.1.5 Determination of viscosity of silicone/talcum mixtures

The viscosity of the water-based silicone and silicone/talcum mixtures at different shear rates was investigated by Brookfield viscometer (Figure 76). The shear rate correlates with the spindle speed. An increase of the spindle speed leads to an increase of the shear rate. The pure silicone has the lowest viscosity of about 150 mPas at slow spindle speed (15 rpm). The viscosity is decreased to about 60 mPas at 120 rpm. The addition of talcum leads to a significant increase of the viscosity, especially at low shear rates. The effect of the talcum on the viscosity is less distinct at high shear rates. All mixtures show a decreasing viscosity with increasing shear rate which corresponds to a thixotropic behavior. Highest viscosity of about 27.000 mPas was obtained for the silicone/talcum mixture with the highest solid content of 40wt% talcum (8 μm), followed by 10wt% talcum (2 μm) with a highest viscosity of 18.000 mPas. This mixture contains 30wt% less talcum but the talcum with the smallest particle size has the highest surface area and thus the strongest impact on the viscosity. The viscosity is mainly governed by the particle size and particle size distribution, but it is also influenced by the particle shape.[127] The impact of particle size on viscosity is also visible when comparing the viscosity of 10wt% talcum (4 μm) and 20wt% talcum (8 μm). The viscosity of the smaller talcum particles is higher compared to 20wt% talcum (8 μm), although double amount of talcum is mixed with the silicone. The mixtures of 40wt% talcum (8 μm) and 10wt% talcum (2 μm) with silicone seems to be the best one in order to reduce silicone migration into the paper due to a high viscosity. Thus, the latter mixtures should be used for further experiments after optimization of the coating process in terms of homogeneous coating and low coat weight, respectively.

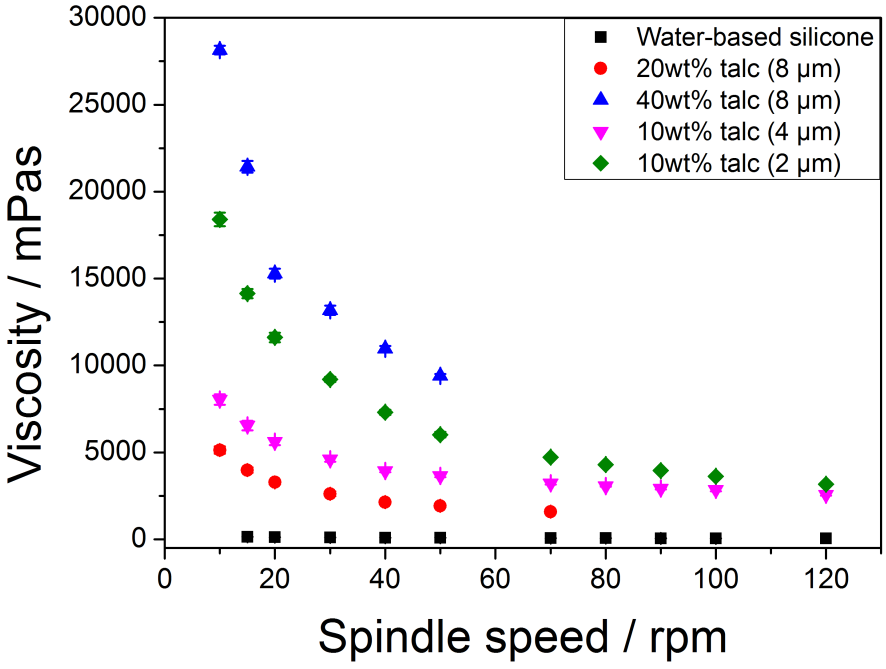

Figure 76: Determination of the Brookfield viscosity of different mixtures of water-based silicone and talcum at 25°C.

6.2 Siliconization of pre-coated base papers

In previous experiments, it was shown that closing paper pores is essential in order to receive low release forces. Penetration of the adhesive tape into paper pores has to be prevented so that the adhesive is not able to mechanical interlock with the paper, leading to high release forces. Additionally, the adhesive will not come in contact with parts of the paper which were not covered by silicone. The siliconized surface should be as smooth as possible because roughness increases the release forces due to an incomplete silicone coating.

As a next strategy, we focused on polymeric pre-coatings prior to siliconization. The paper pores should presumably be closed by polymeric pre-coats. These specific pre-coats should act as a barrier in order to prevent silicone absorption into the paper afterwards. The silicone should stay on the paper surface and a homogeneous layer should be formed. In detail, synthetic polyvinyl alcohol with degree of hydrolysis of 88% (PVA88%) and 99% (PVA99%) as well as bio-based hydroxyethyl cellulose (HEC) and methyl cellulose (MC) are used in order to close the paper surface. The pre-coat should substitute the more complex clay-coating. The polymers should carry OH-groups that the cellulose fibers are able to generate hydrogen bonds to the coating and increase film stability. The solvent-free silicone will be used for the experiments because no complications showed up during coating process with this specific silicone system and it is commonly used in industry. The following results were partially published in Cellulose in 2018.[98]

6.2.1 Applying pre-coats by a roller coater

The polymeric pre-coats (HEC, MC, PVA88%, PVA99%) were dissolved in water at a concentration of 7 wt%. Polymer concentrations above 7 wt% could not be obtained because the polymers do not dissolve completely. The polymeric solutions were applied to the paper by roller coater. The pressure between the rollers was adjusted to 30 N in order to get the highest possible coat weight. After the first coating cycle, about 0.4 g/m^2 coat weight for L40 and 0.7 g/m^2 coat weight for L90 were obtained, which is rather low (Figure 77). Typical barrier coat weights of about 2.0 g/m^2[63] are used for glassine papers. Thus, the papers were coated multiple times by the polymers at one side under the same coating conditions (30 N, 2 m/min) in order to increase the coat weight. Both papers show a linear increase of the coat weight after several coating steps. The coat weight can be adjusted by the number of coating cycles by using this method.

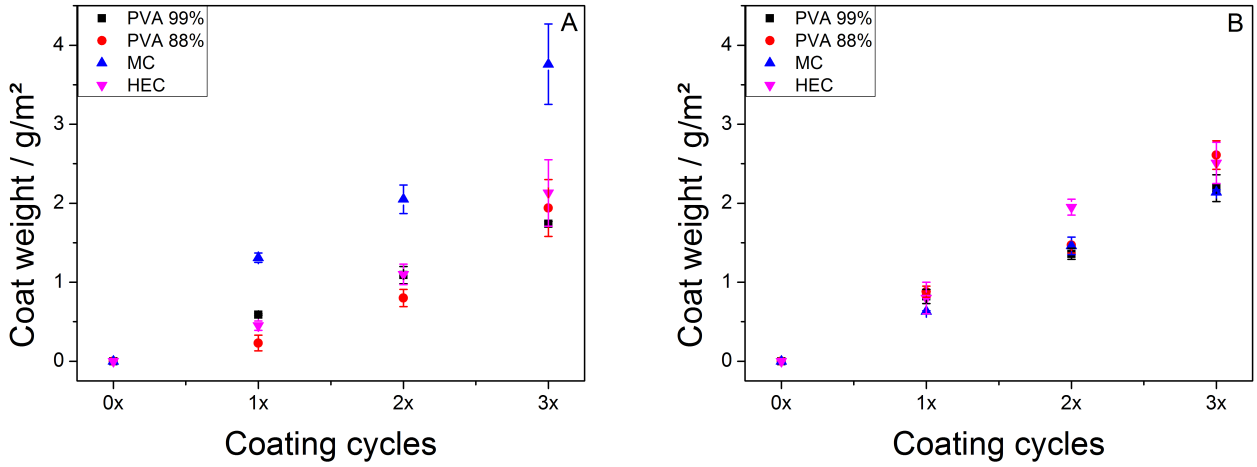

Figure 77: L40 (A) and L90 (B) papers are coated multiple times by a roller coater with various pre-coats (7wt%) in water under the same coating conditions (30 N, 2 m/min). The coat weights is increased with multiple coating cycles.

It can be taken from SEM images that the paper pores got closed to more extent, if multiple coating cycles were applied (Figure 78). It can be seen that less amount of polymer was transferred to L40 compared to L90 which is most likely due to the different sizing of the papers. This is in accordance to the preceding experiments, because more silicone was applied to L40 paper compared to L90 paper. However, coat weights of MC for L40 papers were significantly higher compared to the other polymers, which may be due to a different polarity and rheological property of the MC solution. The coat weights transferred to L90 papers were similar considering same coating cycles.

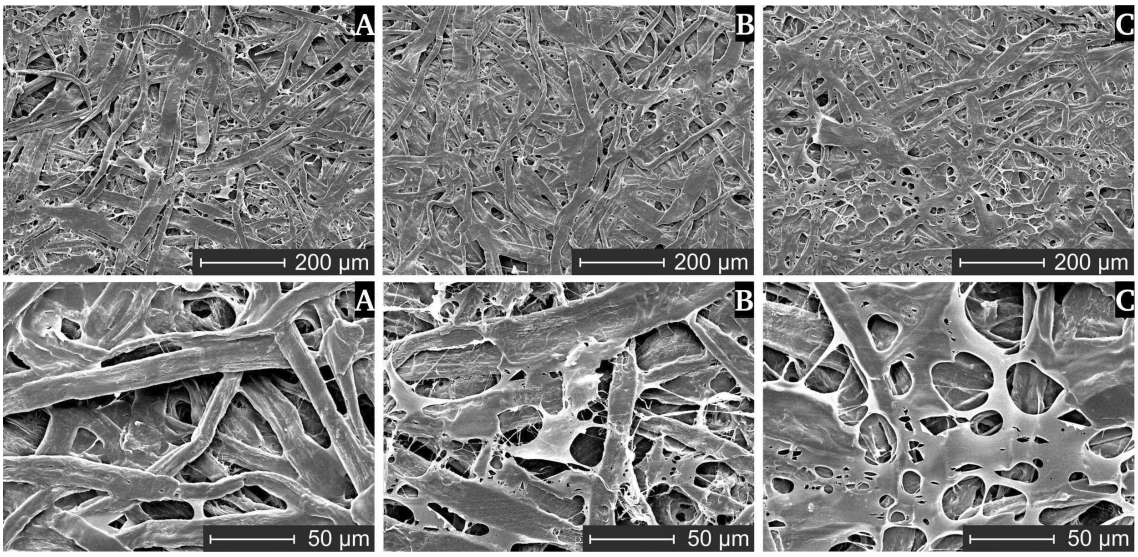

Figure 78: SEM images (topview) of L40 paper surface first coating cycle (A), second coating cycle (B) and third coating cycle with PVA88% (C). The papers were coated three times by a roller coater under the same coating conditions (30 N, 2 m/min). The paper surface is increasingly closed.

Higher coat weights could be obtained by additional coating steps, but the paper got stuck to the roller after a third coating cycle which led to partial creasing of the paper sheet. The coat weight may also be increased by changing the roller material from stainless-steel to a soft material, because the rollers can be deformed to more extent. It has to be mentioned that the stainless steel roller were not completely wetted by the polymeric solutions, which was also previously observed for the water-based silicone. This phenomena is attributed to an instability in film formation, also known in literature as ribbing.[121,122] Thus, the homogeneity of the paper coating was studied by SEM analysis (Figure 79). The paper surface of the uncoated L90 paper possesses large pores (Figure 79, A). Many pores of the paper were closed after applying the film-forming HEC (Figure 79, B) or PVA88% (Figure 79, C). The bio-based HEC seems to be competitive to the synthetic PVA in terms of closing paper pores. SEM images of L90 papers coated by MC or PVA99% show similar results (see Appendix, Figure 110). Nevertheless, the surface of the paper was not homogeneously closed by the pre-coat and some open pores remain. The inhomogenous film formation on the paper is attributed to the instability in film formation on the roller. Additionally, the applied polymers may posses a different wetting behavior on the rollers, which may influence the homogeneity of the coating on the paper, too. However, this assumption could not be confirmed by SEM analysis. In order to overcome the inhomogenous roller wetting, papers were coated by a lab blade coater in the next step.

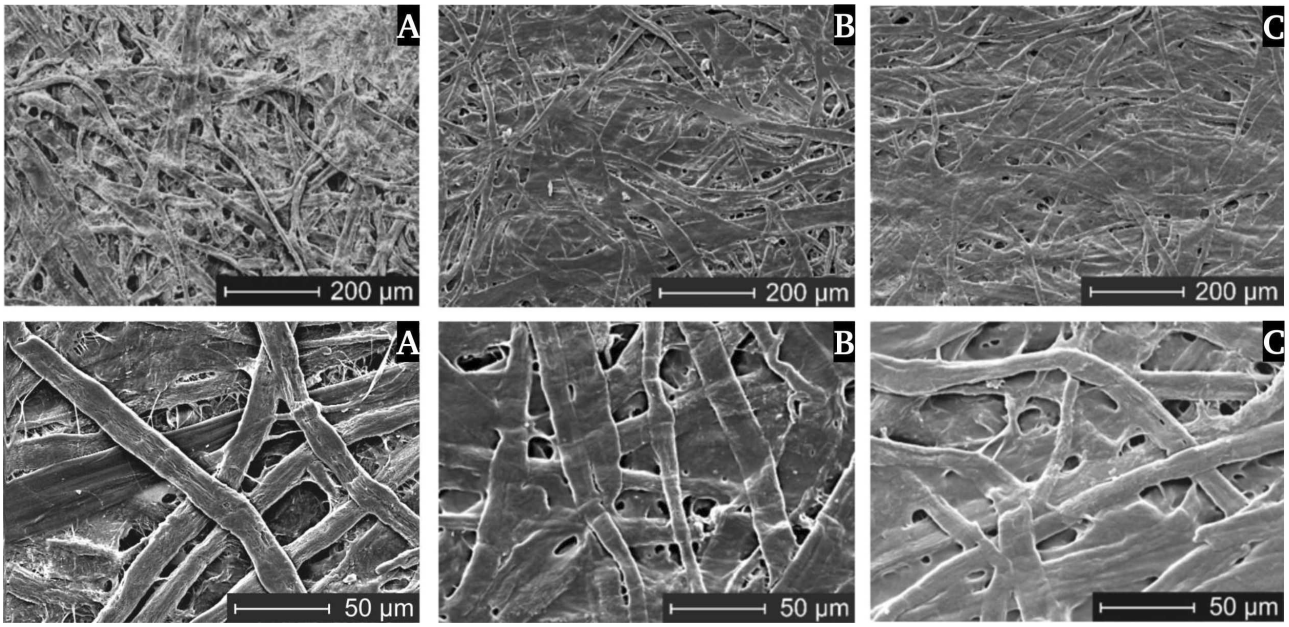

Figure 79: SEM images (topview) of L90 paper surface without any pre-coat (A), coated by 2.5 g/m² HEC (B) and coated by 2.6 g/m² PVA88% (C). The papers were coated three times by a roller coater under the same coating conditions (30 N, 2 m/min). Figure reproduced with permission from reference.[98]

6.2.2 Applying pre-coats by a blade coater

The polymers (PVA88%, PVA99%, HEC, MC) were again dissolved in water to a final concentration of 7wt% and applied on the base papers by a lab blade coater in a single step. The corresponding blade gap sizes of 50 μm and 100 μm were used in order to obtain coat weights in the range of 0.8 - 2.3 g/m^2. Investigations of the paper surface by SEM after coating showed that mainly all pores were closed by the polymeric pre-coat (Figure 80). In contrast to the coating results of the roller coater, in this case, the paper surface was more homogeneous covered by the barrier coating. This was also observed for pre-coated L40 papers. The fiber structure was still visible, but just small pores remain. The paper surface was in contact with the coating solution over the complete paper width during coating process. Thus, the whole surface was coated by the polymeric pre-coat and wetting issues of the roller coater could be circumvented. The bio-based polymers HEC (C) and MC (D) seem to close the paper pores as good as the synthetic PVA88% (A) and PVA99% (B). Penetration of the silicone into the paper was prevented and the silicone stayed on the closed paper surface in most parts. The silicone coating was applied on the pre-coated papers in the next step by using the roller in order to produce the release liner.

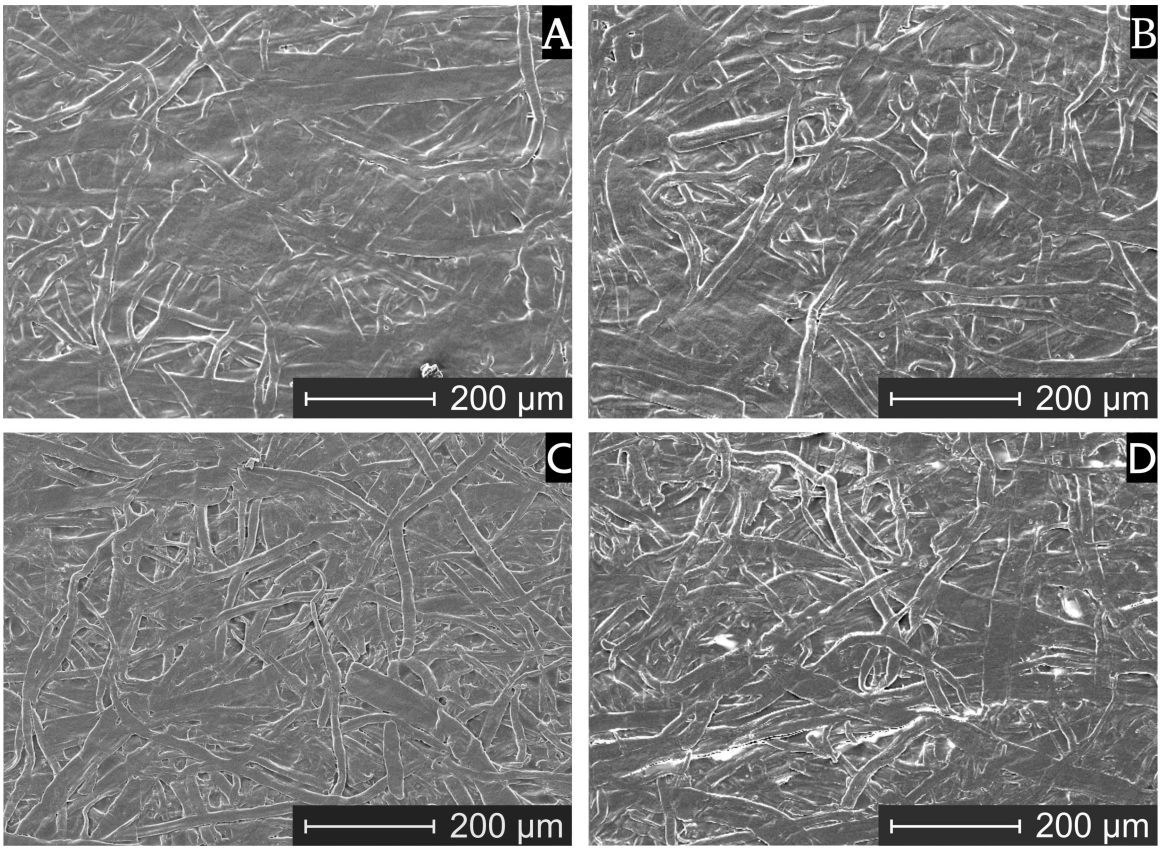

Figure 80: SEM images (topview) of L90 paper coated by PVA88% at 2.2 g/m^2 (A), PVA99% at 2.0 g/m^2 (B), HEC at 1.9 g/m^2 (C) and MC at 2.3 g/m^2 (D) by a blade coater at different magnifications. The paper surface is homogenously closed by the various polymers. Figure reproduced with permission from reference. [98]

6.2.3 Siliconization of roller-coated papers

The pre-coated papers applied via roller coater were coated with solvent-free silicone by using the roller coater (110 N, 2 m/min) in order to study the barrier properties of the used polymers. The silicone was thermally cured by IR-dryer and hot-air dryer (1 min at 150 °C). The silicone transfer was studied as a function of the coat weight of the pre-coatings. It can be seen from the figure that about 0.3 g/m² more silicone was transferred to the L40 paper (A) compared to L90 paper (B) (Figure 81).

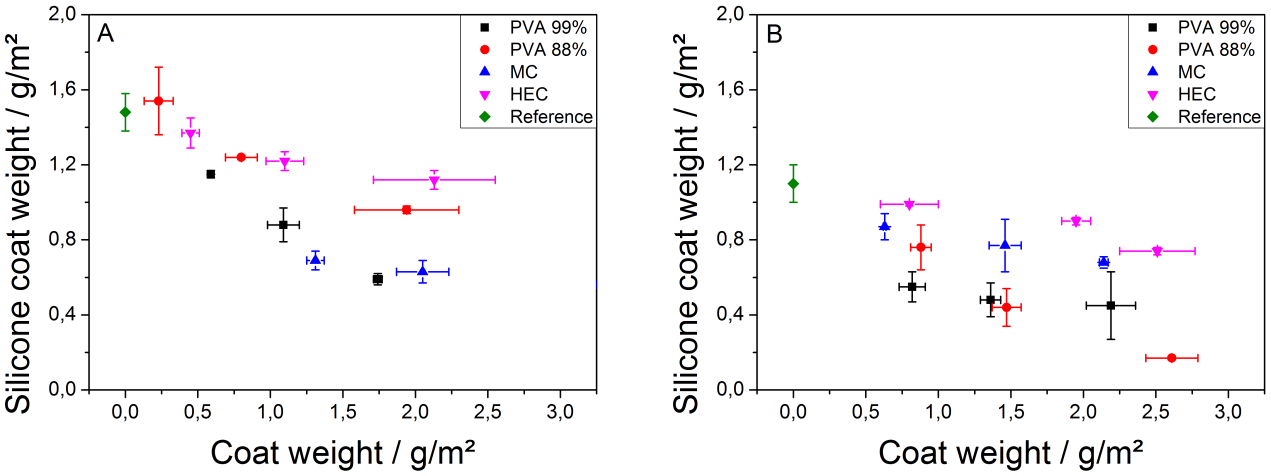

Figure 81: Influence of polymer pre-coat on silicone coat weight of L40 (A) and L90 (B) papers. The various pre-coats (7wt%) dissolved in water are applied by roller coater (30 N, 2 m/min) and the silicone was coated by a roller coater (110 N, 2 m/min). The silicone coat weight is decreased with increasing pre-coat weight.

This behavior is attributed to the different sizing of the papers as discussed before, because the paper was not homogeneously covered by the coating and open pores still remain. If silicone was applied on the pre-coated papers, the silicone coat weight was decreased with increasing pre-coat weight. For instance, the silicone coat weight was reduced from 1.5 g/m² for the untreated L40 paper to about 0.6 g/m² by using 2.0 g/m² PVA99% or MC. This specific behavior was observed for all pre-coated L40 and L90 papers and was independently from the used polymers for pre-coating. It seems that reducing silicone coat weight with increasing pre-coat weight is less distinct for HEC in contrast to PVA88%, which may be due to differences in surface chemistry. The coatability of the paper surface is most likely governed by surface energy and surface porosity[57]. The hydrophilic pre-coats on the paper surface may impair the wetting behavior of the hydrophobic silicone leading to less silicone transfer. Additionally, decreasing silicone coat weight on pre-coated papers may originate from a decreasing amount of open pores on the paper surface and a reduced surface porosity. As previously shown in SEM images, the paper pores were closed to more extent when an increasing amount of polymer was applied to the paper surface. Thus, less silicone was pushed into the paper pores leading to less silicone transfer compared to the reference.

SEM analysis of the paper surface showed that open pores remain on the untreated reference paper as well as for the pre-coated papers after siliconization (Figure 82). The adhesive tape may penetrate into these pores leading to high release forces. Nevertheless, the barrier properties of the pre-coat to

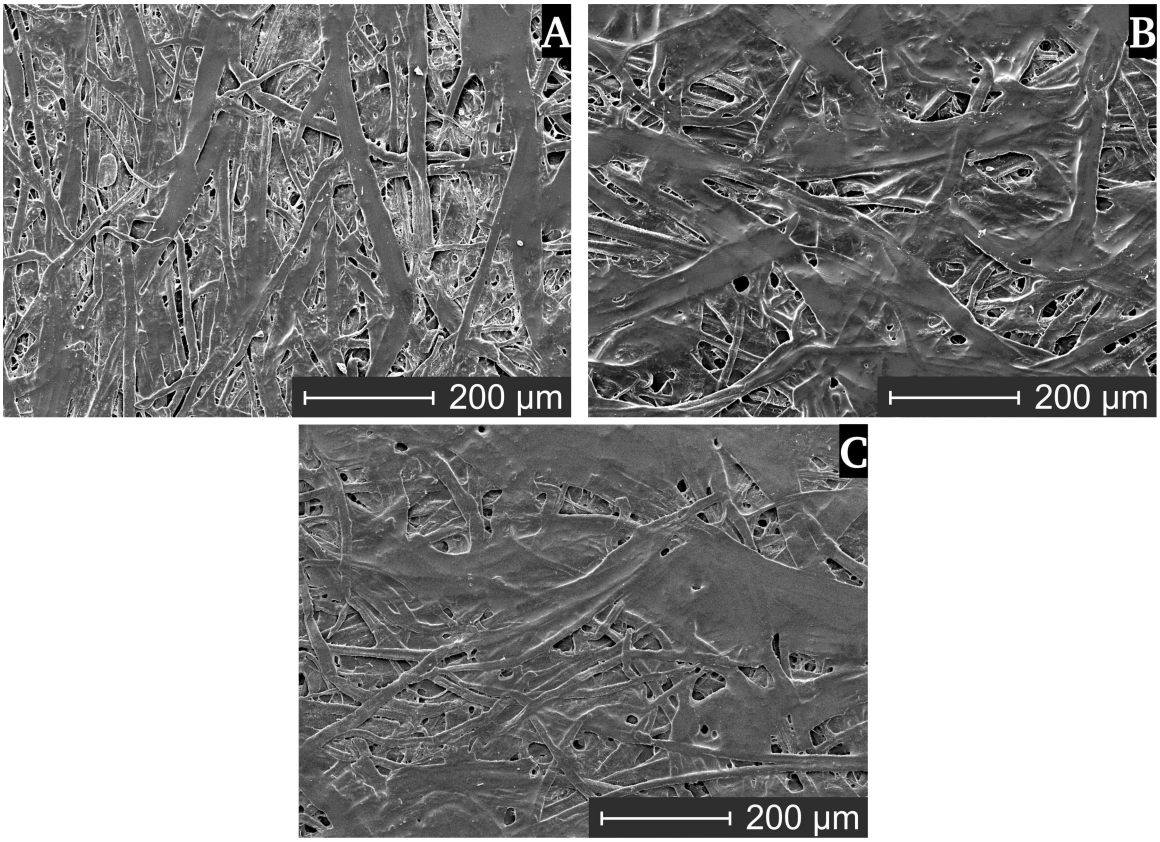

Figure 82: SEM images (topview) of L90 papers coated by silicone (1.1 g/m²) (A), L90 coated by HEC (2.5 g/m²) and silicone (0.7 g/m²) (B) and L90 coated by PVA88% (2.6 g/m²) and silicone (0.3 g/m²) (C). The pre-coatings and silicone were applied by roller coater. Figure reproduced with permission from reference. [98]

the silicone can be seen from the SEM images. Less silicone is absorbed by the paper, if a polymeric pre-coat was applied to the paper surface prior to siliconization step. In order to learn more about the the relationship between silicone transfer and surface wetting behavior, papers coated by PVA88% were used for reference experiments. This specific polymer was selected, because many studies in literature have been using this particular polymer. Base papers were coated by PVA88% and analyzed by static contact angle measurements (Figure 83).

The water contact angle of uncoated L40 base paper was about 10° higher compared to L90 base paper, which is attributed to the different used sizing agents. A hydrophobic contact angle (> 90°) was observed for both papers. The water contact angle changed from hydrophobic to hydrophilic, if the papers were coated by PVA88% (1.5 g/m²). In particular, the static contact angle of coated L40 paper was reduced by 50°, going from 122° to 72° (Figure 83, A). The hydrophobic sizing agent was overlaid by the hydrophilic PVA, which increases the surface energy and led to a poor wetting by the hydrophobic silicone. The inverse behavior was observed when comparing the silicone contact angle of untreated base paper with PVA-coated paper. Silicone contact angle changed from 15° to 35° due to the application of PVA88%. This led to the assumption that the the silicone wetting on PVA-coated papers was not prevented, but diminished by the hydrophilic pre-coat. This may result in less silicone transfer from roller to the paper surface. In order to further strengthen this assumption, a smooth and non-porous PET-foil was

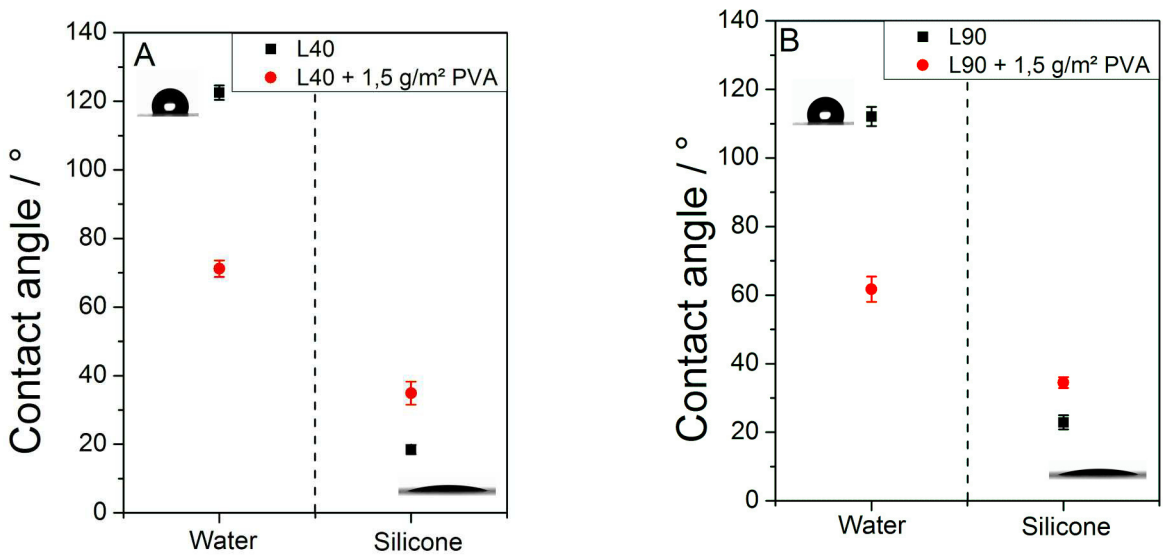

Figure 83: Contact angle measurements of L40 (A) and L90 (B) base papers with water droplet (4 μL) and silicone droplet (4 μL). Papers are coated by PVA88% (1.5 g/m²) and contact angle measurements are performed again.

coated by PVA88% (12 g/m²) and subsequently siliconized (1 g/m²). The surface of the siliconized foil was analyzed by Si-EDX-mapping in order to visualize silicone distribution on the foil (Figure 84). As one can infer from the figure, the foil was not homogenously covered by silicone and non-siliconized areas were observed. This suggests that silicone transfer and wetting were affected by the surface energy.

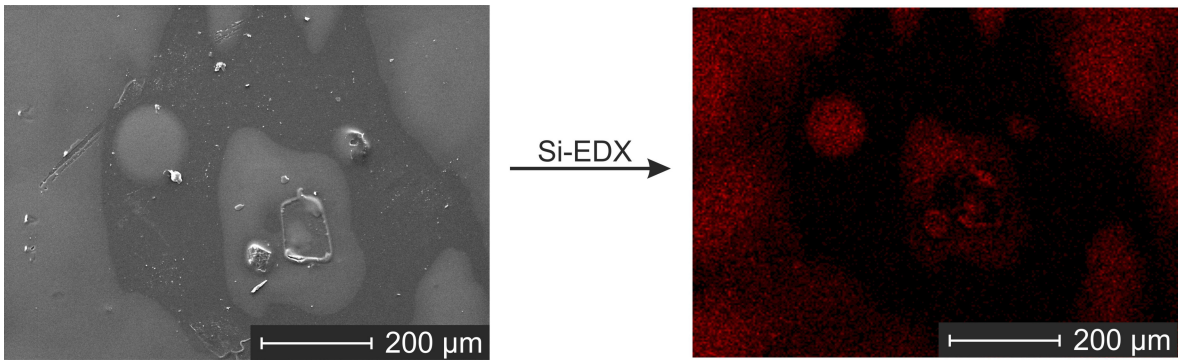

Figure 84: SEM analysis (topview) of PVA-coated foil (12 g/m²) which was subsequently siliconized (1 g/m²). The silicone coverage is investigated by Si-EDX mapping and featured by red colour. Figure reproduced with permission from reference.[98]

6.2.4 Siliconization of blade-coated papers

The papers pre-coated via blade coater were siliconized by a roller coater in a second step (110 N, 2 m/min) in order to study the barrier properties of the pre-coated polymers. As previously observed for the pre-coated and siliconized papers by roller coater, the silicone coat weights was again decreased with increasing pre-coat weight (Figure 85). Silicone coat weight for L40 paper was decreased from 1.5 g/m² to about 1 g/m² by using various pre-coats (Figure 85, A). Minimum silicone coat weight of about 0.7 g/m² was obtained for L90 paper when the paper surface was pre-coated with 2.0 g/m² PVA99% (Figure 85, B). Silicone penetration into the paper was prevented by the pre-coatings and the silicone stayed on the closed paper surface (Figure 86). The fiber structure, which was visible after applying the pre-coatings, is covered by the silicone in most parts. The barrier properties of the bio-based HEC or MC seems to be comparable to the synthetic PVA.

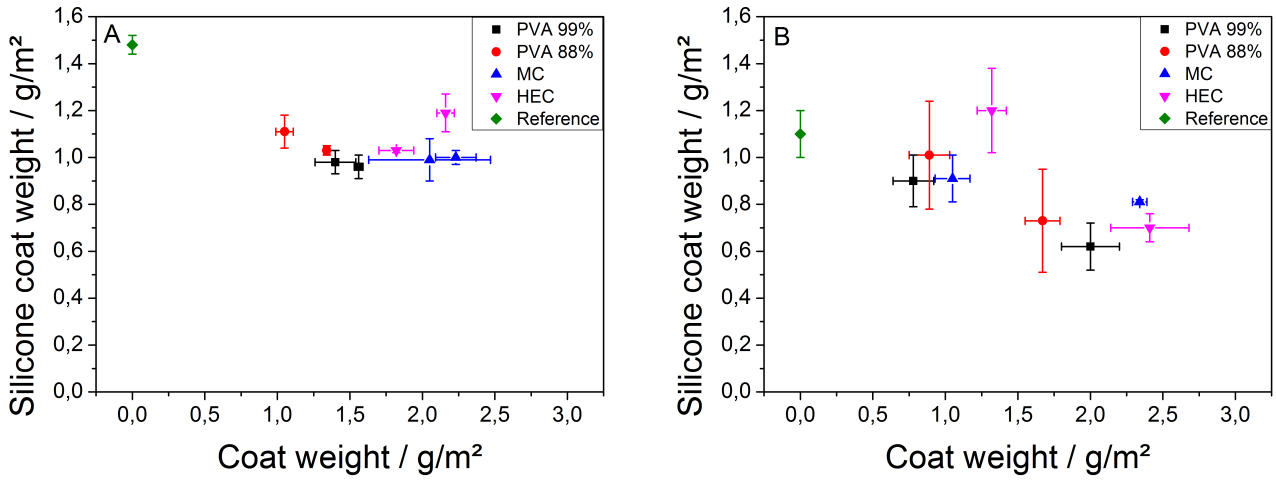

Figure 85: Influence of polymer pre-coat on silicone coat weight of L40 (A) and L90 (B) papers. The various pre-coats (7wt%) dissolved in water are applied via blade coater (50 μm & 100 μm, 50 mm/s) and the silicone was coated by a roller coater (110 N, 2 m/min).

Similar amounts of silicone were transferred to the pre-coated papers, if the pre-coats were applied by blade coater. Especially for siliconized L40 papers, the silicone coat weight for various polymers was the same (1 g/m²) (Figure 85, A). In contrast to that, the silicone coat weight seemed to be depended on the pre-coated polymer when the pre-coats were applied by roller coater. The wetting of the rollers by the various polymers may be different depending on the used polymers. This led to an inhomogenous closure of the paper pores on one side and different silicone coat weights on the other side. The surface of blade-coated papers was fully covered by the polymer and almost all pores were blocked. Thus, the transferred silicone amounts were similar and independent of the applied polymer in the pre-coat.

Another point is that the silicone coat weights of papers pre-coated by blade should be lower compared to roller coater, because the paper pores were closed to more extent and less silicone is pushed into the pores. The homogeneous coating by the hydrophilic polymers lead to an increase of the surface energy over the whole paper surface, which reduces the wetting by the hydrophobic silicone. However, similar or even higher amounts of silicone were transferred to the pre-coated papers by blade coater

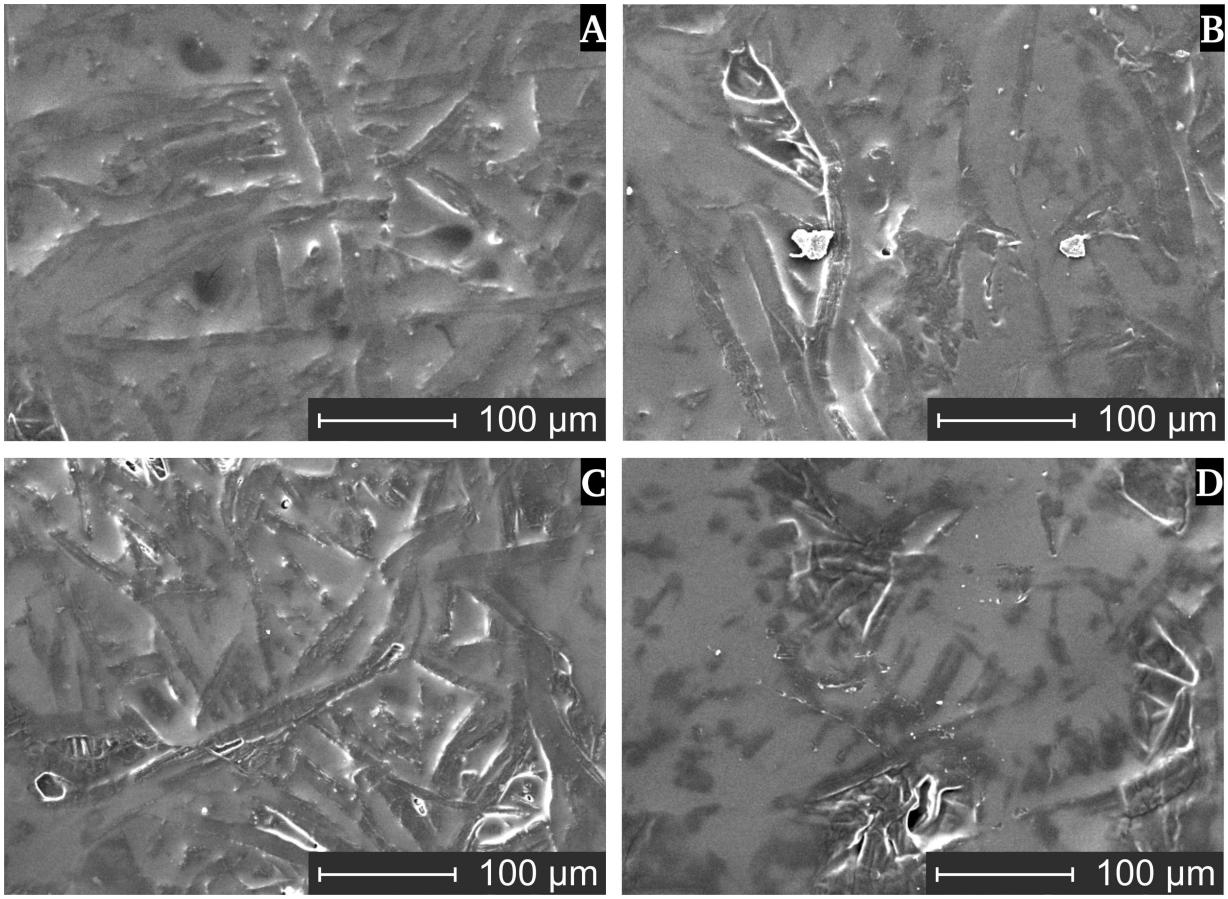

Figure 86: SEM images (topview) of L40 papers coated by silicone (1 g/m²) and PVA88% (1.1 g/m²) (A), PVA99% (1.0 g/m²) (B), HEC (1.8 g/m²) (C) and L90 coated by MC (2.0 g/m²) (D). First, the pre-coatings were applied on the papers by blade coater and afterwards the silicone was coated with a roller coater.

when comparing same pre-coat weights. In particular, 0.6 g/m² silicone was transferred to L90 paper with about 2.0 g/m² PVA99% coated by blade coater. The same silicone coat weight was achieved for L90 paper with about 2.0 g/m² PVA99% coated by roller coater. These results are in contrast to the prediction and may be explained by the influence of a third parameter on the amount of transferred silicone. The pores of the paper surface were closed in most parts and less silicone was pushed into paper pores. Along with this, the contact area between paper surface and roller was increased and more silicone was transferred to the paper. Thus, silicone transfer rate depends on surface porosity, surface energy and contact area. Extended research has to be performed in order to determine the specific influence of each parameter on silicone transfer, which is not the focus of this thesis. The barrier properties of the applied pre-coats strongly depend on the homogeneity of the coating on the paper surface.

6.2.5 Synthesis of FITC-PVA

In order to study the distribution of the pre-coating on the paper surface in detail, PVA88% was stained by a fluorescent dye and the coated papers were investigated by confocal laser scanning microscopy (CLSM). Fluorescein isothiocyanate (FITC) was attached to PVA by an addition reaction in order to stain the PVA for CLSM-measurements (Scheme 14). The reaction mixture was precipitated in isopropanol. Covalent

attachment of FITC to PVA was indirectly proven by measuring the fluorescence of the precipitation agent on the TLC-plate. No fluorescence was detected on the TLC-plate after four purification steps, but the product still showed strong yellow color. This indicates that FITC was covalently attached to PVA. The concentration of attached FITC to the PVA backbone was calculated according to the Lambert-Beer law by using the extinction at 494 nm (Figure 87) and the extinction coefficient (ϵ_{494} = 77.000 $cm^{-1}M^{-1}$ [128], in buffer $pH = 9$). FITC-concentration in PVA was calculated to $7.6 \cdot 10^{-6}$ M.

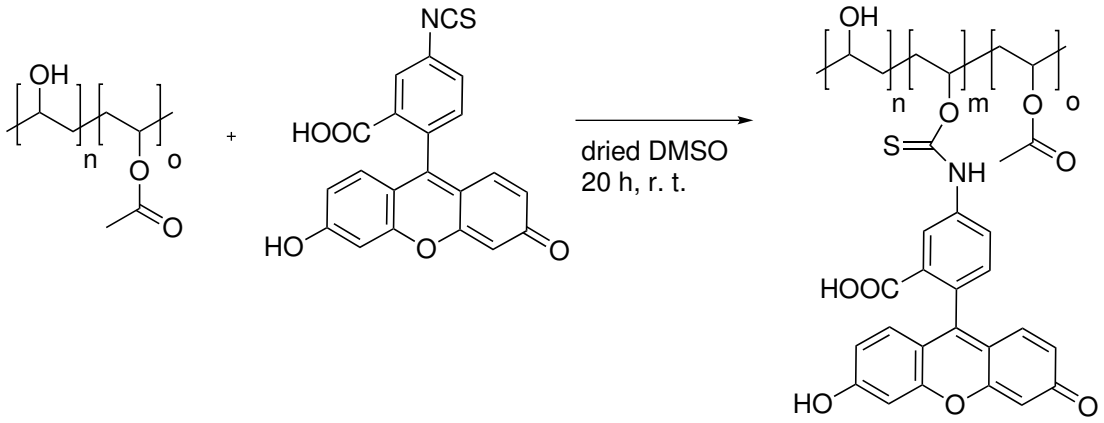

Scheme 14: Synthesis of FITC-PVA.

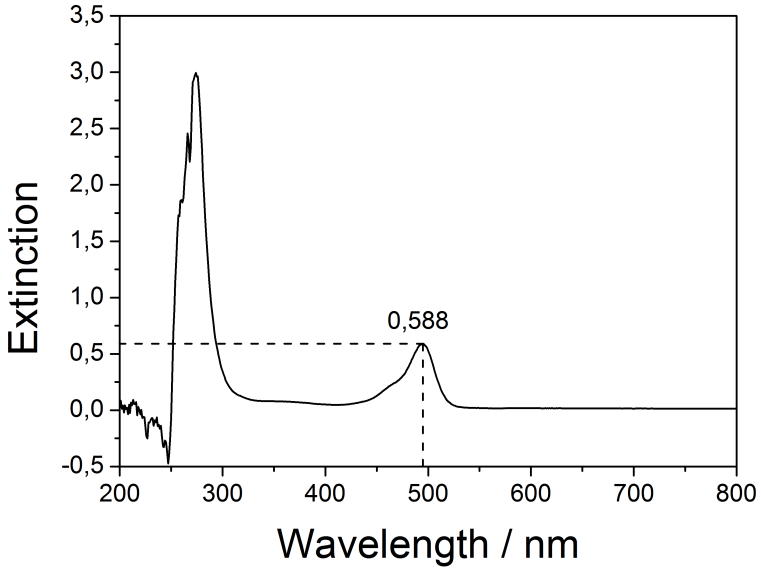

Figure 87: UV/Vis spectrum of FITC-PVA in borax-buffer at $pH = 9$. The extinction maximum at 494 nm was used for the calculation of the FITC concentration in the PVA.

6.2.6 Investigation of the distribution of FITC-PVA on paper by CLSM

For detailed investigation of the coating homogeneity on pre-coated papers, PVA88% was stained by fluorescein isothiocyanate (FITC). For the modification of PVA, it was important that FITC was covalently attached to the PVA backbone so that generation of artifacts were prevented. FITC-PVA was dissolved in

water to a final concentration of 7 wt% and coated on paper by using the roller coater (30 N, 2 m/min) and the blade coater (100 μm, 50 mm/s) at same coating conditions as before. The coated papers were investigated by confocal laser scanning microscopy (CLSM) and FITC-PVA is displayed by green fluorescence. Fluorescence images showed that the papers were inhomogenoues coated by FITC-PVA when the polymer was applied by roller coater after the first coating cycle (Figure 88, A). The instable film formation on the rollers is attributed to this phenomena, as featured by green fluorescent stripes. In order to increase the coat weight and the coating homogeneity, papers were coated three times by the roller coater. The stripes disappeared after third coating cycle, but the coating was still not homogeneously distributed (Figure 88, B). Black parts on the paper are visible, which were not coated by FITC-PVA. The coating homogeneity was significantly increased when similar amounts of FITC-PVA were applied to the paper with the blade coater (Figure 88, C). The complete paper surface showed green fluorescence, which indicates full coverage by FITC-PVA without any defects. The paper surface was in contact with the polymer solution over the whole width when the coating was applied by a blade coater. Thus, the barrier properties of the pre-coats against silicone were enhanced, if the polymer was coated by blade coater. This may also affect the release forces, which were investigated in the next step.

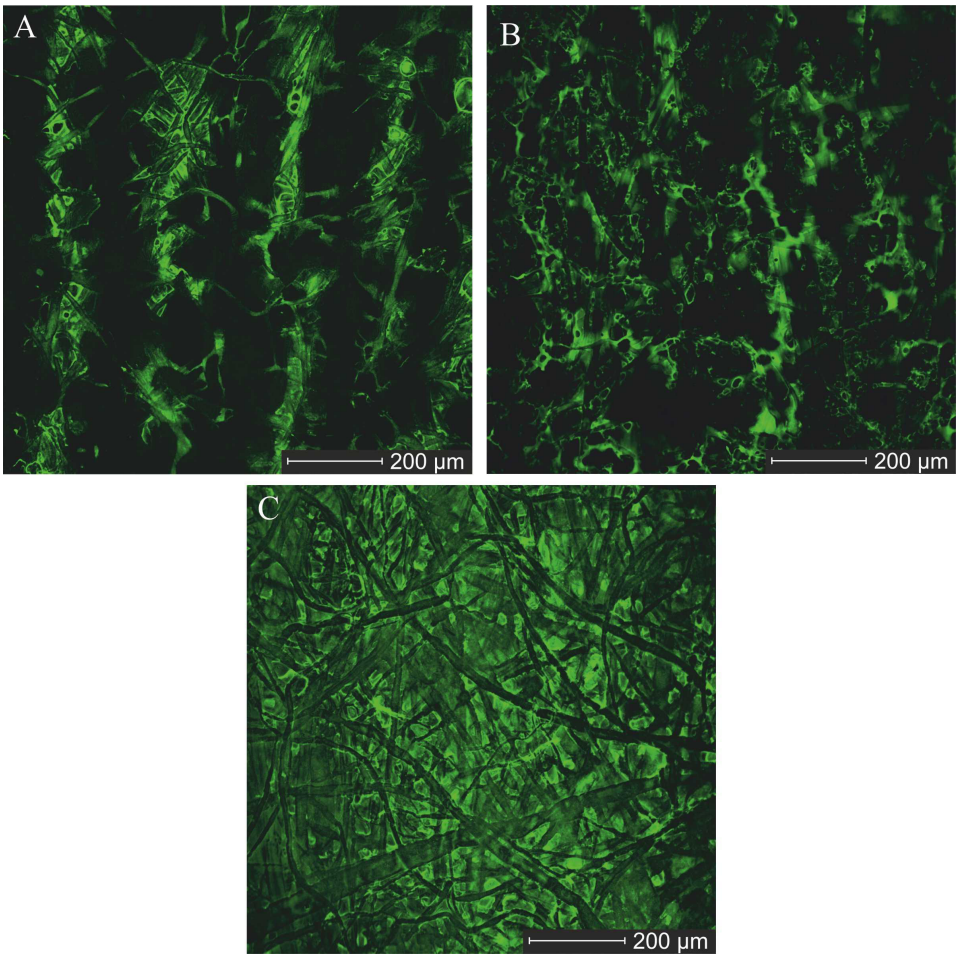

Figure 88: Fluorescence images of L90 paper coated by FITC-PVA on roller coater after first coating cycle (A, 0.6 g/m²) and third coating cycle (B, 1.8 g/m²). FITC-PVA coated by blade coater (C, 2.1 g/m²). The green fluorescence corresponds to FITC-PVA. Figure reproduced with permission from reference.[98]

6.2.7 Determination of Bendtsen air permeability of pre-coated papers

In order to characterize homogeneity of the coatings in more detail, one may also study gas-permeability of coated/uncoated samples. As such, the barrier properties of the pre-coated papers were determined by measuring the Bendtsen air permeability. The air permeability of the uncoated base papers L40 and L90 was high due to its high porosity and large pores. The L40 paper carries the highest air permeability of about 1000 $^{ml}/_{min}$ whereas the L90 paper with 400 $^{ml}/_{min}$ was less permeable for air (Figure 89). The air permeability of L90 was significantly higher compared to L40, because the L90 paper is composed of more than double amount of cellulose fibers, which resulted in a higher paper thickness. Thus, the air needs more time in order to permeate through the paper and the paper resistance against air was increased for L90 paper. If about 2 $^{g}/_{m^2}$ polymer was coated with the blade coater on the base papers, the air permeability was significantly decreased compared to the reference. Additionally, at this coat weight, both papers showed similar air permeability. Some pores remain open, but most part of the paper surface was closed. Thus, silicone penetration into the paper is remarkably reduced. Moreover, the bio-based polymeric pre-coats show barrier properties as good as those of the synthetic polymers.

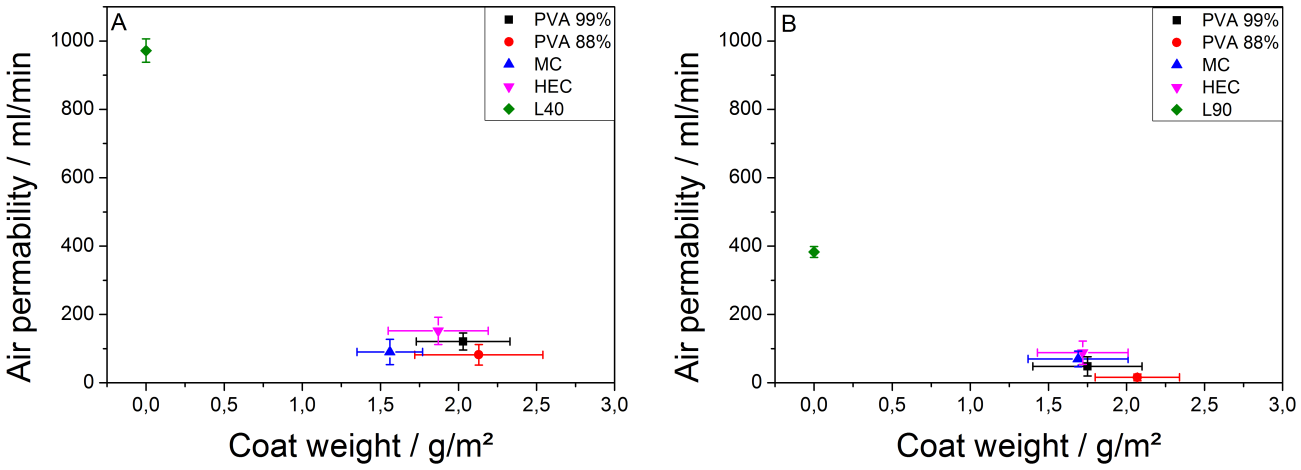

Figure 89: Determination of Bendtsen air permeability of blade-coated L40 (A) and L90 (B) papers and the uncoated reference papers.

6.2.8 Release properties of siliconized papers pre-coated with different polymers

The release forces of siliconized papers were measured in order to compare them to common release liner in industrial applications. For this purpose, an acrylic tape having a width of 25 mm was applied on the siliconized surface of the release liner according to the FINAT 10 method. The release liner is stored under specific weight between two glass plates so that the tape was in intimate contact with the paper surface. Release forces of the adhesive tape from the siliconized paper were measured at an angle of 180°. First, release forces of siliconized papers with the polymer pre-coat and silicone applied by the roller coater were studied. As one can infer from the figure, release forces of siliconized L90 papers were higher in contrast to siliconized L40 papers (Figure 90).

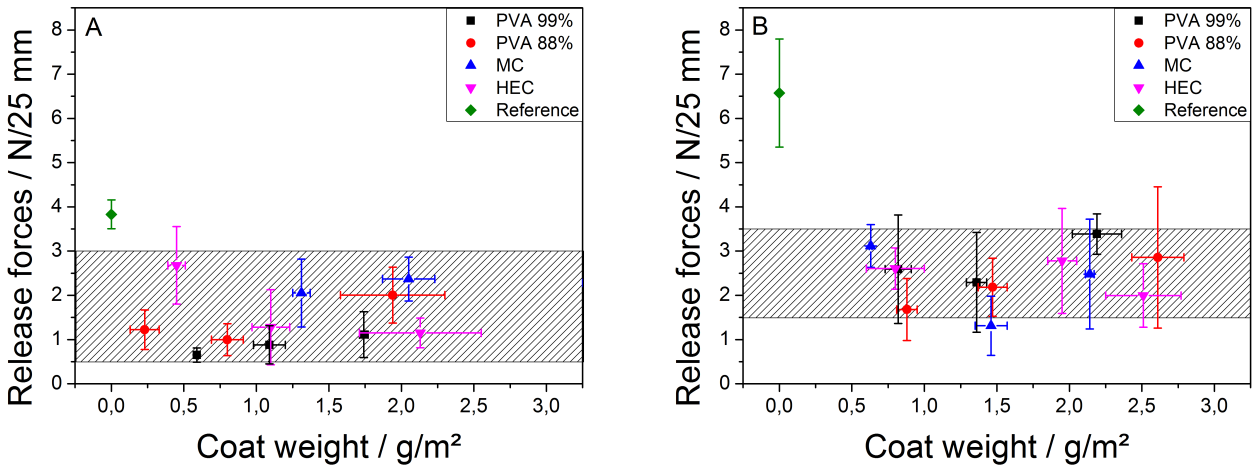

Figure 90: Release forces of siliconized L40 (A) and L90 (B) papers with various pre-coats applied by the roller coater. Papers were siliconized by roller coater (110 N, 2 m/min).

The different release forces can be clearly observed when comparing the pre-coated papers with the uncoated reference paper. In particular, release forces of about 4 N/25 mm were achieved for L40 reference paper (Figure 90, A) and about 6.5 N/25 mm for the L90 reference paper (Figure 90, B). This behavior is attributed to different amounts of transferred silicone from the roller to the paper. The uncoated L40 reference paper was coated by 1.5 g/m² silicone, whereas just 1.1 g/m² silicone was transferred to L90 paper. Thus, the adhesive in siliconized L40 papers is in contact with the silicone to more extent leading to lower release forces. This behavior was also observed when the papers were pre-coated by a film-forming polymer. The release forces of pre-coated L90 papers as well as the errors were again higher compared to those of pre-coated L40 papers. Nevertheless, release forces of siliconized L40 and L90 papers were significantly reduced by using various polymeric pre-coats compared to those of the uncoated reference papers. In detail, release forces in the range of 0.5 to 3 N/25 mm were achieved for L40 papers and siliconized L90 papers resulted in release forces ranging from 1.5 to 3.5 N/25 mm. Nevertheless, release forces were high compared to common release liner based on CCK papers. The paper surface was not completely covered and closed by silicone, which was shown by SEM images. This leads to increased release forces, because the viscous adhesive tape is pushed into the paper pores coming in contact with non-siliconized parts of the paper. Additionally, the adhesive tape is mechanically interlocked with the

paper when the adhesive creeps into paper pores. The release forces should be reduced with increasing pre-coat weight, because more pores are closed by the pre-coating and the silicone stays on the paper surface to more extent. However, this was not observed in our experiments. This presumably occurs, because less silicone was transferred to the paper when the pre-coat weight was increased. The adhesive tape may come in contact with the pre-coating or other parts of the paper which were not covered by silicone leading to high release forces. Another prerequisite for a good release liner is a good mechanical stability of the silicone coating (no rub-off). Some parts of the silicone coating may be removed from the paper during peel-off and impair the performance of the adhesive tape. Thus, it is important that the silicone anchorage to the paper is sufficient high. Stability of silicone layer to the various pre-coats was good, except of MC. In this case, the coating was easily removed by rubbing with a finger over the coating. MC carriers very few OH-groups, which are important for covalent crosslinking reactions with silicone. Additionally, fewer hydrogen bonds from the coating to the underlying cellulose fibers are formed, which further reduce coating stability. Hence, MC is less appropriate as barrier coating for the production of a release liner.

In a next step, release forces of pre-coated papers by blade coater were measured (Figure 91). It can be seen from the figure that release forces were significantly reduced compared to release papers pre-coated by roller coater. In detail, release forces in the range of 0.5 to 2 $^{N}/_{25\ mm}$ were obtained for L90 papers (Figure 91, B). Even more, release forces smaller than 0.5 $^{N}/_{25\ mm}$ were measured for siliconized L40 papers (Figure 91, A) when neglecting the release forces of papers pre-coated by MC. These papers can be classified to "medium" release and release forces were in the order of CCK papers. Moreover, the barrier property of HEC was competitive to commonly used PVA, which was also displayed in similar release forces. Additionally, the silicone is able to crosslink with OH-groups of the HEC pre-coating which increases the coating stability. The coverage of the pre-coating on the paper was improved by using blade coater. Most paper pores were blocked by the pre-coating and the silicone stayed on the paper surface. The adhesive tape was in contact with the silicone in most parts, which led to low release forces.

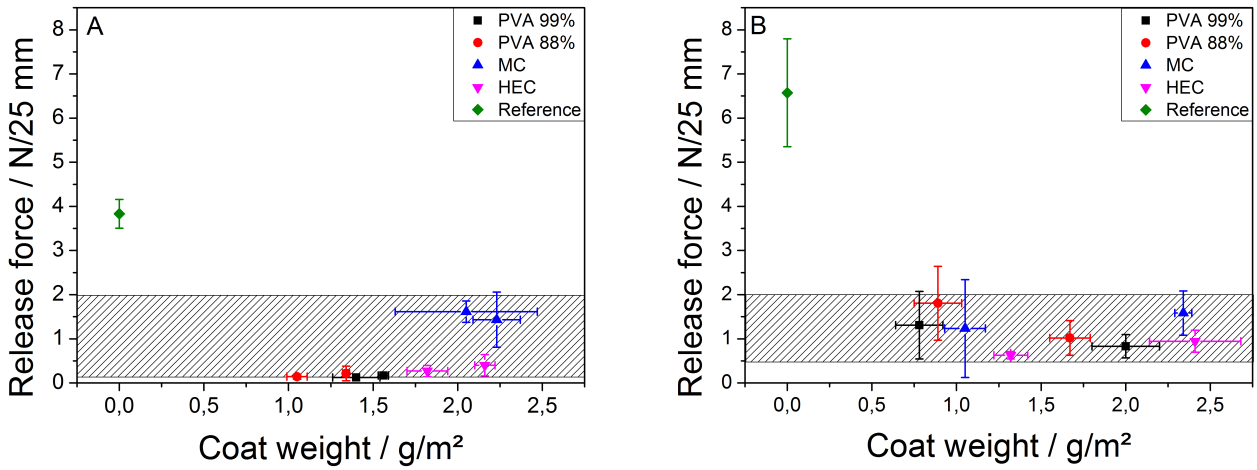

Figure 91: Release forces of siliconized L40 (A) and L90 (B) papers with various pre-coats applied by blade coater. The untreated reference papers were coated with about 1.5 $^{g}/_{m^2}$ (L40) or 1.1 $^{g}/_{m^2}$ (L90) silicone, respectively. Papers were siliconized by a roller coater (110 N, 2 $^{m}/_{min}$).

6.2.9 Comparison of release forces using different coating methods

The coating methods, which were used in order to apply the pre-coats on the paper, were compared with respect to observed release forces. It has been shown that the release forces were affected by the coating method, and the homogeneity of the pre-coatings plays a crucial role. Comparison of the release forces is not trivial, because the silicone coat weight, which affects the release forces, was reduced with increasing pre-coat weight. Thus, paper samples with similar silicone coat weights were selected to analyze the release forces. In particular, L40 papers were chosen having a silicone coat weight of 1.1 g/m² (Figure 92, A) and L90 papers having a silicone coat weight of 0.7 g/m² (Figure 92, B).

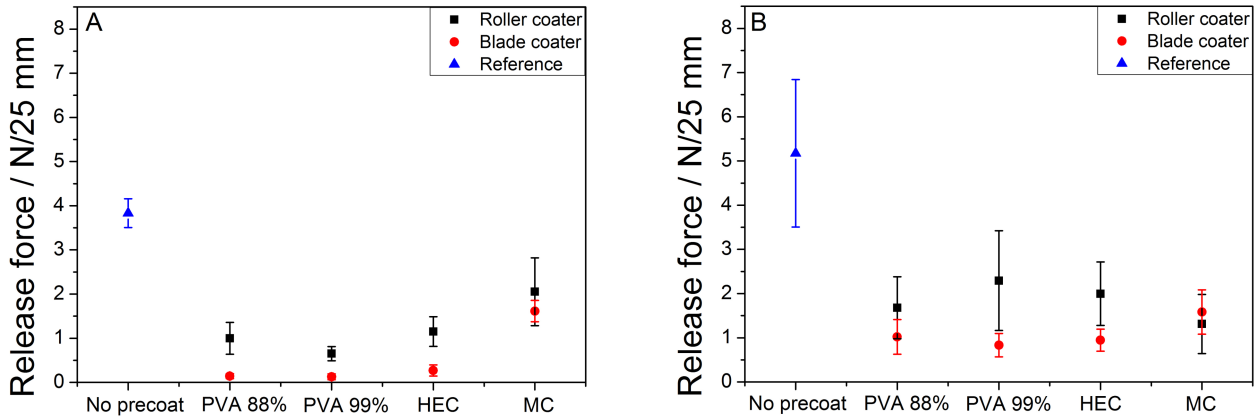

Figure 92: Comparison of the release forces of siliconized L40 papers (A) and L90 papers (B), which were pre-coated by roller or blade coater. Silicone coat weight of pre-coated L40 papers: 1.1 g/m² ± 0.1 g/m², reference: 1.5 g/m² ± 0.1 g/m² silicone. Silicone coat weight of pre-coated L90 papers: 0.7 g/m² ± 0.1 g/m², reference: 1.1 g/m² ± 0.1 g/m² silicone.

The release forces of blade-coated papers were lower compared to roller coater for both paper types. The porous paper surface was closed by the pre-coating to more extent, if blade coating method was used. The pre-coating acts as barrier coating similar to the clay-coating with CCK paper, and silicone penetration into the paper is prevented. The adhesive tape is mostly in contact with the silicone layer, which resulted in low release forces. The papers pre-coated by roller coater were not homogeneously covered by the silicone, which led to higher release forces as discussed above. The release forces and errors of L90 paper were higher compared to L40 papers, because the selected L90 papers have got approximately 0.4 g/m² less silicone. Thus, the paper surface may not fully be covered by the silicone and the adhesive tape comes in contact with non-siliconized parts of the paper, which may explain the higher release forces. Silicone coat weights of about 0.7 g/m² are rather low compared to common applied silicone amounts. Higher silicone coat weights of about 1 g/m² may close the non-siliconized voids and result in lower release forces. The siliconized papers pre-coated with bio-based polymers (HEC, MC) showed promising release forces and they were competitive to synthetic barrier coatings (PVA) or even clay-coating, if applied by blade coater. Nevertheless, the release forces of MC-coated papers were higher compared to HEC, which was attributed to the poor coating stability on the paper surface. Some parts of the coating may be removed from the paper by the adhesive tape, which leads to increased release forces. The release forces of HEC-coated L90 papers and clay-coated S98 paper at 0.7 g/m² silicone coat

weight were in the same range of 1 N/25 mm. This makes the HEC a prominent bio-based candidate in order to replace the synthetic PVA or the clay coating.

6.3 Conclusion

Porous base papers which were not clay-coated nor calendered were used in order to produce a release liner. The untreated papers were coated by about 1.0 g/m² solvent-free and water-based silicone, which is similar to common used silicone coat weights. The corresponding release forces were at this stage too high for release liner applications. Additionally, the papers were partially destroyed during peel off and the errors were huge. This is because the silicone was absorbed by the paper pores and the adhesive tape will creep into these pores and comes in contact with non-siliconized parts of the paper. The release forces were reduced in the range of easy release by applying higher silicone coat weights, but this is not economically. Thus, in a next step, talcum was added to the silicone in order to increase the viscosity and prevent silicone penetration into the paper. This approach combines two individual coating processes into one, which saves costs. The water-based silicone has to be used for coatings of silicone/talcum mixtures, because the talcum was not homogeneously suspended in the solvent-free silicone. Additionally, the mixture has to be preferably applied by blade coater, because the rollers were not homogeneously covered by the coating suspension due to ribbing effects. The paper pores were increasingly closed with higher talcum contents, but release forces were still high due to open pores. The influence of the talcum on the release forces was not completely understood, because only high silicone coat weights of 9 g/m² were obtained by blade coater. Thus, the paper surface was completely closed even by using silicone without talcum, which resulted in low release forces smaller than 0.25 N/25 mm. Even higher coat weights were applied on the paper when talcum was added to the silicone and the release forces were slightly increased. This is most likely due to an enhanced roughness, which was shown by SEM images. The experiments demonstrate that the talcum acts more as a viscosity modifier than a mechanical barrier, so that silicone penetration into the paper is reduced due to the high viscosity. The viscosity is significantly increased by the addition of talcum, which was shown by measuring the viscosity. The role of the talcum as a barrier additive has to be studied in detail for lower coat weights (1-2 g/m²), because high silicone coat weights may suppress the influence of the talcum. Coating experiments have to be performed on a blade coater with adjustable small gap sizes in order to obtain low coat weights. Additionally, talcum may be utilized as a filler in order to reduce silicone consumption. In principal, it was shown that a release liner can be produced starting from a non clay-coated paper by using high amounts of silicone. Nevertheless, this high coat weights are not economically and associated with high costs. Thus, a third method was pursued in order to produce a release liner out of a porous base paper with significant lower silicone consumption.

For this purpose, the pores of the base paper were closed by using film-forming polymers. The pre-coatings should act as a barrier coating and prevent silicone penetration. The barrier properties of commonly used synthetic PVA were compared to new bio-based barrier coatings. The polymers were applied on the paper by blade coater and the roller coater in order to compare both methods. Investigations of pre-coated papers by SEM and CLSM revealed that the coating is inhomogeneously distributed when using the roller coater. The rollers were not fully covered by the coating solution and stripes occur. Application of the pre-coats by blade coater is thus the preferred method to obtain more homogeneous

coatings. It has to be emphasized that the paper pores were closed by the bio-based polymers HEC and MC as good as those of the synthetic PVA. The barrier properties of the film-forming polymers were determined by air permeability measurements. A significant reduction of the air permeability was observed for all polymers at coat weights of about 2 g/m^2, if the polymer was applied by blade coater. Almost all pores were closed by the polymers and silicone penetration into the paper was reduced. A silicone layer was applied on the pre-coated papers in a second step in order to produce the release liner. The results showed that the silicone coat weight was decreased with increasing pre-coat weight. Wetting effect of the hydrophobic silicone to the hydrophilic surface as well as reduced porosity were assigned to this phenomena. Investigation of papers pre-coated by roller coater showed that the silicone penetrates into the paper pores. The insufficient closure of the paper pores by the roller coater leads to improper barrier properties in terms of silicone. This results in high release forces, because the adhesive tape is pushed into the open pores and is mechanically interlocked. Lower release forces and improved barrier properties were obtained for papers which were pre-coated by blade coater. The enhanced barrier properties were analyzed by measuring the Bendtsen air permeability. The air permeability was significantly reduced by using polymeric pre-coats and the barrier properties were improved. Mainly all paper pores were closed by the pre-coating and the silicone stayed on the surface. Thus, the adhesive tape was not able to creep into paper pores. The release forces were significantly reduced from 4 $N/25\ mm$ for the untreated reference to 0.25 $N/25\ mm$ for pre-coated L40 papers. The release forces of pre-coated L90 papers were decreased from 6.5 $N/25\ mm$ for the reference to less than 1 $N/25\ mm$. Especially HEC showed promising barrier properties, which were competitive to the synthetic pre-coats. MC was less appropriate for such applications, because of a poor coating stability on the paper surface. This specific polymer may be removed from the adhesive tape during peel-off and impair the adhesive performance. It was shown that it is possible to produce a release liner with sufficient low release forces out of a porous base paper. Extended refining steps and complex clay-coating of the paper can be replaced by using a film-forming polymer with special focus on bio-based HEC. Release liner produced by this method can be used in label industry or for medical applications such as plaster.

7 Towards a silicone-free release liner based on modified HPC

Most silicone release papers are burned and used for energy production, because recycling of these specific papers is not trivial.[129–131] Additionally, in case of solvent-free silicone, an expensive platinum catalyst is required for curing and crosslinking reactions. For some application, silicone-free release liner are required, because silicone contains unreacted extractables, which can migrate and reduce the adhesive performance or lead to printing issues.[37]. Thus, a silicone-free release liner based on modified cellulose is highly demanded. In particular, HPC was selected for this purpose, because it was already shown by a colleague in the Department of Macromolecular Chemistry and Paper Chemistry that this specific polymer can be easily modified to produce interesting barrier films on paper.[54] Additionally, this polymer is made of a natural resource. As HPC is a biopolymer, it may be hydrolyzed by acid or enzymes and the cellulose fibers may be recovered, because the release coating can be removed from the paper surface. This coating may improve the recycling of release liner papers. Additionally, HPC carries hydroxy groups which can be used for crosslinking reactions without the need of a platinum catalyst. The main challenge is to reproduce the unique properties of silicone in order to obtain low release forces.

7.1 Release forces of HPC derivatives hydrophobised by various acid chlorides

Silicone coatings posses a hydrophobic character ($\theta > 90°$) accompanied with a very low surface energy of 22 $^{mN}/_{m}$, which is one requirement for low release forces.[26] Thus, the hydrophilic HPC was modified with long, hydrophobic alkyl chains to a degree of substitution (DS) of about 3 in order to decrease the surface energy and mimic the properties of the silicone. In brief, the HPC was dissolved in tetrahydrofuran (THF) and treated with 6 equivalents of stearic acid chloride (Scheme 15).

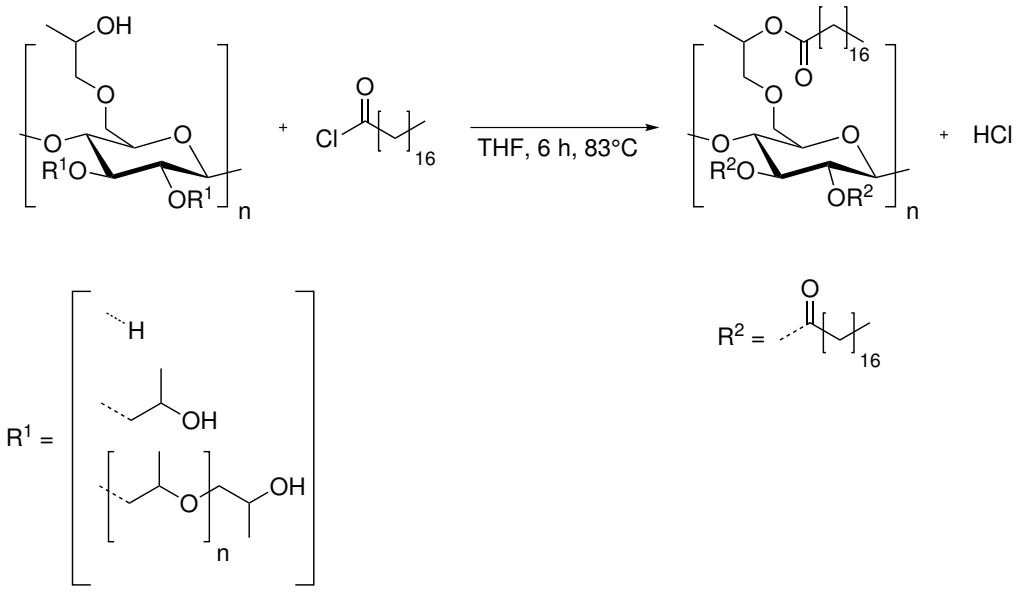

Scheme 15: Modification of HPC by stearic acid chloride to a DS of 3.[54]

After the modification process, all three hydroxy groups per anhydrous glucose unit carry a C_{18}-alkyl chain (HPC C18 DS3). The degree of substitution was determined by ^{1}H-NMR measurements according to the procedure described in literature.[54] HPC-C_{18}-esters with different DS were synthesized in order to investigate the influence of changing DS on release forces. Additionally, HPC was modified by lauric

acid chloride (C_{12}) to a DS of 3 (HPC C12 DS3) via an analog procedure in order to investigate the influence of the chain length on release forces. The HPC esters were developed and kindly provided by M.Sc. Maximilian Nau of the laboratory of the Macromolecular Chemistry and Paper Chemistry, Department Chemistry, TU Darmstadt.

A clay coated paper (S98) was selected as coating substrate and for release force measurements, because this type of paper carries a smooth and closed surface and the coating solution will stay on the paper surface. Hydrophobic HPC esters were dissolved in THF to a final concentration of 10wt% and applied on clay-coated papers (S98) by using the blade coater (150 μm, 50 mm/s). The coated papers were dried at room temperature and static contact angle measurements were performed. The coatings of HPC C12 DS3 (102°) as well as HPC C18 DS3 (104°) showed hydrophobic water contact angles due to the modification process. The coated papers were prepared for release forces measurements as previously described. The release forces of coated papers were investigated as a function of the DS of modified HPC by C_{18}-esters. The release forces were significantly reduced when the DS of HPC C18-coating is increased to a DS of 3 (Figure 93).

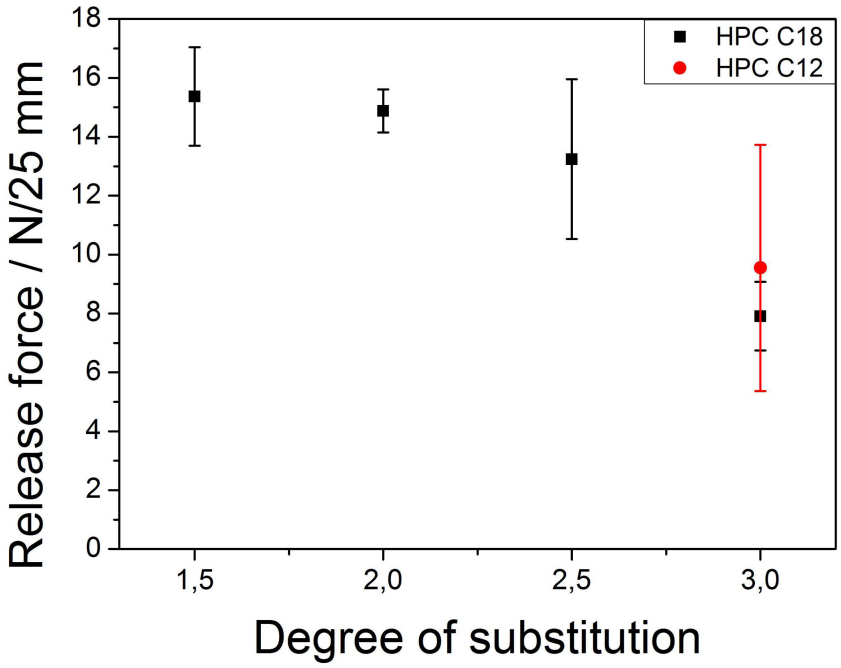

Figure 93: Determination of release forces as a function of the DS of modified HPC by C_{18}-esters and of HPC C12 DS3 on S98 papers. Papers were coated by about 3 ml of the coating solution (10 wt%) using the blade coater (150 μm, 50 mm/s in order to obtain a coat weight of about 2.5 g/m^2.

In particular, the release forces were decreased from about 15 N/25 mm for HPC C18 DS1.5 to about 8 N/25 mm for HPC C18 DS3. The reason for this observation is probably that physical interactions between the acrylic tape and the HPC-coating were reduced due to the decreased surface energy, when the hydroxy groups of the HPC were fully esterified by C_{18}-alkyl chains. Nevertheless, the release forces were high compared to siliconized release liner (< 1 N/25 mm). The release forces of HPC C12 DS3 were similar compared to HPC C18 DS3, but the standard deviation of C_{12}-esterified HPC was significant higher. As the contact angle of C_{12}- and C_{18}-modified HPC DS3 does not differ significantly, release forces were affected by another property. It has to be mentioned that the coating of HPC C12 DS3 feels very sticky

in contrast to HPC C18 DS3-coating,which suggests a low glass transition temperature (T_g) or melting temperature (T_m).
Therefore, phase transitions were investigated by using differential scanning calorimetry (DSC). The melting temperature of HPC C12 DS3 was determined at -38°C, whereas the melting temperature of HPC C18 DS3 is about 39°C. This measurement explains the sticky character of HPC C12 DS3 and the increased error of release force. The highly viscous acrylic tape may penetrate into the HPC C12 DS3-coating to more extent, which leads to higher release forces and increased error bar. The coating stability of both coatings on CCK paper was checked as before by a simple finger rub-off test. The coating of HPC C12 DS3 has a bad rub-off and the sticky coating is smeared during test procedure. The sticky character of this specific polymer makes it improper for release liner applications. Thus, all upcoming experiments will focus on coatings with HPC C18 DS3. The coating of HPC C18 DS3 seems to be more stable, but the anchorage to the paper surface was insufficient. The coating itself did not stick at room temperature and it seemed to be stable on the paper surface, but the coating started to smear during rub-off test due to the increased temperature. The coating has to be stable on the paper surface so that the adhesive is not affected by the release coating. Thus, the coating stability of HPC C18 DS3 on CCK paper was investigated in detail.

7.2 Investigation of coating stability of HPC C18 DS3 on CCK-paper

In order to investigate the coating stability of HPC C18 DS3 after peel-off of an adhesive tape, the dissolved polymer was stained with a fluorescent dye. In brief, a solution of rhodamine B in THF (500 μL, 0.05 $^{mg}/_{ml}$) was added to a solution of HPC C18 DS3 in THF (10wt%, 15 ml). The coating was applied on paper surface by blade coater (150 μm, 50 $^{mm}/_{s}$). The coated paper as well as the adhesive tape were investigated by fluorescence microscopy after peel-off measurements. Part of the coating was ripped off from the paper surface during peel-off, which is nicely illustrated by a matching image of the adhesive tape (Figure 94, A). A lack of fluorescence was observed on the coated paper surface, and the geometric shape matches the part of the fluorescent area on the adhesive tape (Figure 94, B). This experiment proves that the coating is insufficiently anchored to the clay-coating. Additionally, the adhesive performance of the adhesive tape is impaired by this instable coating. Thus, in order to improve the coating stability, the coating has to be fixed to the paper surface in the next step by covalent bonds.

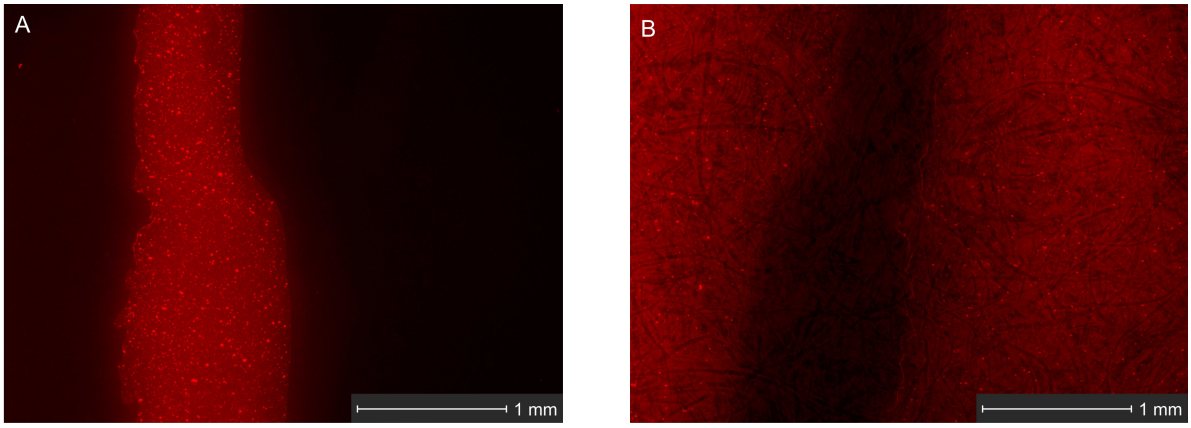

Figure 94: Fluorescence images of adhesive tape after peel-off (A) and S98 paper coated by HPC C18 DS 3 after peel-off (B). The coating was stained by rhodamine B and is displayed as red fluorescence.

7.3 Crosslinking of HPC and modified HPC with C_{18}-chains

The anchorage of the coating to the clay topcoat as well as the intrinsic stability of the coating itself should be improved by using a crosslinker. This crosslinker undergo crosslinking reaction with residual hydroxy groups from the modified HPC and with the hydroxy groups from additives in the clay-coating. The crosslinking-reaction should be as fast as for silicone curing to save energy and should be preferably started by heat. In order to find an appropriate crosslinker, preliminary studies were performed with pure HPC. Glutaraldehyde and glyoxal were selected as a potential crosslinking agent of the series of dialdehydes, since thermal crosslinking reactions with hydroxy groups are known in literature and this aldehydes are used on an industrial scale.[132–134] HPC also exhibits hydroxy groups which can be used for this kind of reaction. The hydroxy groups react with the dialdehyde via the formation of an acetal leading to crosslinking (Scheme 16).

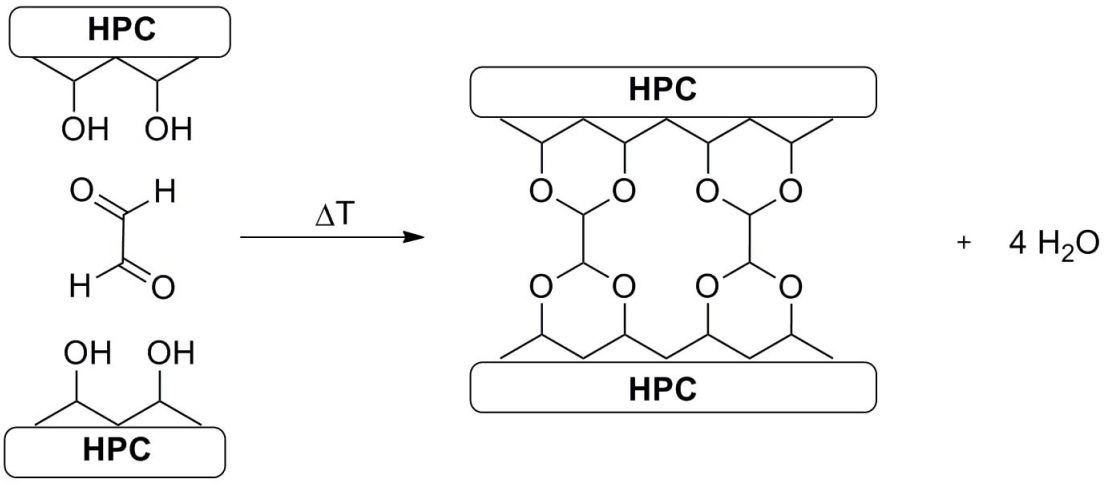

Scheme 16: Crosslinking reaction of HPC with glyoxal via the formation of an acetal.

Different amounts of glyoxal related to the mass of HPC were added to HPC, which was dissolved in THF. The solvent of all samples was removed under reduced pressure at room temperature prior to heat treatment. The crosslinking reaction was performed in dry state in order to better compare the

crosslinking results. The different amounts of solvent affect the speed of the crosslinking reaction, which may falsify the crosslinking results. The mixtures of HPC and glyoxal were heated to 150°C for different times. Note, the amount of HPC was kept constant for all experiments. Crosslinking was qualitatively checked by swelling experiments with deionized water and rated as:

+	High amount of swollen gel
0	Low amount of swollen gel
-	No swelling, dissolved by solvent

Table 9: Swelling results of HPC with various amounts of glyoxal in water.

Glyoxal / wt%	1 min	3 min	6 min	9 min
2	0	0	+	+
4	+	+	+	+
6	+	+	+	+

Swelling experiments show that small amounts of HPC are crosslinked by using 2wt% glyoxal and after 1 min at 150°C (Table 9). The swelling is improved by increasing crosslinking time or glyoxal content. Formation of the acetal may be further supported by addition of acid. This is supported by images of the hydrogel in swollen state (Figure 95). The amount of swollen hydrogel is significantly increased when using 4wt% or 6wt% glyoxal, respectively. The reference experiment without any glyoxal does not show any swelling and the HPC is dissolved by the water. These results demonstrate that glyoxal can be well utilized in order to crosslink HPC.

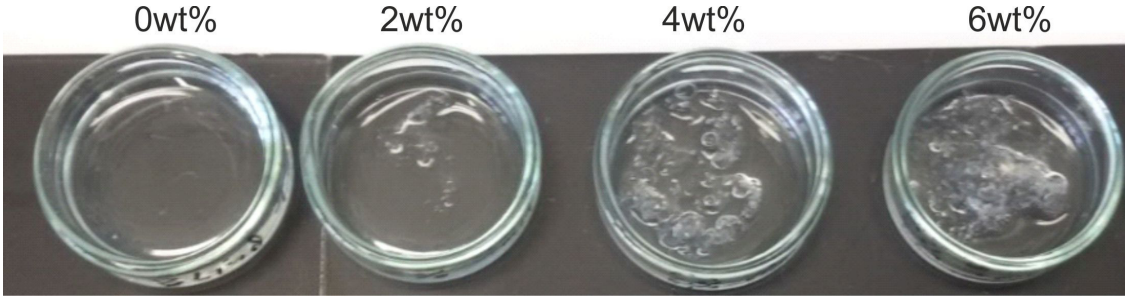

Figure 95: Images of HPC with various amounts of glyoxal after swelling in water. The mixtures were crosslinked for 1 min at 150°C.

As a second crosslinker, glutaraldehyde was reacted with HPC according to the same procedure as for glyoxal. The swelling experiments show that the HPC is not crosslinked after 1 min or 3 min, respectively, even when 6wt% of crosslinker were added (Table 10). Small amount of swollen hydrogel was observed for extended crosslinking times (6 min or 9 min). Glutaraldehyde is less appropriate for crosslinking reaction of HPC in contrast to glyoxal. The reaction kinetic of glutaraldehyde seems to be significant lower compared to glyoxal. Additionally, predominantly intramolecular reactions may occur in the reaction of HPC with glyoxal, whereas slower intermolecular reactions may be preferred when using glutaraldehyde due to a higher chain length. Different reaction kinetics were observed in the reaction between PVA with glutaraldehyde and butenedial.[135] The reaction of PVA with both aldehydes follows a kinetic of first

order, but the activation energy for the butenedial was about 50% higher and the rate of bond formation was one order of magnitude slower. This shows that the reaction rate is significantly influenced by the structure of the aldehyde.

Table 10: Swelling results of HPC with various amounts of glutaraldehyde in water.

Glyoxal / wt%	1 min	3 min	6 min	9 min
2	-	-	0	0
4	-	-	0	0
6	-	-	0	0

7.4 Crosslinking of HPC C18 DS3 with glyoxal

Glyoxal, which successfully crosslinks HPC, was now mixed with HPC C18 DS3 in order to check the reproducibility of the crosslinking results. The HPC C18 DS3 was dissolved in THF and different amounts of glyoxal were added to the polymer. The crosslinking procedure was performed under the same conditions as for the HPC and THF was used instead of water for the swelling experiments. The amount of swollen HPC C18 DS3 was significantly reduced compared to HPC, because mainly all hydroxy groups were modified by C_{18}-esters and just few hydroxy groups were accessible for crosslinking reaction (Table 11). No swollen gel was observed by addition of 2wt% glyoxal after 1, 3 or 6 min in oven, respectively, but significant amount of swollen organogel was observed with 4 and 6wt% glyoxal after 3, 6, or 9 min in oven. This indicates that some hydroxy groups were accessible for crosslinking reactions even at DS of 3. One explanation may be that hydrolysis of the ester occur after addition of glyoxal. The 40wt% glyoxal solution is stored under acidic condition (pH =1) in order to stabilize the glyoxal. For crosslinking experiments, the glyoxal solution was diluted to 1wt% and than added to the HPC. The diluted solution is still acidic (pH = 3) and may support hydrolysis of the HPC-esters. This correlates with the observation that higher amounts of glyoxal and extended reaction time were needed for a significant amount of crosslinked polymer. Another explanation may be that the DS was determined by ^{1}H-NMR and the DS posses an error of about 0.2. Thus, some residual hydroxy groups remain even at DS of 3 which can be utilized for crosslinking reactions.

Table 11: Swelling results of HPC C18 DS3 with various amounts of glyoxal in THF.

Glyoxal / wt%	1 min	3 min	6 min	9 min
2	-	-	-	0
4	-	0	+	+
6	-	+	+	+

Extended analysis of the swelling behavior of the organogel has been carried out in order to quantify the swelling ratio. The swelling ratio was calculated by gravimetric measurements (Equation 7.1).[136,137]

$$\text{Swelling ratio} = \frac{m_s - m_d}{m_d} \cdot 100\% \tag{7.1}$$

In particular, the mass of the organogel in swollen state (m_s) is subtracted and divided by the mass in dry state (m_d). The swelling was enhanced with increasing amount of added glyoxal (Figure 96). The swelling ratio from 4wt% to 6wt% glyoxal was not significantly increased which indicates that a maximum swelling ratio was achieved. Thus, further increase of the glyoxal amount may not influence the swelling behavior. A maximum swelling ratio of about 350% was achieved with 6wt% glyoxal after 3 min at 150°C, which corresponds to 3,5-fold increase in volume compared to the non-crosslinked reference. No swelling was observed for the HPC C18 DS3 samples with 0wt%, and 0.5wt% glyoxal. The polymer was dissolved by the THF and removed from the crystallization dish. The results show that the crosslinker is capable of sufficient crosslinking the HPC C18 DS3. The paper surface carries hydroxy groups from additives in the clay-coating (e.g. PVA), which can be utilized for crosslinking reaction with the hydrophobic HPC. Additionally, the release forces may be further reduced by the crosslinked release coating, because of the force-dissipative character similar to crosslinked silicones. It is known that interfacial slippage occurs during release of an adhesive tape from a crosslinked silicone coating, which contributes to the unique low adhesion properties of silicones.[16,34] Crosslinking of HPC C18 DS3 may also support the release of an adhesive tape in our case.

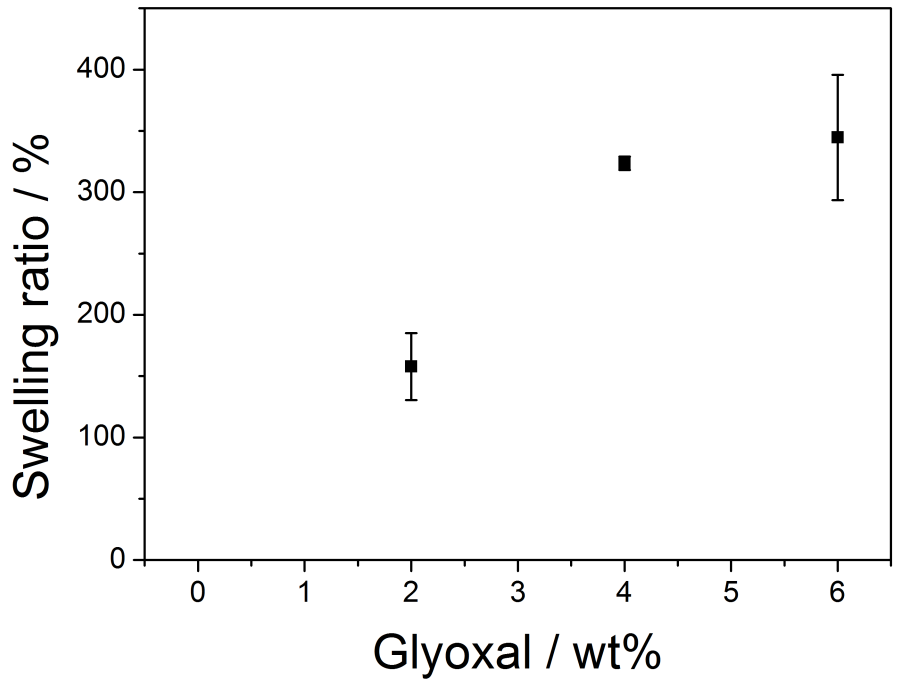

Figure 96: Determination of the swelling ratio of crosslinked HPC C18 DS3 in THF as a function of various amounts of glyoxal. The polymer was crosslinked in an oven for 3 min at 150°C.

7.5 Measuring the release forces of HPC C18 DS3 on CCK-paper after crosslinking

The hydrophobic HPC C18 DS3 was dissolved in THF and mixed with different amounts of glyoxal in order to investigate the influence of glyoxal on the release forces and on coating stability. The coating solution was applied on clay-coated S98 paper by using the blade coater (150 μm, 50 $^{mm}/_{s}$) and thermally crosslinked for 3 min at 150°C. Investigation of the coated paper by SEM showed that the structure of the CCK-paper is homogeneously overlaid by the coating of the hydrophobic HPC (Figure 97).

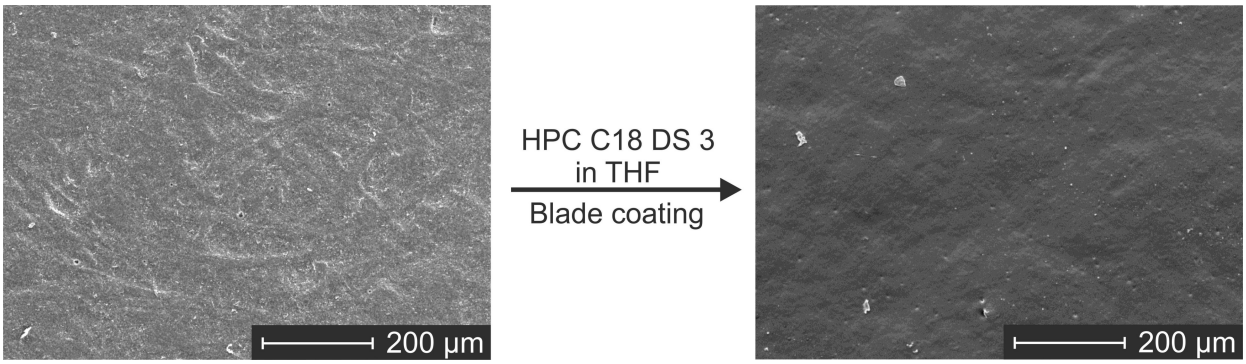

Figure 97: SEM images (topview) of S98 paper prior and after coating of HPC C18 DS 3 by blade coater (150 μm, 50 $^{mm}/_{s}$).

The curing temperature of 150°C is above the T_g of HPC C18 DS3 and thus rearrangements of the polymer chains of the coating may occur which may influences the release forces. In order to study this influence, the release forces of papers were compared which were dried at 150°C and at room temperature. The release forces of coatings with low amounts of glyoxal (0.5wt%) were in the range of 7-8 $^{N}/_{25\ mm}$ and the heat treatment does not affect the release forces. (Figure 98). Parts of the coating were removed during peel-off-testing, which is reasonable because no crosslinking was observed for 0.5wt% glyoxal in swelling experiments. Poor coating stability was even observed, if 6wt% of glyoxal was added to the coating and dried at room temperature. In contrast to this, the rub-off is significantly improved when this coating was dried at 150°C. Moreover, the release force seems to be slightly lower compared to the coatings with 0.5wt% glyoxal. The addition of crosslinker to the modified HPC and drying at elevated temperature leads to crosslinks which improve the coating stability as well as the anchorage to the paper surface. Long-term measurements were performed in order to study the stability of release forces over several days. This is important, since release liners are stored over weeks prior to final application and release forces have to be constant over this time. Thus, the release liner, together with the applied adhesive tape were stored at standard climate conditions for 15 days and the release forces were measured afterwards. The release forces did not change significantly after 15 days compared to the release forces after 2 days and the variations were in the margin error. The rub-off-results of the samples which were stored for 15 days were the same as for the samples after 2 days. Only the coating which is mixed with 6wt% glyoxal and cured at 150°C exhibits no rub-off and a chemical stable coating. Release forces of about 6 $^{N}/_{25\ mm}$ were obtained for the coating which was mixed with 6wt% glyoxal and dried at 150°C after 15 days. This specific value is lower compared to the other samples, which indicates that the release of an adhesive tape is supported by introducing crosslinks into the release coating. Nevertheless, release forces of the HPC-coated paper are still high in contrast to siliconized release liner,

but this bio-based, silicone-free release coating represents a promising alternative to silicone for tight release applications without using an expensive platinum catalyst.

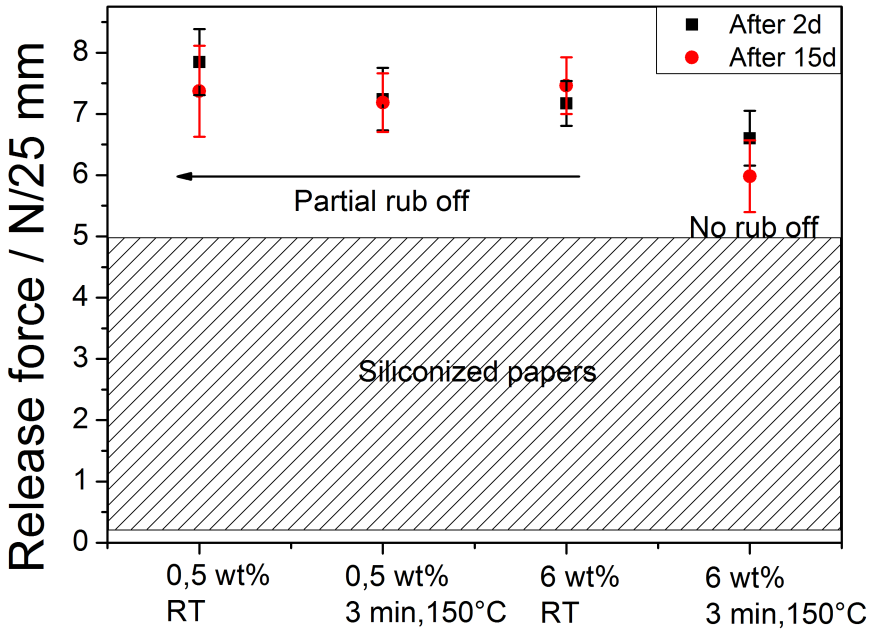

Figure 98: Determination of the release forces of HPC C18 DS3 in THF with 0.5wt% and 6wt% glyoxal. The polymer was applied by blade coater (150 μm, 50 mm/s) to a coat weight of about 2 g/m² and finally dried at room temperature or in oven for 3 min at 150°C. Release forces were measured after 2 d and 15 d storing in climate room.

7.6 Investigation of the anchorage of hydrophobic HPC-esters to the paper surface

The anchorage of the HPC-coatings with DS 2.5 and 3 on the paper surface were indirectly determined by extraction experiments and measuring the static contact angle (Figure 99). The HPC C18 DS2.5 was selected as an additional experiment, because it possesses more hydroxy groups which can undergo crosslinking with glyoxal. This polymer was as well developed by M.Sc. Maximilian Nau in a parallel Ph.D. thesis. All coated papers posses a hydrophobic contact angle (> 90°) prior to extraction, which originates from the hydrophobic modification of HPC. The contact angle of HPC C18 DS3 is slightly higher (104°) compared to the contact angle of HPC C18 DS2.5 (99°). This is most likely due to the different substitution pattern of HPC. The contact angle of HPC C18 DS2.5 is slightly reduced by free hydroxy groups. The hydroxy groups may increase the crosslink density and improve the layer stability. The samples were extracted for 4 h in THF in order to remove unbound polymer and the contact angles were measured again. The contact angles of the coatings without glyoxal were significantly reduced below 90°. Thus, the coating exhibits a poor anchorage to the paper and the coating is dissolved from the paper surface. In contrast to this, the contact angles of coatings which were mixed with glyoxal show no change in the contact angle after extraction. This indicates that the anchorage to the paper surface is improved by the addition of glyoxal as a crosslinker. The glyoxal increases the coating stability by forming a network and additionally it can react with hydroxy groups on the paper surface leading to an improved anchorage. Nevertheless, it cannot be excluded that part of the coating was dissolved by THF even if glyoxal was added. The layer stability of modified HPC with DS of 2.5 seems to be as good as for a DS of 3.

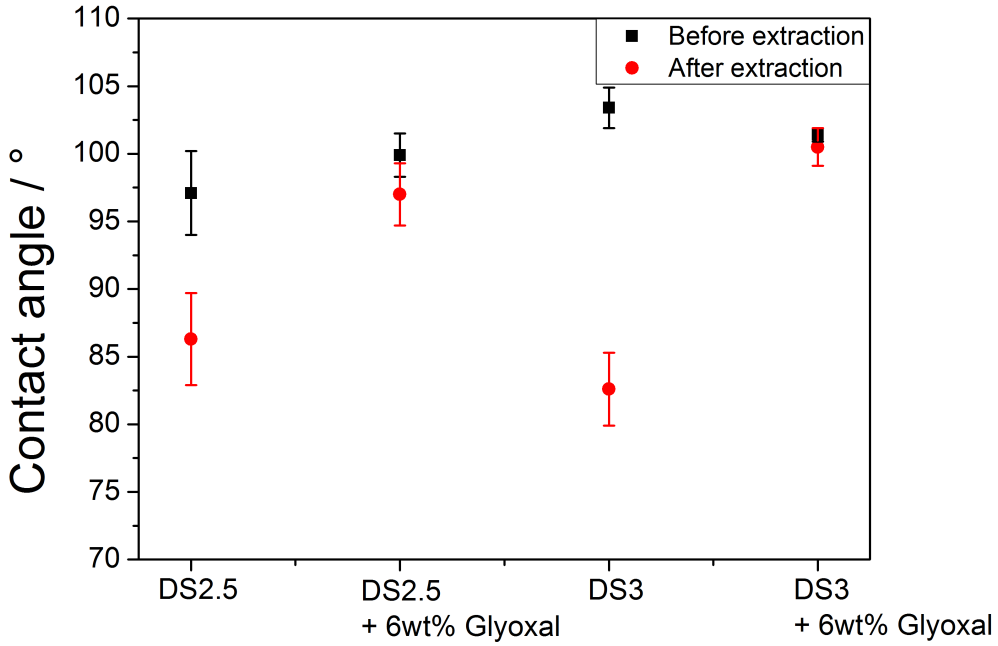

Figure 99: Determination of the static contact angle of papers coated by HPC C18 with DS of 2.5 and 3.0 prior and after 4 h soxhlet extraction with THF. The polymers were dissolved in THF and coated on DN135 by using the blade coater (150 μm, 50 mm/s). The coatings were cured for 5 min at 150°C.

7.7 Development of a water-based suspension of hydrophobised HPC C18 with DS3

In the preceding experiments, HPC C18 DS3 was dissolved in THF and coated on the paper by blade coater, which is possible in lab scale. In contrast to this, production of a release liner according to this method in industrial scale is impractical, because THF is harmful and the coating device would have to be covered by a shell equipped with an air exhauster. Thus, the coating process has to be established in order to enable a coating of modified HPC without the use of THF. A suspension of modified HPC in water has to be developed in order to overcome this challenge. In brief, the HPC C18 DS3 was dissolved in THF to a concentration of 1wt% and precipitated dropwise into a mixture of isopropanol and water (90:10). The suspension did not sediment even after seven days. Thus, a solution of calcium chloride in water was added as a flocculant in order to accelerate sedimentation. The particles sedimented immediately after the addition of the flocking agent. The precipitation agent was decanted and the solid was filtered off. The particles were washed by water and suspended in water which was mixed with a surfactant (Tween 20) in order to stabilize the suspension. This suspension was stable for at least one hour without any mixing process (Figure 100). Analysis of the particle size by SEM showed that small particles ($< 1\ \mu m$) were agglomerated to large particles (5-50 μm) due to the flocculant (Figure 101). This procedure allows the production of water-based suspensions with easy handling and in high yields. The suspension was used in a next step for coating experiments on roller coater and blade coater.

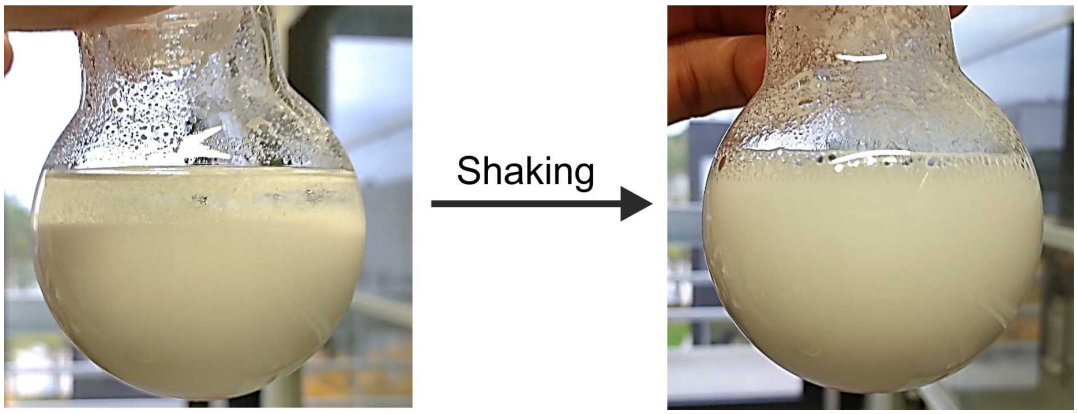

Figure 100: Dipersion of HPC C18 DS 3 (5wt%) in water together with Tween 20 as a surfactant. The suspension was stable for at least one hour without any mixing process.

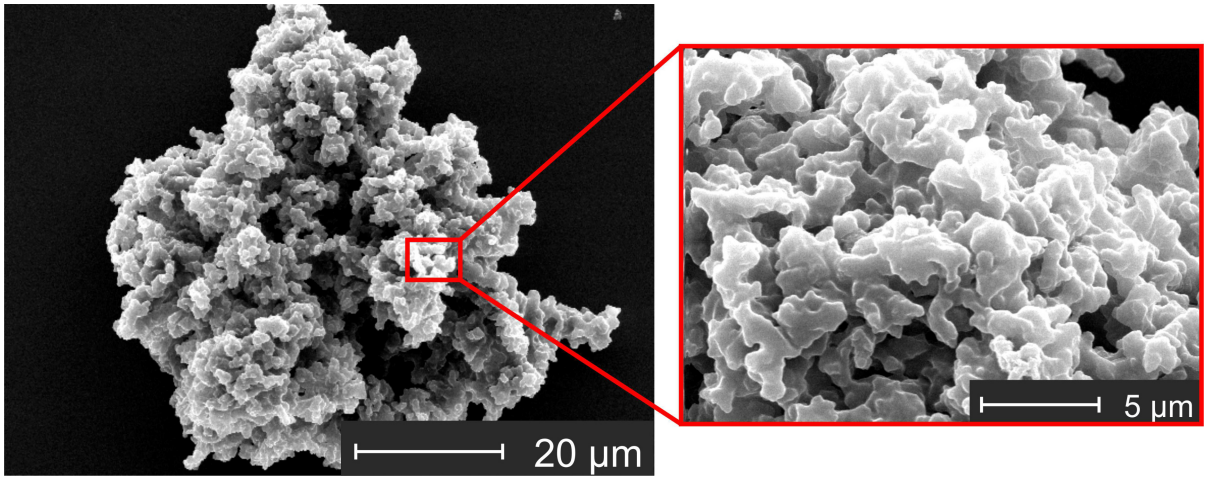

Figure 101: SEM-analysis of HPC C18 DS 3 particles after precipitation in isopropanol/water and flocculation by $CaCl_2$-solution. Small particles are agglomerated to large particles.

7.8 Coating of a water-based suspension of HPC C18 DS3 on CCK paper

First, a water-based suspension of HPC C18 DS3 was applied on S98 paper by using the roller coater. Multiple coating cycles were performed in order to obtain sufficient coat weight. However, the maximum obtained coat weight after four coating cycles was in the order of 0.5 g/m^2. The coating suspension is only poorly transferred from the storage pan to the paper and defects in the coating were observed. The coating process may be enhanced by addition of viscosity modifier to the suspension in order to increase the transfer rate and obtain homogeneous coatings. As an alternative method, the blade coater was used for the coating process in order to increase the coat weight and improve the coating homogeneity. The wet coating film seems to be homogeneously distributed over the paper surface, but coating defects were observed after drying for 3 min at 150°C. The water was removed during drying and it seems that the particles form big agglomerates, leaving non-coated areas (Figure 102). The particle structure was not present anymore, because the coating was heated above the glass transition temperature. The particles were molten together and they form a film, but defects emerged in the coating. This non-coated areas lead to high release forces and paper rupture. The suspension and the coating procedure has to be adjusted in order to obtain a homogeneous coating with sufficient coat weight. This will be investigated in further work since this is a complex process and these engineering challenges are beyond the scope of this thesis.

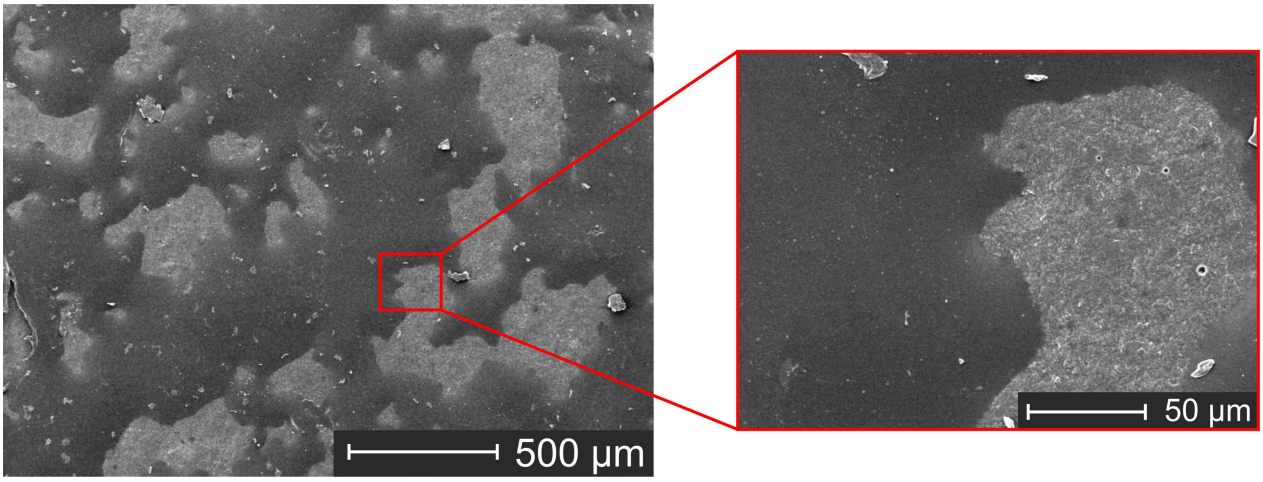

Figure 102: SEM images (topview) of S98 after coating of a water-based suspension of HPC C18 DS3 by blade coater (150 μm, 50 $^{mm}/_{s}$). The coating was dried for 3 min at 150°C. The paper was inhomogeneously coated by the water-based suspension.

7.9 Conclusion

Concluding the results of this chapter, a silicone-free biopolymer was studied which can be utilized as a release liner coating for tight release applications. The bio-based HPC was modified first with long alkyl chains with different DS in order to generate hydrophobicity. This is one property of a silicone release liner, which facilitates low release of an adhesive tape. The release forces were decreased with increasing degree of substitution. Lowest release forces of about 8 $^{N}/_{25\,mm}$ were obtained for HPC C18 DS3, but the coating was not stable on the paper surface and partially removed by the adhesive tape during peel-off. Thus, a crosslinker was introduced, which supports the coating stability itself as well as anchorage to the paper surface. The crosslinking was qualitatively checked by swelling experiments. It was found that glyoxal successfully crosslinks HPC after heat treatment. Glyoxal is also able to crosslink HPC C18 DS 3 after 3 min at 150°C, which indicates that not all hydroxy groups were substituted by alkyl ester chains even at DS of 3. Additionally, hydrolysis reactions may occur after addition of an aqueous and acidic glyoxal solution ($pH = 3$). This may generate free hydroxy groups which can be used for crosslinking reactions with glyoxal. Coating of the hydrophobic HPC together with 6wt% glyoxal showed an improved layer stability and anchorage to the paper surface. This was also shown by extraction experiments and measuring the contact angle of the coatings. The contact angle was significantly reduced after extraction with THF if no glyoxal was added, because the unbound polymer was washed off from the paper surface. In contrast to this, the coating seems to be stable on the paper surface when glyoxal was added to the coating, which was shown by a hydrophobic contact angle after extraction. The rub-off test also confirmed that no coating was removed from the paper. The release forces of HPC C18 DS3 were reduced to about 6 $^{N}/_{25\,mm}$ by the addition of 6wt% glyoxal and curing at 150°C compared to the coating without any crosslinker. This may be explained by the force-dissipative character of the crosslinked coating similar to crosslinked silicone release coatings.

As an outlook, in a next step, the coating of HPC C18 DS3 was switched from a solution in THF to a water-based suspension. This is important for industrial coating processes, because water is harmless

and does not need any expensive safety precautions. Application of the water-based suspension on CCK paper by roller coater and blade coater resulted in an inhomogeneous coating and coating defects. The coating suspension and the coating process have to be optimized in order to get a more homogeneous coating.

8 Summary and Outlook

Silicone release liners exist since over 50 years and the production process has been permanently improved. Most widely used production route for release liner starts with a clay-coated base paper. The large open pores of the base paper are typically coated by pigments in order to close the paper pores. This coating acts as a barrier and penetration of the silicone into the paper is prevented to large extent. Thus, silicone consumption is reduced and the thin silicone coating (typically about 1 μm), which is applied by multiple roller coater, stays on the paper surface. The adhesive is transferred onto the release liner in a second step followed by applications of a label paper to obtain the final product. The clay-coating is a complex mixture and consecutive calendering steps are always necessary in order to compress and smoothen the paper surface. Additionally, commonly used silicone systems use a platinum catalyst, which is expensive and cannot be recovered. Moreover, recycling of silicone-based release liner is not trivial and needs harsh conditions. Thus, the objective of this thesis was to investigate and research new routes for the production of a release liner with the focus on saving, resources and introducing biogenic polymers. Special emphasis was placed on non-clay-coated base papers as a cheaper substrate for the development of a release liner. Film-forming polymers were applied on the porous base paper and utilized as a barrier coating similar to the clay-coating. Final goal of this thesis focused on first demonstration studies of a silicone-free release liner based on modified cellulose.

In this thesis, clay-coated papers as well as porous base papers were used as substrates for coating experiments. The papers were characterized with respect to surface chemistry and surface morphology by using static contact angle measurements, infrared spectroscopy, mercury intrusion porosimetry, white light interferometer and scanning electron microscopy, respectively. SEM investigations showed, that the porous base papers L40 and L90 carry huge open pores in the range of 10 to 40 μm, whereas these pores were closed by clay-pigments at S98, DN135 and DNC135 papers. Silicone penetration into the paper is thus prevented by using a clay-coating and just small open pores (< 1 μm) remain on the paper surface. Analysis of the surface of the base papers by FT-IR showed typical signals for functional groups like C-OH (1024 cm^{-1}) or OH (3310 cm^{-1}) from the cellulose backbone. These signals disappeared when a clay coating is applied on the paper surface and new signals from the clay pigments appeared. The porous base papers L40 (122°) and L90 (112°) possess a hydrophobic contact angle due to different sizing agents, whereas the clay-coated papers (S98, DN135, DNC135) carry a hydrophilic surface (65°). The clay-coating also influences the median pore diameter as well as paper porosity, which were determined by mercury intrusion experiments. The pore diameter and the paper porosity were significantly reduced by the clay-coating. The median pore diameter was decreased from 12 μm for the non-clay coated papers to about 7 μm for the CCK paper. The pores were blocked by the pigments, which also reduce the porosity. The roughness of the paper surface was determined by white light interferometry. An arithmetic average roughness of about 2 μm was measured for the base papers L40 and L90. The paper roughness was significantly reduced to 1.3 μm when the paper surface was clay-coated and calendered (S98). Even more, if higher amounts of clay pigments were applied on the paper surface, the roughness is reduced to 0.8 μm (DN135, DNC135). The parameters, which were determined by various methods are essential in order to interpret different coating behavior and release forces of an adhesive tape.

As a first step, the silicone coat weight has to be adjusted to industrial standards (1 g/m²) in order to obtain appropriate silicone coat weight for the fabrication of a release liner. This was achieved by using the 3-roller system and the film press setup. The silicone coat weight was determined with respect to changing coating parameters. A silicone coat weights of minimum 5 g/m² was obtained with the film press setup, which is too high. The 3-roller system was found to be the most suitable system to reach low silicone coat weights. It was shown that different amounts of silicone were applied on the paper depending on the roller material, the coating speed and the roller pressure between dosing and applicator roll as well as on the paper substrate. An increasing silicone coat weight was observed with increasing coating speed and decreasing roller pressure. Especially at low roller pressure, different amounts of silicone were transferred to the paper at same coating conditions depending on the paper substrate. In detail, most silicone was applied on L40 paper followed by L90 paper and lowest silicone coat weight was achieved for the clay-coated S98 paper. The silicone coat weight can be well adjusted by changing the roller pressure between dosing and applicator roll at constant coating speed. Several optimization steps were necessary in order to obtain low silicone coat weight (1 g/m²) similar to common silicone coat weight of release liner. In particular, rollers composed of stainless steel were acquired and a connection bridge between dosing and applicator roll as well as a second pressure cylinder were installed. Silicone coat weight of about 1 g/m² was achieved at a roller pressure between dosing and applicator roll of 110 N and a coating speed of 2 m/min by using stainless steel rollers. The release forces measured with this specific silicone coat weight strongly depend on the paper substrate. The silicone coat weights were correlated to the corresponding release forces, which facilitates precise adjustment of release forces by changing the coat weight. The force which is needed to remove an adhesive tape from its release liner significantly depends on the surface chemistry, surface porosity and surface roughness, respectively. In detail, release force of 0.2 N/25 mm was observed for the siliconized CCK paper (S98), whereas about 3 N/25 mm was measured for siliconized porous base paper (L90) at similar silicone coat weight of 1 g/m², respectively. This difference is caused by the barrier property of the clay-coating. The silicone is retained on the paper surface and the adhesive is in complete contact with the release coating. In contrast to that, the silicone penetrates in to the porous base paper, when the paper surface is not sealed by a barrier coating. The viscous adhesive creeps into the pores leading to a mechanical interlocking and coming in contact with non-siliconized areas, which leads to high release forces. Additionally, it was shown that the roughness of the CCK papers influences the release forces. Less defects in the silicone coating were observed when the paper is very smooth. It can be summarized that the smoother the paper surface, the better the silicone coverage and the lower the release forces.

Silicone penetration into the paper significantly affects the release forces. Thus, in one approach, silicone was mixed with different amounts of talcum particles in order to reduce the silicone flow into the paper pores during coating process. The particles act as a barrier additive and the increased viscosity even supports this barrier effect. A water-based silicone was selected for this purpose, because this specific silicone yields stable suspensions with the talcum. During coating process on the 3-roller system, the rollers showed incomplete wetting of the water-based silicone/talcum-mixtures, also known as ribbing. This lead to inhomogeneous coatings on the papers, which resulted in coating defects and high release forces. Thus, in order to increase the coating homogeneity, the coatings were applied by lab blade coater using the smallest blade gap size (50 μm). High coat weights of about 9 g/m² were achieved with this

method, which resulted in low release forces of 0.3 N/25 mm. This easy release properties are competitive to CCK release liner, but high amounts of silicone were necessary. The release forces of silicone/talcum mixtures were slightly higher compared to release forces of pure silicone coatings, which is probably due to an increased roughness. It was shown that the talcum can be used as a viscosity modifier in order to reduce silicone penetration into the paper. Nevertheless, the influence of talcum is not fully understood, because paper pores are closed even by using pure silicone in high amounts. In order to investigate the function of talcum in silicone formulations in detail, lower coat weights of about 1-2 g/m² have to be applied by blade coater or a different roller material has to be used for the 3-roller system in order to obtain more homogeneous coatings and improved roller coverage.

In another approach, silicone penetration into the paper was reduced by closing the pores of the paper surface by various film-forming polymers. Synthetic polymers (PVA88%, PVA99%), which were commonly used as barrier coatings, were used as a reference. The barrier properties were compared with new bio-based barrier coatings (HEC, MC). The polymers were applied by using the 3-roller system in various coat weights and the surface coverage was investigated by SEM. Paper pores were increasingly closed with higher polymer amount, but some open pores still remained. This is most likely due to an inhomogeneous wetting of the rollers, which lead to defects in the coating. In contrast to that, the coating homogeneity was significantly enhanced when the polymers were coated by lab blade coater. Mainly all pores were blocked by the polymers, which was featured by SEM analysis. A detailed analysis of the pre-coated papers with respect to the coating homogeneity was performed by labeling the PVA with a fluorescent dye. Investigation of the pre-coated papers by confocal microscopy revealed that the coating was inhomogeneously distributed on the paper surface by the roller coater after first coating cycle, which was depicted as green fluorescent stripes. Coating the same paper up to three times, increases the PVA coverage, but there existed still parts of the paper surface, which were less or not coated by the polymer. In contrast to that, the coating homogeneity was significantly increased when the polymer was applied on the paper by using the blade coater. These results show that barrier properties and the resulting release forces strongly depend on the coating method. The barrier properties were determined by measuring the Bendtsen air permeability. The air permeability was significantly reduced from 1000 ml/min for L90 to about 100 ml/min at a pre-coat weight of 2 g/m² by using the blade coating method. Additionally, the bio-based polymers show same performance in closing paper pores and acting as barrier coating as compared to commonly used synthetic polymers.

In a next step, a thin silicone layer was applied on the pre-coated papers in order to produce the release liner. It was observed that less silicone was transferred to the papers at same coating conditions, if the coat weight of the pre-coatings was increased. This behavior originates from the paper surface, which is increasingly closed with growing polymeric pre-coat. Silicone penetration into open pores is reduced and less silicone is transferred to the paper. Comparing the release forces of the siliconized papers, which were either pre-coated by roller or blade coater, huge differences con be observed. Papers pre-coated by blade coater show significant lower release forces compared to papers which were pre-coated by roller coater. The barrier properties were enhanced due to a more homogeneous coating when the polymers were applied by blade coater. The silicone on blade-coated papers stays on the paper surface in most parts and the adhesive is in intimate contact with the silicone layer. In contrast to this, some part of the silicone is pushed into the open pores of the roller-coated papers. The adhesive migrates into these pores

and comes in contact with non-siliconized parts of the paper, which results in higher release forces. Thus, the barrier properties of papers with respect to silicone, which were pre-coated by blade coater are better in contrast to the roller-coated papers. The release forces were significantly reduced from 6.5 N/25 mm for the uncoated L90 paper to about 0.6 N/25 mm for the pre-coated L90 paper by using HEC. Even lower release forces, below 0.5 N/25 mm, were obtained for pre-coated L40 papers, because more silicone was transferred to this paper. MC closes paper pores as good as the HEC or the synthetic polymers, but this specific polymer suffers from a poor chemical coating stability. The anchorage of the polymer to the paper fibers was impaired, because less hydroxy groups were accessible for hydrogen bonds with the cellulose fibers. Additionally, the formation of covalent bondings between the silicone layer and the MC by post-curing processes was diminished due to less amounts of accessible hydroxy groups. The silicone may be removed by the adhesive during peel-off, which negatively affected the performance of the adhesive tape. As no silicone rub-off is required by the industry, MC is a less appropriate candidate for barrier coatings in release liner applications. However, for future experiments, the amount of hydroxy groups in MC may be tailored in order to get a sufficient layer stability to the paper at one side, but enabling a detachment of the release coating by mechanical abrasion of the coating on the other side. This would further support the recycling process of siliconized release liner, because the silicone layer can be more easily removed from the paper. With these sets of experiments, it was shown that it was possible to produce a release liner starting with a porous base paper by using different film-forming, bio-based polymers. The release forces obtained by this method were applicable for wide variety of applications in the range of easy and medium release. This process saves cost and resources, because extensive refining and calendering steps can be avoided. Especially, the bio-based polymers showed promising barrier properties, which were competitive to the commonly used synthetic barrier polymers. Additionally, the bio-based pre-coatings support the recycling of release liner, because the coating can be easily hydrolyzed by acid or base and removed from the paper. Beside the investigated polymers, other biogenic polymers like starch or polylactic acid may also be possible candidates as barrier coatings for silicone.

In the last part of the thesis, a silicone-free release liner was studied as a proof-of-concept demonstration based on modified hydroxypropyl cellulose (HPC). The release coating, based on the cellulose backbone, can be decomposed by acid or enzymes, which supports recycling of release papers. HPC was reacted with stearic acid chloride (C18) to yield different degrees of substitution (DS). The resulting polymers were dissolved in THF and applied on CCK paper by blade coater. It was shown that the release forces can be adjusted by tailoring the DS of HPC C18. Lowest release forces of about 8 N/25 mm were obtained when all three hydroxy groups of the HPC were substituted by C_{18}-esters, which is high compared to silicone release liner. Fluorescent labeling of the release coating and analysis of the adhesive tape by fluorescence microscopy after peel-off-testing revealed that the coating was not stable on the paper surface. Parts of the coating were removed by the adhesive tape during peel-off, which affects the adhesive performance. Glyoxal was used as a crosslinker, which successfully undergoes crosslinking reactions with the hydroxy groups of unmodified HPC at 150°C. The crosslinker should improve the coating stability and the anchorage to the paper surface. The crosslinking reaction was indirectly proven by swelling experiments in water. Crosslinking experiments with glyoxal were reproduced with HPC C18 DS3 and swelling experiments were performed in THF. Surprisingly, it was shown that the modified HPC

crosslinks with glyoxal even at a DS of 3. One reason may be that, residual hydroxy groups remain even at DS of 3, because the DS is determined by ^{1}H-NMR-measurements and carries an error of about 0.2. Another reason may be the acidity of the added glyoxal ($pH = 3$), which enables hydrolysis reactions of the HPC-esters. The obtained free hydroxy groups can be than used for crosslinking reactions with the glyoxal. In a next step, CCK papers were coated by mixtures of HPC C18 DS3 and glyoxal and cured at room temperature or at 150°C, respectively. The coating stability was not enhanced when the coating was cured at room temperature. In contrast to this, thermally curing at 150°C resulted in significant increase in coating stability and no rub-off of the coating was detected from the paper surface. Additionally, long-term measurements of release forces were performed, because release forces have to be stable during storage. It seems that release forces of the coatings with 6wt% glyoxal, which were crosslinked at 150°C after 15 days, were further reduced compared to coatings cured at room temperature. In particular, release forces of 6 $^{N}/_{25\ mm}$ were obtained for the thermally cured coating with 6wt% glyoxal, whereas about 7 $^{N}/_{25\ mm}$ were measured for coatings which were cured under ambient conditions after 15 days. The obtained release forces were higher compared to siliconized release liner, but still interesting for some tight release applications, such as for sealants in roofing or medical devices. Thus, the release liner based on hydrophobic HPC represents a silicone-free alternative without using an expensive platinum catalyst. As an outlook for the application of the hydrophobic HPC coating in large scale, the HPC C18 DS3 was switched from a solution in THF to a water-based suspension. The modified HPC was precipitated, concentrated to a suspension of 5wt% in water and stabilized by addition of a surfactant. The suspension was applied on CCK papers by using the blade coater. The coating was cured at 150°C, but coating defects were observed in the SEM images in the coating. The coating suspension and the drying process have to be improved for future experiments in order to obtain more homogeneous film coatings.

On the base of the performed experiments, the recycling conditions for release paper made of HPC C18 DS3 have to be studied in detail. The question is, whether the release coating can be separated from the substrate in order to improve recyclability of such papers. As a next step, in order to combine both approaches of this thesis, an improved water-based suspension of HPC C18 DS3 together with glyoxal has to be coated on a pre-coated base paper with HEC to obtain a silicon-free release paper without using a CCK paper. Finally, as low amounts of extractables are required from the industry, the extractables in release liner made of pre-coated base papers and modified HPC have to be analyzed.

9 Experimental Section

9.1 Reagents and solvents

Catalyst C 05	Wacker
Chloroform-d_3	Sigma-Aldrich
Crosslinker V24	Wacker
Dehesive 920	Wacker
Dimethylsulfoxide-d_6	Sigma-Aldrich
Ethanol	Brenntag
Fluorescein isothiocyanate	Acros Organics
Glyoxal (40wt% in water)	Sigma-Aldrich
Glutaraldehyde (50wt% in water)	Sigma-Aldrich
Polyvinyl alcohol 87-89% hydrolyzed	Alfa Aesar
Polyvinyl alcohol 99% hydrolyzed	Sigma-Aldrich
Hydroxyethyl cellulose (Tylose H10 YG4)	Shin-Etsu
Hydroxypropyl cellulose (100.000 g/mol)	Alfa Aesar
Methyl cellulose (viscosity 15 cP, 2% solution in water)	Acros Organics
Rhodamine B	Sigma-Aldrich
Stearic acid chloride	Sigma-Aldrich
Syl-off 7920 emulsion	Dow Chemical
Syl-off 7922 catalyst	Dow Chemical
Tetrahydrofuran	Brenntag
Tween 20	Sigma-Aldrich

Paper substrates

Porous base papers L40 and L90	Sappi, Alfeld
CCK papers S98, DN135, DNC135	Sappi, Alfeld

Drying of THF

Sodium and benzophenone were added to THF and stirred under reflux until the solvent got a blue color. After that, THF was distilled off and the solvent was stored over mole sieve (4 Å) under argon atmosphere.

Purification of stearic acid chloride

The black mixture of stearic acid chloride and other acid chlorides was purified by distillation under vacuum (0.14 mbar) using an ether bridge. The liquid was heated to 170 °C and the product was collected in a receiver flask which was cooled by liquid nitrogen. First 10% of the liquid were removed due to impurities and then the pure product was collected. The stearic acid chloride was obtained as a colorless to yellowish liquid and stored under argon atmosphere. The purity was checked by ^{1}H-NMR (Figure

103). – ^{1}H-NMR (300 MHz, $CDCl_3$): δ = 0.88 (t, 3 H, ^{3}J = 7.3 Hz, H-18), 1.26 (m, 28 H, H-4-17), 1.71 (m, 2 H, ^{3}J = 7.0 Hz, H-3), 2.88 (t, 2 H, ^{3}J = 7.0 Hz, H-2).

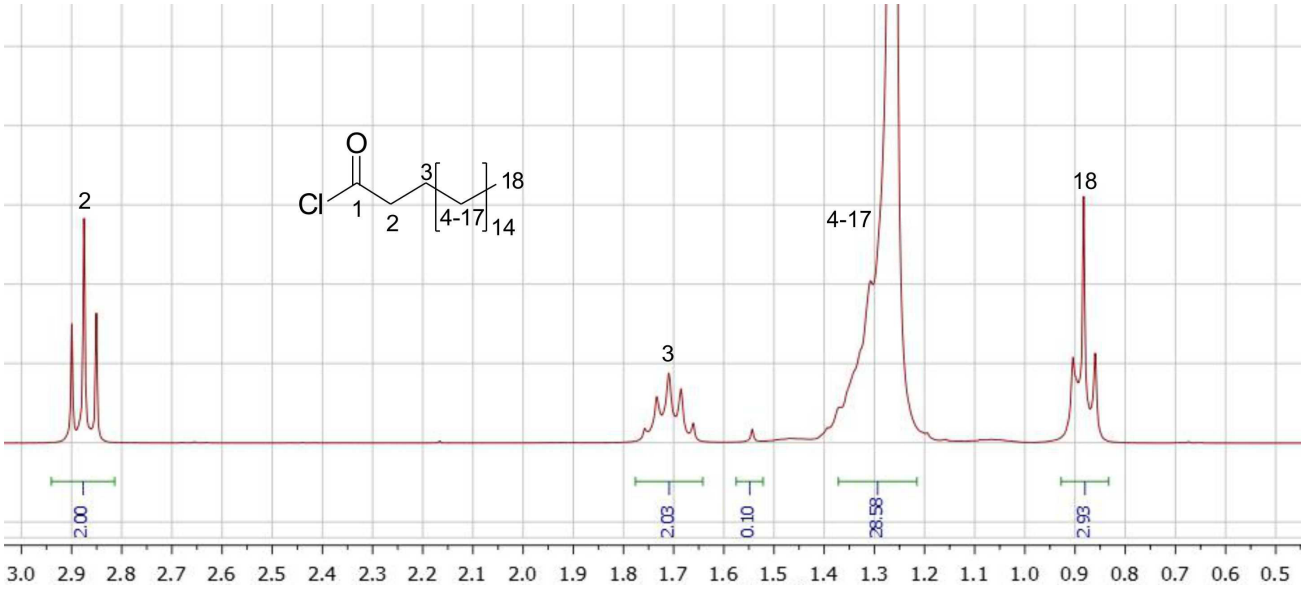

Figure 103: ^{1}H-NMR of purified stearic acid chloride in $CDCl_3$.

Preparation of borax buffer

Borax buffer was prepared by dissolving $Na_2B_4O_7$ x 10 H_2O (9.53 g) in distilled water (0.5 L). The *pH* of the borax solution (85.6 ml, c = 0.05 M) was adjusted to 9 by addition of hydrochloric acid (14.4 ml, c = 0.1 M). The *pH* was checked by a *pH*-meter.

9.2 Instrumentation

ATR FT-IR spectroscopy

Infrared spectra were recorded on a PerkinElmer Spectrum One FT-IR spectrometer, equipped with a ATR unit. For each individual FT-IR spectrum, 10 scans were accumulated with a resolution of 4 cm^{-1}.

Atomic force microscopy (AFM)

The surface topography was investigated by using the atomic force microscope Dimension ICON AFM (Bruker) in PeakForce-Tapping mode. The cantilever ScanAsyst Fluid from Bruker with a tip radius of 10 nm was selected for the measurements. This cantilever possesses a spring constant of 0.86 N/m and a resonant frequency of 70 kHz. All measurements were performed with a drive frequency of 2 kHz and a PeakForce amplitude of 300 nm. The PeakForce was set to 1 nN. The images were recorded with a scan size of 50 μm and a resolution of 256 x 256 pixel. The resulting images were analyzed by using NanoScope Analysis software.

Bendtsen air permeability

The air permeability was measured by using a Bendtsen air permeability tester with a maximum air pressure of 2.2 kPa. The paper sample was placed beneath the air performance test head having a diameter of 3.5 cm, and the air permeability was measured at minimum five independent spots.

Brookfield viscosimetry

The Brookfield viscometer LVDV-II+ was used in combination with spindle DIN-87, LV3 and LV4 in order to determine the viscosity. The correct spindle has to be selected depending on the viscosity of the test sample. The fluid is filled in the tempered container (25°C) and the spindle is immersed in the liquid up to the groove of the spindle. The fluid is tempered for 15 min and the measurement is started with small rpm. The viscosity was taken after 10 s and then the spindle speed was increased.

Contact angle measurement

Static contact angles were measured via the sessile-drop method using a DataPhysics Contact angle OCA 35 instrument and 4 μl droplets of deionized water. The resulting contact angle was measured after 5 s. A silicone droplets (4 μl) were applied by using an Eppendorf pipette. The contact angles measurements were performed under controlled climate conditions at 23 ± 1 °C and 50 ± 2% relative humidity. Minimum five contact angles were measured in order to calculate the mean value.

Drying balance

Concentration of a solution was checked by using the drying balance (Sartorius MA45). Specific volume (1 ml) or weight (1 g) was applied on the aluminium shell and the drying process was started. The drying balance was heated to 100 °C until complete solvent was evaporated and the weight stayed constant. The concentration of the solution was calculated with the final weight of the residue.

Fluorescence microscopy

Fluorescence was recorded using a Olympus BX60 microscope, equipped with a mercury arc lamp. Fluorescent micrographs were captured using an Olympus XM10 camera and appropriate excitation and emission filters. Data acquisition was performed by using an Olympus AnalySIS software. Image analysis was performed using ImageJ software. Confocal laser scanning microscopy was performed using a LEICA TCS SP8 (Leica Microsystems) equipped with an HC PL FLUOTAR 10x/0.30 NA dry objective. The sample was either excited at λ_{ex} = 488 nm for FITC or at λ_{ex} = 552 nm for rhodamine B. The detector was adjusted to 500 – 550 nm for the fluorescence of FITC or to 570 - 650 nm for the fluorescence of rhodamine B.

Mercury porosimetry

The mercury intrusion experiments were either performed on a Micrometrics Autopore IV 9500 at the PMV (Papierfabrikation und Mechanische Verfahrenstechnik), TU Darmstadt or on a mercury porosimeter Porotec Pascal 140/440 (Thermo Fisher) in the research group of Prof. Schneider, TU Darmstadt. In brief, the paper samples were weighed and rolled into the penetrometer. The mercury intrusion volume was measured at low and high mercury pressure and used for the determination of the median pore

diameter and the porosity.

Nuclear Magnetic Resonance (NMR) spectroscopy

NMR spectra were recorded in deuterated solvents on a AC300 Avance II or AR300 Avance III spectrometer at 25°C by the NMR department of the TU Darmstadt. Analyte concentrations were adjusted to 15 $^{mg}/_{mL}$ for ^{1}H-NMR spectra and 30 $^{mg}/_{mL}$ for ^{13}C-NMR spectra using either AC300 Avance II or ARX300 Avance III spectrometer at 25°C. Data analysis was performed using MestreNova (MestreLab Research S.L.).

Scanning electron microscopy (SEM) and EDX-mapping

Paper samples were sputtered with a Cressington 208HR Sputter Coater prior to SEM analysis by a conductive layer of platinum (80%) and palladium (20%) with a layer thickness of approximately 12 nm. SEM images were obtained on a Philips HREM XL 30 FEG XL Series which is equipped with a secondary electron (SE) detector and a x-ray detector. The electron beam was adjusted to 12 kV and a spot size of 3. Si-EDX-mapping measurements were recorded in order to determine the silicone distribution. Radiation of K_α from silicium was selected, and the image was averaged by 16 scans with a resolution of 256 x 200. Dwell time was set to 1000 μs and counts per second were adjusted to at least 900 by changing the spot size.

UV-Vis Spectroscopy

UV-Vis absorption spectra were recorded on a Varian Cary60 UV-Vis in a range of 200 – 800 nm. The base line of the pure solvent was subtracted from the corresponding spectra. Absorption measurements were performed in quartz cuvettes with a thickness of 10 mm at room temperature.

White light interferometry

Surface roughness was analyzed with a Zygo NewView 6k by using a 10x Mirau objective. Paper samples were sputtered by a 50 nm gold layer prior to measurement. A 150 μm scan length was selected in order to collect the topographical image.

9.3 Paper samples

Paper samples were kindly provided by Sappi Alfeld GmbH with a size of 210 x 297 mm (DIN A4). Porous base papers L40 and L90 are one-side machine-glazed and not calendered. The fibers were lightly refined to 30 °SR prior to sheet formation. Additionally, they are surface sized by different sizing agents. The top side of S98 is clay-coated and calendered. Papers to the name of DN135 have a double amount of clay-coating compared to S98 and they are calendered in case of DNC135. Overview of selected papers are shown in Table 12.

Table 12: Overview of selected papers.

Abbreviation	Grammage / g/m²	Info
L40	40	AKD-sized, one-side machine-glazed, not calendered
L90	90	Resin-sized, one-side machine-glazed, not calendered
S98	98	CCK topside coating, calendered
DN135	135	Double amount of clay compared to S98, not calendered
DNC135	135	Double amount of clay compared to S98, calendered

9.4 Coating methods for silicones

9.4.1 Solvent-free silicone

Solvent-free silicone was used from Wacker and mixed as recommended by the manufacturer. In detail, the base polymer with vinyl groups (Dehesive 920), the crosslinker with silane groups (V24) and the catalyst (Cat. C05) were mixed in a ratio of 10:0.26:2.2. The catalyst C05 is a mixture of Dehesive 920 base polymer and the catalyst with a platinum content of 0.115 %. First, crosslinker (V24) was added to the Dehesive 920 in a beaker on the balance. After vigorous stirring, the catalyst (C05) was added and again stirred prior to transfer to the storage pan of the roller coater.

9.4.2 Water-based silicone

Water-based silicone emulsion from Dow was mixed as recommended by the manufacturer. The base polymer (Dow 7920) was mixed with the catalyst (Dow 7922) in a ratio of 90 : 10.

9.5 Surface coating via a roller coater

Surface coating of water-based polymer solutions and silicone was performed by using different roller materials and coating setups of the Sumet roller coater. A minimum fill height of the storage pan was necessary so that the roller was in contact with the solution. In particular, a minimum volume of 50 ml was needed for the 3-roller system and 80 ml for the bigger storage pan of the film press setup. Usually the paper was clamped at the front of the sample carrier for the coating process. Unfortunately, this led to an incomplete coating of the paper surface. Thus, a setup was developed to fix the paper on the surface of the sample carrier by adhesive tape, which resulted in a complete surface coating of the DIN A4 paper (Figure 104). A cardboard was fixed to the sample carrier and a hole with the size of a DIN A4 paper was cutted in the middle of the cardboard. The sample carrier protects the cardboard from silicone contamination and allows fixations of the paper by adhesive tape for complete coating. Minimum three papers were coated for each test series.

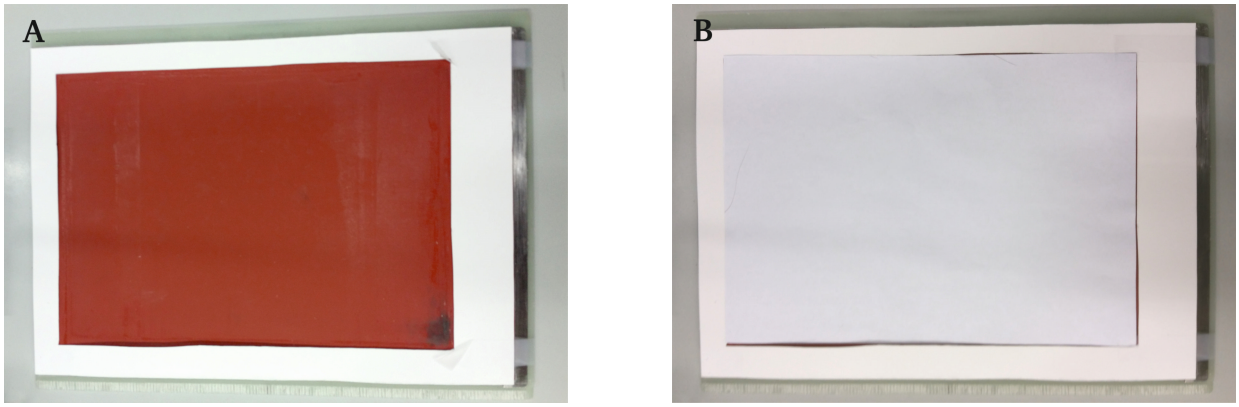

Figure 104: Sample carrier with a cardboard for protection against silicone contaminations (A) and for fixation of a DIN A4 paper to get complete coating (B).

9.5.1 3-Roller-system

The 3-roller system, equipped with a roller material composed of rubber and stainless steel, was used for silicone coatings. The roller pressure between dosing and applicator roll was varied from 30 to 200 N and the speed was changed from 2 to 8 $^{m}/_{min}$. The 3-roller system composed of stainless steel roller was used in order to obtain low silicone coat weights (1 $^{g}/_{m^2}$). The dosing roll is driven by the applicator roll and both rollers having the same speed. The pressure of the pressure roll, which pushes the sample carrier with the paper on the applicator roll, was held constant at 800 N if not other denoted. The silicone coating was first cured by an IR-dryer (100 %) after the sample carrier is passed through the roller and then kept constant for 1 min at 150 °C by air dryer. Both types of silicone were dried under these conditions. If water-based coatings were applied to the paper, the stainless steel rollers have to be purified by HCl (12%) prior to coating in order to remove residual silicone contamination. Water-based solutions (7 wt%) and HPC C18 DS3 dispersions were applied on the paper at a minimum roller pressure of 30 N and 2 $^{m}/_{min}$ by using stainless steel rollers. A roller pressure below 30 N led to inhomogeneous coatings because the dosing roll and applicator roll were not constantly in contact. Coating of water-based solutions were dried for 30 s at 60 °C. A detailed overview about the coating setup is given in the methods section in figure 18.

9.5.2 Film press setup

The influence of coating parameters on silicone coat weight was studied by using the film press setup. For this purpose, metering bars with different groove sizes (0 μm, 10 μm, 20 μm, 30 μm) were used. The coating speed was varied from 10 - 35 $^{m}/_{min}$ and the pressure of the metering bar to the applicator roll was changed from 40 - 110 N. Silicone coating was cured by an IR-dryer (100 %) after the sample carrier passed the roller and then kept for 1 min at 150 °C by air dryer. The pressure of the pressure roll stayed constant at 800 N. A detailed overview about the coating setup is given in the methods section in figure 19.

9.5.3 Blade coating procedure

Water-based polymer solutions (7 wt%), aqueous dispersions of HPC C18 DS3 (7 wt%) and HPC esters dissolved in THF were applied onto paper substrates by using the blade coater (BYK Film Applicator) with blade gap sizes of 50 μm, 100 μm and 150 μm (Figure 105). The polymer solution (2 mL) was filled in the blade with a syringe and then the blade moved with a constant speed of 50 $^{mm}/_{s}$ along the paper so that the solution spreads over the substrate. Coatings of water-based solution were dried for 2 min at 60 °C in oven. Water-based silicone emulsion and silicone/talcum-mixtures were cured for 1 min at 110 °C. Coatings of esterified HPC with glyoxal were dried at 150 °C

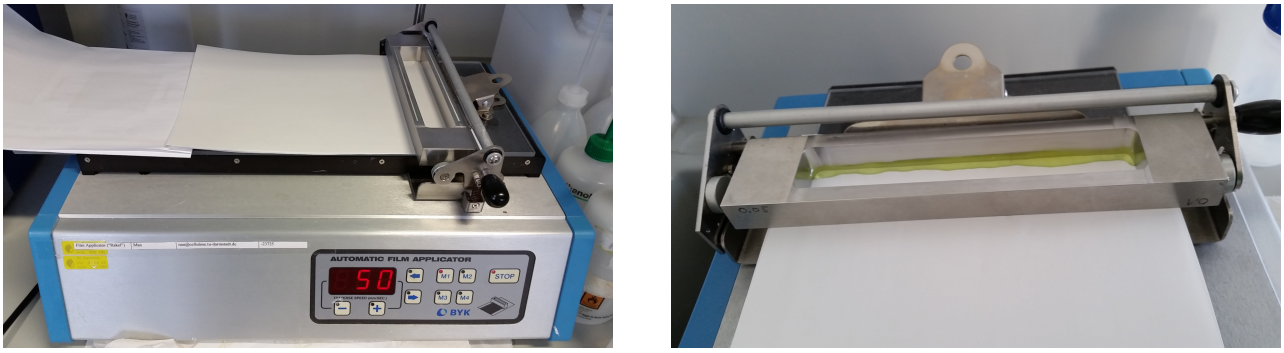

Figure 105: Blade coater (left) and traverse of blade filled with stained PVA solution (right).

9.6 Determination of coat weight

In order to determine the coat weight, papers were stored in a climate-controlled room over night (23 ± 1 °C, 50 ± 2 % r. H.) and weighed before and after each coating step. The silicone mass was determined by using an analytical balance (Sartorius CPA324S). Coat weight is defined as the mass of coating (g) per surface area (m^2). Minimum three papers were weighed for each test series and used in order to determine the coat weight.

9.7 Sample preparation for SEM cross sections

A paper stripe (3 mm width) was cut from the paper sample and freezed in liquid nitrogen for 1 min. After this time, the paper was broken in the liquid nitrogen by using two tweezers and the sample was stuck to the carbon tape on the SEM holder.

9.8 Staining of HPC C18 DS3 with rhodamine B

A stock solution of rhodamine B (1 mg) in THF (20 ml) was prepared. The HPC C18 DS3 was dissolved in THF (20 ml, 10 wt%) and rhodamine B solution (500 μl) was added.

9.9 Swelling experiments

For the investigation of the swelling behavior, 1 ml of a 7wt% solution of HPC or HPC C18 DS3 in THF were transferred in a weighted glass dish and the respective amount of crosslinker was added. The 40wt% glyoxal solution was diluted to 1% for better handling. The solvent was removed under reduced

pressure (800 mbar) and the crosslinking was performed at 150°C at different times. The mixture was cooled, the sample mass in dry state was determined and the swelling agent was added. In case of HPC, water was added and THF was used for swelling experiments of HPC C18 DS3. After 30 min, the swelling agent was decanted and a filter paper was used to remove residual liquid. The mass in swollen state was determined and the swelling ratio was calculated.

9.10 Measuring release forces and rub-off test

The release forces of an adhesive were measured from a siliconized paper according to FINAT 10 in an angle of 180°.[97] The siliconized paper was cut into five strips (27 mm x 175 mm) for measurement of the release forces. Acrylic tape (Tesa 7475, 25 mm x 35 mm) was applied on the release liner strips by a standardized FINAT pressure roll. Double-sided sticky tape (Tesafix 4965, 25 mm x 175 mm) was fixed to the non-coated backside of the paper strips, and the samples were stored between two flat glass plates under a pressure of 70 g/cm² for 20 h. After this time, the paper strips were transferred to the climate room (23 ± 1 °C, 50 ± 2% r. H.) for 4 h. Paper strips were stuck to the metal plate by double-sided adhesive tape and then fixed to the Zwick setup. The protruding site of the adhesive tape was fixed to the clamp. The release forces were measured by a Zwick Z 1.0 equipped with a Xforce HP 20 N load cell in an angle of 180° and a constant speed of 300 mm/min (Figure 106). Stability of silicone anchorage on the paper was qualitatively checked by rubbing a finger over the siliconized paper according to common procedures in industry. The rub-off was judged as good, if no silicone was removed from the paper (no rub-off).

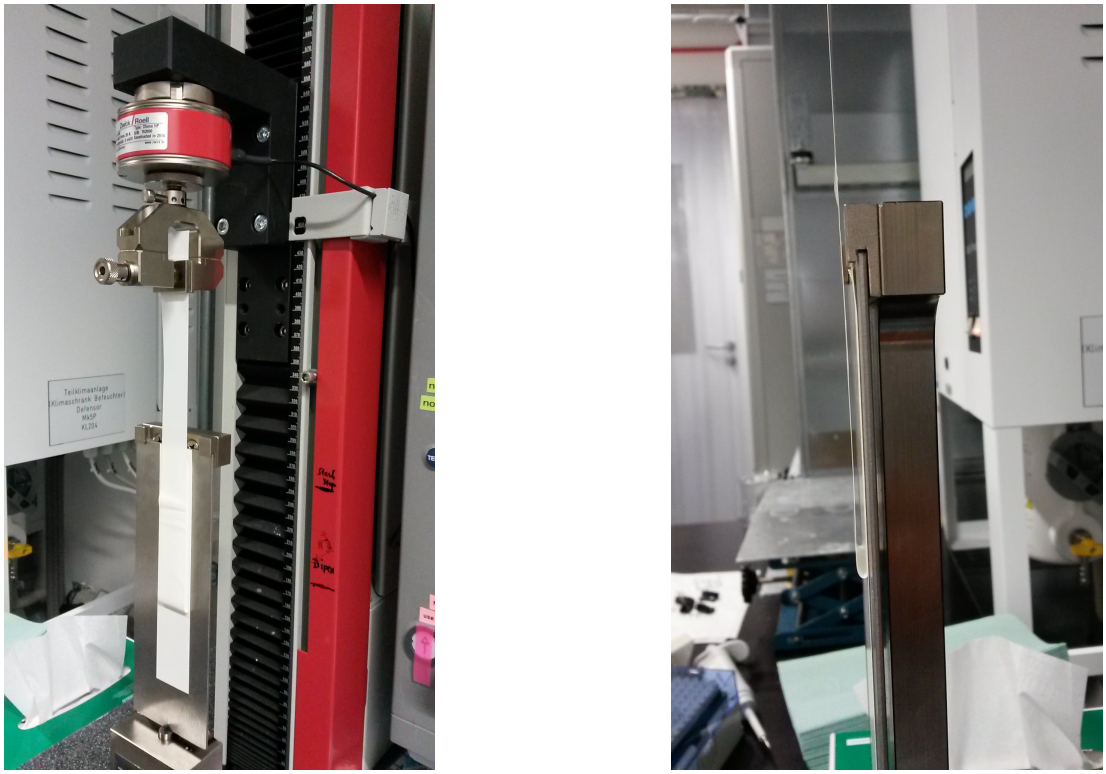

Figure 106: Adhesive tape is removed from the release liner in an angle of 180° according to FINAT 10. View from the front (left) and from the side (right).

9.11 Syntheses

The following protocols of the synthesis of the HPC-esters have been developed in a parallel thesis by M.Sc. M. Nau and have been recently published.[54]

9.11.1 Synthesis of FITC-PVA

A solution of FITC (100 mg, 0.257 mmol, 2.25 eq.) in dry DMSO (20 ml) was added to a solution of PVA 88% (5.00 g, 0.114 mol, 1 eq.) in dry DMSO (300 ml) and stirred at room temperature for 19 h over argon atmosphere. The solution was precipitated in isopropanol (1.2 L) and centrifuged (5 min, 4500 rpm). The polymer was dissolved in water (60 ml) at 70 °C and precipitated in isopropanol (1.2 L). The residue was centrifuged, filtrated and again dissolved in water (60 ml) at 70 °C. This procedure was repeated three times, until no fluorescence was detected in the precipitation agent on the TLC-plate. The solid was freeze–dried and the product was obtained as a yellow, fluffy solid (3.41 g, 0.077 mol). In order to determine the FITC concentration, modified PVA was dissolved in borax buffer (c = 0.05 mol/L; pH = 9). The solution was used to fill in a quartz cuvette with 10 mm thickness, and a UV/Vis spectrum of the solution ($c = 10^{-4}$ M) was recorded from 200 – 800 nm. The FITC concentration was calculated according to the Lambert-Beer law by using the extinction coefficient at λ_{ex} = 495 nm.

9.11.2 Synthesis of HPC C18 with DS 2.5

Esterification of HPC with stearic acid chloride was done according to the procedure described in literature.[54] HPC was dried over night in an oven at 60 °C under vacuum. The following procedure describes the synthesis of HPC C18 with DS of 2.5. Dried HPC (10.0 g, 20.6 mmol, 1 eq.) was dissolved in THF (225 ml) over night to give a 5 wt% solution. A solution of stearic acid chloride (40.6 g, 134 mmol, 6.5 eq.) in THF (200 ml) was added dropwise to the HPC solution. The mixture was then heated to 83 °C and the formed hydrochloric acid was removed by sodium hydroxide solution in a gas washing bottle. The reaction was finished after 5 h by addition of ethanol (30 ml). The solution was precipitated in methanol (1.5 L) and the precipitation agent was decanted. The residue was dissolved in THF (200 ml) and the product was purified by inverse-precipitation with methanol (500 ml). After third purification step, the viscous solid was transferred into a crystallizing dish and dried in oven at 70 °C over night. Liquid nitrogen was added to the crystallizing dish and the crushed product was isolated (13.6 g). The product was analyzed by ^{1}H-NMR (Figure 107).

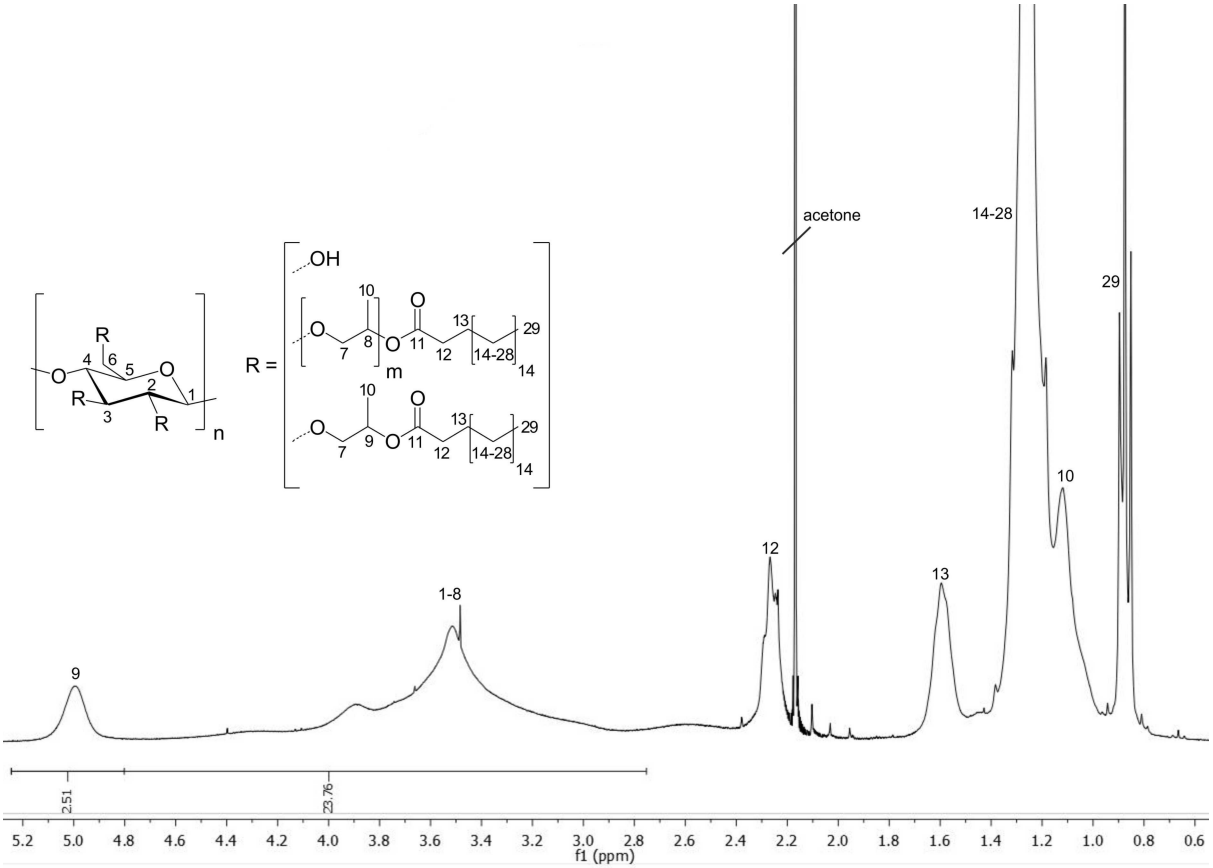

Figure 107: ^{1}H-NMR of HPC esterified with stearic acid chloride in $CDCl_3$.

9.12 Preparation of water-based dispersion of HPC C18 DS 3

Fully esterified HPC with stearic acid chloride (DS 3) was kindly provided by a colleague of the Macromolecular Chemistry and Paper Chemistry research group. HPC C18 DS 3 (5.00 g) was dissolved in THF (500 ml) to get a 1 wt% solution. The solution was precipitated dropwise in a 5 L beaker comprising a mixture of IPA/H_2O (90 : 10; 3 L) at a stirring speed of 400 rpm. Then, 100 μL of a solution of $CaCl_2$ (0.5 g) in water (20 ml) was added to the suspension to induce flocculation. The precipitation agent was decanted and the solid was filtrated and washed by water (3 x 50 ml). The wet solid was transferred to a flask and a mixture of water (50 ml) and surfactant (Tween 20, 90 μL) was added to get a 5wt% stable suspension. The concentration was checked by the drying balance.

Bibliography

[1] Pocius, A. V. *Adhesion and Adhesives Technology*; Carl Hanser Verlag GmbH & Co. KG: München, 2012.

[2] Andriot, M., Ed. *Silicone Release Coatings for the Pressure Sensitive Adhesive Industry. In: Andriot M., DeGroot J.V., Meeks R. Silicones in industrial applications*; Nova Science Publisher, New York, 2009.

[3] Mukherjee, S., Ed. *The Science of Clays*; Springer Netherlands: Dordrecht, 2013.

[4] Bollström, R.; Nyqvist, R.; Preston, J.; Salminen, P.; Toivakka, M. *Tappi J.* **2013**, *4*, 45–51.

[5] Vähä-Nissi, M.; Lathi, J.; Savolainen, A.; Rissa, K.; Lepistö, T. *54th Appita Annual Conference* **2000**, *2*, 581–590.

[6] Benedek, I. *Pressure-Sensitive Adhesives and Applications*; CRC Press: Boca Raton and FL, 2004.

[7] Orlych, G. *PSTC Tech XXVI Global Conference, Orlando, May 12–14* **2004**,

[8] Chalk, A. J.; Harrod, J. F. *JACS* **1965**, *87*, 16–21.

[9] Lewis, L. N.; Stein, J.; Gao, Y.; Colborn, R. E.; Hutchins, G. *Platinum Metal Rev.* **1997**, *41*, 66–75.

[10] Eduok, U.; Faye, O.; Szpunar, J. *Progress in Organic Coatings* **2017**, *111*, 124–163.

[11] Brook, M. A. *Chemistry - A European Journal* **2018**, *24*, 8458–8469.

[12] Desorcie, J. L.; Stein, J. *Journal of Inorganic and Organometallic Polymers* **1991**, *1*, 591–604.

[13] Clarson, S. J., Fitzgerald, J. J., Owen, M. J., Smith, S. D., van Dyke, M. E., Eds. *Science and Technology of Silicones and Silicone-Modified Materials*; ACS Symposium Series; American Chemical Society: Washington and DC, 2007.

[14] Simpson, T. R. E.,; Tabatabaian, Z.; Jeynes, C.; Parbhoo, B.; Keddie, J. L. *Journal of Polymer Science Part A: Polymer Chemistry* **2004**, *42*, 1421–1431.

[15] Saint-Gobain, 8000 Series Film Release Liner. `http://fffcs.com/pdf/ProductLiterature/Film/AFF1017A.pdf`, 2009; [Online; accessed 05-February-2018].

[16] Amouroux, N.; Petit, J.; Léger, L. *Langmuir* **2001**, *17*, 6510–6517.

[17] Satas, D. *Handbook of pressure sensitive adhesive technology*, 2nd ed.; Van Nostrand Reinhold: New York, 1989.

[18] Ghatak, A.; Vorvolakos, K.; She, H.; Malotky, D. L.; Chaudhury, M. K. *The Journal of Physical Chemistry B* **2000**, *104*, 4018–4030.

[19] Pocius, A. V.; J., K. D.; J., Y. D.; Tirell, M.; Thakkar, B.; Mangipudi, V. S. *Plast. Eng.* **1997**, *53*, 31–36.

[20] Leger, L.; Creton, C. *Philosophical Transactions of the Royal Society A: Mathematical, Physical and Engineering Sciences* **2008**, *366*, 1425–1442.

[21] Chaudhury, M.; Pocius, A. V. *Adhesion Science and Engineering: Surfaces, Chemistry and Applications*; Elsevier, 2002.

[22] Packham, D. E., Ed. *Handbook of adhesion*, 2nd ed.; Wiley: Chichester, 2007.

[23] Clint, J. H. *Curr. Opin. Colloid Interface Sci.* **2001**, *6*, 28–33.

[24] Sun, S.; Li, M.; Liu, A. *International Journal of Adhesion and Adhesives* **2013**, *41*, 98–106.

[25] Orlych, G. *Dow Corning Corporation* **2005**,

[26] Eckberg, R. P. *Silicone Release Coatings. In: Tracton A.A. Coating materials and surface coatings* **2007**, *47*, 1–10.

[27] Horgnies, M.; Darque-Ceretti, E.; Felder, E. *Int. J. Adhes. Adhes* **2007**, *27*, 661–668.

[28] Do Amaral, M.; Roos, A.; Asua, J. M.; Creton, C. *Journal of Colloid and Interface Science* **2005**, *281*, 325–338.

[29] Horgnies, M.; Darque-Ceretti, E.; Combarieu, R. *Journal of Adhesion Science and Technology* **2004**, *18*, 1047–1061.

[30] Kowalski, A.; Czech, Z. *International Journal of Adhesion and Adhesives* **2015**, *60*, 9–15.

[31] Yamauchi, T.; Cho, T.; Imarnura, R.; Murakarmi, K. *Nordic Pulp Paper Res. J.* **1989**, *4*, 43–47.

[32] Pelton, R.; Chen, W.; Li, H.; Engel, M. R. *The Journal of Adhesion* **2001**, *77*, 285–308.

[33] Zhao, B.; Pelton, R. *J. Adhes. Sci. Technol.* **2003**, *17*, 815–830.

[34] Zhang Newby, B.-m.; Chaudhury, M. K. *Langmuir* **1997**, *13*, 1805–1809.

[35] Zhang Newby, B.-m.; Chaudhury, M. K. *Langmuir* **1998**, *14*, 4865–4872.

[36] Gordon, G. V.; Schmidt, R. G. *The Journal of Adhesion* **2006**, *72*, 133–156.

[37] Muschelewicz, K. J.; Pittillo, C. V.; Allen, B.; McEwen, T. *Tech 30 Global Conference VI, Orlando, May 16–18* **2007**,

[38] Wiliams, P. L. *Anti-stick coating* **1958**, US 2829073.

[39] Schwarcz, A.; Niskayuna, N. Y. *Release agents suitbale for use with pressure sensitive adhesive tapes* **1976**, *US 3970599*.

[40] Kinning, D. J. *The Journal of Adhesion* **1997**, *60*, 249–274.

[41] Li, L.-H.; Macosko, C.; Korba, G. L.; Pocius, A. V.; Tirrell, M. *The Journal of Adhesion* **2001**, *77*, 95–123.

[42] Belosinschi, D.; Chabot, B.; Brouillette, F. *BioResources* **2012**, *7*, 902–912.

[43] Martinez, P.; Kwon, J. Y.; Guerin, D.; Ryu, J.-Y. *Pira specialty papers EU 2016, Manchester, April 7* **2016**,

[44] Adamko, M. A.; Friedman, M.; Waldenberger, D. *Silicone-free release films* **1996**, *US 5817386 A*.

[45] Lonc, G.; Spitzer, J. *Release coating for tapes* **2001**, *WO 2001049801 A1*.

[46] Brandenburg, R. *Silikonfreies Trennpapier* **2004**, *DE 102004012734 A1*.

[47] Ando, M.; Inokuchi, S.; Nonaka, N. *Release liner and pressure-sensitive adhesive sheet* **2006**, *EP 2087995 A1*.

[48] Emslander, J. O.; Clements, J. C. *Release materials* **2008**, *US 20110143134 A1*.

[49] Eevers, W.; Issaris, N.; Wasbauer, I.; Dubreuil, M. F.; Vangeneugden, D. *Release Liner* **2010**, *EP 1978067 B1*.

[50] Brown, P. L.; Stickles, D. L. *Pressure sensitive adhesive release liner and fluorosilicone compounds, compositions and method therefor* **1986**, *US 4736048 A*.

[51] Berlioz, S.; Stinga, C.; Condoret, J.; Samain, D. *International Journal of Chemical Reactor Engineering* **2008**, *6*.

[52] *Handbook of adhesion*; Advances in Carbohydrate Chemistry and Biochemistry; Elsevier, 2010.

[53] Schmid, M.; Sängerlaub, S.; Miesbauer, O.; Jost, V.; Werthan, J.; Stinga, C.; Samain, D.; Stramm, C.; Noller, K.; Müller, K. *Polymers* **2014**, *6*, 2764–2783.

[54] Nau, M.; Seelinger, D.; Biesalski, M. *Cellulose* **2018**, *134*, 44949.

[55] Andersson, C. *Packag. Technol. Sci.* **2008**, *21*, 339–373.

[56] Hult, E.-L.; Ropponen, J.; Poppius-Levlin, K.; Ohra-Aho, T.; Tamminen, T. *Industrial Crops and Products* **2013**, *50*, 694–700.

[57] Bollström, R.; Tuominen, M.; Määttänen, A.; Peltonen, J.; Toivakka, M. *Prog. Org. Coat.* **2012**, *73*, 26–32.

[58] Zhu, Y. D.; Allen, G. C.; Adams, J. M.; Gittins, D. I.; Hooper, J. J.; Skuse, D. R. *Polymer Chemistry* **2013**, *4*, 4386.

[59] Iyengar, G.; Point, S. *Better curing coated release liner substrate* **2012**, *US 2012/0121893 A1*.

[60] Reinhardt, B.; Viehmeyer, V.; Hottenträger, M. *Release base paper having silicate containing primer coats* **1998**, *US 5,807,781*.

[61] Knauf, G. H. *Release liner base stock for printed films or labels* **2001**, *US 6,210,767 B1*.

[62] Schuman, T.; Wikström, M.; Rigdahl, M. *Surface and Coatings Technology* **2004**, *183*, 96–105.

[63] Koskinen, K. *Method for manufacturing base paper for release paper* **2005**, US 2005/0123629 A1.

[64] Bertrand, J.-F. *A method of manufacturing of glassine paper* **2014**, *WO 2014091071 A1*.

[65] Dufour, M. *Cellulosic fibre-based support containing a modified PVA layer methods for production and use* **2013**, *US 2013/0010134 A1*.

[66] Dudek, E.; Michel, S. *Impregnation materials for Release Papers* **2013**, *DE 102013107329 A1*.

[67] Anthony, R.; Xiang, Z.; Runge, T. *Prog. Org. Coat.* **2015**, *89*, 240–245.

[68] Rastogi, V.; Samyn, P. *Coatings* **2015**, *5*, 887–930.

[69] Tang, X. Z.; Kumar, P.; Alavi, S.; Sandeep, K. P. *Critical Reviews in Food Science and Nutrition* **2012**, *52*, 426–442.

[70] Ghista, D. N., Ed. *Biomedical Science, Engineering and Technology*; InTech, 2012.

[71] Aldana, D.; Villa, E.; De Dios Hernández, Miguel,; Sánchez, G.; Cruz, Q.; Gallardo, S.; Castillo, H.; Casarrubias, L. *Polymers* **2014**, *6*, 2386–2403.

[72] Gicquel, E.; Martin, C.; Garrido Yanez, J.; Bras, J. *J. Mater. Sci.* **2017**, *52*, 3048–3061.

[73] Syverud, K.; Stenius, P. *Cellulose* **2009**, *16*, 75–85.

[74] Lavoine, N.; Desloges, I.; Khelifi, B.; Bras, J. *J. Mater. Sci.* **2014**, *49*, 2879–2893.

[75] Mazhari Mousavi, S. M.,; Afra, E.; Tajvidi, M.; Bousfield, D. W.; Dehghani-Firouzabadi, M. *Cellulose* **2017**, *24*, 3001–3014.

[76] Tracton, A. A. *Coatings materials and surface coatings*; CRC Press: Boca Raton and FL, 2007.

[77] Colas, A. *Dow Corning, Life Sciences* **2005**,

[78] Anthony, J. *Basic silicone chemistry - a review* **2009**, *Silicone Spectator*.

[79] Colas, A.; Curtis, J. *Silicone Biomaterials: History and Chemistry & Mediacal Applications of Silicones*; Elsevier, 2004.

[80] Vert, P. T.; Cray, S. *Tech 30 Global Conference VI, Orlando, May 16–18* **2007**,

[81] Stäubner, M.; Schmid, H. *Entwicklung eines Strichkonzepts zur Herstellung von Silikontrennpapieren unter Einsatz der Merhschicht-Curtain Coater Technologie* **2010**, *PTS-Forschungsbereicht IGF 16407*.

[82] Kuo, A. C. M. *Silicone Release Coatings for the Pressure Sensitive Industry – Overview and Trends* **1998**, *Dow Corning Corporation*.

[83] Smook, G. A.; Kocurek, J. *Handbook for pulp and paper technologists* **2003**, *Angus Wilde Publications*.

[84] Benjamin, D. F.; Anderson, T. J.; Scriven, L. E. *AIChE Journal* **1995**, *41*, 1045–1060.

[85] Wilson, M. C. T.; Gaskell, P. H.; Savage, M. D. *European Journal of Applied Mathematics* **2001**, *12*.

[86] Roesler, G. *Fall Technical Conference, Scottsdale, AR, USA* **2007**,

[87] Howatt, G.; Breckenridge, R. *J. Am. Ceram. Soc.* **1947**, *30*, 237–242.

[88] Berni, A.; Mennig, M.; Schmidt, H. *Sol-Gel Technologies for Glass Producers and Users*; Springer US, 2004.

[89] Wengeler, L.; Schmitt, M.; Peters, K.; Scharfer, P.; Schabel, W. *Chemical Engineering and Processing: Process Intensification* **2013**, *68*, 38–44.

[90] Chou, Y. T.; Ko, Y. T.; Yan, M. F. *J. Am. Ceram. Soc.* **1987**, *70*, C–280–C–282.

[91] Pitchumani, R.; Karbhari, V. M. *J. Am. Ceram. Soc.* **1995**, *78*, 2497–2503.

[92] Tok, A. I.; Boey, F. Y.; Lam, Y. C. *Mater. Sci. Eng. A* **2000**, *280*, 282–288.

[93] Zhang, G.; Wang, Y.; Ma, J. *Mater. Sci. Eng. A* **2002**, *337*, 274–280.

[94] Gao, B.; Liu, H.; Gu, Z. *Langmuir* **2014**, *30*, 15041–15046.

[95] Endres, I.; Tietz, M. *Tappi J.* **2007**, *6*, 24–32.

[96] Gordon, G. V.; Perz, S. V.; Tabler, R. L.; Stasser, J. L.; Owen, M. J.; Tonge, J. S. *Silicone Release Coatings: A Closer Look at Release Mechanisms* **1998**, *Dow Corning Corporation*.

[97] Jack, A. *FINAT technisches Handbuch* **2001**, 26–27.

[98] Gradowski, S. v.; Torborg, C.; Biesalski, M. *Cellulose* **2018**, *17*, 6510.

[99] *Hariharan,P. Basics of Interferometry*; Elsevier, 2007.

[100] Depiereux, F.; Konig, N.; Pfeifer, T.; Schmitt, R. *IEEE Transactions on Instrumentation and Measurement* **2007**, *56*, 2279–2283.

[101] Meggitt, B. T. In *Optical Fiber Sensor Technology*; Grattan, K. T. V., Meggitt, B. T., Eds.; Springer US: Boston and MA, 2000; pp 193–238.

[102] Bandyopadhyay, S. *International Conference on Optics & Photonics* **2015**,

[103] Grattan, K. T. V., Meggitt, B. T., Eds. *Optical Fiber Sensor Technology*; Springer US: Boston and MA, 2000.

[104] Raz, E. *Review of Scientific Instruments* **1996**, *67*, 3416–3419.

[105] Zygo, *MetroPro Reference Guide OMP-0347K* **2006**,

[106] Sobhana, S. S. L.; Bogati, D. R.; Reza, M.; Gustafsson, J.; Fardim, P. *Micropourous and Mesoporous Materials* **2016**, *225*, 66–73.

[107] Djomgoue, P.; Njopwouo, D. *J. Surf. Eng. Mater. Adv. Technol.* **2013**, *3*, 275–282.

[108] Madejova, J. *Vib. Spectrosc* **2003**, *31*, 1–10.

[109] Giesche, H. *Particle & Particle Systems Characterization* **2006**, *23*, 9–19.

[110] Yusoff, N. S.; Ahmad, M. S.; Akil, H. M.; Ariffin, K. S.; Ariffin, A. *J. Reinf. Plast. Compos* **2010**, *29*, 3442–3449.

[111] Wacker, *Technical data sheet Dehesive 920*; 2014.

[112] Whitesides, G. M.; Bowden, N.; Brittain, S.; Evans, A. G.; Hutchinson, J. W. *Nature* **1998**, *393*, 146–149.

[113] Chen, X.; Hutchinson, J. W. *Journal of Applied Mechanics* **2004**, *71*, 597.

[114] Rayven, Release Liner Values. http://www.rayven.com/values-rayven.php, 2015; [Online; accessed 05-May-2018].

[115] Elkem, Our full spectrum of silicone release solutions. http://www.elkem-silicones.cn/ZH/Our_offer/KEC/ListInstance_Brochure_Title/Silcolease_Brochure.pdf, 2018; [Online; accessed 17-December-2018].

[116] Film, M. P. Pressure-Sensitive Label Facestock & Release Liners. http://www.m-petfilm.com/applications/pressure-sensitive-label-facestok-release-liner/, 2018; [Online; accessed 17-December-2018].

[117] Tesa, *Product information Tesaband 7475*; 2014.

[118] Bikerman, J. J. *Tappi Journal* **1961**, *44*, 568–571.

[119] Johnson, L. M.; Gao, L.; Shields IV, C.; Smith, M.; Efimenko, K.; Cushing, K.; Genzer, J.; López, G. P. *J. Nanobiotechnology* **2013**, *11*, 22.

[120] IMERYS, *Product data sheet Steamic T1 CA*; 2011.

[121] Hasegawa, T.; Sorimachi, K. *AIChE Journal* **1993**, *39*, 935–945.

[122] Lie, K. N.; Chiu, Y. M.; Jang, J. Y. *Journal of Mechanics* **2009**, *25*, 167–175.

[123] Lopez, F. V.; Rosen, M. *Latin American Applied Research* **2002**, *32*, 247–252.

[124] Gutoff, E. B., Cohen, E. D., Eds. *Coating and drying defects: Troubleshooting operating problems*, 2nd ed.; 2006.

[125] Lee, J. H.; Han, S. K.; Lee, J. S.; Jung, H. W.; Hyun, J. C. *Korea-Australia Rheology Journal* **2010**, *22*, 75–80.

[126] Rotenberg, B.; Patel, A. J.; Chandler, D. *J. Am. Chem. Soc.* **2011**, *133*, 20521–20527.

[127] Koca, H. D.; Doganay, S.; Turgut, A.; Tavman, I. H.; Saidur, R.; Mahbubul, I. M. *Renewable and Sustainable Energy Reviews* **2018**, *82*, 1664–1674.

[128] Sabnis, R. W. *Handbook of fluorescent dyes and probes*.

[129] Hess, J.; Sena-Gomes, R.; Davie, L.; Sykes, M. *Tappi Pulping Conference* **2001**,

[130] Venditti, R.; Gilbert, R.; Zhang, A.; Abubakr, S. *Tappi Recycling Symposium* **2000**,

[131] Ledbetter, M. D.; Trojan, K. L. *Process for recycling waste film and product made therefrom* **2011**, US 2011/0168325 A1.

[132] Gebben, B.; van den Berg, Hans W.A.,; Bargeman, D.; Smolders, C. A. *Polymer* **1985**, *26*, 1737–1740.

[133] Tillet, G.; Boutevin, B.; Ameduri, B. *Prog. Polym. Sci.* **2011**, *36*, 191–217.

[134] Zhang, Y.; Zhu, P. C.; Edgren, D. *Journal of Polymer Research* **2010**, *17*, 725–730.

[135] Hansen, E. W.; Holm, K. H.; Jahr, D. M.; Olafsen, K.; Stori, A. *Polymer* **1997**, *38*, 4863–4871.

[136] Begam, T.; Nagpal, A. K.; Singhal, R. *J. Appl. Polym. Sci.* **2003**, *89*, 779–786.

[137] Park, H.; Guo, X.; Temenoff, J. S.; Tabata, Y.; Caplan, A. I.; Kasper, F. K.; Mikos, A. G. *Biomacromolecules* **2009**, *10*, 541–546.

Appendix

Analysis of base papers by SEM

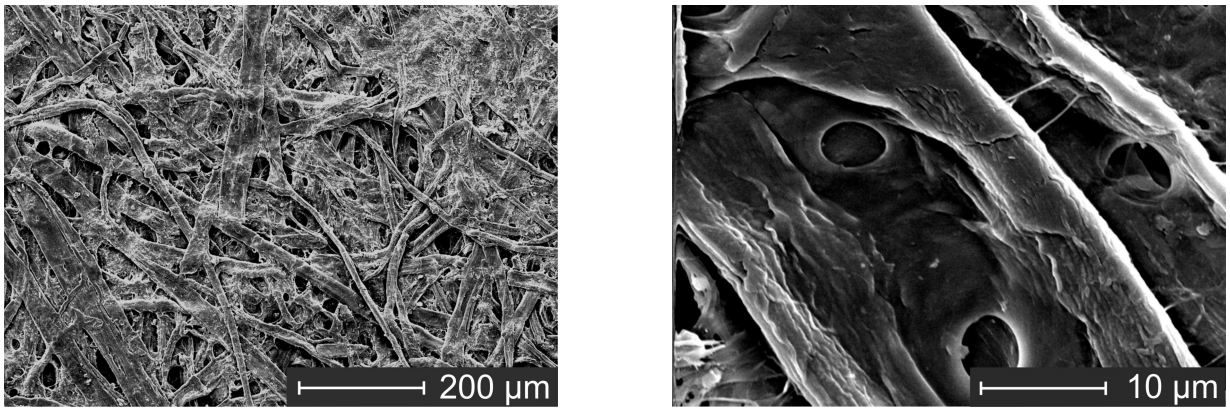

Figure 108: SEM images (topview) of L90 at different magnifications.

SEM images of different sorts of talc

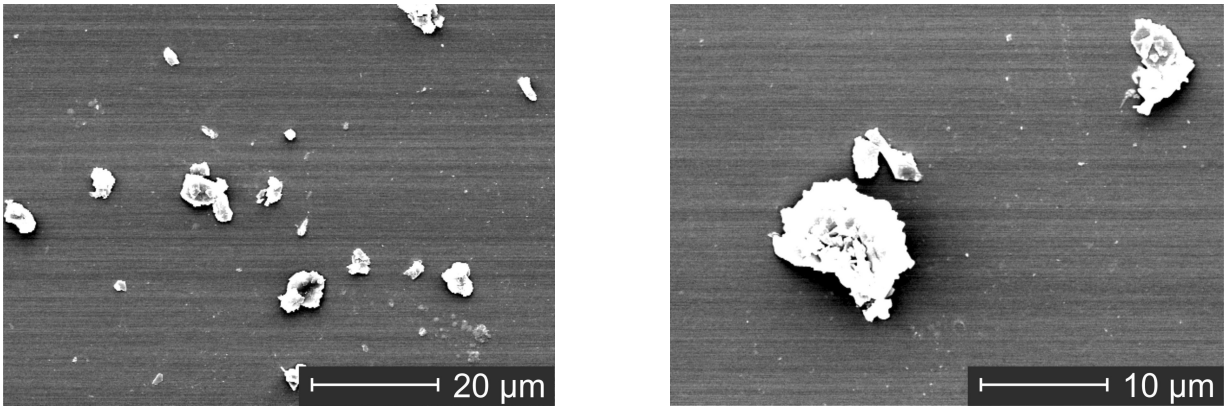

Figure 109: SEM images of talcum T1 CA having a particle size ranging from 4-12 μm.

SEM images (topview) of pre-coated base papers

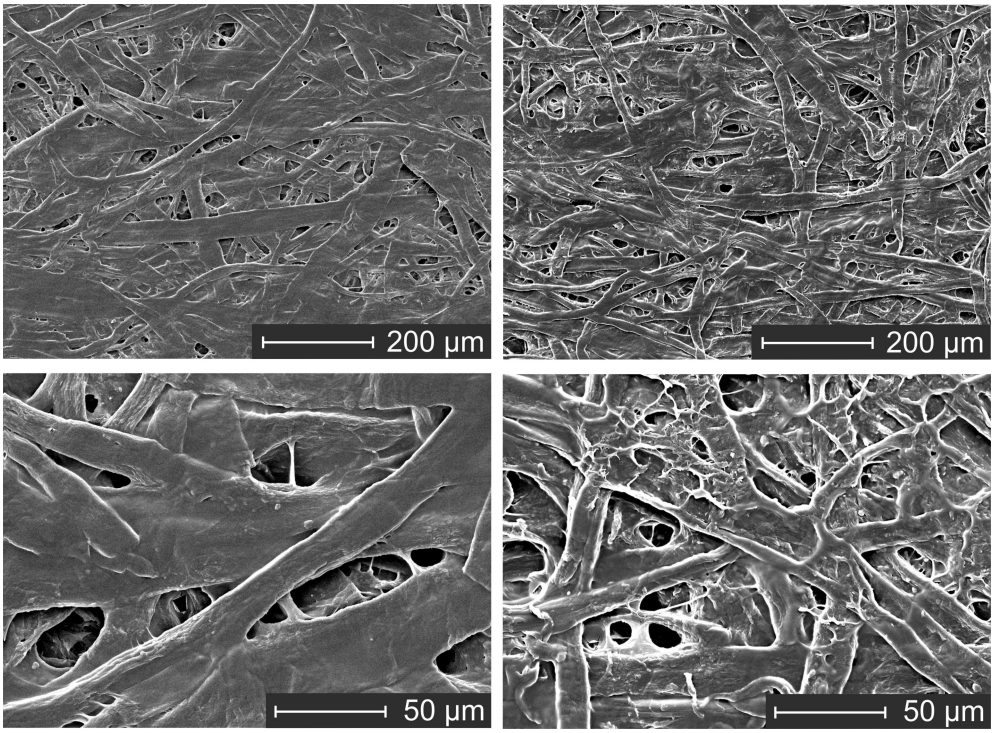

Figure 110: SEM images (topview) of L90 coated by 2.2 g/m² PVA99% (left) and 2.1 g/m² MC (right). The papers were coated three times by roller coater at same coating conditions (30 N, 2 m/min)

Curriculum Vitae M. Sc. Sebastian von Gradowski

Persönliche Daten

Sebastian von Gradowski
Mühlenkamp 21
D-40229 Düsseldorf

Geburtsdatum: 19.02.1989
Geburtsort: Ahlen / Nordrhein-Westfalen

Beruflicher Werdegang

09/2018 – heute	Henkel AG & Co. KGaA, Düsseldorf Produktentwickler für wasserbasierte Klebstoffe

Akademische Ausbildung

11/2014 – 03/2019	Technische Universität Darmstadt Promotion am Institut für Makromolekulare Chemie und Papierchemie unter der Leitung von Prof. Dr. M. Biesalski Promotionsthema: ,,Biogenic Polymers: From Barrier Coatings towards the Design of novel low-adhesive Release Liner“
10/2012 - 10/2014	Universität Siegen, Studienfach: Chemie Abschluss: Master of Science (M. Sc.) Masterarbeit: ,,*Synthesis and Investigation of Dextran-Based Hydrogels for Enhanced Bone Healing*"
10/2009 - 09/2012	Universität Siegen, Studienfach: Chemie Abschluss: Bachelor of Science (B. Sc.) Bachelorarbeit: ,,*Synthese und Untersuchung von H_2O_2-sensitiven Fluoreszenzsonden*"

Schulbildung

04/2002 - 03/2008	Freiherr-vom-Stein-Gymnasium, Betzdorf-Kirchen Abschluss: Abitur
08/1999 - 02/2002	König-Wilhelm-Gymnasium, Höxter